Version 2.0

NIWA
Taihoro Nukurangi

A biophysical model for the Marlborough Sounds

Part 2: Pelorus Sound

Prepared for Marlborough District Council

June 2015

10 June 2015 12.24 p.m.

Version 2.0

Prepared by:
Niall Broekhuizen
Mark Hadfield
David Plew

For any information regarding this report please contact:

David Plew
Hydrodynamics Scientist
Hydrodynamics
+64-3-343 7801
david.plew@niwa.co.nz

National Institute of Water & Atmospheric Research Ltd
PO Box 8602
Riccarton
Christchurch 8011

Phone +64 3 348 8987

NIWA CLIENT REPORT No:	CHC2014-130
Report date:	June 2015
NIWA Project:	MDC13301

10 June 2015 12.24 p.m.

Contents

Tables

Figures

Reviewed by

Graham Rickard

Approved for release by

Charles Pearson

Formatting checked by

David Plew

Executive summary

The Marlborough District Council contracted NIWA to undertake biophysical modelling of the Queen Charlotte and Pelorus Sounds. The purpose of the modelling was to describe the effects of existing and proposed mussel and fin-fish farms on water quality. This report presents results for Pelorus Sound. Results for Queen Charlotte Sound and Tory Channel were presented in a previous report.

The biophysical model consists of a three-dimensional hydrodynamic model (with 20 layers in the vertical) coupled to a biogeochemical model (which models water quality, plankton, and other biological and chemical attributes). We used the ROMS hydrodynamic model with the Fennel biogeochemical model, with additional components added to simulate mussel and fish farms. The biogeochemical model includes: (a) the inorganic nutrients ammonium and nitrate, (b) a single phytoplankton class, (c) a single zooplankton class and (d) three classes of particulate organic detritus (slow and fast sinking natural detritus and very fast sinking organic detritus stemming from mussel and fish farms (mussel faeces and pseudo-faeces, fish faeces and waste food)). The abundances of most of these are characterized by means of nitrogen concentration, but the phytoplankton is characterized by two variables: nitrogen concentration and chlorophyll concentration.

A total of seven farming/biogeochemical scenarios were modelled:

- No mussel or fish farms (with benthic denitrification operating) [henceforth, NM-NF-WD].
- Existing mussel farms (no fish farms, with benthic denitrification operating) [EM-NF-WD].
- No mussels, existing fish farms with benthic denitrification [NM-EF-WD].
- Present day/existing farms scenario (with benthic denitrification operating): mussel farms in operation in 2012 (counted by aerial-surveys), and New Zealand King Salmon Ltd. Salmon farms that operated during 2012/2013 (Waihinau Bay, Forsythe Bay, and two farms in Crail Bay). [EM-EF-WD]. We were instructed to treat results from this scenario as a 'baseline' against which to compare alternative scenarios.
- *Approved farms*: as for the *present day* scenario, but also including the additional mussel and fin fish farms that have been approved or existed but were not occupied during the 2012 aerial survey [AM-AF-WD]. The additional salmon farms are Richmond, Waitata and Port Ligar[1]. We also include a small farm in Beatrix Bay licenced for hapuku, although we assume the feed schedules and physiology are the same as for salmon.
- Existing mussel farms, no fish farms, without benthic denitrification [EM-NF-ND].
- Existing mussel and fish farms without benthic denitrification [EM-EF-ND].

In the *with denitrification* scenarios it is assumed that 75% of any particulate organic nitrogen (from any source) which settles to the bed will be lost from the system through denitrification (whilst the remaining 25% is returned to the water column as ammonium). In the *without denitrification*

[1] The Port Ligar farm was included in error. The licence for a salmon farm at that site has been rejected.

scenarios, none of the sedimenting particulate organic nitrogen is lost from the system. It is all returned to the water column as ammonium.

Simulations spanned 500 days (24 May 2012 to 6 October 2013), consisting of a 135 day spin-up period followed by 365 days (1 year) over which the model outputs were analysed.

Horizontal grid resolutions from 100 m to 400 m were tested. Finer resolution grids provide greater detail of the spatial distributions of both physical (hydrodynamic) and biogeochemical properties, but the simulations take significantly more time to run (halving the size between grid points increases the computation time by a factor of approximately 8). The 200 m model reproduces the essential aspects of the hydrodynamics of Pelorus Sound with acceptable accuracy and allows simulations with the full biophysical model for periods of over one year. The 200 m resolution grid was used when making the biophysical simulations reported within this document.

The hydrodynamic model was compared to current meter data collected from a variety of locations and periods during 1994–1995 and 1997–1998, and for shorter durations (FRIA assessments) during 2005. Temperature and salinity were compared with monthly profiles collected by Marlborough District Council at 11 stations from 2012–2013.

Analysis of the hydrodynamic model output allows us to make the following conclusions about the physical behaviour of the Sound.

- Peak tidal flows through the Waitata Reach vary from 20–30,000 $m^3 s^{-1}$ at neap tide to 50–60,000 $m^3 s^{-1}$ at spring tide.
- However, movement of nutrients and tracers through Pelorus Sound is driven primarily by estuarine circulation. The dominant supply of freshwater is from the Pelorus River.
- The estuarine circulation involves a flow of approximately 5000 $m^3 s^{-1}$ of brackish water at the surface out from Pelorus Sound into Cook Strait, and a similar inflow of ocean water below.
- Sustained low river flows cause the estuarine circulation to weaken, leading to longer residence times within the Pelorus Sound. However the estuarine circulation is seldom, if ever, entirely absent.
- Surface salinities decrease (the water becomes fresher) as one moves from outer to inner Pelorus Sound, but the influence of surface freshening events from increased river flow occurs through the Sound.
- Stratification in Pelorus Sound is generally driven by salinity. In summer time, when river flows are generally low, warmer surface temperatures can strengthen stratification. In winter, surface salinities can be sufficiently low to allow the surface water to become cooler than that of deeper waters.
- The biophysical model was validated using field data collected from 7 stations in Pelorus Sound by Marlborough District Council. We used model coefficients derived during calibration against 3 years of data when we modelled the Queen Charlotte Sound. The comparison between the modelled state variables (NO_3-N, NH_4-N, chlorophyll, phytoplankton nitrogen, zooplankton, small and large detritus) suggests that the model reproduces the majority of the respective long-term averages and the

respective amplitudes of the seasonal cycles moderately well, but frequently fails to reproduce the phase of the seasonal cycle accurately. For example, the onset of springtime phytoplankton growth (and associated reductions of NO_3 concentrations) is late relative to the field data. Similarly, during late summer/early autumn the simulated NO_3 concentrations start to rise later than the field measurements suggest they should. In comparison with the field data, the model appears to over-predict the summertime concentrations of phytoplankton carbon biomass and of chlorophyll. We believe that the apparent quantum of over-prediction is deceptively large. In the model, the phytoplankton and chlorophyll state-variables represent the entire phytoplankton community. In contrast, the field determinations of phytoplankton biomass and chlorophyll used techniques that would have counted only those members of the total phytoplankton community that have cell sizes greater than approximately 2 µm. Other studies suggest that phytoplankton <2 µm represented an average of 29% (~5-65%) of the total phytoplankton community in the upper 15 m of the water of Beatrix Bay. We have made no attempt to calibrate the model to the field-data from Pelorus.

- In some cases there are no direct analogues in the field data for modelled state variables, thus we need to infer their values.
- Because the model has only one phytoplankton class, it has no ability to mimic seasonal changes in phytoplankton community structure.
- Our Cook Strait boundary conditions are based upon scarce field data (monthly measurements at only two depths).
- The insolation intensities that are applied are not corrected for possible seasonal-scale variations in cloud-cover or seasonal and hour-by-hour variations in topographic shade (though the latter will be significant only in narrow parts of the Pelorus system).
- The hydrodynamic model produces summer-time water temperatures which are a bit too low. Since phytoplankton and zooplankton physiology is temperature dependent, this (or possibly incorrect parameterisation of the temperature dependence) could have subtle influences upon emergent population growth rates and standing stocks.
- The wind-fields driving the model derive from wind models that have relatively coarse spatial resolution compared to the width of the channels in Pelorus Sound. In combination with the steep topography, this implies that wind-driven surface-flows and mixing may not be well represented in the hydrodynamic model.

In the context of this modelling, nitrogen release from fish farms, and mussel-farm induced nitrogen transformations (and net removal) are the key mechanisms by which farming might influence water quality. If the model did not reproduce the annual averages and amplitudes, its ability to describe the influence of farms would necessarily be called into question. Fortunately, whilst the model is not accurately reproducing the phases of some seasonal cycles, it is reproducing the annual averages and the amplitudes of the seasonal cycles fairly well. In particular, it reproduces the switch from winter-time light limited phytoplankton growth to summertime nutrient (nitrogen) limited growth. Thus, we believe that the model is performing sufficiently well that it can plausibly predict the magnitude of changes induced by the different scenarios.

Our biophysical modelling is aimed at understanding the influences that mussel farming and fish farming have upon nutrient dynamics and the plankton community. Indeed, at the outset, the focus was upon fish-farming. There are important differences between mussel farming and fish farming. Fish farms rely upon adding feed into the environment. Mussel farms require no feed input. Instead, the crop draws feed out of the environment. Fish farms are net sources of readily bio-available nutrient (much of the nutrient added in feed passes into the environment). Mussel farms are a net sink for nutrient (a small fraction of the nutrient within the particulate organic detritus which the mussels are assumed to consume is eventually harvested). Nonetheless, much of the consumed nutrient is recycled into the environment as ammonium and as faeces and pseudo-faeces. This is a natural part of the mussel growth processes. The mussels serve to: (a) convert living plankton into living mussel flesh, (c) ammonium, and (d) dead particulate organic detritus. They serve to convert dead particulate organic detritus into: (a) living mussel flesh, (b) ammonium, (c) recycled/recreated dead particulate organic detritus. Since some of the ingested food is subsequently released back into the environment as ammonium, mussels can serve to speed the transformation of particulate organic nitrogen back into a dissolved form that is readily consumed by phytoplankton.

Based on the output from the model, we infer that with respect to the ecological and water quality responses of Pelorus Sound:

- Phytoplankton growth tends to be limited by low light intensities and short day-length during the winter months. During the summer months, it tends to be limited by a scarcity of nutrient (nitrogen). As a result of this difference, some of the effects of mussel and fish-farming differ between winter and summer months. For this reason, we often draw a distinction between winter- and summer- periods when summarising the simulated effects of mussel and/or fish farms in the following bullets[2].
- Relative to the nominated baseline scenario (EM-EF-WD), a no mussel, existing fish with denitrification simulation (NM-EF-WD) yields:
  - Winter-time: lower concentrations of ammonium and nitrate but higher concentrations of particulate organic detritus (dead plankton etc.,) phytoplankton and zooplankton. The largest changes in relative concentration are seen in Kenepuru Sound and the largest relative concentration changes are within the zooplankton. There, time-averaged near-surface winter-time seston[3] concentrations in the NM-EF-WD simulation are more than double those of the EM-EF-WD scenario (for zooplankton in Kenepuru, substantially more than double). The Beatrix/Crail/Clova system also exhibits similar (but smaller) changes.
  - Summertime: lower concentrations of ammonium, nitrate, higher concentrations of detritus and zooplankton, but phytoplankton concentrations which are similar to (or lower than) those of the EM-EF-WD scenario. During summer, mussels convert particulate organic nitrogen (not directly exploitable by phytoplankton) to ammonium (directly exploitable by phytoplankton). Phytoplankton growth is normally nutrient limited during this time, but in the immediate vicinity of the

[2] Note also, that in this summary, we focus upon inferences drawn from the *with denitrification* simulations.

[3] Collectively, phytoplankton, zooplankton and other small particulate material are referred to as seston. The mussels feed upon phytoplankton, zooplankton and detritus. They release detritus (as faeces and pseudo-faeces). Fish also generate faeces. None of this faecal and pseudo-faecal material is part of the seston because they sink very rapidly whereas, by definition, seston is supposed to be approximately neutrally buoyant.

mussel farms, phytoplankton (which survive passage through the farms) find a plentiful ammonium supply. This enables them to grow quickly – more than offsetting the losses that the population suffered to mussel grazing (the 'excess accrued phytoplankton biomass being fuelled out of the detritus that was consumed). Once again, the largest changes are in Kenepuru Sound.

- Relative to the nominated baseline scenario (EM-EF-WD), a with mussel, no fish with denitrification simulation (EM-NF-WD) yields:
  - Winter-time: lower ammonium, nitrate and natural[4] detritus concentrations. With the exception of ammonium, the concentrations differ by less than approximately 1%. Phytoplankton and zooplankton concentrations that are almost identical to those of the EM-EF-WD scenario.
  - Summer-time: lower ammonium, nitrate, natural detritus, phytoplankton and zooplankton. The largest changes (declines in the absence of fish farms) are in Crail Bay (reflecting the presence of licensed farms in Crail Bay and Beatrix Bay and the slower flushing time of these bays in comparison with Waitata reach (which also harbours an existing fish farm at Waihinau Bay). Within Beatrix/Crail/Clova, time-averaged summertime phytoplankton concentration is predicted to be up to about 10% lower in the absence of fish farms. Zooplankton concentration is predicted to be up to about 15% lower.
- Turning to a comparison of the approved farms scenarios (AM-AF-WD) with the baseline (EM-EF-WD), the model predicts that the relatively few additional mussel farms present in the 'approved farms' scenarios (over and above those of the 'existing farms' scenario) induce water-quality changes that extend out to about bay-scale but amount to only a few percent of the simulated baseline (existing farms) concentrations. Changes are evident in nutrient (esp. ammonium) and seston concentrations. The changes include: increased ammonium concentrations in the vicinity of the farms and depressed concentrations of particulate organic detritus and zooplankton. During the winter, phytoplankton concentrations are slightly depressed by the additional mussel farms. During the summer, they are depressed in the immediate vicinity of the new mussel farms but can become slightly elevated further afield.. The changes induced by these additional farms amount to a few percent of background concentrations. These are small relative to natural variability. For example, during winter, mussel grazing is predicted to induce local depletion of up to approximately 10% relative to the background/baseline (existing farms) simulation. In contrast, field data suggest that the extrema of phytoplankton population biomass can vary three or more fold over the course of a year. Indeed, it can sometimes fluctuate by almost that much over time-scales of weeks and space scales of km or less.
- The model predicts that effects induced by additional fish farming will extend through the entire Pelorus system. The effects upon nutrients are more localised[5] (and, therefore, more intense) than the effects upon phytoplankton, zooplankton or natural

[4] The small and large detritus classes of the model that receive dead plankton etc *cf* the XL-detritus class that receives faeces and pseudo-faeces from the mussels and fish.

[5] Because there are few fish-farms in total. In contrast, there are many mussel farms distributed through much of the Pelorus system

detritus. Relative to the present-day, the modelling suggests that the approved additional fish and mussel farms will induce winter-time phytoplankton biomass changes of <5% and summer-time changes of <15% at most[6]. In winter, phytoplankton biomass will increase slightly in the main channel of central and inner Pelorus but decline within Crail/Clova/Beatrix Bays. In summer, it will increase throughout Pelorus. The greatest (but still relatively small) changes will be in the vicinities of the new fish farms (i.e., in Beatrix/Crail/Clova Bays, and around Richmond/Waitata/Port Ligar).

- Wintertime light limitation acts as a 'bottleneck' which limits the response of short-lived organisms to the increased nutrient concentrations.
- Nutrient inputs associated with the additional fish farms are predicted to increase summertime near-surface phytoplankton standing stocks by 5–10% relative to the existing conditions. The simulated phytoplankton concentrations are higher than is the norm for New Zealand coastal waters, but they would not be higher than values that are intermittently recorded in our coastal waters. That said, the field data indicate that the 'existing conditions' simulation may be over-estimating summertime near-surface phytoplankton abundance[7]. We believe that this underlying (possible) over-estimation implies that the 'additional fish farms' scenario will also contain this embedded tendency to over-estimate.
- Even if the real-world summertime phytoplankton concentrations were to reach those predicted by the model, they would probably not be high enough to begin to change the perceived colour of the water. Nor would they be sufficiently high (for long enough and over sufficiently large areas) for the system to be classified as eutrophic.
- At the whole of Pelorus scale, the majority of the farm derived nitrogen is predicted to be lost through denitrification at the seabed of the Pelorus system rather than by export to Cook Strait.

Deposition footprints of the 8 farm sites were predicted with a particle-tracking model. The deposition modelling shows that deposition of waste from each farm is highest immediately beneath that farm. Footprints beneath farms located in low velocity areas (Beatrix, Crail, Forsyth, Port Ligar, Waihinau) extend only a short distance, but in higher current areas (Waitata, Richmond), footprints are predicted to extend several hundred metres from the farm perimeters in the along-shore direction (although the intensity of deposition at these distances is very low). Historical data from existing NZKS farms indicate that Benthic Enrichment Scores of around 5 are increasingly likely to be exceeded when deposition rates exceed 5–10 kg solids m^{-2} y^{-1}. The deposition modelling suggests that few, if any, of the new farms will be able to operate at their maximum consented annual feed loads without breaching agreed benthic standards. With that in mind, it is worth noting that the consent conditions for the new farms require that each farm be developed in a staged manner (contingent upon meeting the agreed environmental standards). Thus, there are safe-guards in place that will help to prevent excessive degradation of the seabed around the farms.

[6] Excluding the XL-detritus class. Uneaten fish feed and fish faeces passes into this class. Inevitably, when a new fish farm is added, the relative concentration of this material increases dramatically in the vicinity of the new farm.

[7] The degree of over-estimation may not be as large as one would infer from a simple visual comparison of field data and model: the modelled quantity is total phytoplankton, but the sampling by Marlborough District Council does not capture the smallest phytoplankton which can contribute a substantial fraction of the total phytoplankton community biomass.

1 Introduction

1.1 Background

The Marlborough District Council is the regional authority overseeing the Marlborough Sounds, where approximately 80% of New Zealand's aquaculture production occurs. The majority of the area used for aquaculture is occupied by mussel farms, however there are also a small number of salmon farms, particularly in Queen Charlotte Sound. At the commencement of this project, applications had been submitted to the Environmental Protection Authority for additional finfish farm sites. In light of these applications and the possibility of future proposals to expand finfish aquaculture, the Marlborough District Council (MDC) desired an improved range of tools to enable it to predict ecological implications with more certainty. MDC commissioned NIWA to undertake biophysical modelling of the Queen Charlotte and Pelorus Sounds in order to help it understand potential effects of future aquaculture developments. The information provided from the modelling will be used to help plan for longer term, and identify both risks and opportunities.

The primary motivation for the biophysical modelling is to assess the influence of aquaculture. In the later part of the project, the Marlborough District Council has expressed interest in whether the models can be used for assessing the effects of other activities, such as catchment land-use changes. This is possible (indeed the models incorporate freshwater flows and nutrients from rivers and runoff) but modelling the effects of land-use change or changes in nutrient loads from activities other than aquaculture is outside the scope of the current project.

The two sounds (Queen Charlotte and Pelorus) are modelled separately in this project. This report describes the results for the Pelorus Sound. Results for Queen Charlotte Sound were be presented in a previous report: A biophysical model for the Marlborough Sounds, Part 1: Queen Charlotte Sound and Tory Channel (Hadfield, Broekhuizen, Plew 2014a).

1.2 Definition of a biophysical model

In this report, we use the term "biophysical model" to describe a numerical (computer) model that couples physical (hydrodynamic) processes with biological and chemical processes.

The biophysical model is comprised of several component sub-models.

- The ROMS (Regional Ocean Model) hydrodynamic model, which simulates the physical behaviour of water including currents, salinity and temperature.
- A nutrient/phytoplankton/zooplankton/organic detritus (NPZD) model. The particular model that we have adopted includes a simple description of the benthic mineralisation of deposited detritus. For that reason, we will refer to it as the *biogeochemical model*.
- A mussel farm model which focuses upon feeding, respiration and excretion.
- A fish farm model which also focuses upon feeding, respiration and excretion.

The four sub-models are implemented within a single code-base and we will refer to the collective implementation as the *biophysical model*. The biogeochemical model component relies on predictions of transport by water currents by the hydrodynamic model, thus the accuracy of the biogeochemical modelling component depends greatly on the hydrodynamic model adequately

capturing the physical behaviour of the region to be modelled. The hydrodynamics affect the biogeochemical modelling, but we do not allow for the presence of mussel and fish farms to influence hydrodynamics since we believe any such feedback will be negligible at the regional scale. Consequently, this report first focuses on describing the performance of the hydrodynamic model before considering the biogeochemical predictions of the complete biophysical model.

1.3 Scope of this project

The scope of this project is to

1. Conduct 3D hydrodynamic simulations of the Queen Charlotte Sound and Pelorus Sound that accurately simulate tidal, wind-driven and residual currents; and model the changes in stratification over seasonal and annual time periods.

2. Couple the hydrodynamic model with a water quality/biogeochemical model to simulate:

    - The influence of present day aquaculture activities on nutrient concentrations, phytoplankton and zooplankton. This *existing conditions* or *present day* scenario contains (a) those mussel farms which were shown to have backbones in the water during aerial-survey operations flown in 2012; and (b) salmon farms that were licensed to operate during the 2012/2013 period. For Pelorus Sound these are the two salmon farms in Crail Bay, and the farms in Waihinau and Forsythe Bays.

    - A future scenario considering additional mussel and salmon farms that have been approved or existed but were not occupied at the time of the 2012 aerial survey. This is referred to as the *approved farms* scenario. The addition salmon farms are Richmond, Waitata and Port Ligar. We also include a small farm in Beatrix Bay which is licenced for hapuku, although we assume that feed schedules and physiology are the same as for salmon.

    - A *worst case* scenario, which is the same as for *approved farms* but with benthic denitrification processes turned off (such that all particulate organic nitrogen, from any source, which settles to the seabed is returned to the bottom-most layer of the water-column as ammonium).

3. Simulate the deposition of waste matter (faeces) emanating from the fish farms.

In addition to the scenarios described above, we also ran simulations with:

- no mussel or fish farms
- existing mussel farms but no fish farms
- no mussel or fish farms with denitrification turned off.

While these scenarios were not required under the agreed scope, we included them as they provide useful information on the relative effects of denitrification processes in the model; and also of mussel and fish farms both with respect to each other, and also to the background (no marine farms) conditions of Pelorus Sound.

1.4 Outline of this report

In the following sections of this report, we describe

- Section 2: The hydrodynamic model, the area modelled, and the data used as input to this model.
- Section 3: Results from the hydrodynamic modelling, including a comparison to observed data.
- Section 4: The biogeochemical components of the biophysical model and its parameterisation.
- Section 5: Results from the biophysical modelling. Specifically, the following results are presented:
  - *No farms* with benthic denitrification.
  - *Existing mussel farms only* with benthic denitrification.
  - *Existing mussel and fish farms* with benthic denitrification.
  - *All approved mussel and fish farms* with denitrification.
  - *Existing mussel farms* without benthic denitrification.
  - *All approved mussel and fish farms* without denitrification.
  - *No mussel farms, existing fish farms with denitrification*[8]
- Section 6: A discussion of the performance, limitations, and implications of the biophysical modelling.
- Section 7: A description of and results from the deposition model used to simulate finfish farm benthic footprints.

[8] This scenario was not required in the contract. We ran it for our own edification and offer it in that spirit but the readers should note that this scenario was run on a 400 m resolution spatial grid whereas all of the other ones were run on 200 m grids.

2 Hydrodynamic model: Methods

2.1 Model description

The hydrodynamic model used in this project was ROMS (Haidvogel, Arango et al. 2008), a widely accepted ocean/coastal model. ROMS has a number of optional sub-models, including several alternative biological models. The current project uses the Fennel biological model as described in Section 4.1.

ROMS is a fully 3 dimensional model and is able to simulate the currents forced by tides and wind, as well as the effects of density differences caused by variations in temperature and salinity. In the vertical, ROMS uses a terrain-following coordinate system, i.e., a fixed number of levels (here 20) is fitted between the bottom and the surface; this system is well suited to coastal situations and copes well with large tidal variations in sea level. In the horizontal, ROMS uses a structured rectangular (as used in this project) or curvilinear grid. There are several aspects of the ROMS structure that relate to its suitability for the present application.

1. The ROMS grid cannot be fitted around complicated coastlines: instead land is represented by masking out grid cells. This leads to some inefficiency, because in the model grids used for this project less than 50% of the area is occupied by water.

2. The horizontal spacing of a ROMS grid cannot be reduced for better resolution in specific areas, e.g., around a fish farm or in a small bay.

3. ROMS uses a time splitting scheme for the equations of motion, i.e., it solves for the depth-average velocity on a short time step and for the vertical variations from that depth average on a longer time step. For the 200 m simulations described here the short time step was 1.5 s and the long-time step was 12 s. The time-splitting scheme is computationally efficient when the maximum depth in the model domain is large (a few hundred metres or more) but has no advantage in shallower water.

4. ROMS uses an explicit time-stepping scheme, which means that the time step is constrained to a maximum that depends on the grid spacing and the flow speed.

2.2 Model grids and bathymetry

The Pelorus Sound model domain (i.e., the area over which the calculations are performed) is shown in Figure 2-1. It was designed to cover the Sound, plus the area immediately outside in Cook Strait. The domain axes were rotated by 40° anticlockwise from true north/east to better align the domain with the Sound. The exact placement of the boundaries was fine-tuned to avoid instabilities caused by the strong Cook Strait tidal currents interacting with the topography near the boundary.

The model bathymetry was constructed from a number of sources, including:

- a digital terrain model of Marlborough Sounds at 25 m resolution generated from NIWA bathymetry data
- contour data (most digitised from LINZ hydrographic charts) held in the NIWA marine bathymetry database
- high-resolution coastline data (to fix the zero contour in the model), and

- land elevation data (also to improve interpolation near the coast.

These data were collated and interpolated onto the model grid with the GMT[9] mapping tools. A terrain-following model like ROMS requires a further smoothing process to limit the steepness of the bathymetry. At the 200 m and 100 m resolutions this does not degrade the accuracy of the bathymetry significantly, e.g., at 100 m resolution (Figure 2-1) the model captures sharp features like the pair of dramatic, scour-induced depressions near Cape Jackson.

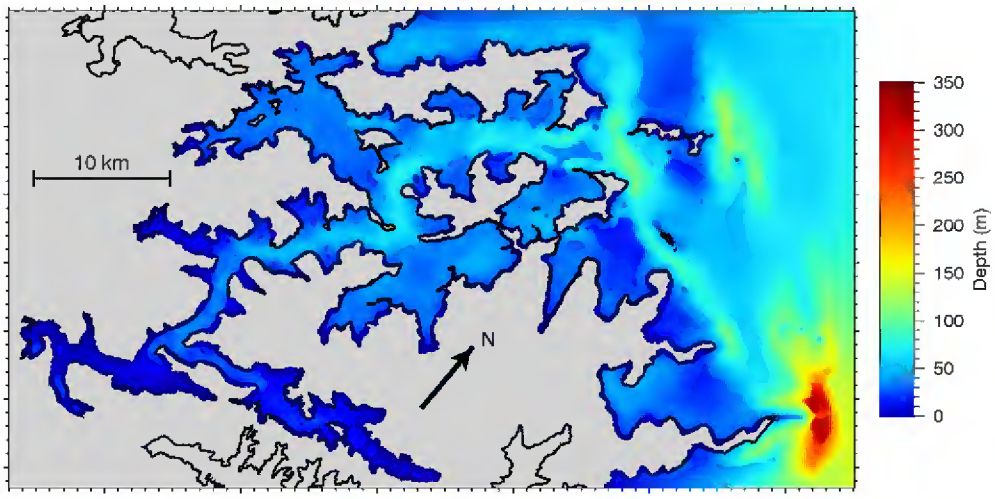

Figure 2-1: The Pelorus Sound model domain and bathymetry. A map showing the model bathymetry and land mask (100 m grid) with LINZ coastline data (black). Note that while parts of the neighbouring Croisilles Harbour and Queen Charlotte Sound are within the domain, these regions were blanked out (shown as grey in the above figures) and were not modelled here.

2.3 Hydrodynamic model simulations

The majority of model simulations described in this report have been for a period of 500 days (24 May 2012 to 6 October 2013) which allows for 135 days to spin-up various components of the model (notably the biogeochemical model) followed by 365 days over which the model output is analysed. Given the short model time steps that are required in coastal situations, a simulation of this duration can be very expensive computationally. Running the model on finer resolution grids allows spatial variability in both physical and biological properties to be better represented, but this comes at the cost of the model taking longer to execute. There is a balance to strike between sufficiently fine resolution and manageable execution time. To examine this issue we set up a series of model grids on the same domain, with different horizontal grid spacing. We employed three such grids: 400 m, 200 m and 100 m.

The execution time (Table 2-1) increases by a factor of approximately 8 with each halving of the resolution, except that between 400 m and 200 m the factor is somewhat smaller because the 400 m grid is not large enough to use the computer efficiently. The addition of biogeochemical processes with the mussel and fish farm parameterisations results in a very large (~ 5–6 times) increase in execution time. This results in part from the extra tracers and processes that the model has to handle, but mainly because the introduction of a fast-sinking detritus class (Section 4.1) required a

[9] http://gmt.soest.hawaii.edu/

change in the model's advection scheme (i.e., the set of model code that moves material through the model grid). With the biogeochemical and aquaculture options activated, the model used the ROMS implementation of the MPDATA advection scheme (Margolin and Smolarkiewicz 1998), which guarantees that concentrations can never become negative. For the hydrodynamics and tracer-flushing simulations we used the usual ROMS third-order upwind scheme (Shchepetkin and McWilliams 1998), which allows small negative concentrations: this is normally acceptable, but leads to problems when the model deals with fast-sinking material. The MPDATA scheme increases execution times by a factor of 2–3.

Table 2-1: Grid resolution and execution time. Time required to execute the Pelorus Sound model for 500 days at three different grid resolutions on a single node of the NIWA supercomputer, Fitzroy. Values in italics have been estimated by extrapolation.

Execution time (days)	400 m	200 m	100 m
Hydrodynamics only	0.6	2.8	25.0
Hydrodynamics plus 6 tracers	0.8	4.2	*37.5*
Hydrodynamics plus biogeochemical model, mussel farms and fish farms	3.0	17.7	*158.0*

The 500-day period (24 May 2012 to 6 October 2013) described above was used for the biogeochemical simulations. In addition several hydrodynamics-only simulations were carried out for earlier periods in which hydrodynamic field data were available (Section 2.5):

- 20 May 1994 to 24 June 1995, bracketing a period of measurements in Beatrix Bay
- 24 May 1997 to 28 June 1998, bracketing a period of measurements in Beatrix Bay and outer Pelorus Sound
- 8 July 2004 to 12 August 2005, bracketing a period of measurements for a FRIA (Fisheries Resource Impact Assessment) programme in Pelorus Sound.

2.4 Initial and boundary conditions

The simulations described in this report were all carried out in forward mode, i.e., the model's temperature, salinity, velocity, sea surface height and biogeochemical variables were set to a plausible initial state and then stepped forward in time subject to various forcings from the surface (wind stress, heat flux, freshwater fluxes), the bottom (bottom drag), the open ocean lateral boundaries (specified temperature, salinity, velocity, etc.,) and inflows from point sources like rivers. There was no process of adjustment towards observations during the model run (i.e., data assimilation), as there would be in a forecasting model, for instance.

The initial and boundary data for the hydrodynamic variables were taken from a larger-scale model covering Cook Strait (Figure 2-2) at a resolution of 2 km. The Cook Strait model was run for the same periods as the Pelorus Sound simulations, with model fields saved as consecutive six-hour averages. These data were then interpolated to the boundaries of the Pelorus Sound model and written to data files that were read by the latter model. This process is known as one-way, off-line nesting.

The Cook Strait model itself required lateral boundary data. For the 2004–2005 and 2012–2013 simulations this was taken from a global ocean analysis and prediction system operated by the US

Naval Research Laboratory, using the HYCOM[10] ocean model. (The specific dataset used here is the HYCOM/NCODA Global 1/12° Analysis on grid GLBa08.) The HYCOM system provides daily snapshots of the three-dimensional state of the global ocean on a 1/12° grid; at NIWA we have archived a subset of this data around New Zealand since 2003. For the 1994–1995 and 1997–1998 periods, lateral boundary data for the Cook Strait simulations was taken from an implementation of ROMS for the New Zealand region, forced by six-hourly surface fluxes, essentially repeating the work of Rickard, Hadfield and Roberts (2005). In either case the purpose of the Cook Strait model was to generate realistic temperature, salinity and currents at the entrance to Pelorus Sound.

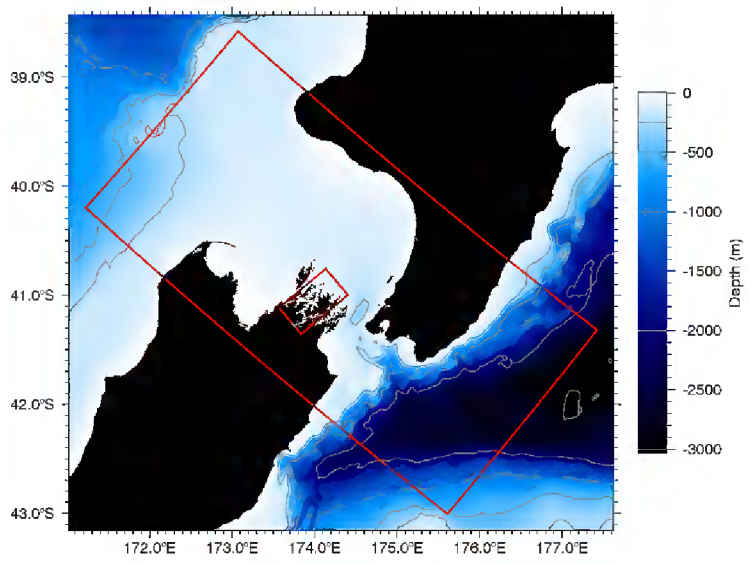

Figure 2-2: The Pelorus Sound and Cook Strait model boundaries.

In principle, the Cook Strait model could include tidal fluctuations in sea-surface height and velocity, which would then be passed into the Pelorus Sound model through its lateral boundaries. However this would require the outer model data to be saved at intervals of ~30 minutes, which would require very large output files. Therefore tides were not represented in the Cook Strait model but were applied at the boundaries of the Pelorus model. Amplitude and phase data for 13 tidal constituents (M2, S2, N2, K2, K1, O1, P1, Q1, 2N2, MU2, NU2, L2, T2) were interpolated from the output of the NIWA New Zealand region tidal model (Walters, Goring, Bell 2001). The ROMS tidal forcing scheme then calculated tidal sea surface height and depth-averaged velocity at each time step and added them at the boundaries.

Surface stresses generated by the wind are an important factor in forcing currents in Cook Strait and (we expect) in Pelorus Sound. For the 2012–2013 simulation, these stresses were calculated using 3-hourly winds from the NZLAM 12 km regional atmospheric model[11]. For the 2004–2005 and earlier simulations the winds came from a global (1/4°, six-hourly) ocean surface wind dataset called CCMP (Atlas, Hoffman et al. 2010). In both cases, the surface stress was calculated from the wind speed using the following equation.

[10] http://hycom.org/
[11] NZLAM is part of the NIWA Ecoconnect environmental forecasting system: http://EcoConnect.niwa.co.nz/

Equation 2-1: Formula for calculating model surface stress from wind speed

$$\tau = \rho_{air} C_D {U_h}^2$$

where τ is the stress, ρ_{air} the density of the air, U_h the wind speed and C_D a wind-speed-dependent term called the drag coefficient (Smith 1988). For the larger Cook Strait model, it was found in a previous modelling exercise (Hadfield 2013) that the modelled currents agreed well with measurements, but only when the drag coefficient was multiplied by a factor of 1.4. A similar adjustment—though often by a smaller factor—has been found to be necessary in coastal modelling exercises around New Zealand by us (Hadfield and Zeldis 2012) and others (e.g., P. McComb *pers. comm.*). For the Pelorus Sound model the drag coefficient was not increased as the speed of the modelled wind-driven currents matches the measurements reasonably well without any adjustment. The relatively coarse spatial resolution of the wind datasets means that they will not reproduce the topographic channelling of the wind that is seen in Marlborough Sounds and this can be expected to limit the accuracy of the hydrodynamic model. It is possible to run an atmospheric model at much finer resolution to generate more detailed wind fields, but this is outside of the scope of the current work. We note that from mid-2014 NIWA have an atmospheric model running at 1.5 km resolution which may give improved results in the Marlborough Sounds compared to the 12 km model. Unfortunately this could not be used for the present study but could be considered in the future.

Surface heat fluxes in both the Cook Strait and Pelorus Sound models were calculated using data (6-hourly averages) from a global atmospheric analysis system called the NCEP Reanalysis (Kalnay, Kanamitsu et al. 1996), with a heat flux correction term that causes the model sea surface temperature (SST) to be nudged towards observed SST (the NOAA Optimum Interpolation 1/4° daily SST dataset (Reynolds, Smith et al. 2007)). The heat flux correction prevents the modelled SST from departing too far from reality due to any biases in the surface fluxes, but has a negligible effect on day-to-day variability.

The surface freshwater flux (precipitation minus evaporation) was calculated from a combination of NCEP Reanalysis 6-hourly evaporation data and daily rainfall from the Crail Bay climatological station (NIWA Climate Database[12] agent number 4232). The average annual rainfall at Crail Bay is 1675 mm. Applied over the area of Pelorus Sound (inside the boundaries shown in Figure 3-12 below) of 382 km^2, this implies a mean rainfall input of 6.4×10^8 m^3 per year, or 20.3 m^3 s^{-1}.

[12] http://cliflo.niwa.co.nz/

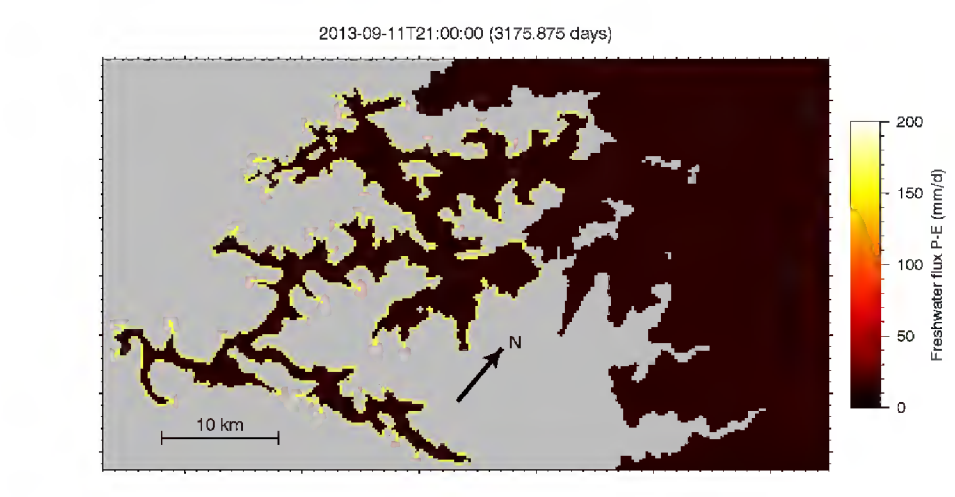

Figure 2-3: Surface freshwater flux. A colour plot showing a snapshot of the surface freshwater flux on the 200 m grid during a moderate rain event (~10 mm d^{-1}), illustrating the extra input of freshwater in a band next to the coast in Pelorus Sound.

The two largest rivers draining into Pelorus Sound (Heath 1974) are the Pelorus River (catchment area 880 km^2, annual mean flow 43 $m^3 s^{-1}$) and the Kaituna River (catchment area 115 km^2, annual mean flow 5 $m^3 s^{-1}$). These two rivers were represented explicitly as point sources in the model. The flow rate for the Pelorus River was constructed from daily average flow data from the NIWA hydrological database (Kathy Walter *pers. comm.*) at the Pelorus at Bryants (58902) and Rai at Rai Falls (58903) stations, with the sum multiplied by 1.2 to account for contributions from catchments downstream of the stations. There is no suitable gauge data for the Kaituna River, so river input to the model was constructed by multiplying the Pelorus River flow by a factor of 5/43. In addition to the largest rivers, there are many smaller rivers and streams, almost all ungauged, draining into Pelorus Sound. We assumed that the catchment area of Pelorus Sound (excluding the Pelorus and Kaituna River catchments and the surface of the sound itself) is 1075 km^2 (Heath 1974) and that, of the rainfall falling on that area every day, 20% is lost to evaporation and the remainder is immediately delivered to the sea at the coastline. This was achieved by applying an increment to the surface freshwater flux (i.e., an extra input of freshwater, see Figure 2-3) of an appropriate amount in all model grid cells that are adjacent to the land mask and inside the boundaries of Pelorus Sound. The annual mean input by this mechanism is 18.0×10^8 m^3 per year, or 45.7 $m^3 s^{-1}$.

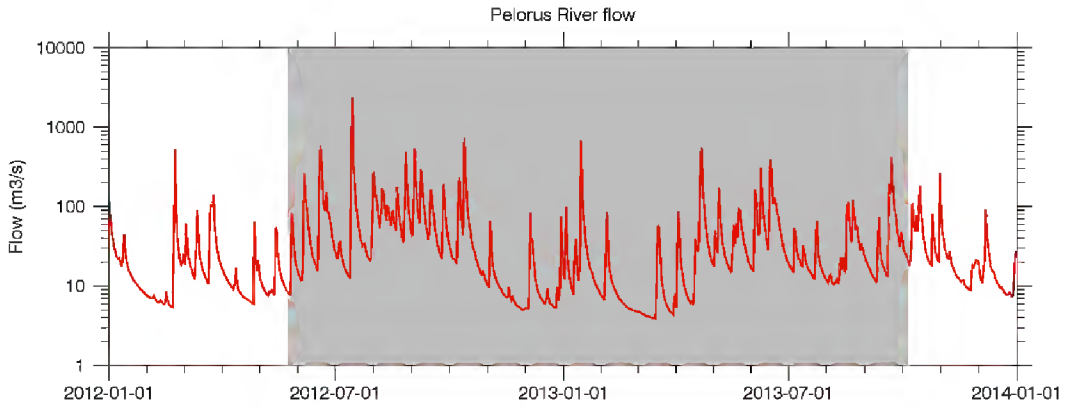

Figure 2-4: Pelorus River flow. Pelorus River flow as input to the model, estimated from the Pelorus at Bryants (58902) and Rai at Rai Falls (58903) stations. The grey rectangle indicates the period of the 500-day 2012–2013 simulation.

2.5 Hydrodynamic field data

2.5.1 Pelorus Sound 1994–1995 and 1997–1998 measurements

Two hydrodynamic measurement campaigns were conducted by NIWA in the 1990s. The first involved a tide gauge and several moorings with current meters and temperature and salinity sensors in Beatrix Bay from September 1994 to June 1995. Selected results were written up by Sutton and Hadfield (1997).The second involved similar instruments deployed in Beatrix Bay and outer Pelorus Sound from July 1997 to February 1998. Current and sea level data from several measurement sites (Figure 2-5) are compared with model output in Sections 3.2.1, 3.3.1 and 3.4.1.

2.5.2 FRIA measurements, 2005

FRIA (Fisheries Resource Impact Assessment) was a programme assessing the effect of aquaculture for the Ministry of Fisheries, a predecessor to the Ministry for Primary Industry. To support these assessments, NIWA and other organisations made hydrodynamic measurements in several aquaculture areas around New Zealand. The Pelorus Sound FRIA measurements were made in February and March 2005: some 19 sites in inner and central Pelorus Sound were occupied by acoustic Doppler current profiler (ADCP) instruments for periods typically between 14 and 28 days. These sites are shown in Figure 2-6 along with an extra site in Port Ligar, labelled as number 20, which was occupied for 22 days in April–May 2005. ADCP pressure and velocity data are compared with hydrodynamic model output in Sections 3.2.2 and 3.3.2.

Permission to use the FRIA Pelorus Sound ADCP data for the present report was kindly granted by the Marine Farming Association[13].

[13] http://www.marinefarming.co.nz/

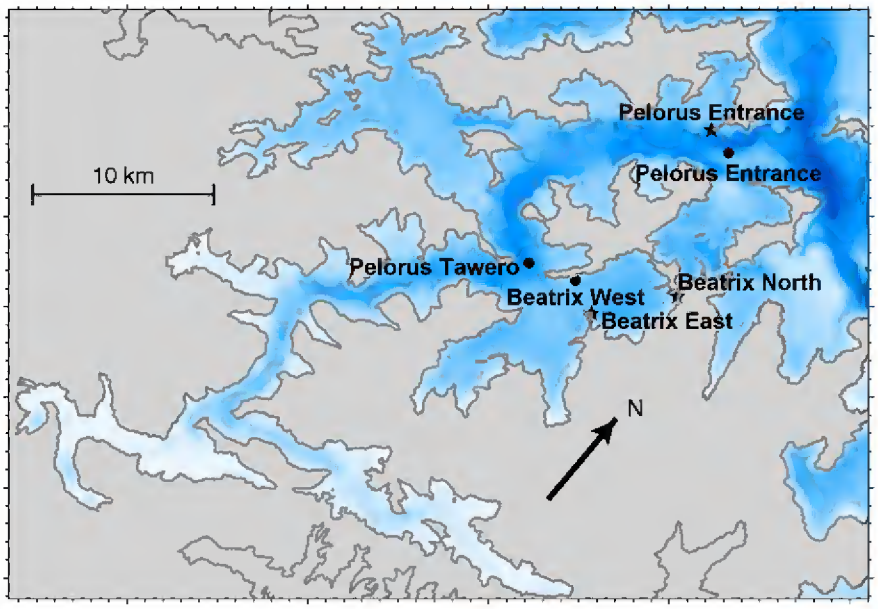

Figure 2-5: Pelorus Sound 1994–1995 and 1997–1998 measurement sites. A map showing the model bathymetry and land mask (100 m grid), with current meter sites indicated by filled circles and tide gauge sites indicated by a star.

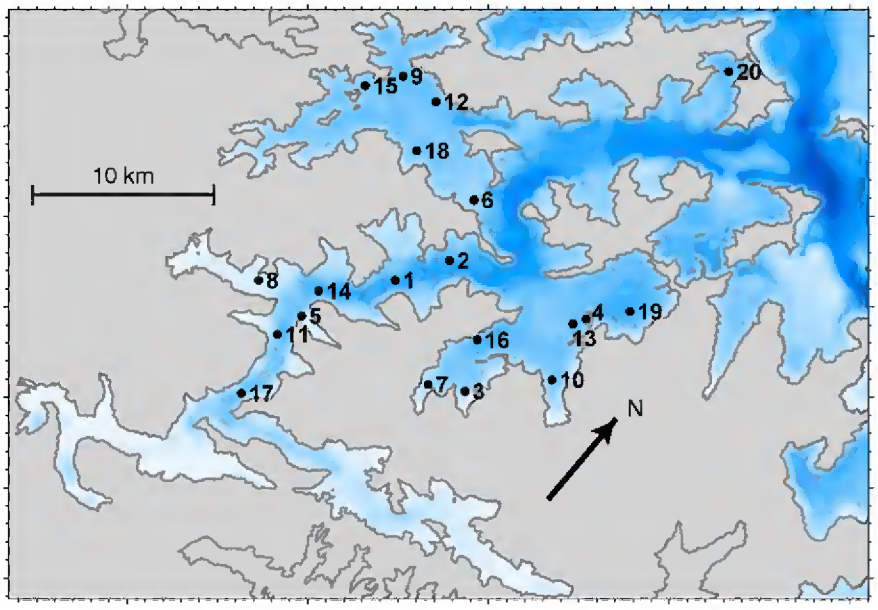

Figure 2-6: Pelorus Sound FRIA sites. A map showing the model bathymetry and land mask (100 m grid), with ADCP sites for the 2005 FRIA project.

2.5.3 Havelock tide gauge data

Sea level time series data for the Havelock tide gauge from 21 April to 14 December 2009 has been kindly supplied by Glen Rowe of Land Information New Zealand, with permission from Port Marlborough. Tidal analyses of these data are compared with model output in Section 3.2.3.

2.5.4 Pelorus Sound CTD surveys, 2012–2014

Beginning in July 2012, Marlborough District Council with NIWA support has measured monthly vertical profiles of temperature and salinity with a CTD (conductivity-temperature-depth) instrument at 11 sites (Figure 2-7) in Pelorus Sound. (At 7 of these sites water quality samples were also collected, see Section 4.4.) The CTD data are compared with hydrodynamic model output in Section 3.1.1.

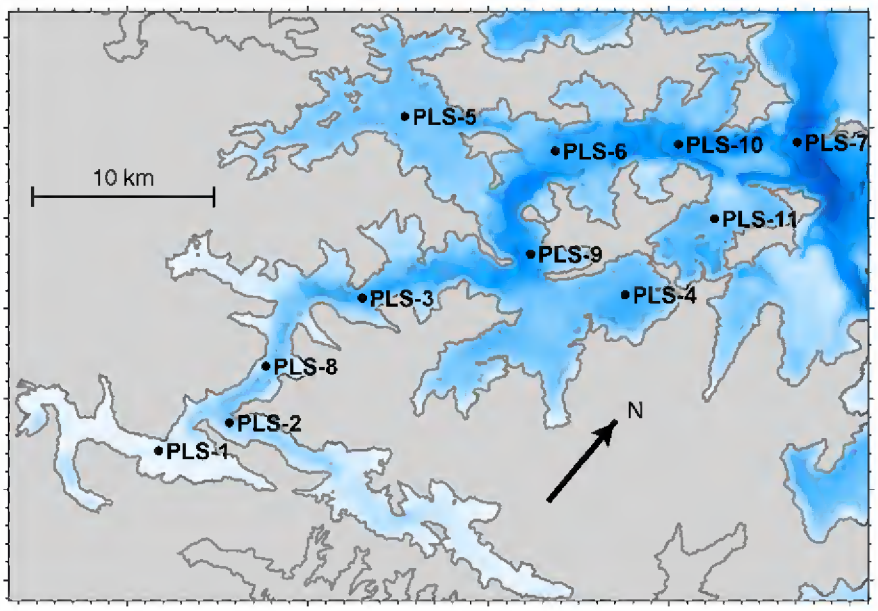

Figure 2-7: Pelorus Sound CTD sites. A map showing the model bathymetry and land mask (100 m grid), with sites occupied by the Pelorus Sound CTD programme. Water quality measurements were also made at seven of these sites.

3 Hydrodynamic model: Results

3.1 Model *vs* observations: temperature and salinity

3.1.1 Pelorus Sound CTD surveys, 2012–2014

Figure 3-1 shows the temperatures measured by the monthly CTD surveys as colour plots against time and depth axes, along with comparable model data. (However note that the way the CTD data are graphed suggests the temperature is uniform throughout the month, but in fact it only applies to a period of an hour or so, and there is considerable within-month variability in the actual temperatures, just as there is in the model.) The panels of Figure 3-1 show 5 sites from inner to outer Pelorus Sound: PLS-1 (Moetapu Bay) in Mahakipawa Arm, PLS-3 (Yncyca Bay) in Popoure Reach; PLS-4 (Beatrix Bay); PLS-5 (Dart Rock) in western Tawhitinui Reach; and PLS-10 (Post Office Point) in Waitata Reach. Site locations are shown in Figure 2-7.

At all the sites there is a clear seasonal variation in near-surface temperature, from 10–12 °C in late winter to 18–20 °C in late summer. At the sites in the inner Sound the winter minimum is lower and the summer maximum higher than in the outer Sound: the time series plots below will show this more quantitatively. The depth profile of temperature is nearly uniform in late winter: perhaps a little cooler at the surface than at the bottom, but again the time series plots show this better. The warming in spring is confined to the top 10 m or so of the water column, but as summer progresses this warm layer thickens and eventually occupies the full depth, down to the 40 m shown in the figures.

Overall, Figure 3-1 suggests that the variation of temperature with depth and time agrees well between the model and the CTD measurements, with the obvious limitation that the CTD data are monthly snapshots.

Figure 3-2 is a comparison of the temperature measured by the CTD with co-located model data—like Figure 3-1 above—but in this case the data are plotted as time series from two depths, 5 and 30 m. At the innermost and shallowest site, PLS-1 (Figure 3-2a), where there are no 30 m data, the 5 m modelled temperature agrees with the CTD data (bearing in mind the limitations of the CTD data). At all other sites there is good agreement between the model and the measurements in winter and early spring, but from late spring to late summer, the model is biased low by 1–1.5 °C. However the difference in temperature between the two depths remains about right.

The model's temperature bias in summer in Pelorus Sound is thought to be a result of the amplitude of the seasonal cycle in SST in Cook Strait being too low. This might be a result of a bias in the surface heat flux formulation (which is based on coarse-resolution data from a global-scale model) or maybe excessive tidal mixing in the areas with high tidal current speeds in Cook Strait (see Figure 3-8 below).

A noticeable feature of the temperature time series at the four deeper sites in Figure 3-2 is that the near-surface is warmer than the water below in summer, but cooler by as much as 1–2 °C in winter. Given that water expands as it warms, a lower surface temperature can only be maintained if the surface water is less saline, and the salinity data presented below confirm that this is the case. This phenomenon of a cool surface water layer in winter was noted in Beatrix Bay by Sutton and Hadfield (1997) and appears to be a ubiquitous feature in Pelorus Sound.

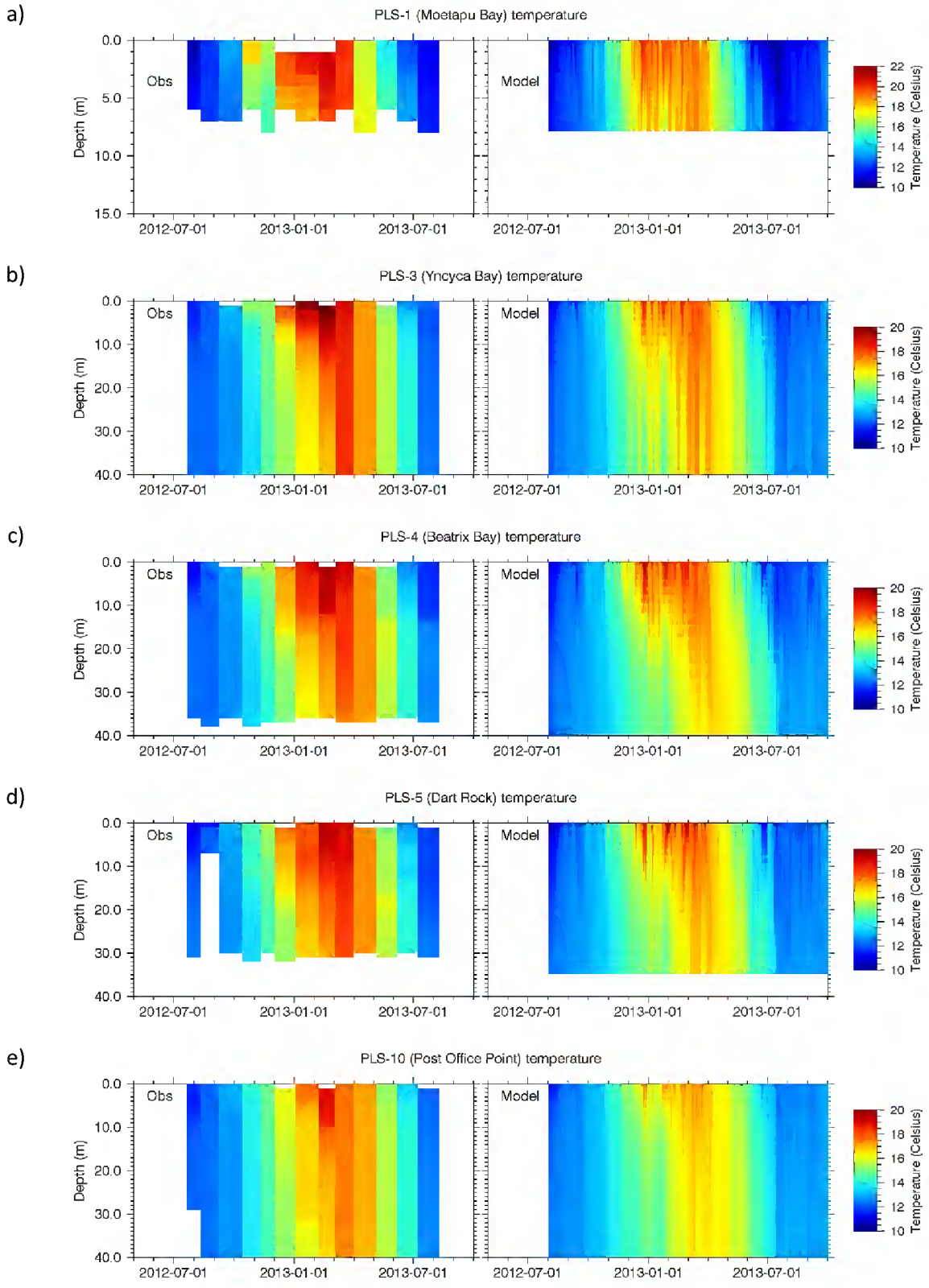

Figure 3-1: Observed and modelled temperature profiles. Temperature versus time and depth from monthly CTD casts (left) and model (right) for 5 sampling locations shown in Figure 2-7: a) PLS-1; b) PLS-3; c) PLS-4; d) PLS-5; e) PLS-10.

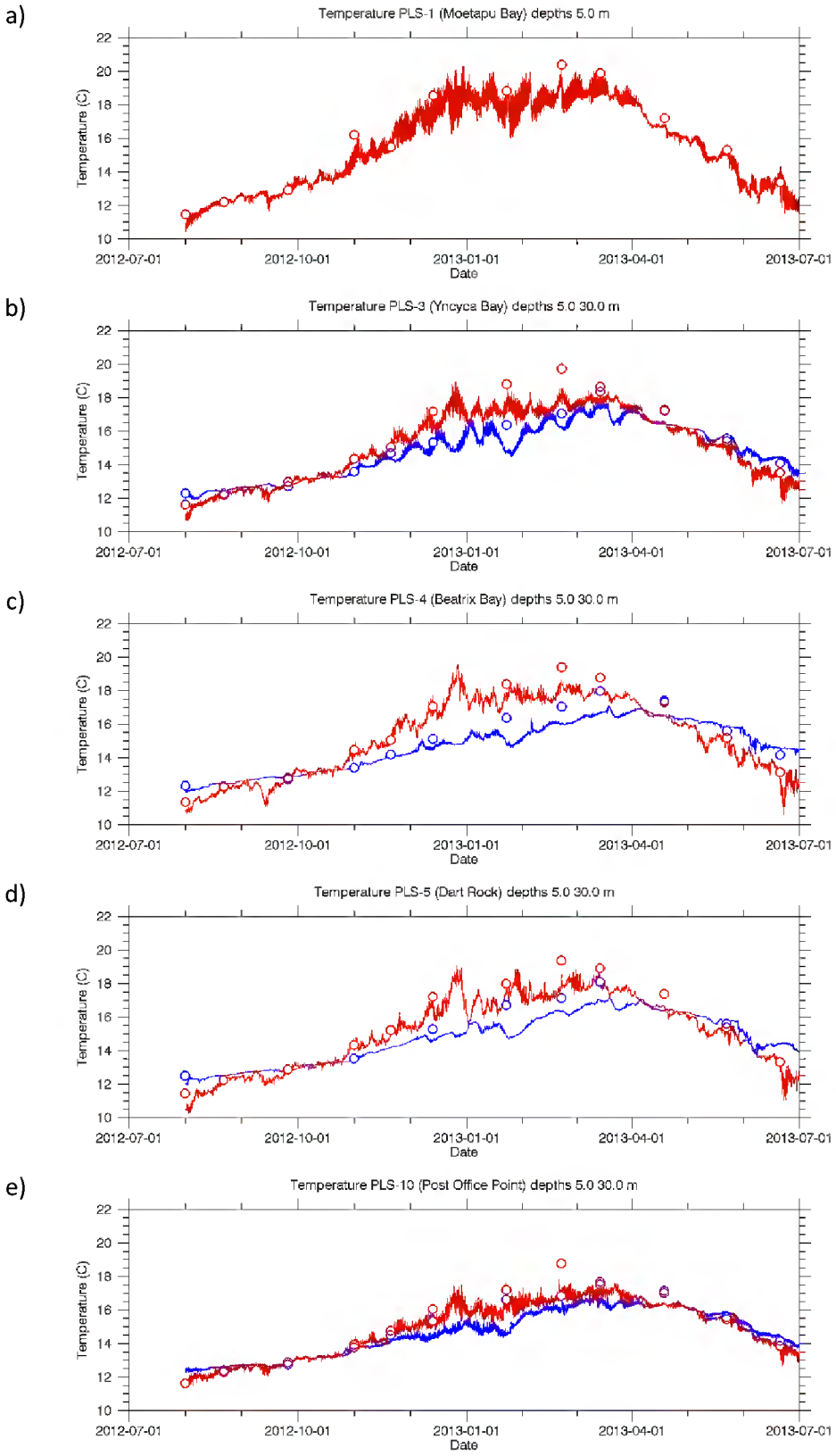

Figure 3-2: Observed and modelled temperature time series. Temperature at two depths (blue lower, red upper) from monthly CTD casts (symbols) and model (lines) for 5 sampling locations shown in Figure 2-7: a) PLS-1; b) PLS-3; c) PLS-4; d) PLS-5; e) PLS-10.

Figure 3-3 shows salinity[14] versus time and depth at the same 5 CTD stations as Figure 3-1. All these plots show there is a low-salinity surface layer that is present much of the time, particularly in winter. Note that the salinity colour scale differs between the panels of Figure 3-3: at the innermost site (PLS-1 Moetapu Bay) the scale spans 20–35 g kg^{-1} and at the outermost site (PLS-10 Post Office Point) it spans 30–35 g kg^{-1}. So the surface salinities fall as one moves from outer to inner Pelorus Sound, but the pattern of frequent surface freshening events occurs throughout the Sound. The timing of the surface freshening events agrees between the model and the measurements (bearing in mind the limitations of the monthly sampling) and the freshening events seem to follow pulses of Pelorus River flow (Figure 2-4).

Salinity time series at the mooring sites are shown in Figure 3-4. Agreement between model and measurements is very good. The model salinity is biased high at the outer site (PLS-10, Post Office Point) in the winter and spring of 2012. This might be a model spin-up issue: the model was initialised with zero freshwater on 24 May 2012 and it may take several months for the freshwater to spread through Pelorus Sound and into Cook Strait. The lack of freshwater input into the Cook Strait model might be an issue too.

A lack of freshwater in Pelorus Sound from late January to late April 2013 is apparent at all the sites. This coincided with a period of low Pelorus River flow (Figure 2-4) and a drought in central New Zealand[15] and was terminated by a Pelorus River flood event with a peak flow of 500 m^3 s^{-1} on 22 April.

[14] The term "salinity" in this report implies absolute salinity as defined by the TEOS-10 standard (Pawlowicz 2010).
[15] http://www.stuff.co.nz/business/farming/drought-recovery/8963794/Drought-worst-in-nearly-70-years

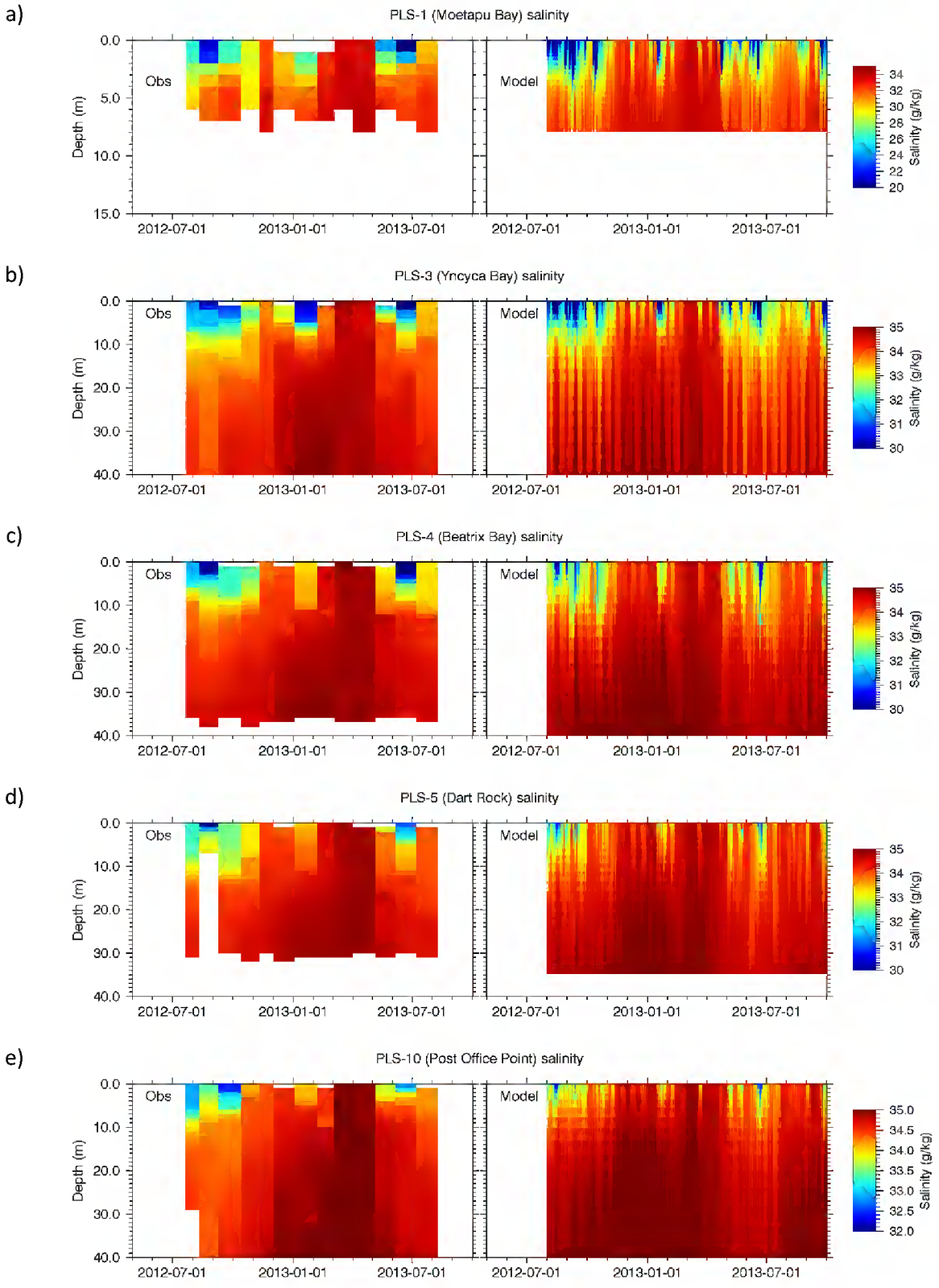

Figure 3-3: Observed and modelled salinity profiles. As Figure 3-1 but for salinity.

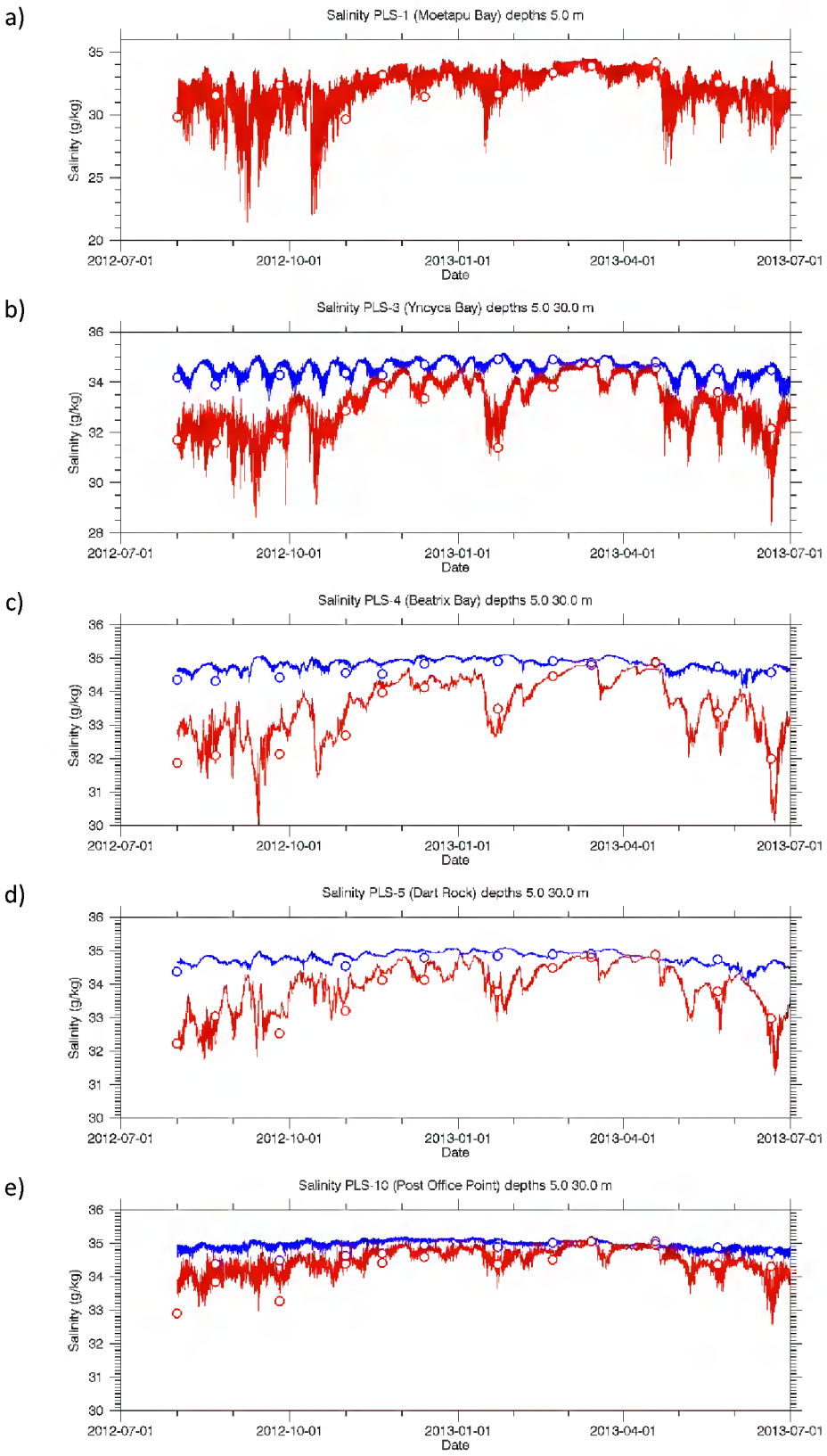

Figure 3-4: Observed and modelled salinity time series. As Figure 3-2 but for salinity.

3.2 Model *vs* observations: tidal height fluctuations

This section considers the accuracy of the model's representation of tidal fluctuations in sea surface height. These are estimated by fitting tidal harmonics of specified frequencies to the data. As is the case elsewhere around New Zealand, the dominant tidal constituent in the area is the lunar, semi-diurnal constituent (M2). The tidal variation is defined by two parameters: the amplitude (metres) and the phase (degrees) in time of the sinusoidal oscillation. A phase difference of 1° corresponds to a time difference of 1/360th of the tidal period: for the M2 tide, the period is 12.42 hours (0.5 lunar days) so a phase difference of 1° corresponds to a shift of 2.1 minutes.

3.2.1 Pelorus Sound 1994–1995 and 1997–1998 measurements

Table 3-1 compares measured and modelled M2 tidal parameters at tide gauge sites occupied in 1994–1995 and 1997–1998 (Figure 2-5). The model matches the amplitude within 6% and the phase within 1.5° (3 minutes) which represents very good agreement.

Table 3-1: Comparison of M2 tidal height parameters for Pelorus 1994–1995 and 1997–1998 tide gauges. M2 tidal sea level parameters from measurements and model. Here "ratio" means model value divided by observed value and "diffce" means model value minus observed value.

Tide gauge site and deployment	Record length (days)	Amplitude (m)			Phase (°)		
		Obs.	Model	Ratio	Obs.	Model	Diffce
Beatrix East 1994-1995 Deployment 55	54	0.878	0.927	**1.06**	270.2	271.6	**1.3**
Pelorus Entrance 1997-1998 Deployment 1	46	0.826	0.824	**1.00**	270.1	270.9	**0.8**
Pelorus Entrance 1997-1998 Deployment 2	69	0.868	0.867	**1.00**	271.7	272.1	**0.4**
Pelorus Entrance 1997-1998 Deployment 3	78	0.829	0.831	**1.00**	271.5	270.9	**-0.6**
Beatrix North 1997-1998 Deployment 1	46	0.881	0.886	**1.01**	270.6	271.7	**1.1**

Note that in Table 3-1, there are separate estimates of the M2 amplitude at one site (Pelorus Entrance) for each of the three 1997–1998 deployments and these estimates differ from each other, varying between 0.826 and 0.868 m. If one estimates the M2 constituent for a sufficiently long period (about one year), one gets a stable estimate representing the true value for that location, which can then be used for tidal predictions well into the future. (The situation is slightly complicated by the nodal variation, which is an astronomically-controlled oscillation of a few percent in amplitude and a few degrees in phase over an 18.6 year period.) However the purpose of the present calculations is not to estimate the true M2 tide, but to compare the model against observations. The M2 tide calculated over a period of a few months will vary from the true value, but ideally the model will capture that variation as long as the model and observations are analysed over the same period.

Table 3-2 presents a similar comparison for the S2 (solar, semi-diurnal) tidal constituent, which has a period of 12 hours and is the largest constituent after M2. Superposition, or "beating", of the M2 and S2 constituents accounts for most of the spring-neap cycle in the semi-diurnal tide. Agreement is not quite as good as with the M2 constituent. The model tends to overestimate the amplitude slightly (implying that the spring-neap variation is being overestimated), with the largest discrepancy being

+13% at the Beatrix East gauge; the phase matches within 4°. It is normal for hydrodynamic models to agree less with the smaller constituents than with the M2, and this still represents good agreement.

Table 3-2: Comparison of S2 tidal height parameters for Pelorus 1994–1995 and 1997–1998 tide gauges. As Table 3-1 but for the S2 constituent.

Tide gauge site and deployment	Record length (days)	Amplitude (m)			Phase (°)		
		Obs.	Model	Ratio	Obs.	Model	Diffce
Beatrix East 1994-1995 Deployment 1	54	0.308	0.346	**1.13**	318.0	314.9	**-3.1**
Pelorus Entrance 1997-1998 Deployment 1	46	0.301	0.316	**1.05**	333.8	337.5	**3.7**
Pelorus Entrance 1997-1998 Deployment 2	69	0.362	0.387	**1.07**	310.5	309.5	**-1.0**
Pelorus Entrance 1997-1998 Deployment 3	78	0.233	0.230	**0.99**	323.0	323.5	**0.5**
Beatrix North 1997-1998 Deployment 1	46	0.323	0.342	**1.06**	334.6	338.4	**3.8**

Similar comparisons are presented in Appendix D for N2 (a semi-diurnal constituent) and O1 (typically the largest of the diurnal constituents) constituents. For N2 (Table D-1) the amplitude is within 8% and the phase is within 6°, which is very good agreement for one of the smaller semi-diurnal constituents. For O1 (Table D-2) the disagreement is larger (up to 46% in amplitude and 27° in phase) but given that the amplitude of this constituent is only 0.01–0.02 m, this level of disagreement is not unexpected and does not indicate a deficiency in the model's description of important hydrodynamic processes.

3.2.2 FRIA 2005 measurements

Table 3-3 compares measured and modelled M2 tidal parameters, the former calculated from ADCP pressure data collected during the FRIA project (Section 2.5.2, Figure 2-6). The FRIA ADCPs were deployed for short periods, the longest being 29 days (site 10 deployment 1); records shorter than 10 days were omitted from this analysis. This leads to quite a lot of variation in the amplitude estimated for the M2 tide, as explained above. Despite this variation, the model agrees with the observations reasonably well, tending however to overestimate the amplitude, by 7–12%. The phase agrees very well. Given the short record lengths, these comparisons should be given less weight than the longer-record comparisons in Section 3.2.1.

Table 3-3: Comparison of M2 tidal height parameters for FRIA 2005 ADCP pressure data. M2 tidal sea level parameters from measurements and model. Here "ratio" means model value divided by measured value and "diffce" means model value minus observed value.

ADCP site and deployment	Record length (days)	Amplitude (m)			Phase (°)		
		Meas.	Model	Ratio	Meas.	Model	Diffce
Site 1 deployment 2	10	0.684	0.731	**1.07**	276.5	276.0	**-0.5**
Site 11 deployment 2	11	0.742	0.801	**1.08**	276.8	276.8	**0.0**
Site 10 deployment 1	29	0.809	0.909	**1.12**	272.6	271.7	**-0.9**
Site 9 deployment 1	14	0.811	0.901	**1.11**	263.0	263.4	**0.4**
Site 8 deployment 2	10	0.675	0.748	**1.11**	276.7	276.6	**-0.1**
Site 6 deployment 1	14	0.809	0.897	**1.11**	96.5	95.8	**-0.7**
Site 15 deployment 1	14	0.816	0.902	**1.10**	97.0	96.7	**-0.3**

The S2 and other constituents have not been calculated from the FRIA ADCP data because of the short record lengths.

3.2.3 Havelock tide gauge data

Table 3-4 presents another comparison of measured and model tidal height parameters, this one using the Havelock tide gauge data (Section 2.5.3). The record length for the tide gauge analysis was 237 days (21 April to 14 December 2009) and for the model analysis it was 365 days (6 October 2012 to 6 October 2013). These record lengths are sufficient to permit stable estimates of the major constituents, therefore it is not necessary to match the modelled and measured time intervals as was done for the Pelorus Sound and FRIA data in the preceding sections.

Table 3-4: Comparison of tidal height parameters for Havelock tide gauge data. Tidal sea level parameters for 6 constituents from measurements and model. Here "ratio" means model value divided by measured value and "diffce" means model value minus observed value.

Constituent	Amplitude (m)			Phase (°)		
	Meas.	Model	Ratio	Meas.	Model	Diffce
M2	0.931	1.057	**1.14**	277.8	276.0	**-1.7**
S2	0.340	0.366	**1.08**	333.2	330.8	**-2.4**
N2	0.147	0.168	**1.14**	269.1	264.5	**-4.6**
K2	0.104	0.073	**0.70**	311.0	330.8	**19.7**
K1	0.051	0.051	**1.00**	340.0	345.7	**5.8**
O1	0.028	0.017	**0.63**	268.0	250.5	**-17.5**

For the M2 constituent the model matches the measured phase to within 2° (~4 minutes) but overestimates the amplitude by 14%. Similar performance is achieved for the two next-largest semi-diurnal constituents, S2 and N2. The model also performs quite well for the largest diurnal constituent, K1, but substantially underestimates the K2 and O1 constituents. Regarding the K2 constituent, it is very close in period to the S2 constituent: the beat period (the period over which the two constituents move in and out of phase with each other) is 182.5 days. This means that accurate estimates of the two constituents requires a long record, and the record lengths here are

marginal. For the O1 constituent, it is known that the NIWA EEZ tidal model that provided boundary forcing for this model does not reproduce this constituent particularly well in Cook Strait (Stanton, Goring, Bell 2001). Overall, the important result of this comparison is that the model somewhat overestimates the amplitude of the major semi-diurnal constituents.

3.3 Model *vs* observations: tidal velocity fluctuations

Tidal velocity variations are conventionally characterised by tidal ellipses, a representation indicating the path taken by the tip of a tidal current vector, which rotates at a constant angular frequency and changes in length (current speed) through a tidal cycle. A tidal ellipse is defined by four parameters:

- **Semi-major amplitude (m s^{-1}):** The semi-major axes are lines from the origin to the two most distant points on the ellipse perimeter. The two axes are equal in length, and this length represents the amplitude of the velocity along the semi-major direction.
- **Eccentricity:** At right angles to the semi-major axes are the semi-minor axes, which connect the origin to the two closest points on the ellipse perimeter. The eccentricity, or "fatness", of the ellipse is the ratio of semi-minor to semi-major axis lengths. The eccentricity can be positive (vector rotates anti-clockwise) or negative (clockwise).
- **Inclination (°T):** The inclination is the orientation of one of the semi-major axes. The choice between the two is arbitrary: here we take the semi-major axis directed towards the north-eastern or south-eastern quadrant and express the inclination as the orientation in degrees clockwise from true north (°T).
- **Phase (°):** The phase relates to the time at which the rotating tidal current vector passes through the semi-major axis. A phase difference of 1° corresponds to a time difference of 1/360th of the tidal period.

The following subsections compare modelled tidal ellipses in Pelorus Sound with measurements from the same measurement campaigns as the section on tidal height fluctuations. Sample graphs are shown below, with a more complete set of graphs and tables in Appendix D.

3.3.1 Pelorus Sound 1994–1995 and 1997–1998 measurements

Suitable data for a tidal velocity comparison are available from three sites, all in the 1997–1998 campaign: Pelorus Entrance, Pelorus Tawero and Beatrix West (Figure 2-5). Of the full set of 3 sites × 3 deployments × 2 levels, 11 time series are suitable for the comparison. Figure 3-5 compares measured and modelled M2 tidal ellipses at the Pelorus Tawero site during deployment 1, when both the near-surface (9 m below the surface) and near-bottom (5 m above the bottom) meters returned good data. The measured and modelled ellipses match reasonably well in orientation and the model appears to under-predict the amplitude somewhat. At the near-surface meter the modelled ellipse is somewhat "fatter" (higher eccentricity) than the measured one. A tabular comparison (Appendix D, Table D-3) confirms these qualitative observations showing *inter alia* that the model over-predicts the amplitude by 30% at the surface and 20% at the bottom, that the model matches the measured inclination to within 3° and that the model phase leads the observations by 10° (20 minutes). This a reasonable performance, given that the Pelorus Tawero site is at a location where the main channel of Pelorus Sound takes a sharp bend and tidal velocities can be expected to vary over small distances. An interesting feature of this location (model and measurements) is the large difference (45–50°) in the inclination of the tidal ellipse between the near-surface and near-bottom meters.

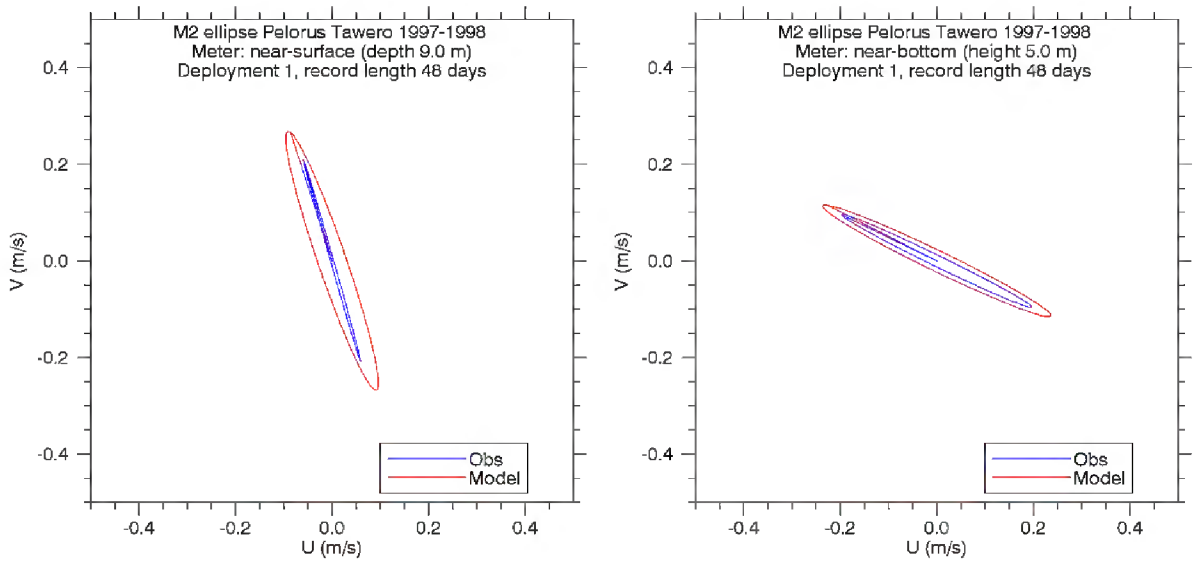

Figure 3-5: M2 tidal velocity comparison (Pelorus Tawero, deployment 1). M2 tidal ellipses from current meters (blue) and model (red). The axes correspond to the velocity components towards due east (*u*) and due north (*v*). The ellipses represent the magnitude and orientation of the tidal velocity variations (see text) and the straight line from the origin to the ellipse represents the phase. The left- and right-hand panels are for the near-surface and near-bottom current meters, respectively.

The remaining model-measurement comparisons are presented in Appendix D, Figure D-1 to Figure D-3 and Table D-3. At the Pelorus Entrance site there is a full set of 3 deployments × 2 levels. The model under-predicts the amplitude by 10–30% and the inclination by 1–10%. At the lower meter the model eccentricity is biased high and the phase is biased high by 20° for deployments 1 and 2 (but only 5° for deployment 3). At this site the instrument metadata indicates a water depth of 68 m, but the model depth interpolated to the same location is 57 m, which suggests significant discrepancies in the bathymetry. (We don't know which, if either, is correct.) Specifically, the model grid (Figure 2-1) indicates that the site is on the northern flank of a bank at about 50 m depth, with a channel 600 m to the north at a depth of 80–90 m and the contours and spot depths on LINZ chart NZ6152 confirm this. In this situation a small error in the instrument position or a small error in the model's bathymetry will affect the tidal currents significantly.

At the Pelorus Tawero site we have already seen the deployment 1 data above; the addition of data from the lower meter in deployment 3 does not change the picture significantly. At Beatrix West there are near-surface datasets from two deployments. The model does reasonably well, over-predicting the amplitude by 10% and 33% and the phase by 13°, but getting the eccentricity and the inclination about right.

S2 current ellipses have been calculated and are presented in tabular form (only) in Table D-4. Overall results are similar to those for the M2 constituent (e.g., amplitude is under-predicted at Pelorus Entrance and over-predicted at Pelorus Tawero) but with somewhat more scatter.

3.3.2 FRIA 2005 measurements

An M2 tidal velocity comparison has been carried out for the 9 suitable time series from the FRIA 2005 campaign. These measurements were made with profiling instruments (ADCPs) rather than current meters. The quantity being compared is the vertical average between 85% and 20% of the water depth. (The former limit is intended to reduce the impact of discrepancies in water depth

between the instrument metadata and the model; the latter is intended to avoid contamination of the ADCP data by surface reflections.) The results are presented in Figure D-4, Figure D-5 and Table D-5. The comparison shows a level of agreement similar to that found in Section 3.3.1. The model/measurement amplitude ratio varies from 0.89 to 1.33, with more over-predictions than under-predictions. The inclination difference is between −3.8° and +8.4°. The phase difference is between −9.0° and +19.1°, with the highest value being an outlier.

3.4 Model *vs* observations: subtidal velocity fluctuations

This section considers the accuracy of the model's representation of sub-tidal currents, i.e., fluctuations in the currents with frequencies below the tidal frequency. Sub-tidal currents were estimated by taking the same velocity data that were tidally analysed in Section 3.2.3, but instead applying a low-pass temporal filter, an operation known as detiding. The filter was the 24G113 filter from Thompson (1983), applied to hourly values; see Figure 1 of that article for its frequency response. The filter removes essentially all fluctuations with a period of less than 2 days from the data and yields rather smooth time series as a result. Note that a comparison between model and measurements, as here, should not be particularly sensitive to the filter characteristics as long as the same filter is applied to both.

3.4.1 Pelorus Sound 1994–1995 and 1997–1998 measurements

Figure 3-6 compares measured and modelled scatter plots of the sub-tidal velocities at the Pelorus Tawero upper current meter during deployment 1. (A tidal vector analysis of the same time series is shown above in Figure 3-5, left-hand panel.) The red ellipse in each scatter plot is a variance ellipse, a conventional representation of the magnitude and pattern of variability in velocity data. A variance ellipse can be characterised by its semi-major axis (in this context called a principal axis), eccentricity and inclination, like a tidal ellipse. However a variance ellipse does not have a phase (since it says nothing about the timing of the variability) and its eccentricity has no sign (since it says nothing about the rotation of velocity vectors). Also, the centres of the variance ellipses are offset from the origin by an amount representing the mean current over the period of the deployment.

Figure 3-6 indicates that both the measured data and the model have a mean of 0.08 m s^{-1} towards a direction of N to NNW. (The numeric values for the mean flow vector are listed in Table D-6.) The variance ellipses are of similar size—indicating broadly similar magnitudes of variability—but different shape, the measured one being elongated to NW-SE (probably because of a large excursion in the data points to the SE) and the modelled one being nearly circular.

To illustrate how the measured and modelled time series match up in time, a direction was first specified (subjectively) for each current meter site representing local channel direction. The directions were: 60° T for Pelorus Entrance; 320° T for Pelorus Tawero; and 50° T for Beatrix West. Figure 3-7 shows separate time series plots of the velocity components along the channel (towards 320° T) and across the channel (towards 230° T). Generally the model produces comparable fluctuations to the measured data in the along-channel and across-channel directions, with several peaks coinciding between model and data, but several not coinciding. Conspicuously, the large negative peak in the along-channel current meter time series (which appears to be real and is probably caused by a wind event) is not reproduced by the model.

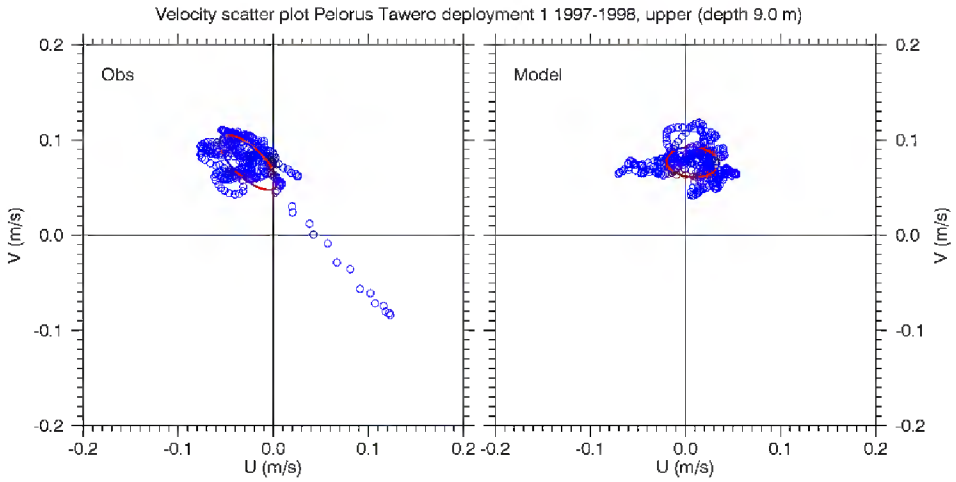

Figure 3-6: Sub-tidal velocity vector comparison (Pelorus Tawero deployment 1). Scatter plots of measured (left) and modelled (right) sub-tidal velocity at the Pelorus Tawero upper current meter during deployment 1. The axes correspond to the velocity components towards due east (*u*) and due north (*v*). The red lines are variance ellipses, representing the magnitude and orientation of the sub-tidal velocity variations (see text).

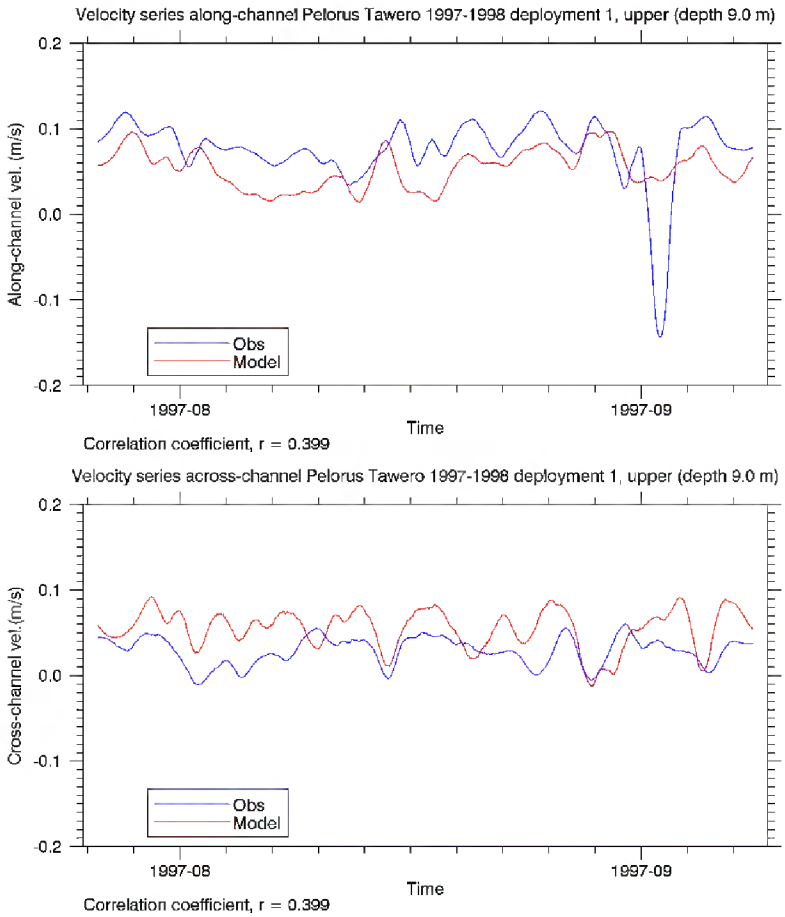

Figure 3-7: Sub-tidal along-channel and across-channel velocity comparisons (Pelorus Tawero deployment 1). Time series of measured (blue) and modelled (red) sub-tidal velocity components in the along-channel (towards 320° T, upper panel) and across-channel (towards 230° T, lower panel) directions at the Pelorus Tawero upper current meter during deployment 1.

The degree of closeness of the match between modelled and measured fluctuations is quantified on the graph with the temporal correlation coefficient, r, which is 0.399 for both directions. (The exact agreement here is a coincidence.) An r value of 0.399 implies an r^2 of 0.16, i.e., the model explains 16% of the variance in the measured data. This is a modest level of agreement, and may well arise by chance.

Appendix D includes a full set of scatter-plot comparisons (Figure D-6 to Figure D-9) along with tabulated parameters in Table D-6. The model does a reasonably good job of reproducing the observed estuarine circulation at Pelorus Entrance (upper flow to NE, lower flow to SW) and Pelorus Tawero (upper flow to N, lower flow to S or SE), although it consistently underestimates the magnitude of the lower, SW flow at Pelorus Entrance. At Beatrix West the mean flow is relatively weak in both model and measurements. Magnitudes of variability are broadly similar between model and measurements. Temporal correlations (Table D-6) are variable, but occasionally large, e.g., 0.8 at Pelorus Entrance deployment 3, lower meter.

3.5 Currents and volume fluxes

The capacity of the environment to dilute and disperse additional dissolved material—whether it be fish farm wastes or substances from other sources—is clearly central to the present project. Before moving to the biophysical model and its results, the remainder of this section presents some relevant analyses of the currents in the main channels of the Pelorus Sound system. A later section (Section 3.6) looks specifically at the transport of dissolved material through and out of the Sound.

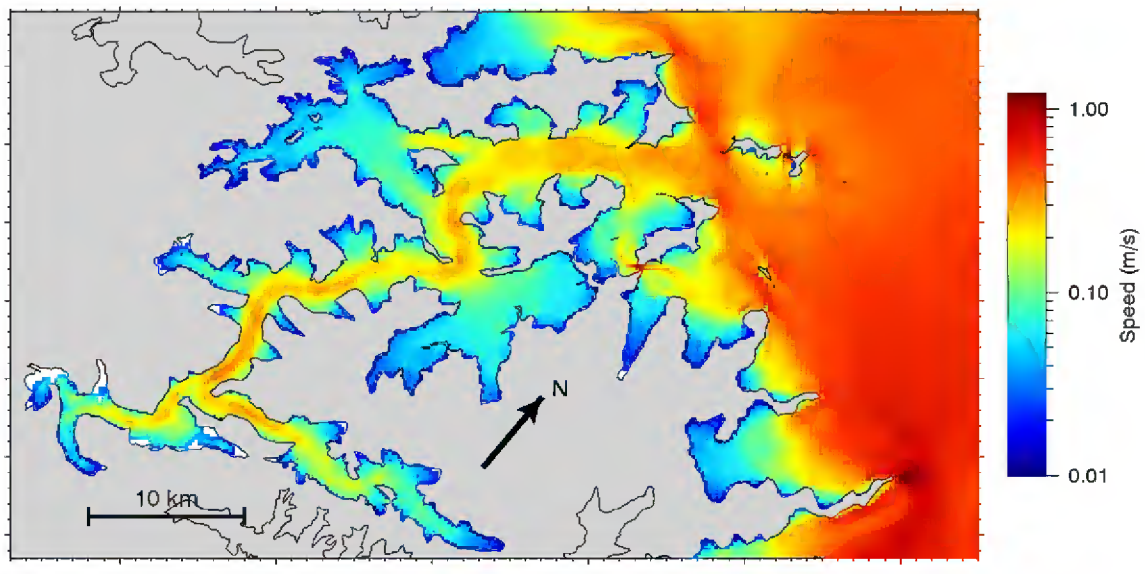

Figure 3-8: Model mean current speed. Mean current speed at 5 m depth, based on one year's hourly data from the 200 m model.

As an approximate indicator of near-field dispersal of nutrients or waste from a mussel farm or fish farm, Figure 3-8 shows the mean current speed at 5 m depth. The largest mean speeds (~1 m s^{-1}) are associated with the strong tidal currents in Cook Strait. There is a band of currents around 0.2–0.3 m s^{-1} through the main channel of Pelorus Sound and into Kenepuru Sound. This band is produced largely by the tides, but the estuarine flow of surface water out of the Sound also contributes.

The analyses in the remainder of this section deal with several sections across Pelorus Sound (Figure 3-9).

Figure 3-10 shows the volume flux through the section labelled Boat Rock Point in Waitata Reach, based on hourly model output. The flux through the Pelorus Sound entrance (Boat Rock Point) is typically 50–60,000 $m^3 s^{-1}$ at spring tide and 20–30,000 $m^3 s^{-1}$ at neap tide. Given that the volume of Pelorus Sound (in the region defined for the flushing calculations of Section 3) is around 10,300 × 10^6 m^3, the peak spring-tide volume flux through Waitata Reach would be large enough to replace all the water in the Sound in 2.0 days, if it were maintained for long enough. Of course, the peak tidal transports are not maintained for several days and fluctuating tidal fluxes are not efficient at flushing the Sound. The true flushing time for Pelorus Sound is on the order of 30–50 days (see Section 3.6 and Table 3-5).

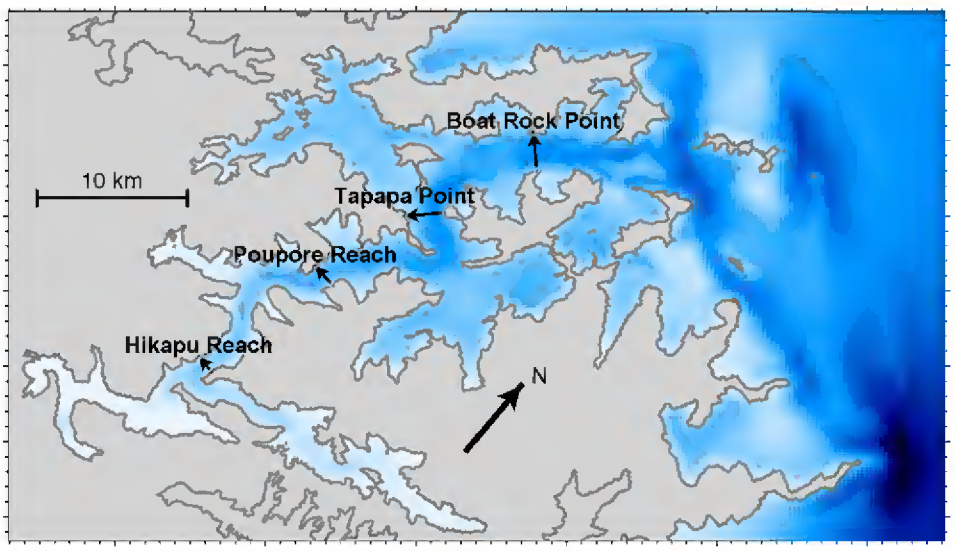

Figure 3-9: Location of sections used for velocity and volume-flux analyses. A map showing the model bathymetry and land mask (200 m grid), with labelled cross-sections.

The black lines in Figure 3-10 are based on a moving-window analysis for the semi-diurnal tide, with the central black line indicating the sub-tidal part of the volume flux. Because Pelorus Sound inside the Boat Rock Point section is a single bay with no other entrance, the sub-tidal flux is required by volume conservation considerations to be very small.

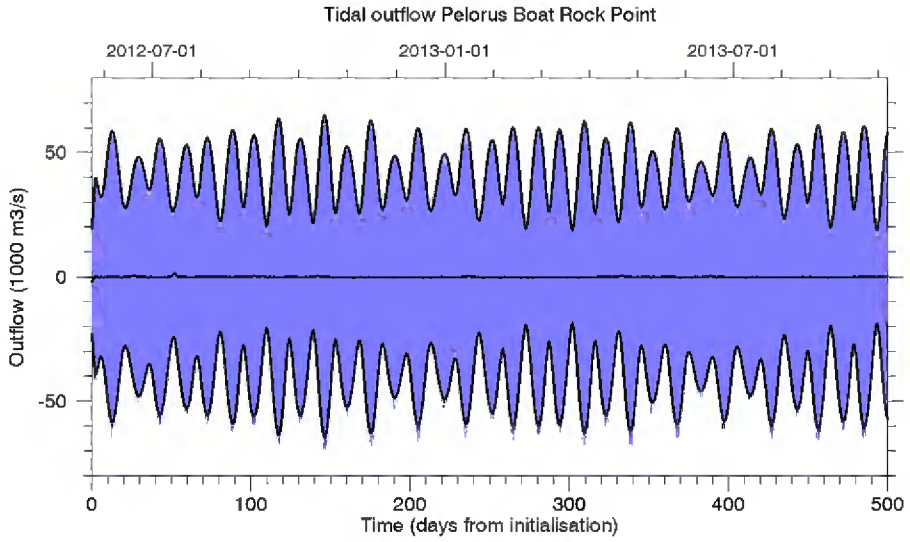

Figure 3-10: Tidal volume fluxes. Time series of volume flux for sections through the Boat Rock Point section across Waitata Reach. The light blue line represents the hourly volume flux (outflow positive) and the thick black lines represent the mean, plus & minus the amplitude of the semi-diurnal tidal flux as estimated by a moving-window tidal harmonic analysis (window width 3.5 days).

The information on volume fluxes presented in this section relates to the vertically-averaged currents. Another important aspect of the currents in Pelorus Sound is the vertical variation. Figure 3-11 shows plots of time-averaged velocity (positive outwards) on four sections across the main channel (see Figure 3-9 for the locations). In all cases there is a layer of outwards flow (~0.2 m s^{-1}) overlying a layer of inwards flow (~0.1–0.2 m s^{-1}). This is the vertical structure expected for an estuarine circulation, in which outward-moving brackish water overlies inward-moving saline water. At the outermost section across Waitata Reach (Boat Rock Point, Figure 3-11d), the interface between the inward and outward flows (the zero-velocity level) is 20 m below the surface and nearly horizontal. At the three sections further inside Pelorus Sound the outflow is displaced to one side or other of the section as the outflowing water snakes through the Sound. Animations (not shown) of these graphs with monthly average data indicate that this vertical structure is set up within 30 days or so of the beginning of the simulation and continues with relatively little change throughout.

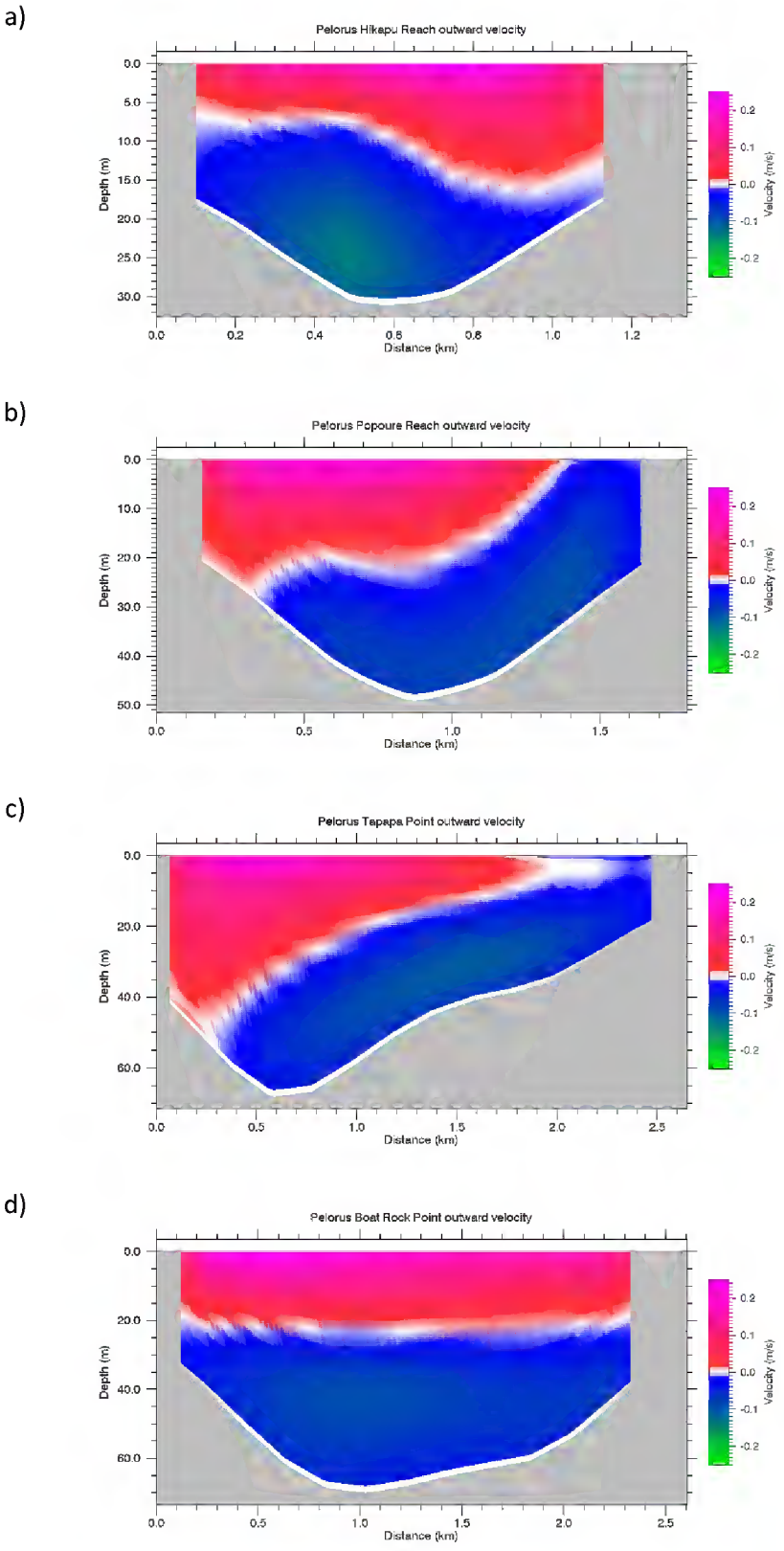

Figure 3-11: Velocity through cross-channel sections. One-year mean modelled velocity perpendicular to sections across Pelorus Sound as shown in Figure 3-9: a) Hikapu Reach; b) Popoure Reach; c) Tapapa Point (Tawhitinui Reach); d) Boat Rock Point (Waitata Reach). Velocity is positive outwards and the view is from the seaward side of the section, looking inwards.

The outwards velocity averaged over the top 20 m of the water column in the Boat Rock Point section is approximately 0.12 m s^{-1} and the width of the channel at this point is 2.2 km. This implies an outward flow in the estuarine circulation of 5300 m^3 s^{-1}, which is an order of magnitude less than the volume flux in the peak spring tidal flow. However the estuarine circulation is very persistent, whereas the tidal flow reverses regularly, so we can expect the estuarine circulation to have a large effect on the flushing of tracers from Pelorus Sound.

3.6 Flushing

A set of simulations was set up to investigate the dilutive capacity of Pelorus Sound for idealised sources of dissolved material. Passive tracers, or virtual dyes, were injected into a hydrodynamic model of the Sound at five sites (Figure 3-12) distributed through Pelorus Sound. There was a release 5 m below the surface at all sites and at the three outer sites (Popoure Reach, Beatrix Bay and Waitata Reach) there was a second release 5 m above the bottom, giving a total of 8 virtual dyes. The model was run at two resolutions, 400 m and 200 m, for the same 500-day period in 2012–2013 as the biogeochemical simulations.

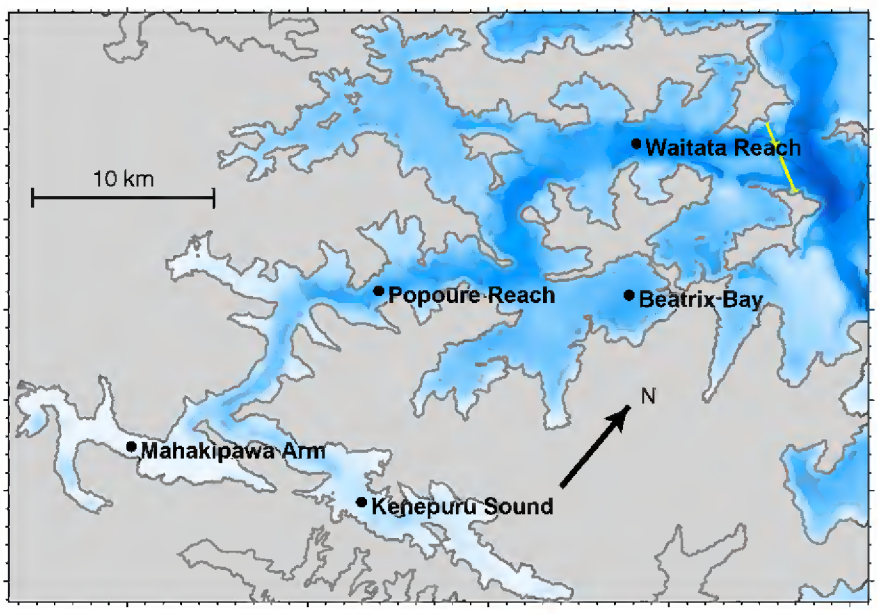

Figure 3-12: Location of passive tracer sources in the flushing simulations. A map showing the model bathymetry and land mask (200 m grid), with source locations for the flushing simulations (black circles and labels) and the boundaries for calculation of volume integrals (yellow lines across Pelorus Sound Entrance and Allen Strait).

The release rate Q of each dye was constant at a nominal 1 kg s^{-1}. The concentration C of the same dye at any location and time is measured in kg m^{-3} and should be proportional to Q (i.e., doubling the release rate should exactly double the concentration). Therefore the ratio between them, C/Q, can be called a normalised concentration: it has units of s m^{-3} and depends on the flow and the location of the source, but not on the release rate. It is convenient to represent this normalised concentration in terms of its reciprocal, called the dilution rate D, which has units of m^3 s^{-1} (Equation 3-1).

Equation 3-1: Definition of the instantaneous dilution rate

$$D = Q/C$$

A simple physical example illustrates the significance of the dilution rate. Consider a source of passive tracer, or dye, in a river. The dye plume will initially be narrow, but within a few hundred metres downstream (or kilometres for a large river, and assuming no major tributaries join in the meantime) the dye will be become uniformly mixed across the river, with a concentration equal to the release rate divided by the river's flow rate. In other words, the dilution rate at large distances downstream is equal to the river flow rate. Within the dye plume closer to the source, the dilution rate is lower (the normalised concentration is higher), because not all of the river flow has mixed into the plume. Note that for a medium-sized river like the Pelorus the mean flow rate is approximately 50 $m^3 s^{-1}$ and for the Clutha River, the largest river by volume in New Zealand, it is approximately 500 $m^3 s^{-1}$.

Within the context of coastal inlets, it is common to introduce the concept of flushing time (Zimmerman 1988; Monsen, Cloern et al. 2002). Here we specify the boundaries of the inlet (as in Figure 3-12), calculate the volume V (in m^3) and evaluate the mass (in kg) of the tracer inside this volume. If the release rate is kept steady for long enough, we expect the mass to reach a more or less steady equilibrium value M_e. The equilibrium flushing time T_e is then defined by Equation 3-2:

Equation 3-2: Definition of flushing time.

$$T_e = M_e/Q$$

This gives a result in seconds, which is normally converted to days for convenience.

From the equilibrium mass M_e and the volume V we can calculate the equilibrium mean concentration $C_e = M_e/V$ and from that we can calculate an equilibrium dilution rate D_e (Equation 3-3), which is representative of the inlet as a whole and applies when there is a balance, more or less, between input of the tracer from the source and flushing through the boundaries.

Equation 3-3: Definition of the equilibrium dilution rate

$$D_e = \frac{Q}{C_e} = \frac{V}{T_e}$$

Although discussions of dilution in coastal inlets often concentrate on the flushing time, the equilibrium dilution rate is often a more pertinent measure, and it involves the inlet volume as well as the flushing time.

The concept of a flushing time originally came from consideration of a well-mixed water body, in which "clean" water from outside enters and is immediately mixed throughout, with the inflow balanced by an equal outflow of mixed water. On a laboratory scale, such a system is called an exponential dilution flask (Ritter and Adams 1976). If a tracer is initially mixed through such a water body, then its concentration will fall away with time according to an exponential curve:

Equation 3-4: Exponential dilution in a *well-mixed* water body

$$C(t) = C(0)e^{-t/T_e}$$

Thus after time T_e the concentration will have dropped to $1/e$ (0.37) times its initial value and after time $2T_e$ it will have dropped to $1/e^2$ (0.14) times its initial value. However coastal inlets are not well mixed (as is quite clear from the figures below) and so do not follow this equation exactly. In other words, we cannot say from the flushing time alone how quickly a dissolved substance will be eliminated from an inlet. Nevertheless the flushing time is still a reasonably good guide to the speed

with which dissolved material is flushed from the system: after one flushing time *most but not all* of the material initially in an inlet will have been flushed out; and complete flushing will generally take several flushing times.

For an indication of how these concepts can be applied to Pelorus Sound, Figure 3-13 shows the time series of the total tracer mass within the Sound for the 8 tracers in the 200 m simulation. The lower horizontal axis in the plot shows time in days from the beginning of the simulation (and the tracer release); the upper horizontal axis shows the date. As explained in connection with Figure 3-12, there are 5 release sites, with near-surface sources only at two sites and both near-surface and near-bottom sources at the remaining three. The vertical axis is the normalised mass of tracer within the Sound, i.e., it is the mass M (in kg) divided by the release rate Q (in kg s^{-1}), yielding a value in seconds, which is converted to days for plotting.

If Pelorus Sound were a simple, well-mixed volume, then all eight lines in Figure 3-13 would follow the same path. They would have an initial linear portion with a slope of 1 (i.e., one day's accumulation of mass per one day of release) and would then tend exponentially towards a horizontal line, at a value equal to the flushing time of the inlet. The actual lines do exhibit some of this behaviour, but deviate in several important respects. For the (black) line representing the tracer released in Mahakipawa Arm, near Havelock, the line rises with a slope of 1 for about 30 days (i.e., no tracer leaves the Sound in this time) and then flattens out at a value of around 35 days. There is a peak with a value of around 50 days in late April 2014. The accumulation of tracers up to that peak coincides with a period of low Pelorus River flow and low freshwater in Pelorus Sound, noted in Section 3.1.1.

The tracer released in Kenepuru Sound (grey) behaves similarly to the Mahakipawa Arm tracer with somewhat larger values. The Popoure Reach (blue) and Beatrix Bay (red) tracers also follow a similar pattern; it is apparent for these release locations that the near-surface (thick line) tracers have lower flushing times than the near-bottom (thin line) tracers. Finally, for the tracer released in Waitata Reach (dark green), the flushing time for the near-surface tracer release is very low, at around 10 days, whereas the tracer released near the bottom has an flushing time comparable to the others at 25–30 days.

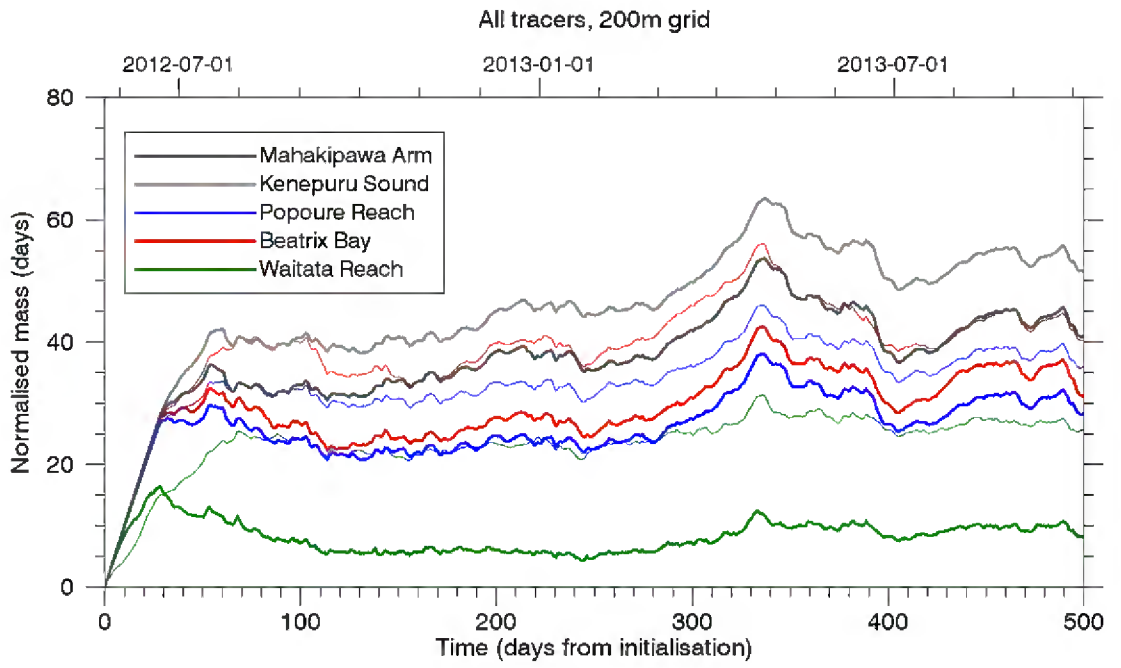

Figure 3-13: Accumulation of tracer from the 200 m flushing simulation. Normalised mass of tracer within Pelorus Sound versus time in the 200 m flushing simulation. See the figure legend for the relationship between the release location (Figure 3-12) and the line colour. For the three outer sites, the near-surface tracer is indicated by a thick line and the near-bottom tracer by a thin line of the same colour.

To estimate an annual-average flushing time and dilution rate for the tracers in Pelorus Sound, we have taken the average normalised mass for each tracer over the final 365 days of the simulation, i.e., from 16 October 2012 to 16 October 2013. The annual-average flushing time (Table 3-5) for the Mahakipawa Arm tracer is 41 days and for the Kenepuru Sound tracer it is 50 days. For the remaining tracers the flushing time is between 25 and 40 days, with the exception of the Waitata Reach near-surface tracer, which has a flushing time of only 7.8 days.

Table 3-5: Equilibrium flushing times and dilution rates for Pelorus Sound. Flushing times and dilution rates evaluated from the data in Figure 3-13 averaged over the last 365 days of the 200 m flushing simulation.

Site	Volume (10^6 m^3)	Flushing time T_e (days)	Dilution rate D_e (m^3 s^{-1})
Mahakipawa Arm	10338	40.9	2930
Kenepuru Sound		49.9	2400
Popoure Reach near-surface		27.5	4350
Popoure Reach near-bottom		35.8	3340
Beatrix Bay near-surface		31.2	3840
Beatrix Bay near-bottom		42.0	2850
Waitata Reach near-surface		7.8	15,370
Waitata Reach near-bottom		25.2	4750

Previous estimates of the Pelorus Sound flushing time were discussed by Broekhuizen and Hadfield (2012) with reference to the evidence of Mr Ben Knight to the EPA King Salmon Hearing (Knight 2012b)—see Table 2-1 of Broekhuizen and Hadfield (2012). Discounting an outlier estimate of 12.9

days, based on questionable tidal prism arguments, there are several estimates between 21 and 49 days, which agree with the current model-based estimates, given the large uncertainties associated with the definition and estimation of flushing time.

It is also useful to compare the flushing behaviour between the 200 m model (which is used for production simulations in this project) and the 400 m model (which is used for development). This comparison is shown for the near-surface sources in Figure 3-14. The differences are very small. We have not run a 100 m model for this comparison (as was done for Queen Charlotte Sound) because the 100 m model is very expensive to run and Pelorus Sound does not have a region like Tory Channel, which has a major influence on mixing and clearly requires fine spatial resolution to be represented accurately in the model. In other words, we do not expect tracer dispersion in Pelorus Sound to be as sensitive to model resolution as it is in Queen Charlotte Sound, and Figure 3-14 supports that expectation.

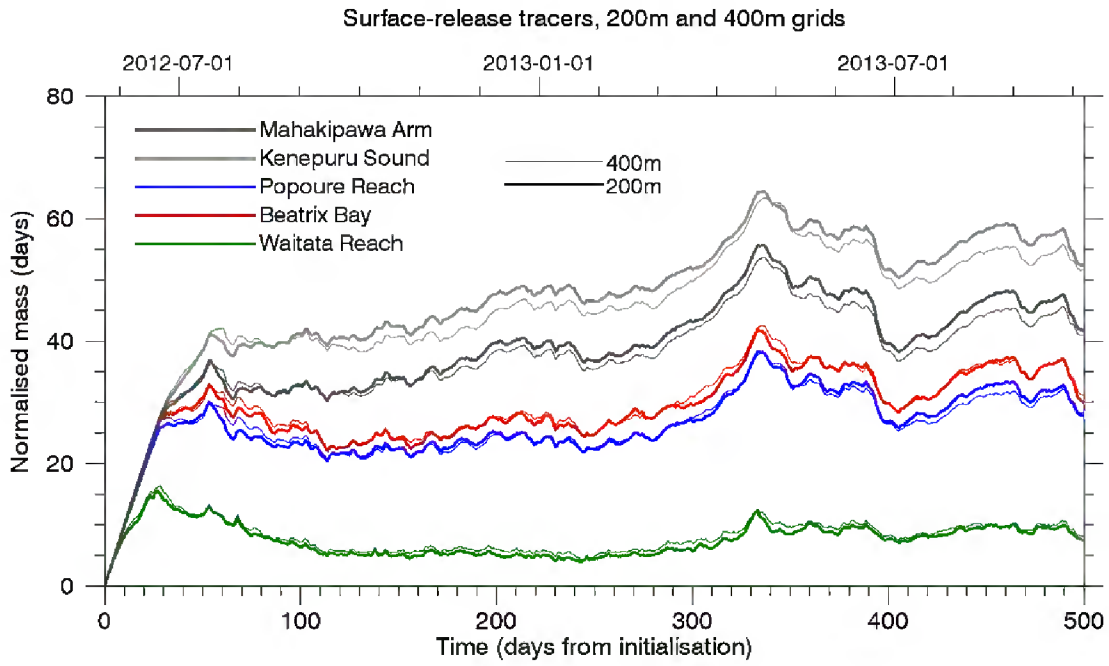

Figure 3-14: Effect of model resolution on flushing. Normalised mass of tracer within Pelorus Sound versus time for near-surface releases from the five sites, from the 400 m (thin) and 200 m (thick) models.

The next five figures (Figure 3-15 to Figure 3-19) show the mean surface concentration for each tracer, normalised and expressed as a dilution rate as described above. For the Mahakipawa Arm source (Figure 3-15) the dilution rate is ~300 $m^3 s^{-1}$ (dark red) and increases through ~1000 $m^3 s^{-1}$ (red–magenta) in Popoure Reach, ~2000 $m^3 s^{-1}$ (blue) in Tawhitinui Reach and ~4000 $m^3 s^{-1}$ (dark green) in Waitata Reach. Outside Pelorus Sound, the tracer plume bends north-westwards and leaves via the northwest boundary of the domain. For a source in Kenepuru Sound (Figure 3-16) the lowest dilution rates occur in Kenepuru Sound and not Mahakipawa Arm, but the pattern is otherwise identical.

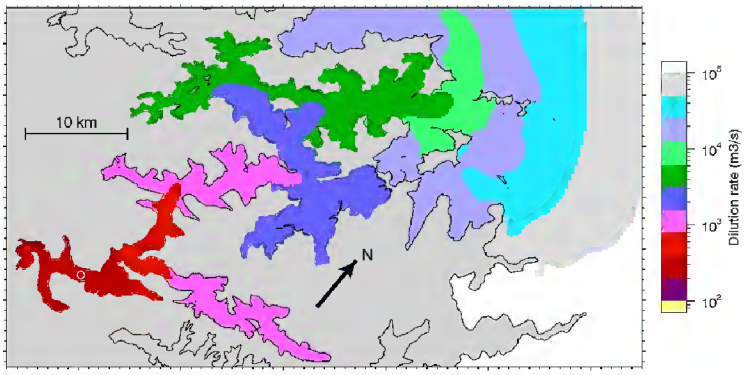

Figure 3-15: Equilibrium concentration for Mahakipawa Arm tracer. Surface concentration of tracer from the Mahakipawa Arm (near-surface) source in the 200 m model, averaged over the final 365 days and expressed as a dilution rate. The source location is indicated by a white circle.

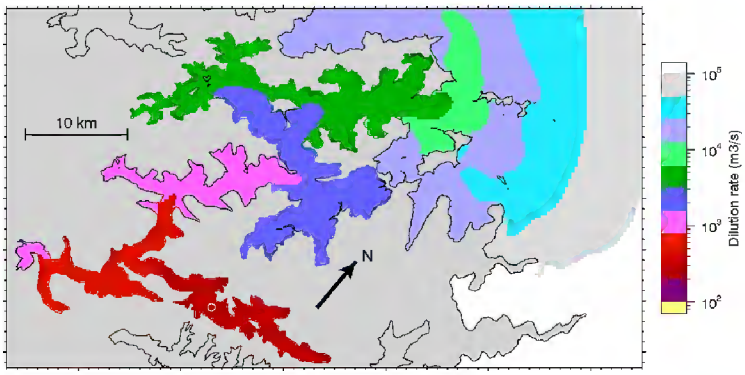

Figure 3-16: Equilibrium concentration for Kenepuru Sound tracer. As Figure 3-15 but for the tracer released in Kenepuru Sound.

For the Popoure Reach tracers the near-surface source (Figure 3-17a) produces a plume with dilution rate ~1000 $m^3 s^{-1}$ (magenta) extending seaward, whereas the near-bottom source (Figure 3-17b) produces a much more extensive area with similar dilution rates throughout Popoure Reach and inner Pelorus Sound. This is a result of the pronounced estuarine circulation in Pelorus Sound, taking surface water towards the sea, to be replaced by inward moving bottom water. In outer Pelorus Sound and Cook Strait the dilution rate pattern is indistinguishable for the near-surface and near-bottom sources, as for the Mahakipawa Arm and Kenepuru Sound tracers. In other words, however tracer material is injected into the inner part of Pelorus Sound, it ultimately moves out through the surface waters of outer Pelorus Sound in the same way.

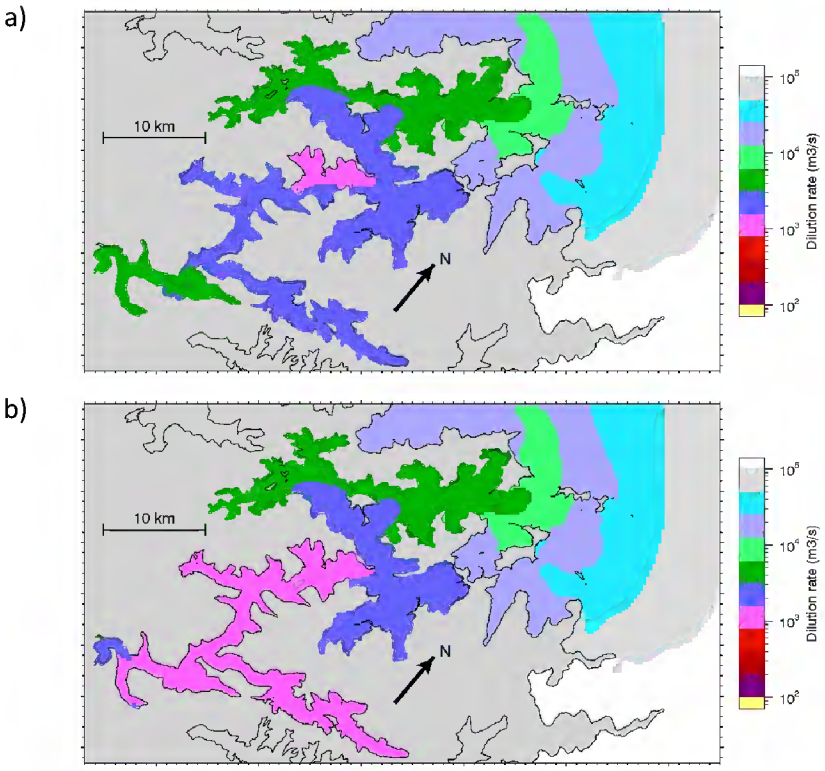

Figure 3-17: Equilibrium concentration for Popoure Reach tracers. Surface concentration of tracers from Popoure Reach (a) near-surface and (b) near-bottom tracer sources in the 200 m model, averaged over the final 365 days and expressed as a dilution rate. The source location is indicated by a white circle.

The Beatrix Bay tracers (Figure 3-18) produce similar patterns to the preceding ones but with the highest concentrations (lowest dilution rates) in Beatrix Bay.

For the tracers released in Waitata Reach, there is a very marked difference between the near-surface and near-bottom sources. The near-surface source (Figure 3-19a) produces a plume (~4000 $m^3 s^{-1}$, dark green) that extends towards Cook Strait and also into Port Ligar, with relatively low concentrations (high dilution rates) everywhere else. The near-bottom source (Figure 3-19b) fills Pelorus Sound with tracer at ~4000 $m^3 s^{-1}$. As with the Popoure Reach tracers, this indicates the effect of the estuarine circulation, which takes near-surface water out of the Sound, but takes near-bottom water into the Sound.

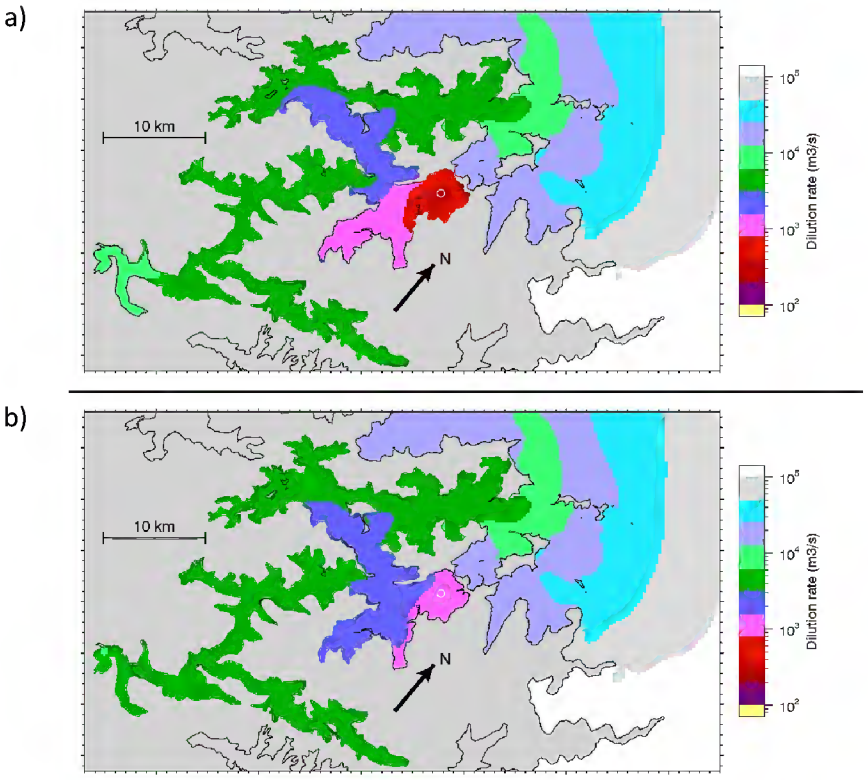

Figure 3-18: Equilibrium concentration for Beatrix Bay tracers. As Figure 3-17 but for tracers released in Beatrix Bay.

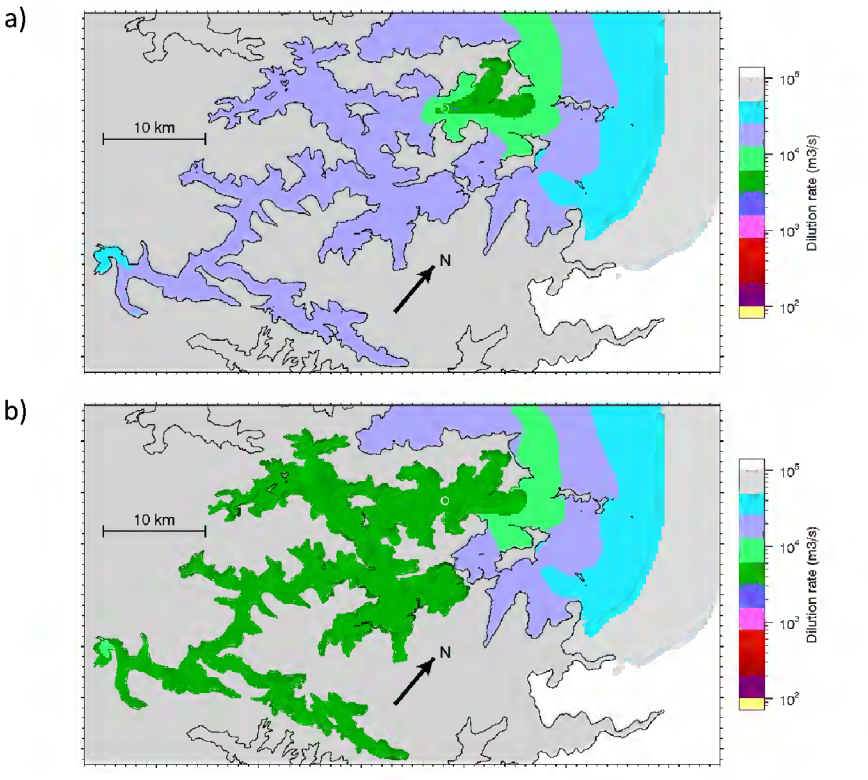

Figure 3-19: Equilibrium concentration for Waitata Reach tracers. As Figure 3-17 but for tracers released in Waitata Reach.

3.7 Hydrodynamic model summary

Grid resolutions from 100 m to 400 m were tested. The 200 m grid reproduces the essential aspects of the hydrodynamics of Pelorus Sound with acceptable accuracy. Comparisons of flushing times derived from the 200 m and 400 m grids show little difference (Section 3.6), which suggests that even the coarser 400 m grid captures the essence of the hydrodynamic behaviour of the Pelorus Sound. The finest grid, 100 m, is too computationally expensive for long simulations (Table 2-1), and in this study is used only for shorter simulations (30 days) for deposition modelling (Section 7).

Comparisons of modelled water levels and currents showed reasonably good agreement with historical field data. For tidal variation in sea level, the model reproduces the observed amplitude for some datasets (the Pelorus Sound 1994–1995 and 1997–1998 measurements) but overestimates it by ~10% for others (the FRIA 2005 ADCP pressure data and the Havelock tide gauge). This indicates that the volume of water moving in and out on each tide is approximately correct, perhaps somewhat overestimated. With regard to tidal currents, the model tends to over predict at some sites, but under predict at others. We note that exact matches between current meter data and model predictions are unlikely due to a number of reasons. In confined waters, small differences in location can result in quite different currents due to the effects of bathymetry (see section 3.3.1). The modelled velocity data are also interpolated from the 200 m model grid onto the location of the current meter, which leads to a degree of smoothing. Comparison of sub-tidal currents (driven by wind and estuarine circulation) from the model and field data show that the model is reproducing the mean currents well, and that the variability in sub-tidal currents is of the correct magnitude, although the timing of fluctuation in the sub-tidal currents do not always agree.

The model's salinity and temperature agree well with observations. The model does tend to under-predict summer temperatures by 1–1.5 °C, however the difference in water temperature between surface and near bed remains about right. This may indicate a deficiency in the model's surface heat flux formulation, which was derived from a global, coarse resolution atmospheric model, or maybe excessive tidal mixing in Cook Strait. However, the model allows stratification to develop to approximately the right extent in Pelorus Sound suggesting that vertical mixing processes are resolved sufficiently well.

The model (and field data) show that the Pelorus Sound is characterised by a strong estuarine circulation with an outward flowing surface layer of brackish water overlying an inward-moving saline water layer. The mean volume flux due to the estuarine circulation (the outward flux in the surface layer) is around 5000 $m^3 s^{-1}$. This compares to peak tidal flows through the Waitata reach of between 20–30,000 $m^3 s^{-1}$ at neap tide and 50–60,000 $m^3 s^{-11}$ at spring tide. However the peak tidal flows are sustained for short periods, and reverse regularly, so the estuarine circulation has a very strong effect on the flushing of Pelorus Sound.

Tracer releases to investigate flushing in different parts of Pelorus Sound indicate that the flushing time is of the order of 30–50 days. However there is considerable variability depending on where the tracer is released into the Sound. Substances released near the surface, particularly in the Waitata and Popoure Reaches, are transported outward by the estuarine circulation, leaving the Sound relatively quickly. Substances released nearer the bed are carried inward by the inward moving saline water, before mixing into the surface layer. Thus substances released near the bed will remain in the Sound for longer.

Based on the above information about flows and flushing, we suggest the following idealised picture of transport through Pelorus Sound:

- Transport in Pelorus Sound is driven primarily by estuarine circulation. The dominant supply of freshwater is from the Pelorus River.
- Low river flows lead to a weaker estuarine circulation and therefore longer residence times within the Pelorus Sound.
- Surface salinities decrease (the water becomes fresher) as one moves from outer to inner Pelorus Sound, but the influence of surface freshening events (from increased river flow) occurs through the Sound.
- Stratification in Pelorus Sound is generally driven by salinity. In summer time, when river flows are generally low, warmer surface temperatures can strengthen stratification. In winter, surface salinities can be sufficiently low to allow the surface water to cool to temperature below that of deeper waters.

Possible improvements to the hydrodynamic model could include:

- Generating surface wind fields to drive the model with a higher-resolution atmospheric model.
- Improving the surface-heat flux by using a higher resolution data set.
- Examining and correcting the reasons for suspected excessive tidal mixing in Cook Strait.
- Improved tidal boundary data from a tidal model of Cook Strait rather than the larger-scale NIWA tidal model.

4 Biophysical model: Methods

As described in the introduction, the biophysical model is comprised of several component 'sub-models':

- The ROMS hydrodynamic model.
- A so-called nutrient/phytoplankton/zooplankton/detritus (NPZD) model. The particular model that we have adopted includes a simple description of the benthic mineralization of deposited detritus. For that reason, we will refer to it as the *biogeochemical model.*
- A mussel farm model which focuses upon feeding, respiration and excretion.
- A fish farm model which also focuses upon feeding, respiration and excretion.

The hydrodynamic model component has been described in the previous sections. In this section, we describe the biogeochemical, mussel farm and fish farm model components.

4.1 Model description

The ROMS code includes several alternative NPZD sub-models to describe water-column nutrient-plankton dynamics. We elected to base our biological modelling upon the Fennel sub-model (Fennel, Wilkin et al. 2006; Fennel, Wilkin et al. 2008; Fennel, Hetland et al. 2011). We made this choice for the following reasons. Firstly, the Fennel model is one of the simpler biogeochemical models that ships with ROMS. The more complex alternatives will impose an unacceptably high additional computational burden and, in some cases, demand data that are not available for the Pelorus system. Secondly, the available field data would be insufficient to calibrate or validate these more complex models. Thirdly, unlike some of the other sub-models, the Fennel model includes a simple description of benthic mineralization of deposited detritus. Finally, we know that there is a more sophisticated benthic diagenesis (nutrient recycling) sub-model being developed by a group in the USA to accompany the Fennel model. We hope to be able to incorporate that model in the future. Since the Fennel model includes benthic mineralization, we will refer to it as a biogeochemical model.

Regardless of which biogeochemical sub-model is selected, it runs 'in-line' with the ROMS hydrodynamic simulation. That is, biogeochemical and hydrodynamic equations are solved simultaneously within the same code-base. The 'in-line' approach differs from the 'off-line' approach. In the latter, the hydrodynamic model is solved first, and the resulting time-series of water-temperature, salinity, and currents etc., are saved to file with (for example) 15 minute temporal resolution. The 'in-line' approach has two great advantages: (a) there is no need to save enormous (100s of GB) files of hydrodynamic results, and (b) the biogeochemical model is able to utilize the fundamental temporal resolution available from the hydrodynamic engine (approximately 12 seconds in our simulations using the 200 m grid).

The Fennel model assumes that nitrogen is the (only) element that might limit biological activity. Field data confirm that nitrogen is the limiting element in the Marlborough Sounds[16]. The standard

[16] The term nitrogen limitation implies that concentrations of inorganic nitrogen (primarily NO_3 and NH_4^+) are sufficiently low to constrain realizable individual phytoplankton cellular growth rates more than light intensity (or any other nutrient) does. Theoretically, it is energetically less expensive to synthesize new nitrogenous tissues using ammonium rather than nitrate. Thus, it is common to assume that,

Fennel model that distributes with ROMS has seven obligate state variables (NO_3, NH_4^+, small and large (slow- and fast-sinking) detritus, phytoplankton nitrogen, phytoplankton chlorophyll and zooplankton nitrogen) and two optional ones (concentrations of dissolved oxygen and dissolved inorganic carbon). We have added an eighth state-variable (representing very-fast sinking detrital nitrogen stemming from mussel and fish farms – specifically mussel pseudo-faeces, and faeces of mussels and fish)[17]. This material is generated only by mussels and fish. In comparison with the other two detrital classes, it sinks very rapidly (5 cm s^{-1}, cf. 0–3 m d^{-1} for the other two detrital classes). It mineralizes as readily as the other detrital classes. With the exceptions of the two optional state variables (O_2, CO_2) and chlorophyll, all the variables are measured in units of nitrogen concentration (mmol N m^{-3}).

The full Fennel model is described in Appendix A. In brief, phytoplankton consume NH_4^+ and/or NO_3 as they grow. Zooplankton consume phytoplankton (and associated chlorophyll). In addition, phytoplankton can die of background processes such as entrapment into small detritus. Large and small organic detritus stems from zooplankton faeces as well as dying phytoplankton and zooplankton. NH_4^+ stems from break-down of the detrital material. In turn, NH_4^+ is oxidized into NO_3. The chlorophyll to phytoplankton nitrogen ratio evolves in response to the ratio of instantaneous photosynthetic rate relative to the local light-dependent maximum rate. The ratio tends to decline under nutrient-limiting conditions and increase under light-limiting ones. All else being equal, a high chlorophyll content permits greater phytoplankton growth than a low one.

In addition to the explicit coefficients of the Fennel model (Table 10-1), there are some features that are turned on/off by means of pre-processor switches when the model is run. Two of these switches influence the fate of particulate material which settles to the seabed. In our 'standard' runs we set them such that 25% of the nitrogenous particulate material which settles on the sea-floor is immediately returned to the water-column as ammonium. The remaining 75% is assumed to be permanently lost through denitrification (Fennel, Wilkin et al. 2006)[18]. In our *worst case* (*no denitrification*) simulations, we set these switches such that all of the sedimenting particulate organic nitrogen would be returned to the bottom-most layer of the water-column as ammonium.

The Fennel model that ships with ROMS does not include mussel farms or fish-farms. NIWA has implemented appropriate mussel farm and fish-farm codes with funding from the Ministry of Business and Innovation and a predecessor body (Foundation for Research in Science and Technology).

The mussel code implements relevant parts of the mussel growth models described in Ren and Ross (2005) and Ren et al. (2010) (with some typographical errors in those papers amended in our code implementation). In particular, the rates of mussel induced particle capture, faecal (and pseudo-faecal) production, NH_4^+ excretion, O_2 uptake and CO_2 production are all incorporated. Mussels are

given the choice, phytoplankton will consume NH_4^+ in preference to NO_3. When the supply of ammonium is inadequate to meet growth demands, nitrate is used to meet the deficit. Whilst this certainly implies additional energy expenditure there is no reduction of realized phytoplankton growth rates in nitrogen-limited waters. This is because, by definition, the realized phytoplankton growth rate is nitrogen limited – they phytoplankton can accrue more than sufficient (non-nitrogenous) carbohydrates (by photosynthesis) to meet even the elevated energetic demands.

[17] In our earlier (Queen Charlotte Sound and Tory Channel) mode, faeces and pseudo-faeces passed into the already existing 'large-detritus' class. Addition of an explicit detrital class for (pseudo-)faecal material was a closing recommendation in Hadfield, Broekhuizen & Plew (2014). The enhancement has been made using NIWA CORE funding from the central Government (project ACEE1502).

[18] The alternative choices were: (a) that the sedimenting material be permanently lost from the system (full denitrification of sedimenting material); or (b) that 100% of the sedimenting particulate nitrogen be instantly returned to the bottom-most layer of the water column as ammonium (no denitrification of sedimenting material).

assumed to have the ability to capture all of the particulate materials in the Fennel model (phytoplankton, zooplankton, small and large detritus). The faeces and pseudo-faeces that they produce pass into a detrital pool that is dedicated to large, very fast-sinking (pseudo-)faecal material[19]. The mussel code does not include a dynamic description of mussel growth (biovolume and weight). Instead, the user supplies a time-series of mussel concentration (mussel m^{-3}) for each of several mussel size-classes. A more detailed description of the ingestion/faeces/excretion components of the mussel model is provided in Appendix B whilst section 4.2 describes the manner in which the spatial distribution of the mussel crop was incorporated into the model.

The fish-farm sub-model works in a manner akin to that of the mussel farm. A detailed description of the uptake and release terms stemming from this model is provided in Appendix C. Section 4.3 describes the manner in which the spatial distribution of the fish crops were mapped onto the model grid.

The fish energetics model is based upon that of Stigebrandt (1999). The original Stigebrandt model is designed to conserve energy, carbon, nitrogen and oxygen. It contains descriptions of a maximal size-specific ingestion rate (J $fish^{-1}$ d^{-1}) from which ingestion (as g food $fish^{-1}$ d^{-1}) can be calculated using a knowledge of the food composition, faecal production, ammonium production, CO_2 production and O_2 demand. As with the mussel model, we have not implemented the fish-growth component of the model. Instead, the user supplies time-series of fish abundance (fish m^{-3}) for each of several fish size-classes. The user also specifies corresponding time-series of fish feed input rates ((kg feed/kg fish live weight) d^{-1}) for each fish size-class. If the implied feed input rate (kg feed m^{-3} d^{-1}) exceeds the implied maximal feed consumption rate, the excess food remains uneaten and its nitrogen content passes into the very fast sinking detritus pool (as do fish faeces).

In the real world, mussels will put on weight over the course of a growth cycle. To achieve that, they must consume more nitrogen than they produce. Thus, in a time-average sense, they are a net sink for environmental nitrogen (though they may be temporary net sources during times when they are receiving insufficient food to offset their respiratory demands). Fish also put on weight over the course of a growth cycle, but they derive their nutrition from an exogenous source (fish feed) rather than from material that is already 'natively' present in the water-column. Any nitrogen that they lose to the environment (faeces and ammonium excretion) augments what is already in the environment. In contrast to mussel farms, fish-farms are a net source for environmental nitrogen.

4.2 Representing the spatial distribution of the mussel crop

Rather than representing each individual mussel line (or mussel farm) as a discrete entity within ROMS, we chose to represent the population of farmed mussels using the grid-structure (spatial resolution) adopted for the ROMS hydrodynamic and water-quality models.

Approximate concentrations of farmed mussels (mussel m^{-3}) within each control-volume of the model domain were derived by adopting several assumptions.

- Since mussel feeding rates etc., are non-linear functions of individual size, we need to prescribe a realistic size-distribution for each population. We know of no data concerning seasonal changes in mussel size structure in the farms within Marlborough Sounds. Thus, we assumed that the size structure remains constant throughout the year, and that all farms share the same size structure. We used four size-classes:

[19] The state-variable is named *XLdetritus* in many of the figures presented later in this report.

32 mm, 47 mm, 72 mm and 100 mm. When required, these lengths were converted to weights using relationships from previous studies (Hickman 1979; Hickman and Illingworth 1980; Orban, Di Lena et al. 2002).

- We assumed that 20% of the length of each dropper was devoid of mussels and that 20% of the length was occupied by each of the four size-classes.
- On the occupied sections of dropper, we assumed that the respective mussel densities for the four size-classes were 170, 150, 130 and 110 mussels per metre length of dropper.
- We assumed that each long line supports 3750 m of dropper per 110 m of backbone (www.NZMFA.co.nz/faq.asp).
- Droppers were assumed to extend from the sea-surface to the lesser of 3 m above the seabed or 15 m below the sea-surface. Time-varying sea-levels imply that the droppers may move into and out of layers of the spatial grid. Almost certainly, the depth to which droppers extend will not coincide with the interface between two model layers. Usually, one intermediate layer (with respect to ordering between sea-surface and sea-floor) will be only partially occupied by the droppers. Thus, the concentration of mussels within each control-volume was recalculated at every time-step of the simulation.
- The mussel farm scenarios were derived from two shape files provided by Marlborough District Council. The first, named "Marine_Farm_Data_13th-Feb2014.shp", contained a series of polygons representing the boundaries of licensed shellfish and fish farms. The second, named "Export_Output_2.shp" contained a series of lines representing mussel farm backbones found in aerial surveys in 2012. All polygons in the first shape file with an approval status of "Active" and a farm type of "Shellfish" were considered to be mussel farms (except that 10 polygons were found to be duplicates and were omitted). We overlaid maps of mussel farms and backbones and assigned those mussel farms that were largely populated by backbones to the *existing farms* category; the remainder were assigned to the *approved farms* category.

Collectively, the above assumptions imply that the size-class specific densities per unit area of mussels within each licenced farming block are 38, 34, 29 and 25 mussel m^{-2} for the 32, 47, 72 and 100 mm size classes respectively. Thus the density totalled over all size classes is 126 mussel m^{-2}.

Figure 4-1 shows the outlines of the *existing farms* and Figure 4-2 the *approved farms*. Black lines in the figures indicate the "Pelorus Sound" region considered for flushing calculations (Section 3.6, Figure 3-12). This region, which includes Forsyth Bay, has an area of 382 km^2. For the *existing farms* scenario, there are 722 mussel farms within Pelorus Sound, with a total area of 24.44 km^2. The *existing plus approved farms* scenario adds another 22 farms with an area of 0.69 km^2, or 2.8% of the *existing farms* area.

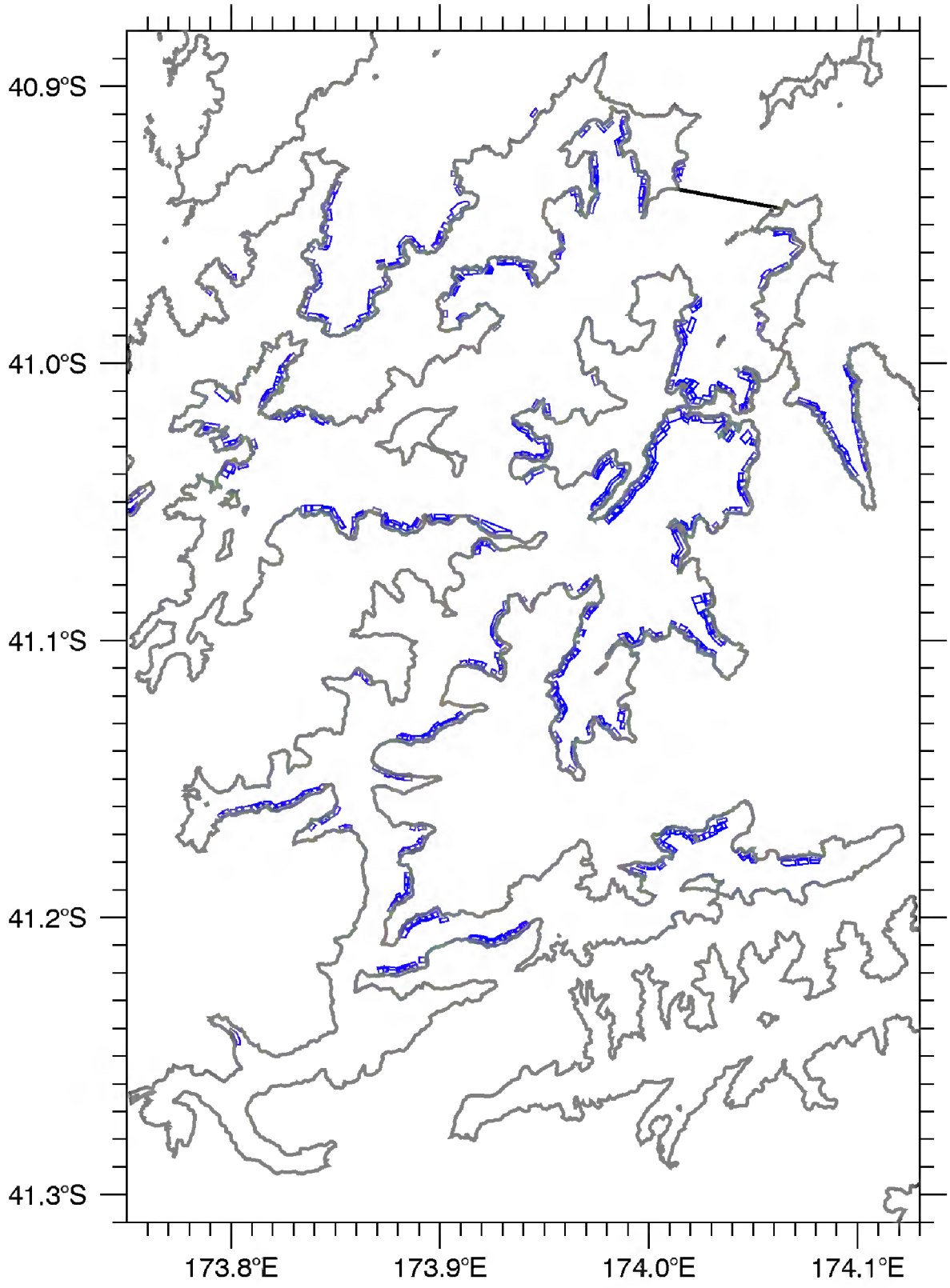

Figure 4-1: Pelorus Sound mussel farm outlines (*existing*). Black lines at the entrance to Pelorus Sound and (barely visible) across Allen Strait indicate the region considered for flushing calculations.

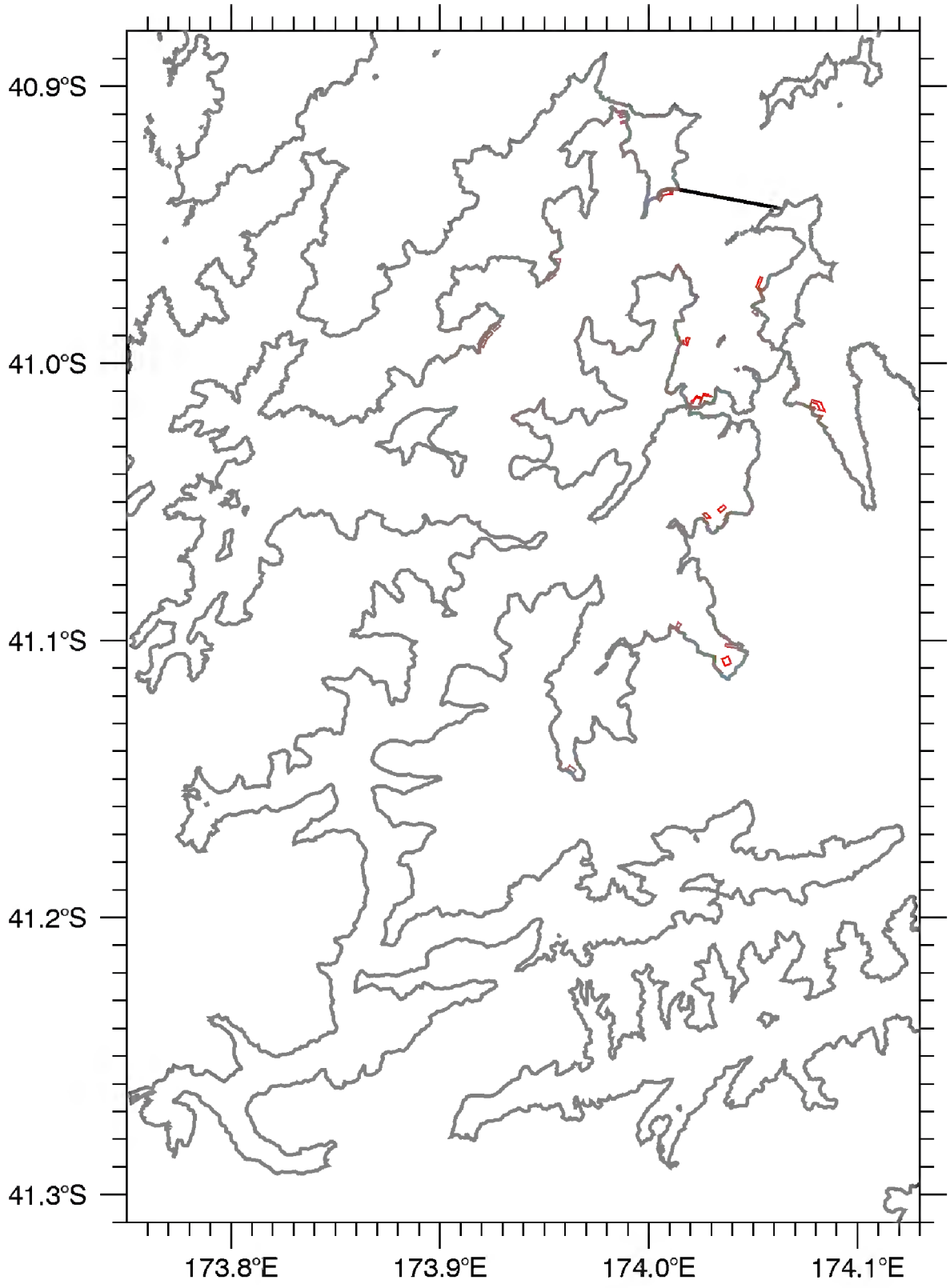

Figure 4-2: Pelorus Sound mussel farm outlines (*approved*).

4.3 Representing the spatial distribution of fish farms

As with the mussel-farms, individual fish-farms were not explicitly represented as discrete entities. Instead, we calculated time-series of farmed-fish concentrations (fish m^{-3}) for each control volume of the model domain[20]. We did so in a manner similar to that for mussels.

- Marlborough District Council provided us with shape files for each farm. In most cases, these included information on the perimeters of the pens. Where that information was not available, we approached NZKS Ltd. They made their engineering drawings available to us and we digitized the locations of the pen perimeters from these.
- We assumed that cages extend to 20 m below the sea-surface.
- We overlaid the farm perimeters upon the model grid to calculate the fractional area of farm within each water-column of the model grid.
- We assumed that the fish crop associated with each farm was evenly distributed throughout the implied farm-volume (and that feed inputs were evenly distributed across its horizontal surface-area).
- For their existing farms, NZKS also provided us with schedules (time-series) of cohort-and-farm-specific: fish abundance, mean live weight and feed-input rates. We used this information to synthesize farm-specific time-series of: (a) fish abundance (per fish farm) within each of several size-classes, (b) feed input rates (kg feed per kg fish per day by fish size-class). This enabled us to calculate high temporal resolution time-series of population size-structure characteristics and feed input rates that are consistent with the prescribed annual-scale consent conditions and plausible farm management practices.
- For the purposes of this exercise, we partitioned each farm's crop into 14 size classes (individual fish live weight, g): 0–100, 100–200, 200–300, 300–400, 400–500, 500–1000, 1000–1500, 1500–2000, 2000–2500, 2500–3000, 3000–3500, 3500–4000, 4000–4500, 4500–5000.
- We have no detailed information on the proposed stocking- and feeding practices at the new fish farming sites. We calculated hypothetical time-series of feed input, fish density, etc., by: (i) assuming that the farms would operate at their maximum (rather than initial) annual feed input rates; and (ii) rescaling the schedules that NZKS provided for their Te Pangu farm (in Tory Channel) such that the realized annual feed input rates were consistent with the prescribed maximum annual feed input rates[21].
- For the purposes of modelling, we assumed that each fish farm was entirely enclosed within a single water-column of the model and calculated fish densities accordingly (Figure 4-3). We recalculated the total concentration of fish of each size-class within each control-volume at every time-step (using linear interpolation between the monthly numbers-at-size schedules which we derived from the information provided

[20] Given the scarcity of fish-farms within Marlborough Sounds relative to the spatial resolution of the model grid, most control-volumes contain no farmed-fish, and those which do contain farmed fish contain fish from only one farm

[21] The new farm in Beatrix Bay is not owned by NZKS and will farm Hapuku rather than salmon. Nonetheless, in the absence of any specific information on Hapuku feed-schedules, we applied the rescaled Te Pangu schedule.

to us by NZKS Ltd.). We also calculated control-volume-specific feed input rates at every time-step.

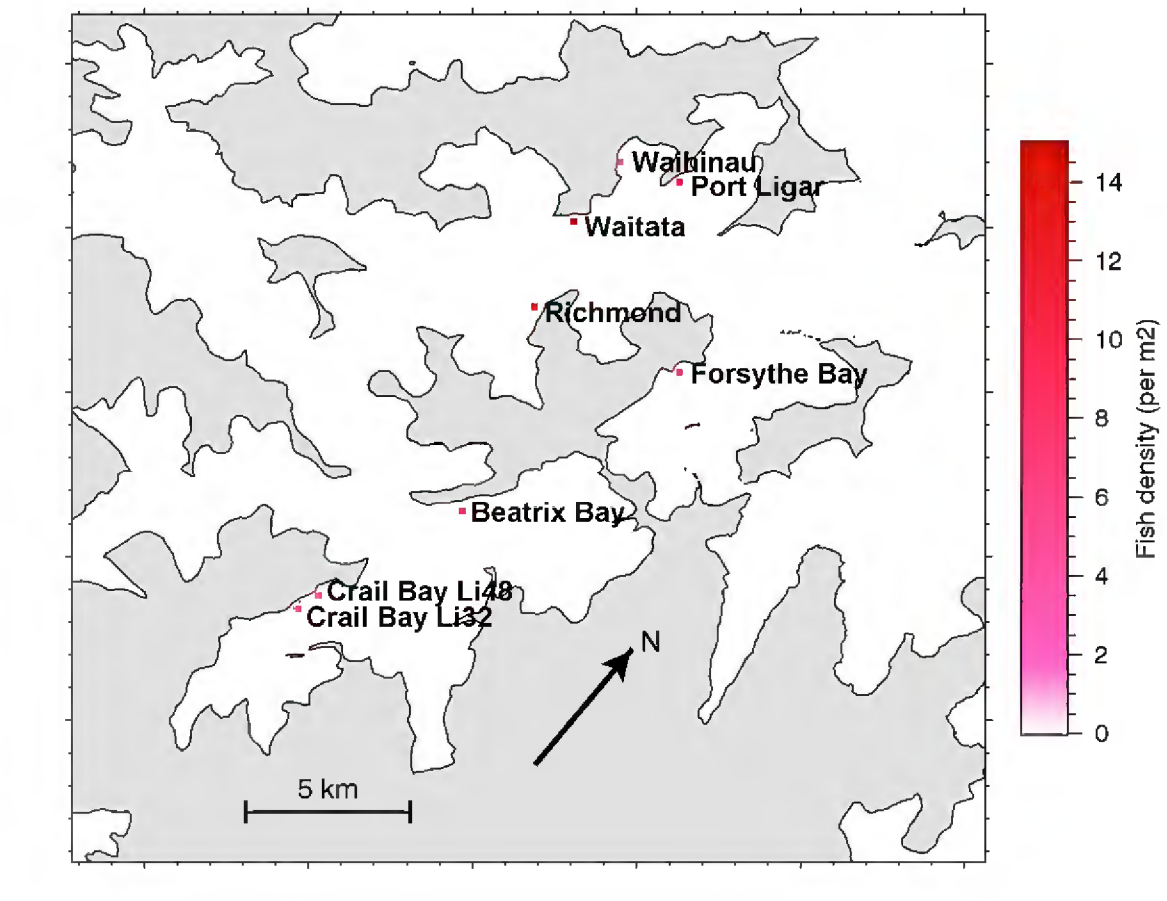

Figure 4-3: Map showing the locations of the eight fish farms. The colour indicates the fish density (fish m^{-2} summed over all of the size classes) averaged over the 200 × 200 m grid cell around each fish farm during the final 12 months of the simulation. The farms at Crail Bay, Waihinau and Forsythe are the 'existing farms'. Those at Beatrix Bay, Richmond, Waitata and Port Ligar are the 'new' farms. The Beatrix Bay farm is licensed for hapuku rather than salmon but our simulations assume that hapuku feed schedules and physiology will be similar to those of salmon. The farms in Crail Bay are occupied only intermittently, but were assumed to be fully utilized in this modelling.

4.4 Water quality data

Marlborough District Council collect water samples at seven stations (PLS-1 to PLS-7, Figure 4-4). Sampling began in July 2012 and has continued at approximately monthly intervals since then. At each station a near-bed sample is collected from approximately 1 m above the seabed using a bottle sampling device. Up until June 2014 (incl.), the same device was also used to collect a near-surface (approx. 1 m below sea-surface) sample. From July 2014 onward, the near-surface samples have been collected using a hose-sampler that extends from the sea-surface to 12 m below the surface.

Each water-sample was held within an ice-packed chilly-bin and shipped to the NIWA chemistry laboratory in Hamilton within 24 hours of collection. Upon arrival at the laboratory, a small volume of each sample was preserved with Lugols (for subsequent plankton counts). The remainder was frozen until needed for nutrient analysis etc., Table 4-1 provides details of the water-quality variables that

are measured. Quantities measured include: nitrate, ammoniacal nitrogen, dissolved reactive phosphorus, total dissolved nitrogen, total dissolved phosphorus, chlorophyll, suspended solids, volatile suspended solids, particulate carbon, particulate organic nitrogen and counts of phytoplankton and zooplankton individuals by species[22]. Phytoplankton and zooplankton carbon concentration was derived from the cell counts using measurements of the sizes of individual plankton and published length-weight relationships. In addition, Secchi disk depth, near-surface water temperature and near-surface dissolved oxygen were measured.

Table 4-1: Water-quality variables measured for Marlborough District Council. Phytoplankton and zooplankton counts are made only on the near-surface water samples.

Property	Description	Detection limit	Method or comment
Ammonium Nitrogen	DRP,NH4-N,NO3-N, Simultaneous Auto-analysis	1 mg N m^{-3}	Astoria
Dissolved Reactive Phosphorus	DRP,NH4-N,NO3-N, Simultaneous Auto-analysis	1 mg P m^{-3}	Astoria
Nitrate + Nitrite Nitrogen	DRP,NH4-N,NO3-N, Simultaneous Auto-analysis	1 mg N m^{-3}	Astoria
Volatile Suspended Solids	Filtration, drying at 104 C, followed by furnacing at 400 C	0.5 mg m^{-3}	APHA 2540D
Inorganic Suspended Solids	Filtration, drying at 104 C, followed by furnacing at 400 C	0.5 mg m^{-3}	APHA 2540D
Suspended Solids	Filtration, drying at 104 C, followed by furnacing at 400 C	0.5 mg m^{-3}	APHA 2540D
Turbidity	Turbidimeter rated against Formazin standards	0.1 NTU	APHA 2130B
Chlorophyll a	Acetone pigment extraction, spectrofluorometric measurement.	0.1 mg Chla m^{-3}	A*10200H
Dissolved Reactive Silicon	Molybdosilicate / ascorbic acid reduction.	1 mg Si m^{-3}	APHA4500Si
Salinity	Salinometer, calibrated against seawater standard	0.1 g kg^{-1}	YSI
Total Dissolved Nitrogen	Persulphate digest, auto cadmium reduction, FIA	10 mg N m^{-3}	Lachat
Total Dissolved Phosphorus	Persulphate digest, molybdenum blue, FIA	1 mg P m^{-3}	Lachat
Particulate Organic Carbon (until June 2014 inclusive)	Catalytic comb @900°C, sep, TCD, Elementar C/N analyser	0.1 mg C m^{-3}	MAM, 01-1090
Particulate Organic Nitrogen (until June 2014 inclusive)	Catalytic comb @900°C, sep, TCD, Elementar C/N analyser	0.1 mg N m^{-3}	MAM, 01-1090
Particulate nitrogen (from July 2014)	Catalytic comb @900°C, sep, TCD, Elementar C/N analyser	0.1 mg C m^{-3}	MAM, 01-1090

[22] The counts were made only for the near-surface water-samples. Furthermore, the counts will yield only qualitative abundance information for the larger (scarcer and more mobile) zooplankton.

Property	Description	Detection limit	Method or comment
Particulate carbon (from July 2014)	Catalytic comb @900°C, sep, TCD, Elementar C/N analyser	0.1 mg N m^{-3}	MAM, 01-1090
Phytoplankton abundance	Water samples fixed with Lugols upon arriving at Hamilton labs. Subsequently, cells settled onto graticule slide. Cells within random fields identified (to lowest practical taxonomic resolution), measured and counted under microscope	-	Cell carbon estimated from cell dimensions and taxon-specific conversion factors
Zooplankton abundance	Counted, as for phytoplankton but no size determinations	-	Niskin bottle samples combined with cell counting are not well suited to capturing larger/more mobile zooplankton in sufficient numbers to permit robust abundance estimates. The counts and derived biomass estimates provide only very imprecise estimates of zooplankton abundance.

4.5 Initial conditions

At the start of each simulation, the initial values of all biogeochemical variables were horizontally and vertically uniform at values representative of winter conditions in Pelorus Sound. The flushing time of Pelorus Sound, and the time-scales of other biogeochemical processes operating within the model are such that the model gradually forgets its initial conditions (as it evolves towards a state that is determined by boundary conditions and internal dynamics) within 50-100 days.

4.6 Model coefficients

The coefficients of the Fennel biogeochemical model, the mussel model and the salmon model are listed in Table 10-1, Table 10-2 and Table 10-3. Almost all of the coefficients were left at their default values. Only two were changed from their default values.

The attenuation coefficient for photosynthetically active radiation (PAR) was specifically tuned for Pelorus Sound. We set this coefficient to 0.15 m^{-1} (based upon measurements of PAR attenuation made during the MDC monthly water quality sampling).

The initial slope of the half-saturation constant for light-limited growth was also changed but we did not tune it to Pelorus specifically. In an earlier exercise (Hadfield, Broekhuizen, Plew 2014b), we had treated this coefficient as a calibration parameter when fitting the model to data from Queen Charlotte Sound. We chose to retain that fitted value for our Pelorus Sound simulations.

The value of one of our two non-standard coefficients is based upon direct measurements of that quantity. The value of the other has not been calibrated to Pelorus Sound data. Thus, we argue that we have made no attempt to calibrate our model to water-quality data from Pelorus Sound. Thus, we argue that the comparisons between simulated- and measured water-quality properties represent validation comparisons rather than calibration attempts. They provide a genuinely independent indication of the model's performance.

4.7 Cook Strait boundary data

There are few historical measurements of water-quality in Cook Strait. Indeed, the only publicly available water quality data that we know of for Cook Strait are those published in Bradford, Lapennas et al. (1986; three summertime surveys during 1980 & 1981). Fortunately, New Zealand King Salmon measured water-quality (nutrients, phytoplankton, chlorophyll, particulate nitrogen, but *not* zooplankton) at five stations around Port Gore monthly from July 2012-April 2013. One of these stations is mid-way across the Port Gore mouth of Cook Strait (Figure 4-4). Earlier numerical modelling (Knight 2012a) suggests that this location will have Cook Strait water-characteristics. Furthermore, the water-quality at this station is markedly different from that of the other four stations (which are well within the bay). It also differs from that of outer Pelorus (PLS7/NZKS7) and outer Queen Charlotte (QCS5) and outer Tory Channel (NZKS22). The nature of the differences are consistent with our belief that the outer Port Gore station is sampling Cook Strait water.

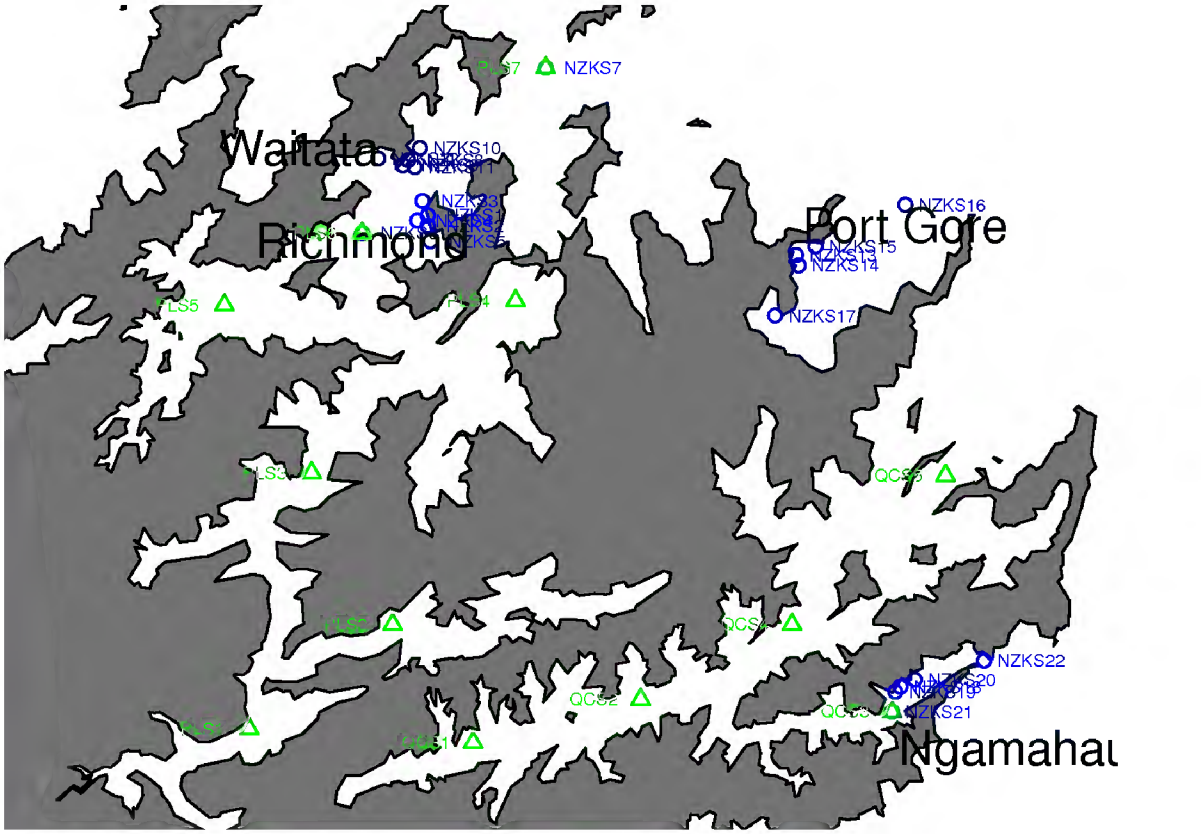

Figure 4-4: Map illustrating the locations of Marlborough District Council (green) and New Zealand King Salmon (blue) water-quality sampling sites. Data from NZKS16 were used to construct the Cook Strait boundary conditions for the NPZD-model.

New Zealand King Salmon Ltd ceased sampling at Port Gore shortly after the Supreme Court upheld the appeal against the Port Gore salmon farm that NZKS had been seeking, but Marlborough District Council continued to sample outer-most Port Gore station (NZKS16) for a further two months. Thus, we have access to one years' worth of monthly data at that station. We generated nominal time-series of sea-surface properties from a 3 month time-centred smoothing curve through the 12 months' worth of near-surface data. We used the corresponding near-bed data to generate a time

series which we assumed to be typical of water at 50 m depth. For the upper 50 m of the water-column, we then used linear interpolation (in the vertical) to derive layer-specific boundary conditions from the smoothed data. Below 50 m, we assumed concentrations were depth invariant (equal to the prescribed values at 50 m).

Zooplankton concentrations have not been measured at the Port Gore station. Thus, boundary conditions for zooplankton were based upon the zooplankton data that Marlborough District Council have gathered at their outer most Queen Charlotte station (station 5). As the zooplankton biomass estimates are imprecise (Table 4-1), we used the time-averaged value from the field data as a temporally invariant boundary condition.

For our modelling, we chose to assume that all dissolved organic nitrogen (DON) is 'old, refractory/inert' material, that is, biologically inactive on the time-scales of interest. Thus, we did not augment the measured NH_4^+ or NO_3^- concentrations so as to generate boundary conditions which implicitly include some reactive dissolved organic nitrogen.

4.8 Catchment boundary conditions

Pelorus Sound has one major river (the Pelorus) flowing into it. Marlborough District Council have collected water-quality samples at a flow recorder station near the Pelorus River mouth at approximately monthly intervals since July 2012 and flow in the river is recorded on a near-continuous basis. They have also gathered similar data near the mouths of three rivers/streams: Kaituna River, Kenepuru Stream, and Cullen Creek. The water-quality monitoring data includes measurements of NH_4^+, NO_3^-, NO_2^- and total suspended solids.

Concentrations of ammoniacal nitrogen and NO_2^- are negligibly small in comparison with those of NO_3^-. Pelorus river NO_3^- concentrations are not correlated with instantaneous flow, or flow over the preceding 24 hours, but they do show clear annual cycles (being higher in the winter than in the summer).

We adopted a constant boundary condition for ammonium in Pelorus River. For nitrate, we generated a time-varying boundary condition by calculating monthly median values from the Pelorus River monitoring data, and then using linear interpolation to obtain instantaneous concentration values.

Since freshwater phytoplankton and zooplankton will not survive in the salty water of Pelorus Sound, we adopted zero-concentration boundary conditions for chlorophyll and carbon concentrations of phytoplankton and zooplankton. Similarly, we assumed a zero concentration boundary condition for the very large faecal detritus class (mussel and fish faeces).

Concentrations of material that would fall into the model classes 'small detritus' and 'large detritus' have not been measured by MDC. Thus, we must look elsewhere in order to synthesize boundary conditions for these two state-variables. Fortunately, Shearer (1989) reports measured NO_2, NO_3, ammoniacal nitrogen (collectively, dissolved inorganic nitrogen, DIN) and total nitrogen (TN) in several streams/rivers that feed into Pelorus Sound. TN-DIN provides a measure of total organic nitrogen (ON). In Shearer's data, the median of the ratio ON/DIN varies between 0.13 (lower Kaituna) and 1.15 (Wakamarina). For the lower Pelorus River, the median ratio is 0.58. We use this last value to derive boundary conditions for in-stream ON concentration (i.e., instantaneous instream ON=0.58 DIN). Finally, we assume that: (i) all of the organic N is bio-available, (ii) that it is all

particulate (such that it can be allocated to either small, or large detritus) and (iii) that it is composed of a 50:50 mix of small and large detritus.

We have chosen to neglect any inputs arising from other (much smaller) point sources such as the Kaituna River, Cullen Creek, Kenepuru Stream and Havelock wastewater plant. We have also neglected any 'diffuse source' inputs that may arise from seeps etc.

4.9 Simulation scenarios

We have made simulations for seven different scenarios:

- No mussel-farms and no fish-farms with benthic denitrification[23] (NM-NF-WD).
- Existing[24] mussel-farms, no fish-farms, with benthic denitrification (EM-NF-WD).
- No mussel-farms, existing fish-farms, with benthic denitrification (NM-EF-WD).
- Existing mussel-farms, existing fish-farms, with benthic denitrification (EM-EF-WD).
- Existing+approved[25] mussel-farms, existing+approved fish-farms, with benthic denitrification (AM-AF-WD).
- Existing mussel-farms, no fish-farms, without benthic denitrification (EM-NF-ND).
- Existing+approved mussel-farms, existing+approved fish-farms, without benthic denitrification (AM-AF-ND).

We will treat the EM-EF-WD scenario as our 'reference condition' – against which results from alternative scenarios will be compared.

All of the simulations were run on the 200 metre resolution grid. Simulations spanned a 500 day period from 24 May 2012 to 6 October 2013. The EM-EF-WD scenario corresponds to present-day conditions in Pelorus Sound.

4.10 Analysis and presentation of biophysical model simulation results

We made our biophysical simulations on the 200 m resolution horizontal grid. Whilst we have finer resolution grids, the model becomes too computationally expensive to permit annual scale simulations at those finer resolutions (Table 2-1). At 200 m resolution, the detailed structures of individual fish farms and mussel farms are not resolved. However beyond, say, 1 km, natural mixing will have eroded the farm-derived steep gradients to sufficient degree that the grid spacing ceases to be significant. Thus, in the far-field the simulated concentrations will be much less subject to bias. In short, the model has been designed with the intent that it be used to derive an understanding of the regional (and large-bay scale) influences of farming rather than the farm-scale/small bay-scale influences.

[23] such that only 25% of sedimenting N particulate N returns to the water-column as NH_4, the remainder being lost

[24] in this context, 'existing' implies those mussel farms which had lines in the water at the time of a 2012 aerial survey in 2010, and the New Zealand King Salmon fish farms that were operating during the 2012/2013 period.

[25] In this context, 'approved' implies those mussel farms which have been approved since the 2012 aerial survey (whether or not they now have lines in the water) and those mussel farms already approved in 2010 which did not have lines in the water at the time of the aerial survey. It also includes the two newly approved NZKS fish farms (Waitata and Richmond) and the small fish farm that has been approved for Beatrix Bay and the Port Ligar fish farm

Simulation results at the locations of each of the seven Marlborough District Council sampling sites within Pelorus Sound were stored at approximately 12 minute resolution. In addition, the 12 hour averaged concentrations for every control-volume were saved once per simulated day.

For the most part, each model state-variable has an unequivocal analogue in the field data, but the situation for model ammonium and model detrital nitrogen is more complex.

Firstly, in reality, non-living organic nitrogen is comprised of both dissolved organic nitrogen (DON) and non-living particulate organic nitrogen (non-living PON). Whilst we have field determinations of DON at the seven MDC sites, the model has no explicit DON pool. Rather a fraction of any newly dead living matter passes into one or other of the two 'standard Fennel' particulate detrital pools (small and large detritus) whilst the remainder passes directly into the so-called ammonium pool. Thus, the question arises: 'how should we apportion real-world DON between modelled ammoniacal nitrogen and the two modelled particulate detrital classes'? Whilst real-world DON concentrations are moderately high (see section 5.2), the majority of marine DON is usually considered to be 'old, refractory' material that is almost inert on the time-scales of interest. We therefore chose to ignore the real world DON when setting our boundary and initial conditions.

Secondly, our direct field determinations of PON measure total (living and non-living) particulate organic nitrogen whereas the model draws distinctions between (living) particulate phytoplankton N, (living) particulate zooplankton N and two classes (small, slow-sinking and large, faster-sinking) of non-living particulate detrital nitrogen.

Plankton nitrogen biomass is known only roughly: from the microscope counts and measurements of individual cells and literature estimates for the volume-specific nitrogen contents of different taxa. Table 4-2 describes the means by which analogues to the model state-variables were derived from the field data.

In short, (i) we assume that field- and modelled ammoniacal nitrogen are direct analogues of one-another, (ii) we derive approximate estimates of living particulate nitrogen from the microscope based counts of phytoplankton and zooplankton and measurements of the dimensions of these plankton, (iii) we use the field determinations of PON as a lower bound for the sum of simulated abundances of large detrital N, small detrital N and living particulate N, (iv) we use the sum of the field determinations of PON and DON as an upper bound for the sum of simulated abundances of large detrital N, small detrital N and living particulate N. Given that we have ignored real-world DON when setting our initial and boundary conditions, we anticipate that the model should yield PON concentrations which are similar to measured PON (rather than similar to the sum of measured PON and DON).

Table 4-2: Means by which the field-data were used to derive analogue values for the model state-values.

Model State-variable	Derivation from field data	Comment
"Nitrate"	NO_3^- + NO_2	
"Ammonium"	NH_4^++NH_3	The model has no explicit DON pool. We choose to lump real-world DON into the model detrital pool (see below)
Chlorophyll-a	Chlorophyll-a	GFC filter (approx. 2 μm pore size)
Phytoplankton carbon concentration	Microscope counts of cells combined with measurements of cell dimensions and literature values for C:volume ratios	The sampling scheme was not designed with zooplankton sampling in mind. The volumes of water that are collected are small. Very motile zooplankton and large jellyfish etc. will be under-sampled. Furthermore derivation of population carbon biomass from cell counts and cell dimensions is error-prone. The zooplankton biomass estimates are certainly very imprecise.
Zooplankton carbon concentration	Microscope counts of cells combined with measurements of cell dimensions and literature values for C:volume ratios	
Total detrital nitrogen (LDetN + SDetN)	(a) PON – phytoplankton N – zooplankton N (b) PON + DON - phytoplankton N – zooplankton N	Given our decision to lump real-world DON into the model detrital pool, (a) & (b) provide lower and upper bounds upon the plausible range of concentrations for the sum of the two model detrital classes. Since we have chosen to ignore real-world DON when setting our initial and boundary conditions, we anticipate that the model should produce PON concentrations that are closer to those of measured PON than those of measured (PON+DON).

For the purposes of illustrating how well the model reproduces the historical field data, we will present time-series plots which show the field data (symbols) and corresponding simulation results (12 minute resolution, from the '*EM-EF-WD*' scenario). We will present the results as a series of seven figures. Each figure corresponds to one of the seven Marlborough District Council monitoring stations. Each figure will contain six panels (one each for nitrate, ammonium, chlorophyll, phytoplankton carbon, zooplankton carbon and particulate organic nitrogen). Each panel will show: (a) time-series of field measurements at the near-surface location (red circles), (b) time-series of field measurements at the near-bed location (blue triangles), (c) corresponding simulated time-series at the net-surface (redline) and near-bed (blue line) locations.

We assess the skill (quality with which the model reproduces the field data) by: (a) visual comparison of the results (from the existing-mussels/existing fish-farms/with denitrification simulation) and field data, and (b) calculation of the two skill-measures (bias, B^*, and unbiased root-mean-squared-difference, $RMSD'^*$) as recommended by Los and Blaas (2010) [who were following Jolliff, Kindle et al. (2008)]:

$$B^* = \frac{1}{N\sigma_D}\sum_{n=1}^{N}(M_n - D_n)$$

$$RMSD'^{*} = \frac{sgn(\sigma_M - \sigma_D)}{\sigma_D}\left[\frac{1}{N}\sum_{n=1}^{N}\left((M_n - \bar{M}) - (D_n - \bar{D})\right)^2\right]^{0.5}$$

M_n and D_n denote the n^{th} corresponding observations in the model- and field time-series, $\bar{M}$ and $\bar{D}$ denote the means of the two time-series, σ_M and σ_D denote the standard deviations of the time-series.

B^* is equal to the ratio of the difference between the two means relative to the standard deviation of the field data. It is a measure of the degree to which the respective long-term means of the model and field time-series are congruent. Values that are close to zero indicate high congruence. Negative values indicate that the model is, on average, under-predicting relative to the field. Positive values indicate that the model is, on average, over-predicting.

$RMSD'^{*}$ is a measure of the match between the residuals (after removal of the respective time-series means) in the two time-series. It provides a measure of the degree to which the model reproduces the amplitude and phase of fluctuations in the field data. Like B^*, $RMSD'^{*}$ is expressed relative to the standard-deviation of the field data. $RMSD'^{*}$ values which are close to zero indicate that the model is reproducing the amplitude and phase of data-fluctuations well. B^* and $RMSD'^{*}$ can be plotted against one another in a standard scatter plot. It can be shown (Jolliff, Kindle et al. 2008) that if a point lies within the unit circle centred upon the origin, then the two time-series must be positively correlated. If a point lies outside the unit circle, the two time-series may be either uncorrelated, or weakly correlated; further, the correlation (if it exists) may be either positive or negative. If a point lies outside the unit circle, the simulation time-series explains less of the variance (of the field data) than the simple mean of the field-data does. Thus, points which lie outside the unit circle are indicative of low model skill.

We illustrate the predicted influences which the various alternative scenarios have upon water quality (relative to the EM-EF-WD scenario), in two ways.

Firstly, we will show a series of false-colour figures of time-averaged results. Secondly, we present seven figures akin to the time-series plots described earlier, but in this case, each panel will show five curves (being the simulated near-surface concentrations under five of the simulated scenarios). These figures indicate how instantaneous water-quality at the seven Marlborough District Council stations is predicted to behave under these scenarios. The intent is to demonstrate that the time-averaging employed to generate the false-colour maps is not masking short-lived, but markedly larger, differences between scenarios.

In the false-colour figures, each figure will contain seven rows and each row will contain three panels (maps). Each row of panels corresponds to one of the model state-variables. Each column presents a different *view* (or *property*) of the state-variable. In this context, *view* or *property* is used as a convenient short-hand to refer to: (i, left-hand map of each row) the time-averaged absolute concentration (of the reference scenario) or (ii, central map of each row) relative concentration (alternative scenario relative to reference scenario), or (iii, right-hand map of each row) time-averaged concentration difference (between reference and alternative scenario) for a particular state-variable.

Each panel is a false colour map of the model domain. Pixel colour at any location in the map is indicative of the numerical value of the property in question at the pixel-location (yellow/red being 'high', and blue being 'low'). The following points are worth noting:

- In each individual plot, the colour-scheme has been selected to yield 'pleasing' colours that allow the full range of values to be readily distinguished. In many of our images of relative (or absolute) change, even the colours at both ends of the colour-scale correspond to changes that are very small (in relative and/or absolute senses).
- The colours should not be interpreted as indicative of whether or not the magnitude of change might be deemed 'acceptable'. For example, 'green' should not be deemed to imply 'safe/acceptable' and 'red' should not be interpreted as meaning 'unsafe/unacceptable'.
- The numerical range spanned by the colour-scale differs for each property that we plot. Thus, when comparing maps of different properties on an individual figure, one must recognise that any specific colour does not necessarily equate to the same numerical value in both maps. Furthermore, even when looking at the same property on different figures, the colour-scales may span differing numerical ranges. A given colour may correspond to a differing numerical value on each of the two panels.

Each row corresponds to a different model state-variable (i.e., ammonium, nitrate, etc.). Within a row, the left-hand most panel will show a time-averaged concentration for the state-variable under a reference scenario (usually, EM-EF-WD). The central panel will illustrate the time-averages of concentration-relative-to-the-reference-scenario (RC_{p}: Equation $4-1$) for an alternative scenario. The right-hand column will show the time-average of concentration difference between the reference scenario and the alternative one. For example, the central column may show results from the EM-EF-ND scenario relative to the EM-EF-WD one and the right-hand panel will illustrate the time-averaged difference between these two scenarios. The time-average of relative concentration is calculated as:

Equation 4-1: Definition of relative concentration

$$RC_p = 1 + \frac{1}{N}\sum_{n=1}^{N}\frac{P_{\mathrm{n}}^{\mathrm{f}} - P_{\mathrm{n}}^{\mathrm{e}}}{\varepsilon + P_{\mathrm{n}}^{\mathrm{e}}},$$

in which *N* is the number of time-levels involved in the time-average, while P_n^e and P_n^f represent the simulated 12-hour average concentration P at time-level n in the baseline and alternative scenarios respectively. The scalar ε (=10^{-100}) was added to avoid the possibility of a division by zero. RC_p takes the value 1 if the time-average of the differences is zero. If, on time-average, the alternative scenario yields lower concentrations than the baseline scenario, RC_p will take a value less than 1. Conversely, if the alternative scenario tends to yield higher concentrations than the baseline scenario, RC_p will take a value greater than 1. Similarly, a negative time-averaged concentration difference implies that the alternative scenario yields a smaller time-averaged concentration than the reference scenario. A positive time-averaged concentration difference implies that the alternative scenario yields a larger time-averaged concentration than the reference one.

5 Biophysical model: Results

5.1 Existing water quality in Pelorus Sound

In this section, we will introduce some of the field data that Marlborough District Council have collected. Data for some other water-properties will be shown in section 5.2 (in which we compare field data and simulation results).

Figure 5-1 presents the time-series of NO_3-N concentrations measured at each of the seven MDC stations. Near surface nitrate concentrations (red symbols) are almost always low at PLS-2 (Kenepuru Sound), PLS-4 (Beatrix Bay) and PLS-5 (Tawhitinui reach). At those sites, they are 'high' only for a month or so during mid/late winter. Elsewhere, near-surface nitrate concentrations are moderately high for a larger fraction of the year (but still low during the summer). Maximum annual concentrations tend to be greater in the main-stem of Pelorus (PLS-1, PLS-3, PLS-6) than in the side-arms (PLS-2, PLS-4, PLS-5) or at the Cook Strait mouth (PLS-7). Near-bed nitrate (blue symbols) dynamics are similar to those of the surface layer – albeit that the amplitude of the near-bed annual cycle is smaller than that of the near-surface one at most sites. Whilst near-surface and near-bed concentrations are similar during winter, they tend to diverge through spring and summer. Divergence is greatest in Beatrix Bay (PLS-4), Tawhitinui (PLS-5) and Waitata reach (PLS-6). It is smallest at the two innermost sites Mahau Sound (PLS-1) and Kenepuru Sound (PLS-2).

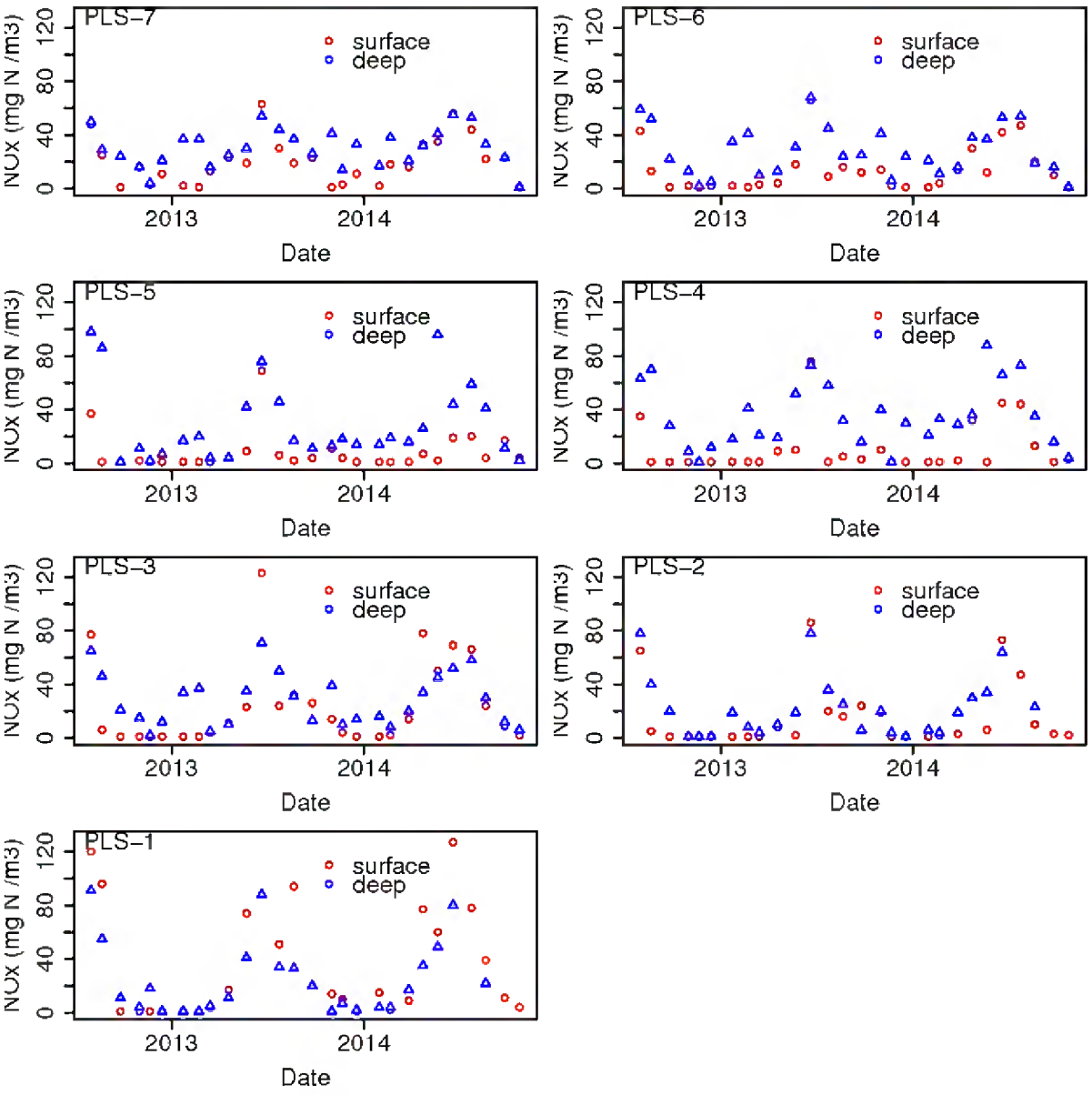

Figure 5-1: Time-series of nitrate concentrations (mg N/m^3) measured at the seven MDC stations in Pelorus Sound.

Figure 5-2 presents the time-series of ammoniacal nitrogen concentrations measured at each of the seven MDC stations. Ammoniacal nitrogen concentrations tend to be highest in mid-late summer. They also tend to be a little higher near-bed than near-surface (Table 5-1). During the summer (December-February, incl.), near-bed and near-surface ammoniacal nitrogen is more abundant than nitrate, but during winter (June – August, incl.) nitrate is more abundant than the ammonium.

Table 5-1: Mean and standard deviation of ammonium and nitrate measured in Pelorus Sound in the MDC sampling. Each observation (value measured at one location in a given month) is treated as an independent record.

Sampling depth	Season	Ammonium concentration mean (standard deviation) [mg N m^{-3}]	Nitrate concentration mean (standard deviation) [mg N m^{-3}]	N
Near surface	Summer	15.3 (8.9)	2.7 (4.9)	434
Near bed	Summer	23.7 (12.2)	17.2 (14.2)	434
Near surface	Winter	12.2 (11.0)	44.1 (37.7)	434
Near bed	Winter	13.0 (9.7)	52.1 (20.1)	434

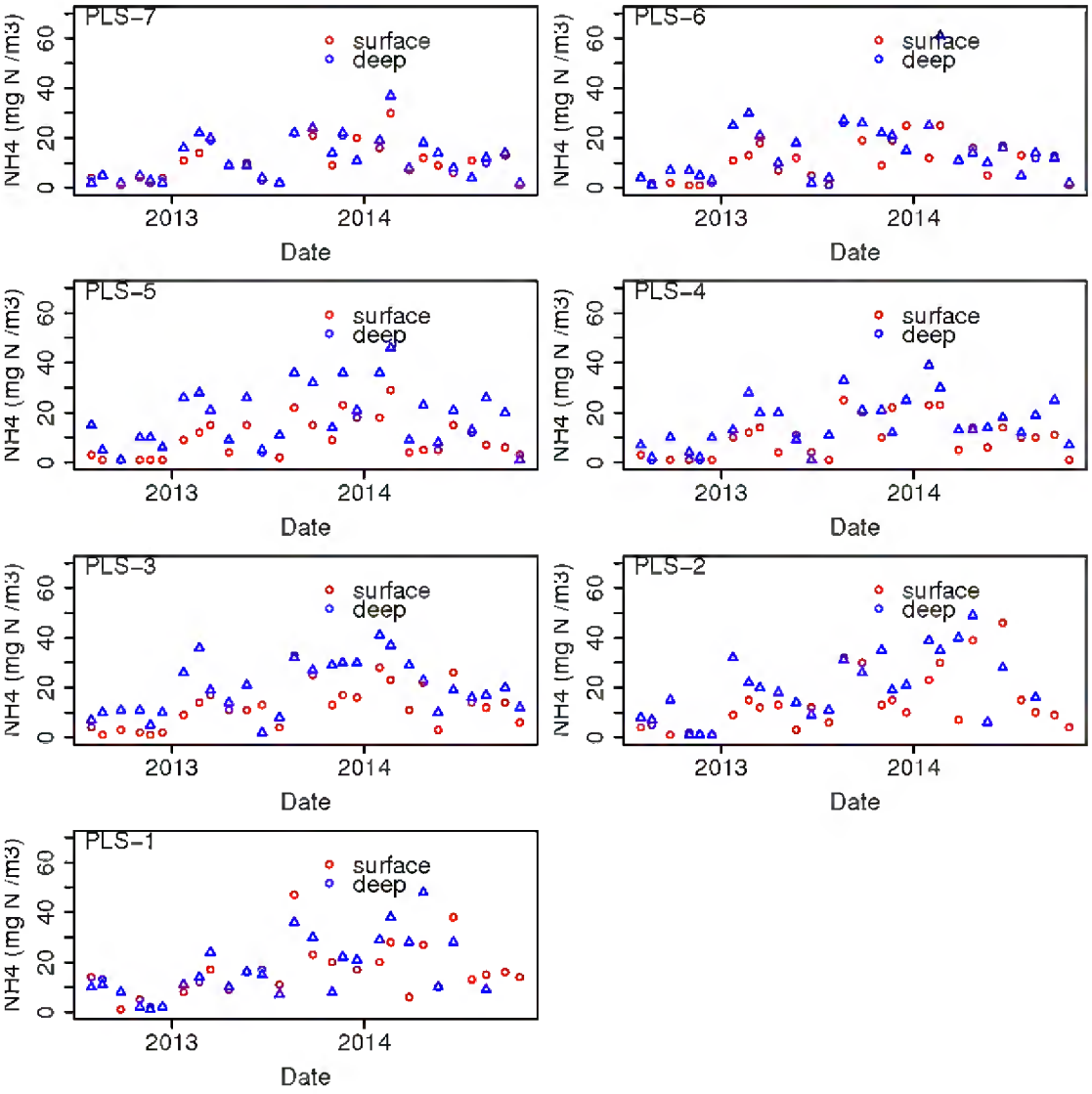

Figure 5-2: Time-series of ammoniacal nitrogen concentrations (mg N/m^3) measured at the seven MDC stations in Pelorus Sound.

Figure 5-3 presents the time-series of chlorophyll concentration measured at the seven MDC stations. Chlorophyll concentrations tend to be highest at the two inner-most stations (PLS-1 and PLS-2) and lowest at the two outermost ones (PLS-6 & PLS-7). At most stations, near-surface chlorophyll concentrations usually exceed near-bed ones but the Beatrix Bay (PLS-4) and Tawhitinui (PLS-5) stations often exhibit so-called *deep chlorophyll maxima*: near-bed chlorophyll concentrations were higher than near-surface ones during both summer periods. Chlorophyll concentrations tend to be greatest in late-winter/early spring and late summer/early autumn – however the month-to-month changes in abundance are much less regular than those of nitrate or even ammonium.

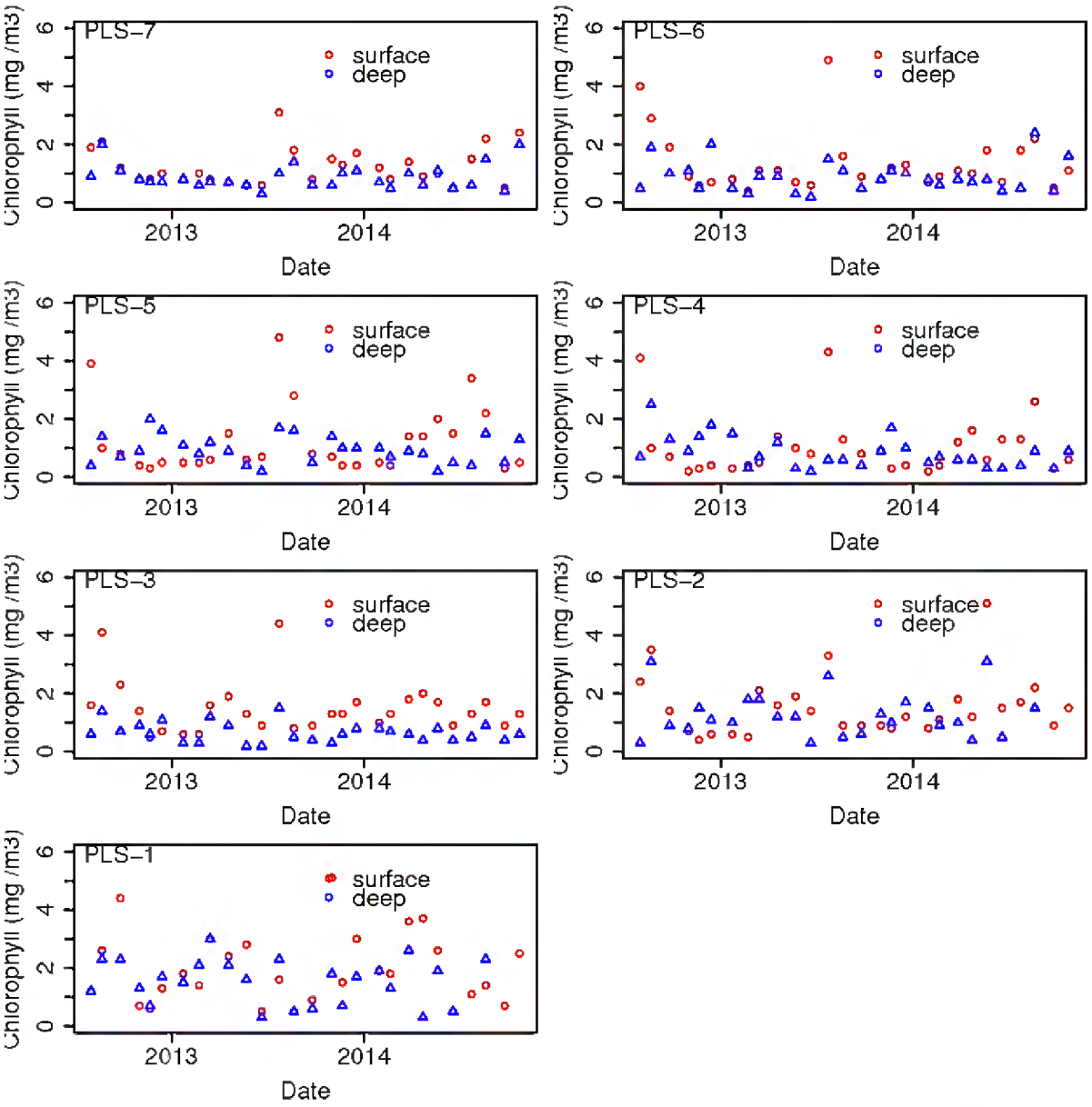

Figure 5-3: Time-series of chlorophyll-a concentrations (mg Chl-a/m^3) measured at the seven MDC stations in Pelorus Sound.

5.2 Comparison of simulation results with field data

We have deliberately made no attempt to calibrate the model to any field data from Pelorus Sound[26]. The coefficients governing the biogeochemical processes are those that we used for the earlier Queen Charlotte modelling (Hadfield, Broekhuizen, Plew 2014b). Since we have not used any Pelorus data to calibrate the model, we can legitimately use the Pelorus data to validate it.

Figure 5-4 - Figure 5-10 present time-series results from the seven Marlborough District Council water quality monitoring stations together with corresponding results from the EM-EF-WD (existing mussel & fish farms, with denitrification) simulation scenario. The congruence between simulation and field measurements tends to be greater at the inner-most (PLS-1 & PLS-2) and outer-most (PLS-7) stations. This probably indicates that: (i) that dynamics at these stations are somewhat constrained/influenced by the boundary conditions which we have applied, and (ii) that the boundary conditions are, indeed 'about right'.

Wintertime maxima- and summertime minima of nitrate concentration are reproduced well at all stations in near-surface waters. Near-bed winter maxima are also replicated well at all stations, but the model under-predicts the extent of the summertime nitrate reduction in the stations that do not lie on the main channel (Tawhitinui & Beatrix Bay). Furthermore, at those stations and also at the two outer stations (PLS-6 & PLS-7), there is a tendency for nitrate concentrations to start rising too early (mid-late summer rather than late-summer-mid autumn). This may be an artefact arising from applying a three-month smoothing window to the Port Gore data from which our boundary conditions were derived.

The field data for ammoniacal nitrogen are less regular than those for nitrate but tend to indicate that ammonium should be more abundant during the summer months and near-bed. The model reproduces those patterns well. The model reproduces the dynamics of particulate organic nitrogen moderately well at all stations – though, perhaps, slightly over-predicting summertime, near-surface PON at stations PLS-3 – PLS-7 and slightly under-predicting the corresponding concentrations in the near-bed water. Jointly, these discrepancies may indicate that our sinking speeds for the small and/or large detrital classes are too low.

Unfortunately, the model appears to over-predict summertime abundances of phytoplankton (as measured by chlorophyll and, more especially, inferred phytoplankton carbon). The over-prediction is worse in the surface layer than the near-bed one, and it is worse in the stations of central Pelorus (PLS-3 – PLS-6) than at the two inner-most stations or the outer-most one. In relative terms, the over-prediction is greater for inferred carbon biomass than for chlorophyll – suggesting that the model is yielding an overly high C:chl ratio. Predicted near-surface PON concentrations are too high during the summer relative to measured PON. Recalling that the model lacks a pool of dissolved organic nitrogen (such that all living nitrogen must pass into PON upon death), it is worth noting that whilst simulated 'PON' exceeds measured PON, it remains well below the sum of measured PON and measured DON. This is consistent with our expectations. Simulated zooplankton concentrations show less variability than is evident in the field data and the simulation does not reproduce the sporadic peaks of zooplankton concentration.

[26] Though, as noted earlier, we did adopt a PAR attenuation coefficient that is consistent with values measured within Pelorus Sound.

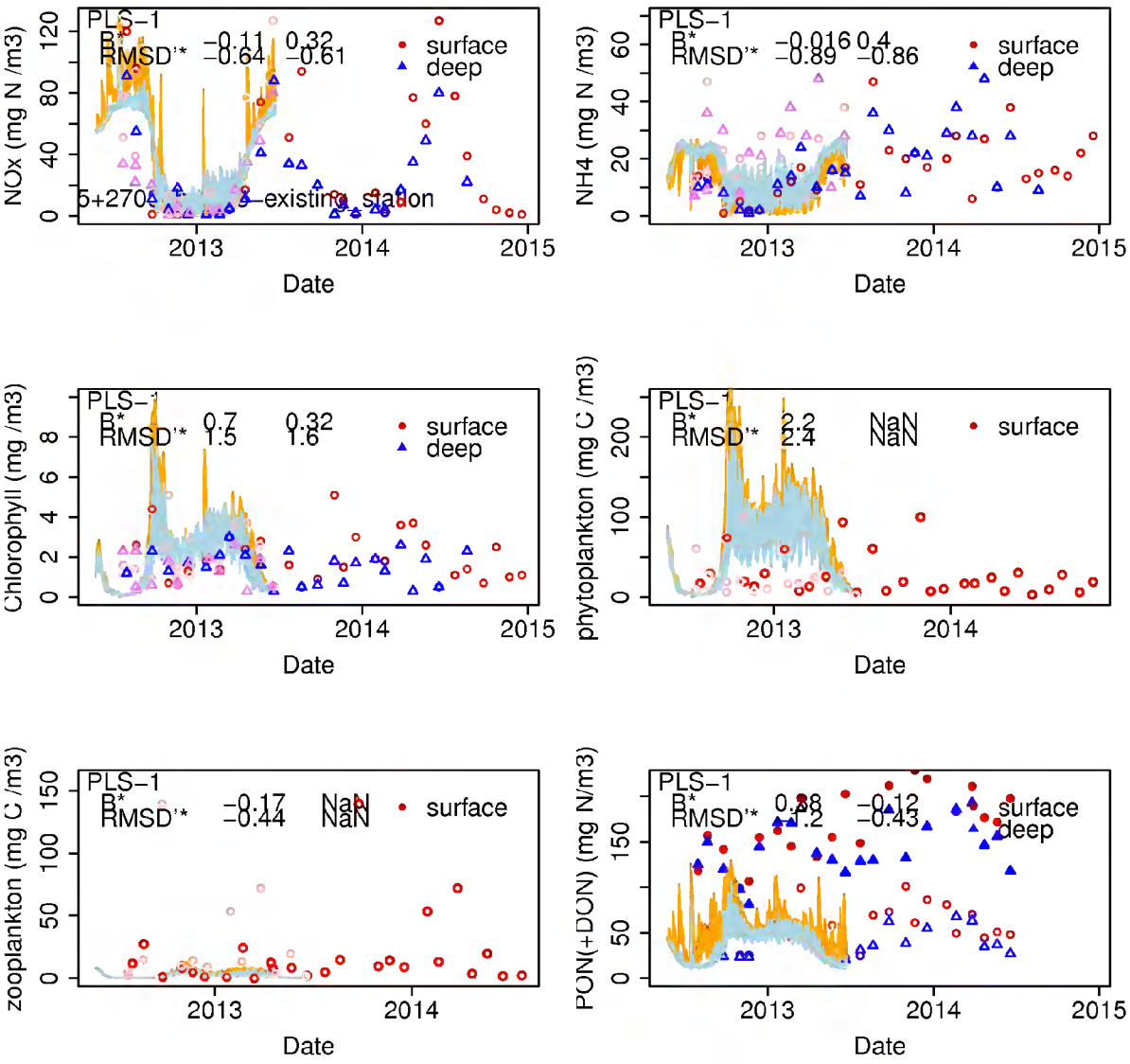

Figure 5-4: Time-series of measured (symbols) and simulated (lines) water-quality characteristics measured at Pelorus station 1. Red symbols are the raw near-surface field-data. Blue symbols are the raw near-bed field data. Pink symbols also represent the near-surface measurements, but in this case measurements made outside of the simulated calendar period have been transposed to a corresponding day-of-year within the simulation period. The violet symbols are the corresponding transposed near-bed field data. The orange and blue lines are the near-surface and near-bed simulation results. Values for B^* and $RMSD'^*$ are also shown. In each case, the left-hand value is for the near-surface simulation/data pair and the right-hand value is for the near-bed simulation/data pair.

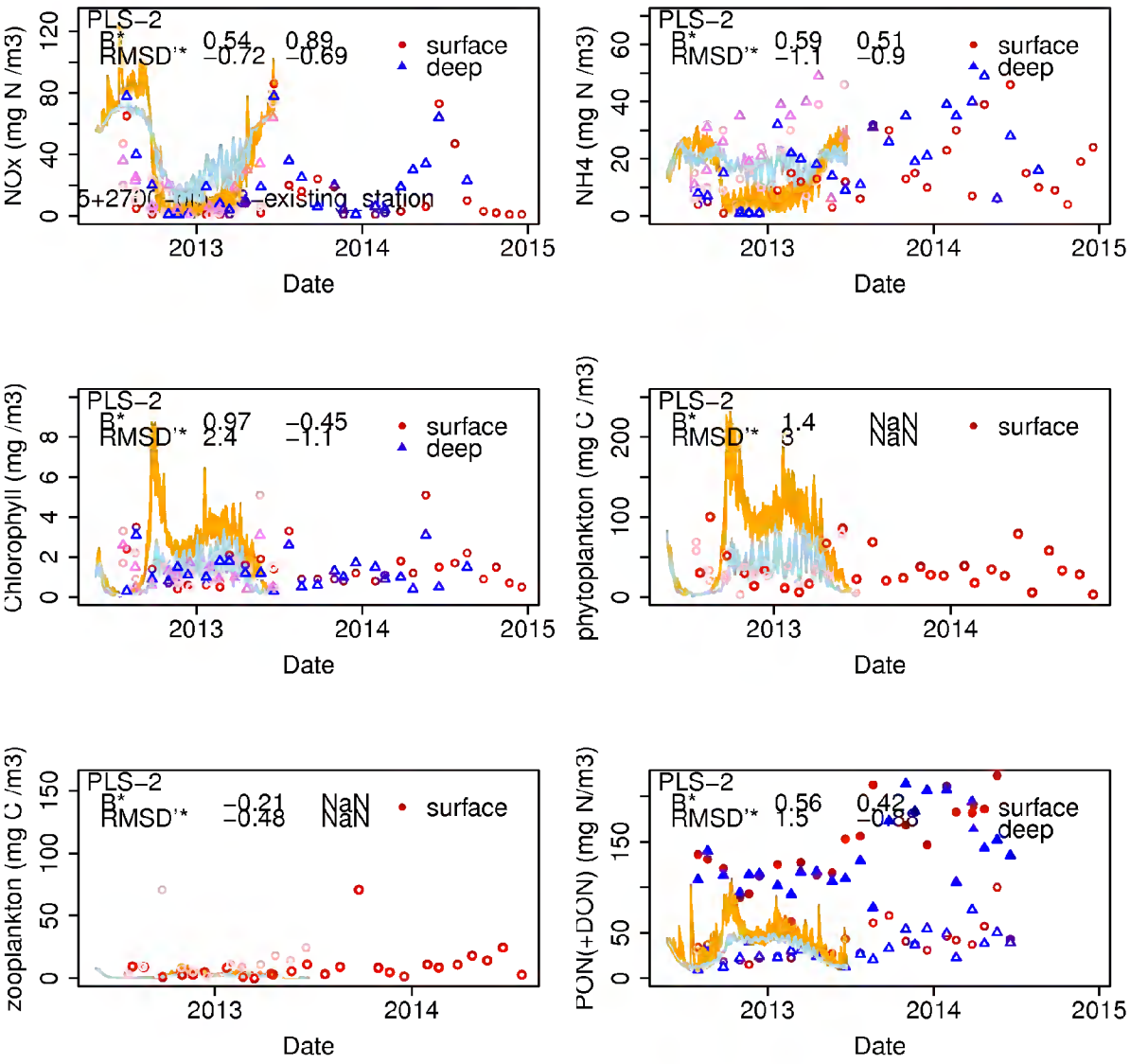

Figure 5-5: Time-series of measured (symbols) and simulated (lines) water-quality characteristics measured at Pelorus station 2. See the caption of Figure 5-4 for further details.

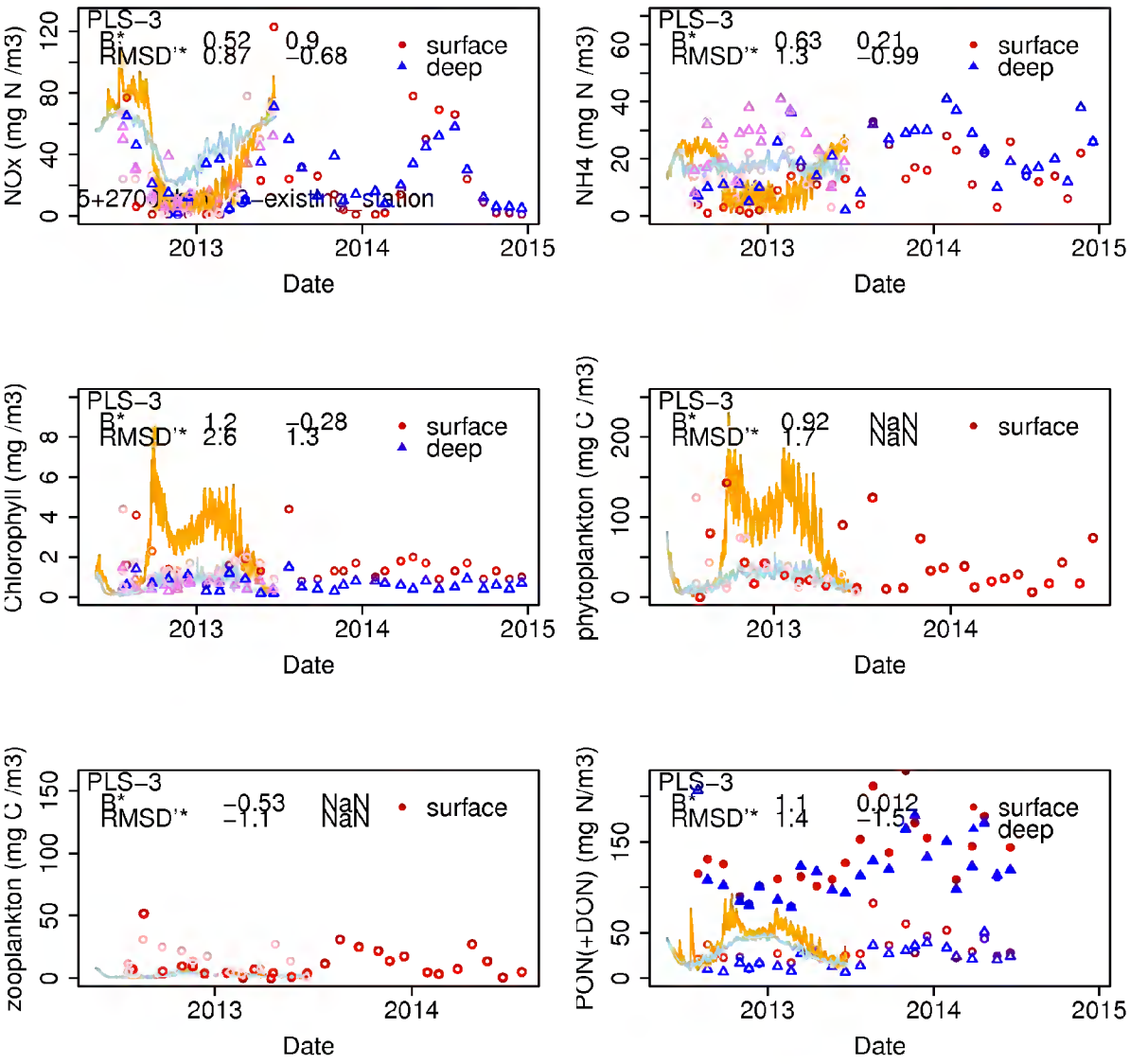

Figure 5-6: Time-series of measured (symbols) and simulated (lines) water-quality characteristics measured at Pelorus station 3. See the caption of Figure 5-4 for further details.

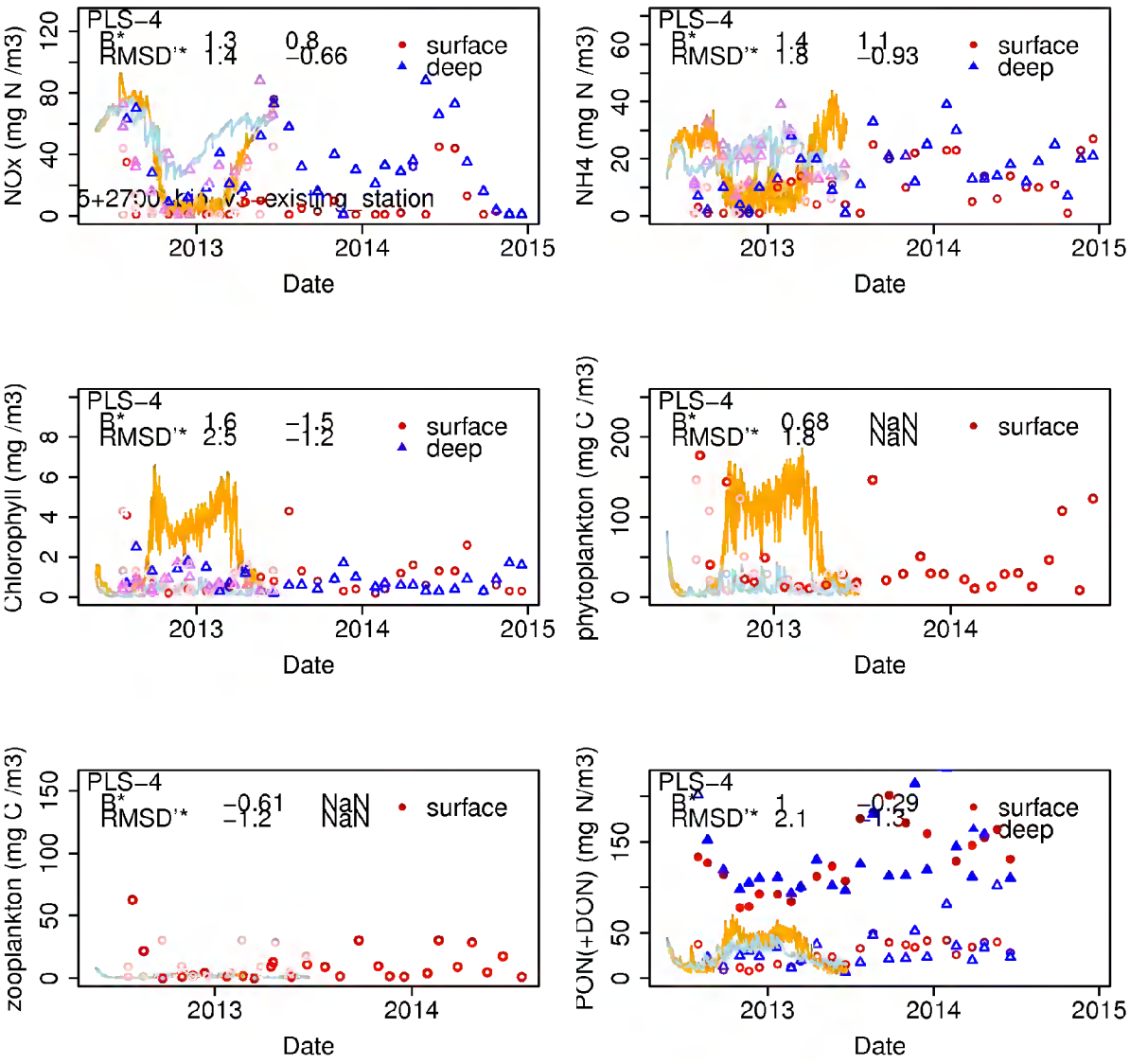

Figure 5-7: Time-series of measured (symbols) and simulated (lines) water-quality characteristics measured at Pelorus station 4. See the caption of Figure 5-4 for further details.

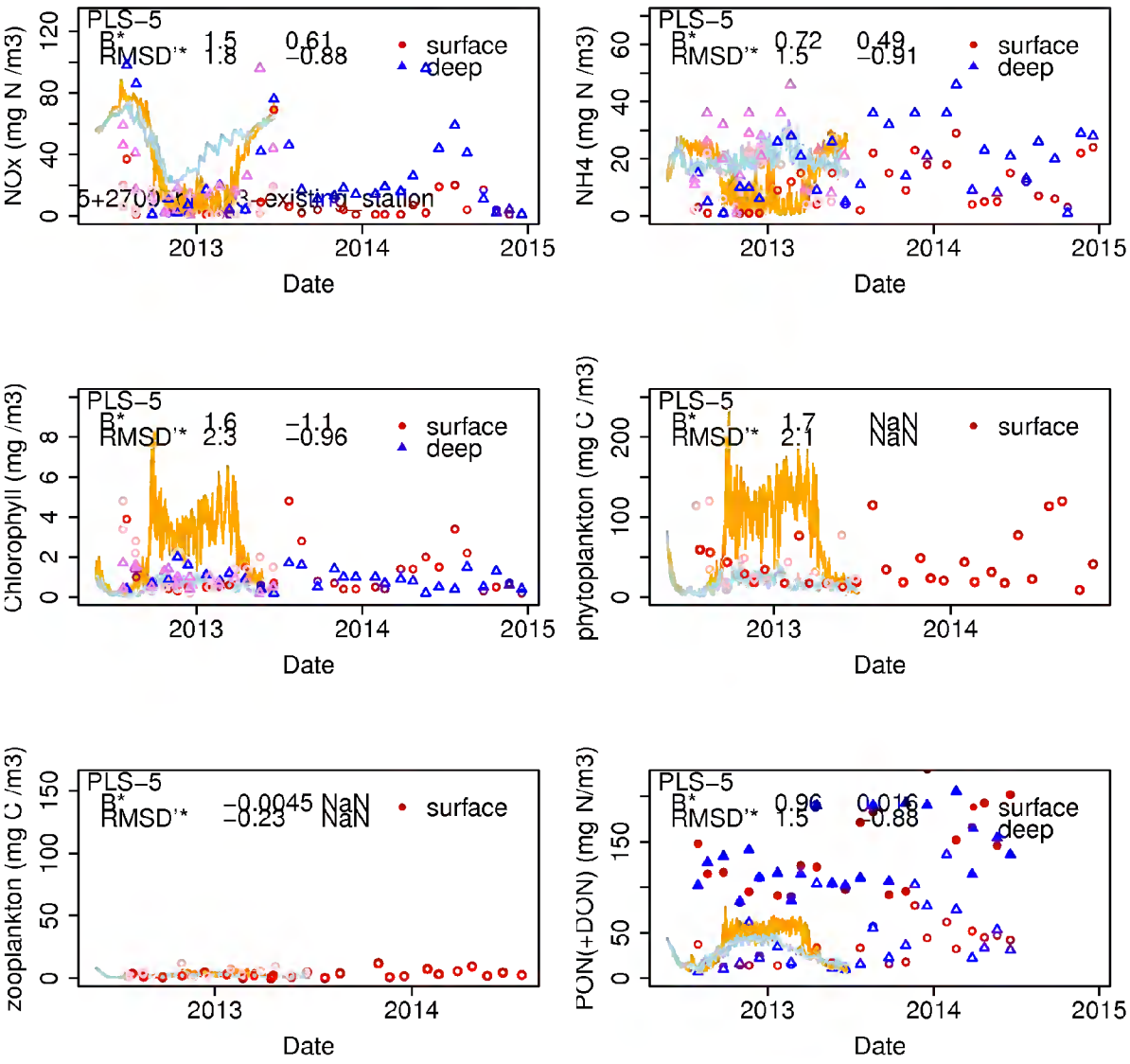

Figure 5-8: Time-series of measured (symbols) and simulated (lines) water-quality characteristics measured at Pelorus station 5. See the caption of Figure 5-4 for further details.

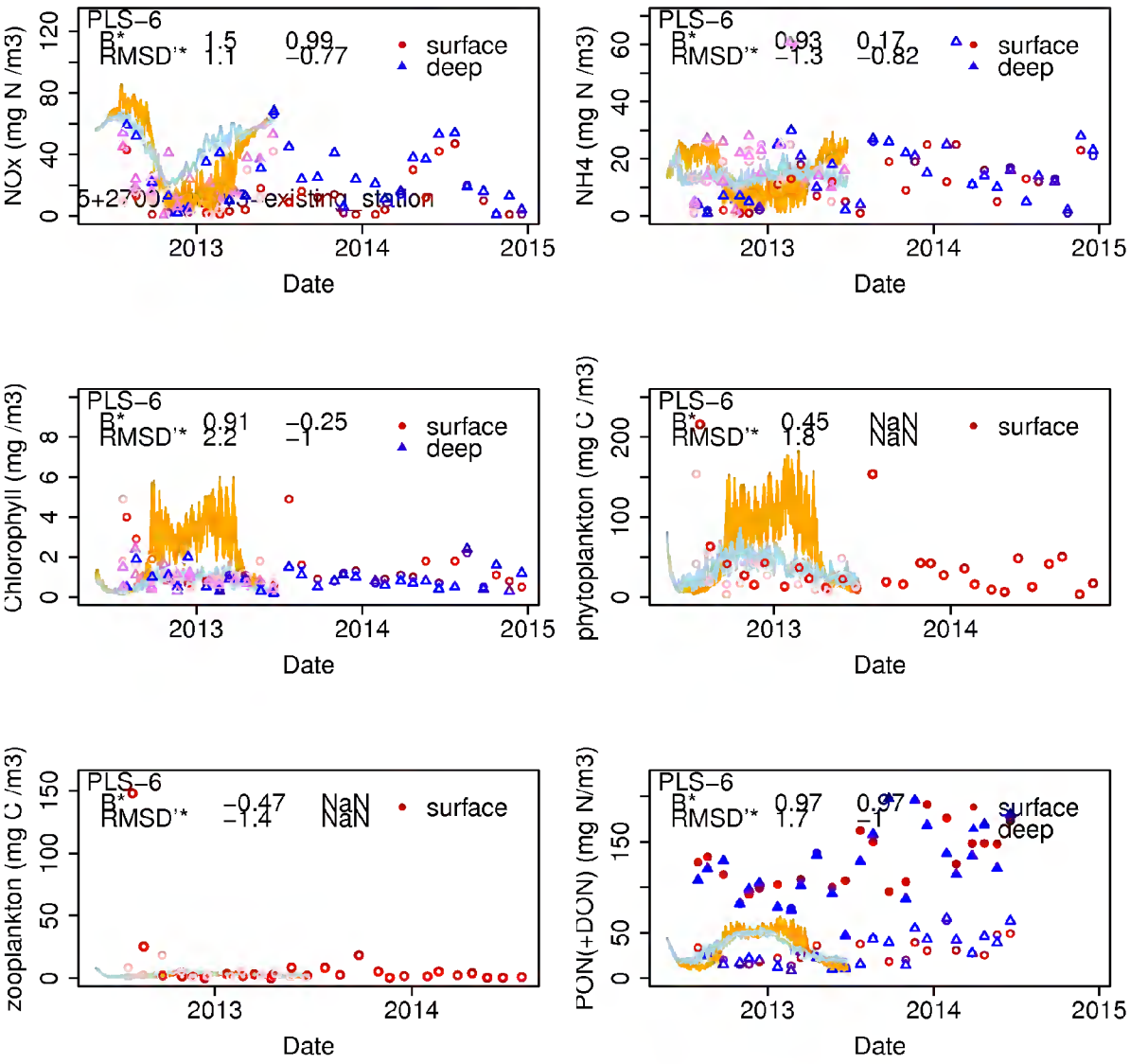

Figure 5-9: Time-series of measured (symbols) and simulated (lines) water-quality characteristics measured at Pelorus station 6. See the caption of Figure 5-4 for further details.

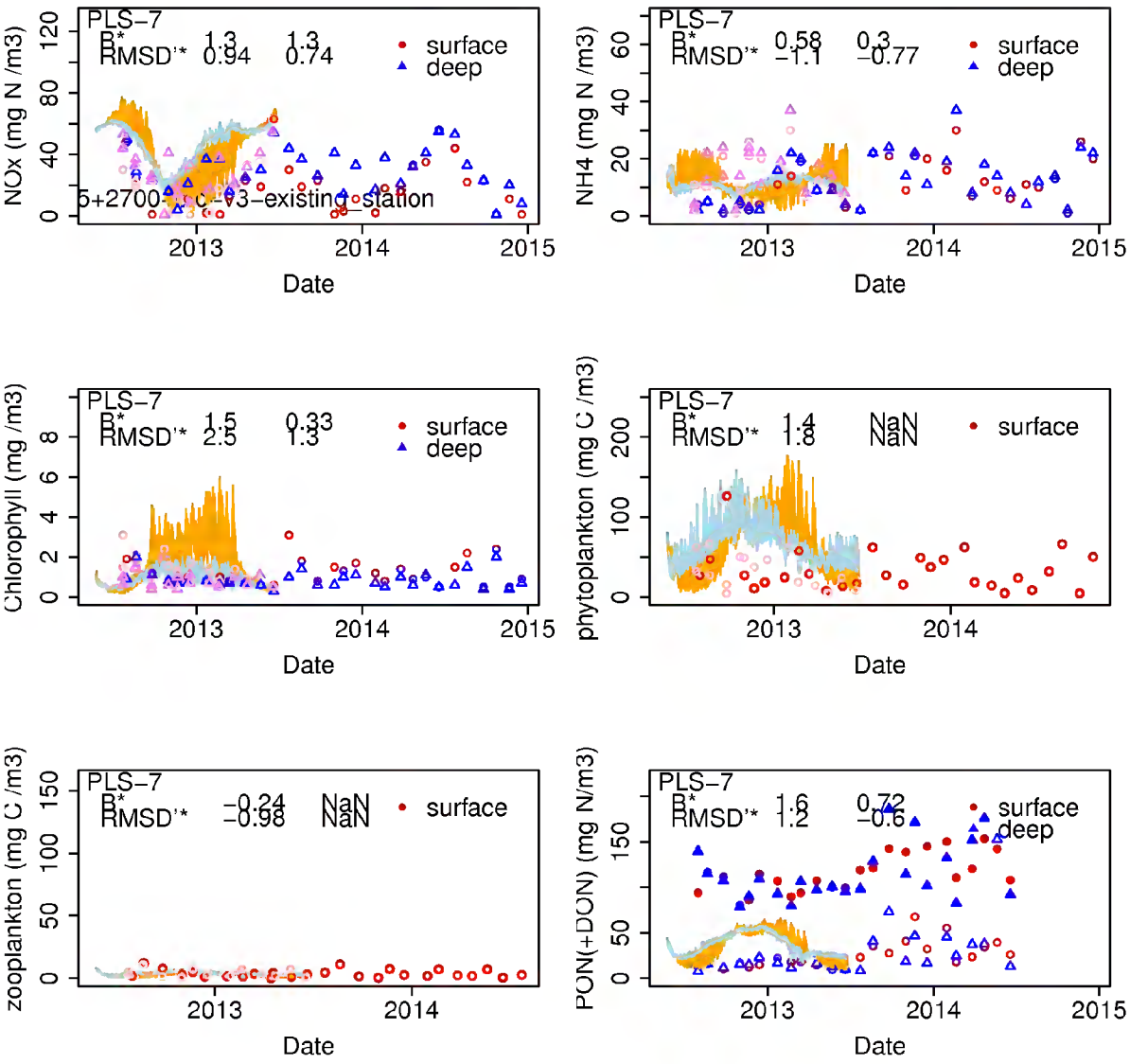

Figure 5-10: Time-series of measured (symbols) and simulated (lines) water-quality characteristics measured at Pelorus station 7. See the caption of Figure 5-4 for further details.

Figure 5-11 presents scatter plots of B^* versus $RMSD'^*$ for each state-variable. Unfortunately, only a minority of points lie within the unit-circle. Arguably, the model tends to reproduce the near-bed data slightly better than it reproduces the near-surface data. Certainly, it reproduces the apparent phytoplankton dynamics (chlorophyll and phytoplankton carbon) less well than it reproduces the dynamics of other state-variables. We will return to this matter in the discussion (section 6.2).

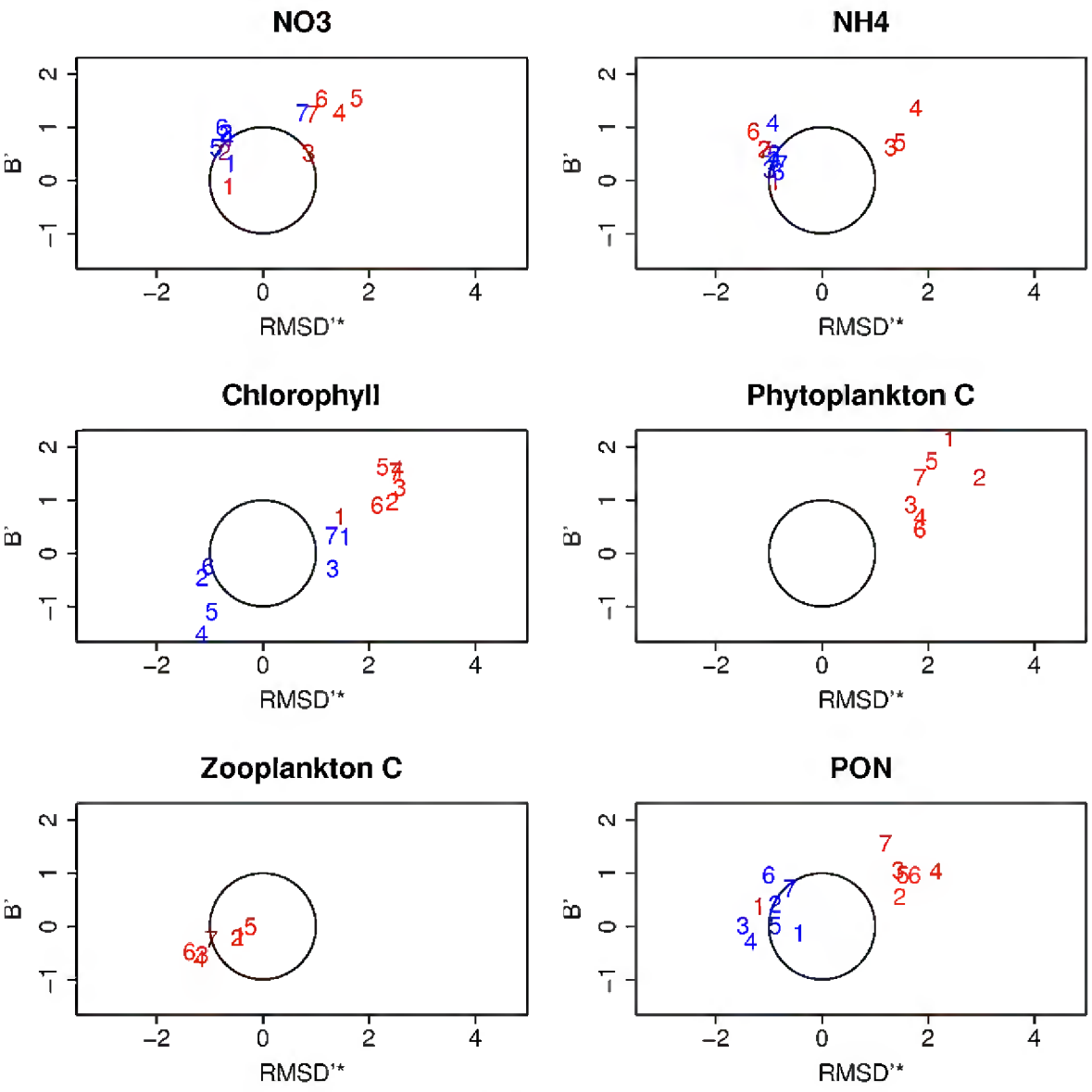

Figure 5-11: Scatter plots illustrating B* and RMSD'* for each state-variable for the EM-EF-WD simulation. Red symbols are for near-surface and blue are for near-bed. The numerals indicate the station number. The unit circle is also shown.

5.3 Denitrification rates

Figure 5-12 illustrates the temporal pattern of denitrification rates under the NM-NF-WD, EM-EF-WD and AM-AF-WD scenarios.

Averaged over the 381 km^2 of Pelorus Sound, simulated denitrification in the EM-EF-WD scenario rates vary from about 0.7 mmol N m^{-2} d^{-1} in winter up to about 2 mmol N m^{-2} d^{-1} in the summer. These are consistent with measurements made during spring, summer and autumn in Kenepuru Sound (0.7–6.0 mmol N m^{-2} d^{-1} under mussel farms and 0.1–0.9 mmol N m^{-2} d^{-1} at control sites) (Kaspar, Gillespie et al. 1985) and during the summer in Beatrix Bay (0.2 mmol N m^{-2} d^{-1} under mussel lines, rising to 0.4 mmol N m^{-2} d^{-1} at control sites) (Christensen, Glud et al. 2003). Whilst the field data are scarce, and we are comparing Pelorus-wide averages with point values, the comparison suggests that the model is yielding plausible denitrification rates.

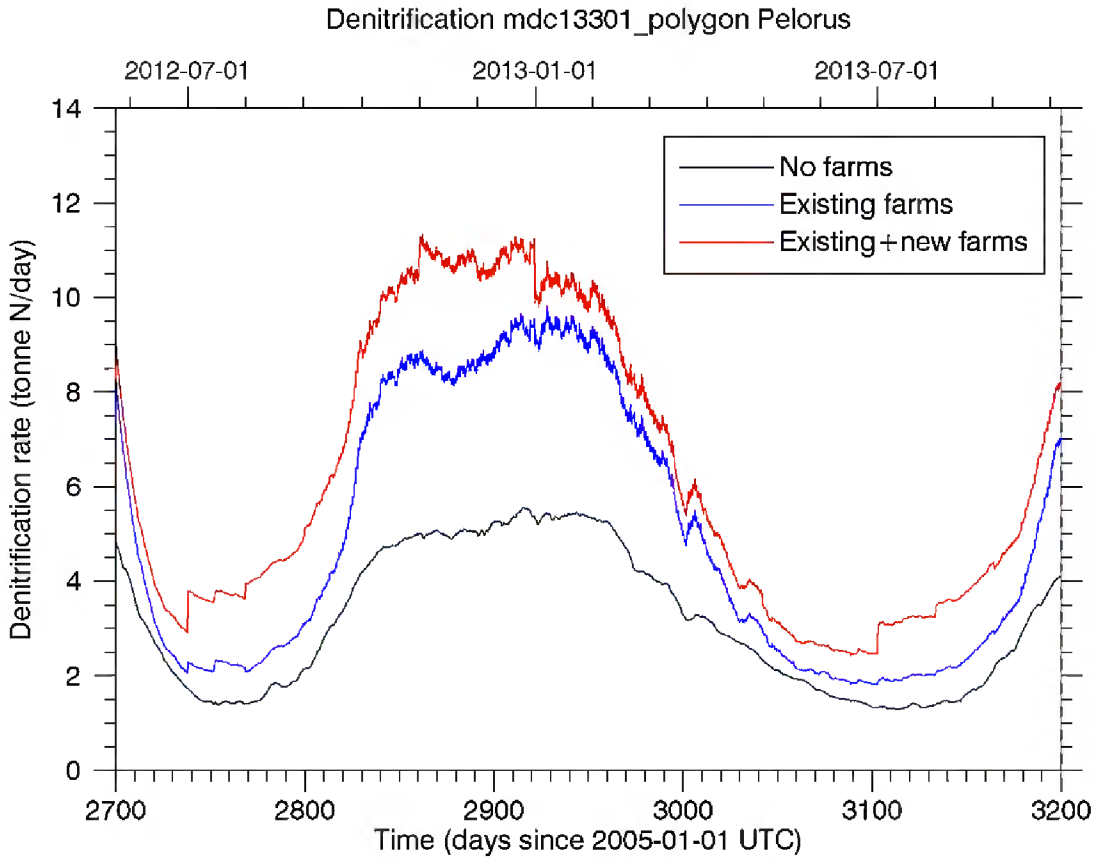

Figure 5-12: Temporal patterns of area-wide benthic denitrification within Pelorus Sound for the NM-NF-WD (black), EM-EF-WD (blue) and AM-AF-WD (red) scenarios.

5.4 Influence of aquaculture and benthic denitrification upon water quality

We start by comparing results from various of the 'existing farm' simulations with the intent of illustrating the relative effects that benthic denitrification, mussel farming and fish farming have upon Pelorus Sound.

The following scenarios were simulated:

- No mussel-farms and no fish-farms with benthic denitrification[27] (NM-NF-WD).
- Existing[28] mussel-farms, no fish-farms, with benthic denitrification (EM-NF-WD).
- No mussel-farms, existing fish-farms, with benthic denitrification (NM-EF-WD) [at 400 m horizontal resolution].
- Existing mussel-farms, existing fish-farms, with benthic denitrification (EM-EF-WD)
- Existing+approved[29] mussel-farms, existing+approved[30] fish-farms, with benthic denitrification (AM-AF-WD).
- Existing mussel-farms, no fish-farms, without benthic denitrification (EM-NF-ND).
- Existing+approved mussel-farms, existing+approved fish-farms, without benthic denitrification (AM-AF-ND).

We will begin by comparing the EM-EF-WD simulation results with the NM-EF-WD, EM-NF-WD and NM-NF-WD scenarios. The intent is to determine the sensitivity of the system to the present-day patterns of marine farming. Subsequently, we will compare EM-EF-WD with AM-AF-WD scenario to determine how much the system may change in the future once all existing and approved farms are operating. Finally, we will make two further comparisons. In both, we use a 'with denitrification' scenario as a reference, and a 'without denitrification' scenario as the alternative. These comparisons are designed to: (i) examine the system's sensitivity to denitrification, (ii) give an indication of the extent by which the system might change under a 'worst case' scenario (in which benthic denitrification ceases) such that the system will become more prone to eutrophication.

We have made comparisons for both the surface-most layer and the bottom-most layer of the discretized domain. Within this section, we focus upon the results from the surface-most layer. Appendix D presents plots that are conceptually equivalent to those presented within this section but which are for the bottom-most (rather than top-most) layer.

5.4.1 "Existing mussel/existing fish/with denitrification" versus "no mussel/existing fish/with denitrification"

Figure 5-13 (winter time-average, surface layer) and Figure 5-14 (summer time-average, surface layer) present comparisons of the EM-EF-WD and NM-EF-WD scenarios. During the winter, the absence of mussels is predicted to induce declines in the concentrations of ammonium (up to approx. 60% decline) and nitrate (up to approx. 30% decline) throughout much of Pelorus. Conversely, concentrations of mussel prey (small- and large-detritus, phytoplankton (as chlorophyll) and zooplankton) tend to increase (up to approx. 2-3 fold increase for detritus and phytoplankton and up to 10-fold increase for zooplankton). Of course, concentrations of XLdetritus (fish faeces and mussel faeces/pseudo-faeces) drop dramatically in the immediate vicinities of each

[27] such that only 25% of sedimenting N particulate N returns to the water-column as NH_4, the remainder being lost

[28] in this context, 'existing' implies those mussel farms which had lines in the water at the time of a 2012 aerial survey and the New Zealand King Salmon fish farms that were operating during the 2012/2013 period.

[29] In this context, 'approved' implies those mussel farms which have been approved since the 2012 aerial survey (whether or not they now have lines in the water) and those mussel farms already approved in 2012 which did not have lines in the water at the time of the aerial survey. It also includes the two newly approved NZKS fish farms (Waitata and Richmond) and the small Ngai Tahu fish farm that has been approved for Beatrix Bay.

[30] We erroneously included a fish farm at Port Ligar within the 'approved farms' scenarios. In reality, the application for a Port Ligar salmon farm has been rejected.

(now absent) mussel farm[31]. The changes (whether decreases or increases) are greatest in the Beatrix/Crail/Clova bays and Kenepuru Sound.

During summer, the qualitative responses of detritus and zooplankton to mussel absence are similar to that of winter: ammonium and nitrate concentrations are predicted to decline whilst detritus and zooplankton concentrations are predicted to rise. The effects tend to be greatest in Beatrix/Crail/Clova and Kenepuru. The summertime response of phytoplankton to mussel removal differs from that seen in the winter. Firstly, the removal of mussels is predicted to have little influence upon concentrations of phytoplankton (chlorophyll) within most of Pelorus (incl. Beatrix/Crail/Clova and Tawhitinui) and to induce a decline in chlorophyll concentration within Kenepuru. Secondly, when mussels are removed, the model shows relative summertime increases of phytoplankton concentration (up to about 30%) at the head of Forsythe Bay, in the western arm of Guards Bay and inner Port Gore that were not evident during the winter.

It is worth noting that, in both winter and summer, simulated concentrations of small detritus (SdetritusN) within Pelorus Sound tend to be higher than those out in Cook Strait, whilst simulated concentrations of large detritus (LdetritusN) tend to be lower than those out in Cook Strait. This is a feature that is repeated in all our scenarios. Our field data measure only total particulate organic nitrogen (PON). We have no way of directly measuring only non-living particulate organic matter[32], and no data on the size-composition of this particulate organic matter. When formulating the Cook Strait boundary conditions, we arbitrarily chose to split the PON 50:50 between LdetritusN and SdetritusN. The qualitatively differing spatial gradients of LdetritusN and SdetritusN in our simulations might be evidence that we should have allocated more of the PON into the SdetritusN class.

[31] This material sinks very rapidly, so even when farms are present, concentrations are negligibly small in those grid-cells which do not contain farms.

[32] though we can estimate it by subtracting estimates of phytoplankton and zooplankton biomass from total organic mass

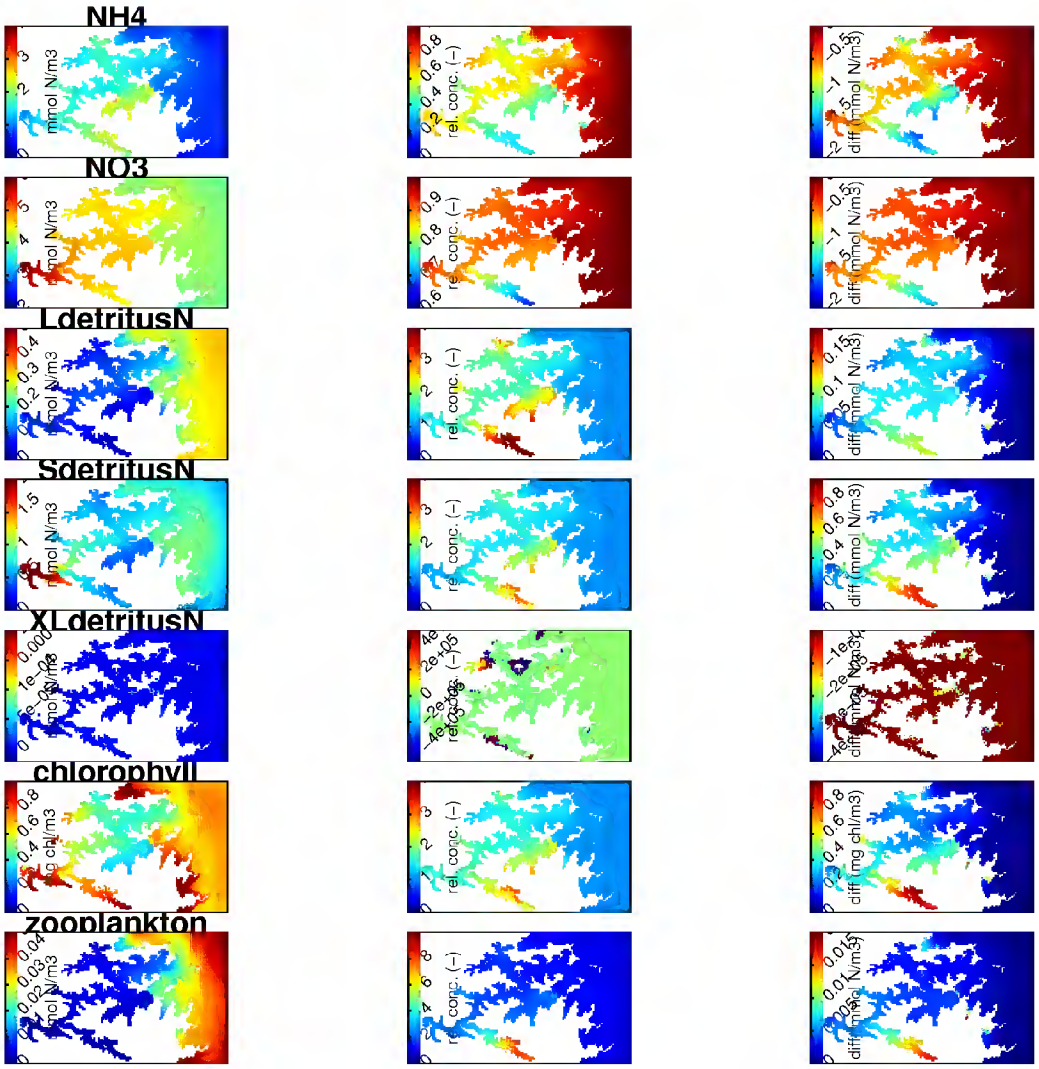

Figure 5-13: Comparison of winter time-averaged surface-layer concentrations in the EM-EF-WD and NM-EF-WD scenarios. The left-hand panel illustrates the time-average in the surface-most layer for the reference scenario (EM-EF-WD). The central panel illustrates the time-averaged relative concentration (alternative scenario relative to reference). The right hand column illustrates the time-averaged concentration difference (alternative scenario - reference scenario). These results are from simulations made with 400 m horizontal resolution.

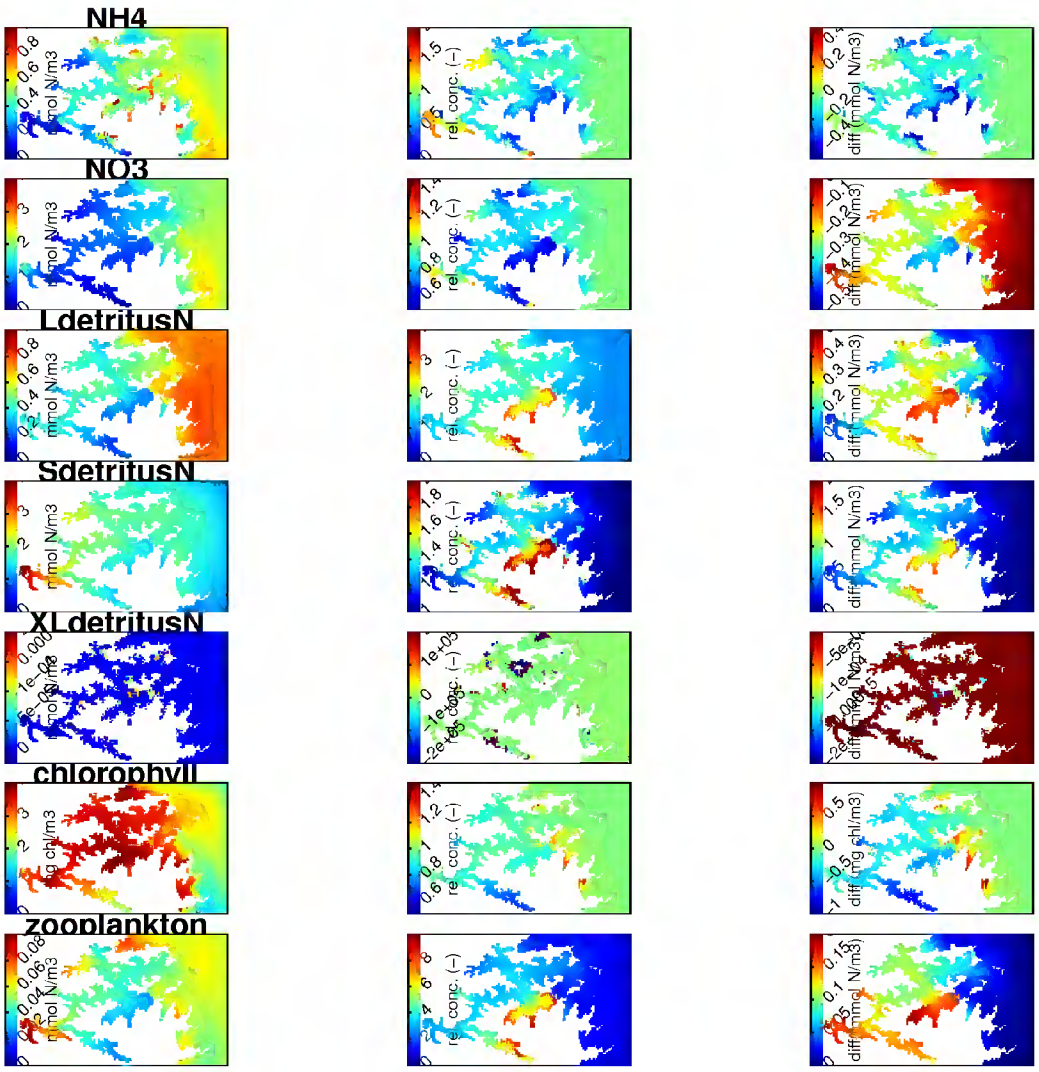

Figure 5-14: Comparison of summer time-averaged surface-layer concentrations in the EM-EF-WD and NM-EF-WD scenarios. Refer to the caption of Figure 5-13 for further explanation. These results are from simulations made with 400 m horizontal resolution.

5.4.2 "Existing mussel/existing fish/with denitrification" versus "existing mussel/no fish/with denitrification"

Figure 5-15 (surface-layer, winter) and Figure 5-16 (surface layer, summer) illustrate the differences between the EM-EF-WD and EM-NF-WD simulations. A casual glance at the colour patterns in the panels might leave the reader with the (false) impression that the existing fish farms are having dramatic effects throughout Pelorus. Inspection of the numerical values on the colour-scales for relative concentration- and for concentration difference will reveal that the magnitudes of change are very small indeed during winter (<2% relative change for all state-variables except ammonium and XLdetritus (mussel and fish faeces and mussel pseudo-faeces[33])). During the summer, the fish

[33] The relative change for the state-variable XLdetritus is very much larger in some places. In those places, the 'baseline' concentration of XLdetritus is very small. Despite the 'large' (20% or more) relative change, the absolute incremental change is small.

farms do appear to be having bigger effects upon the concentrations of living material and derivative detritus – removal of the fish-farms causes concentrations of SdetritusN, LdetritusN and chlorophyll to drop throughout much of outer Pelorus and Beatrix/Crail/Clova (esp. Crail – which hosts a fish-farm in the EM-EF-WD scenario). The chlorophyll declines are several times greater than those of small and large detritus. The biggest chlorophyll declines are seen in Crail Bay – where they amount to almost 10%. Elsewhere, on Pelorus, they are 5% or less. Zooplankton declines by 5-10% through all of Pelorus and by 10-20% within Crail.

The model suggests that, during winter, mussel farms have a greater impact upon the dynamics of nutrients and seston within Pelorus Sound than fish farms do. During the summer the effects of fish farms and mussel farms are of more similar absolute magnitude (but, at some places and/or times, of differing signs to those associated with mussel farming).

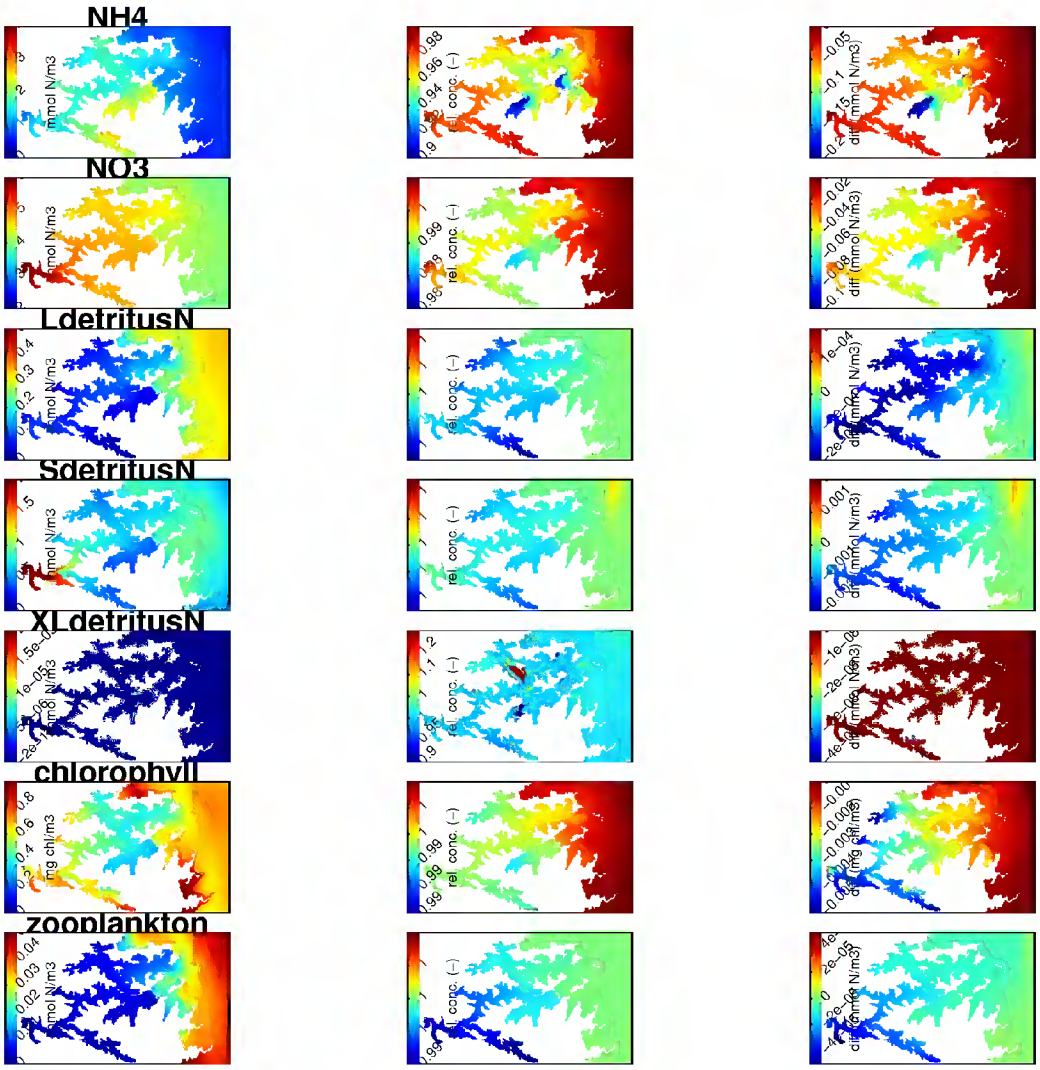

Figure 5-15: Comparison of winter time-averaged surface-layer concentrations in the EM-EF-WD and EM-NF-WD scenarios. Refer to the caption of Figure 5-13 for further explanation. These results are from simulations made with 200 m horizontal resolution.

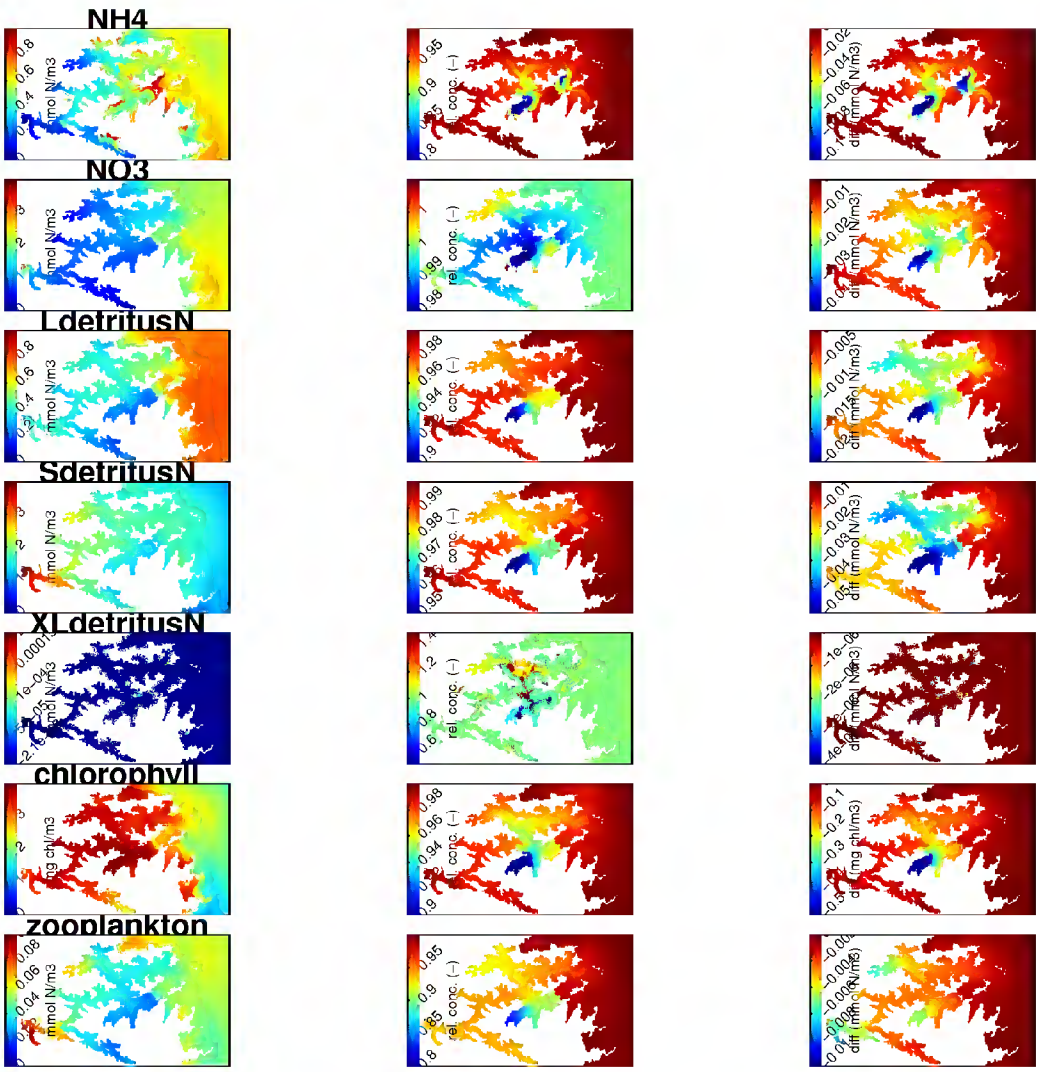

Figure 5-16: Comparison of summer time-averaged surface-layer concentrations in the EM-EF-WD and EM-NF-WD scenarios. Refer to the caption of Figure 5-13 for further explanation. These results are from simulations made with 200 m horizontal resolution.

5.4.3 "Existing mussel/existing fish/with denitrification" versus "no mussel/no fish/with denitrification"

Figure 5-17 (near-surface, winter) and Figure 5-18 (near-surface, summer) illustrate the differences between the EM-EF-WD scenario and the NM-NF-WD scenario. As one might anticipate (on the basis of the results presented in preceding subsections), the effects of removing the mussel farms (lower concentrations of dissolved nutrient, higher concentrations of detrital nitrogen and zooplankton, but mixed increases and decreases of chlorophyll) dominate over the effects of removing the existing fish farms during the winter. The differences between EM-EF-WD and NM-NF-WD tend to be greater in summer than winter.

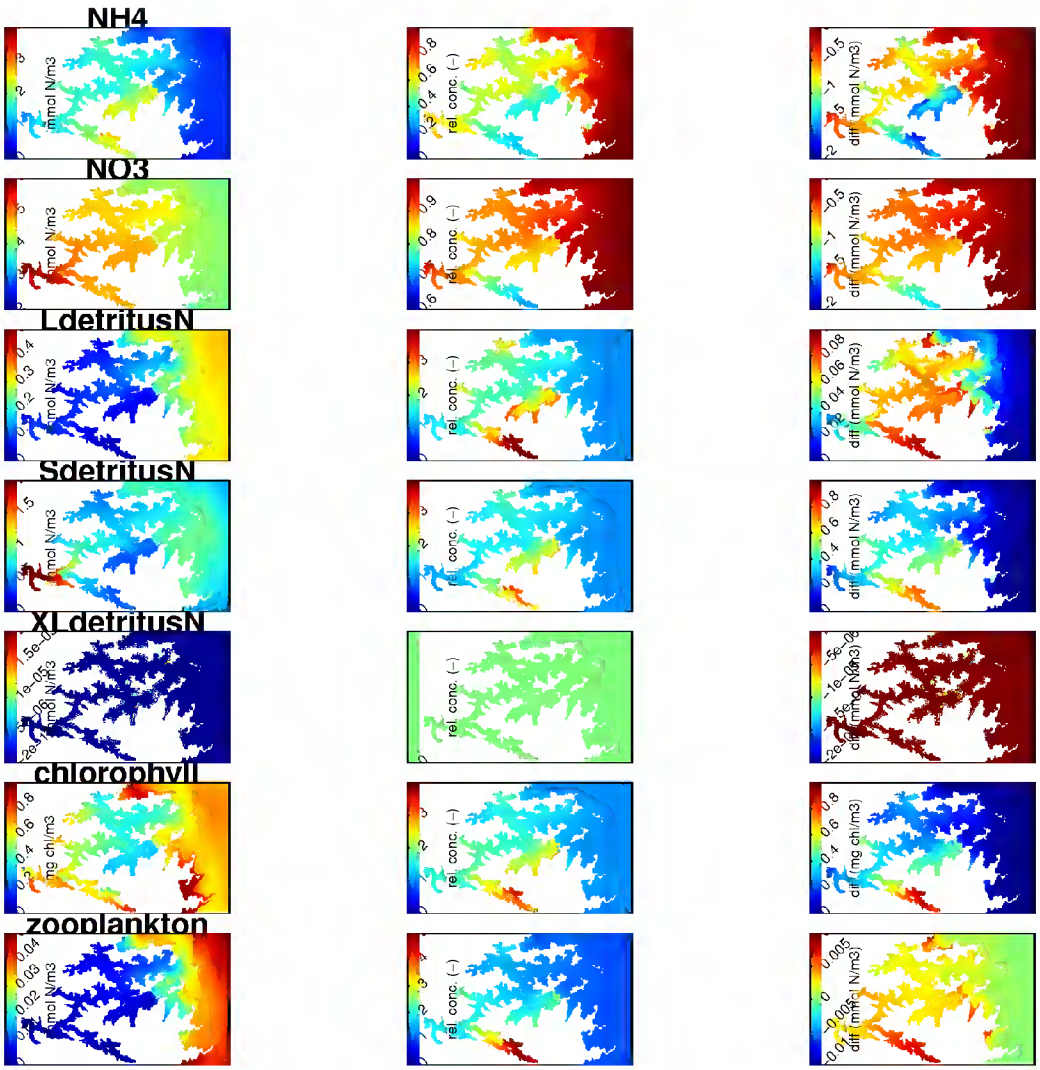

Figure 5-17: Comparison of winter time-averaged surface-layer concentrations in the EM-EF-WD and NM-NF-WD scenarios. Refer to the caption of Figure 5-13 for further explanation. These results are from simulations made with 200 m horizontal resolution.

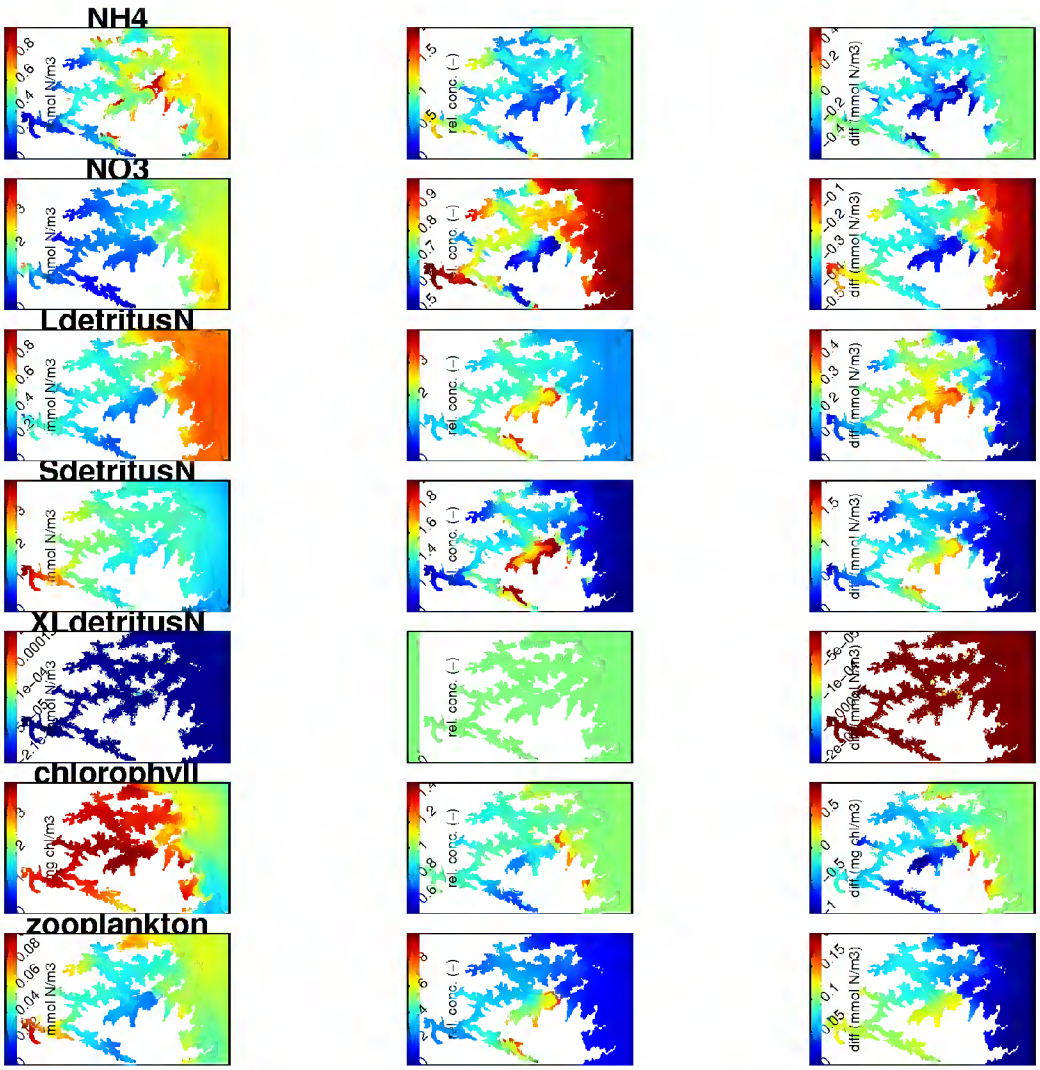

Figure 5-18: Comparison of summer time-averaged surface-layer concentrations in the EM-EF-WD and NM-NF-WD scenarios. Refer to the caption of Figure 5-13 for further explanation. These results are from simulations made with 200 m horizontal resolution.

5.4.4 "Existing mussel/existing fish/with denitrification" versus "approved mussel/approved fish/with denitrification"

Figure 5-19 (surface layer, winter) and Figure 5-20 (surface-layer, summer) illustrate the differences between the EM-EF-WD and AM-AF-WD scenarios.

During winter, ammonium concentrations in outer Pelorus are predicted to rise by 10-20% (driven by the presence of the new salmon farms at Waitata, Richmond and Port Ligar). There is also a small increase within Beatrix/Crail/Clova (driven by the new fish farm within Beatrix Bay). There are some very large changes in the relative concentration of XLdetritus – but these arise in regions where the background concentration is tiny. The absolute changes in the concentration of XLdetritus are very, very small (<1 µmol N m^{-3}) in comparison with total (SdetritusN+LdetritusN+XLdetritusN) detrital N concentrations (~ tens of mmol N m^{-3}). Changes in the concentrations of other state-variables

(LdetritusN, SdetritusN, phytoplankton N and chlorophyll, and zooplankton) are small (up to 5% for zooplankton in Kenepuru, but usually <2% for zooplankton elsewhere and for other state-variables).

During summer, the AM-AF-WD yields higher concentrations of all state-variables throughout most of Pelorus. Ammonium concentrations show the biggest relative changes (more than doubling in the immediate vicinity of the new fish farms). Nonetheless, even close to the fish-farms, the ammonium concentrations remain well below those considered toxic to marine organisms (Anon 2000). Phytoplankton (as chlorophyll) concentrations are predicted to rise by up to about 10% (less than 0.5 mg Chl m^{-3}) in the vicinities of Beatrix Bay and Waihinau/Port Ligar (near the Waitata and Port Ligar farms). They are predicted to rise by up to 0.2 mg Chl m^{-3} throughout the remainder of outer and central Pelorus, Tawhitinui Reach and Crail/Clova Bay. Zooplankton concentrations are predicted to increase throughout all parts of Pelorus Sound. The biggest increases are at the head of Pelorus, Kenepuru, Beatrix/Crail/Clova and head of Tawhitinui. In these regions, the increase is around 10–15%.

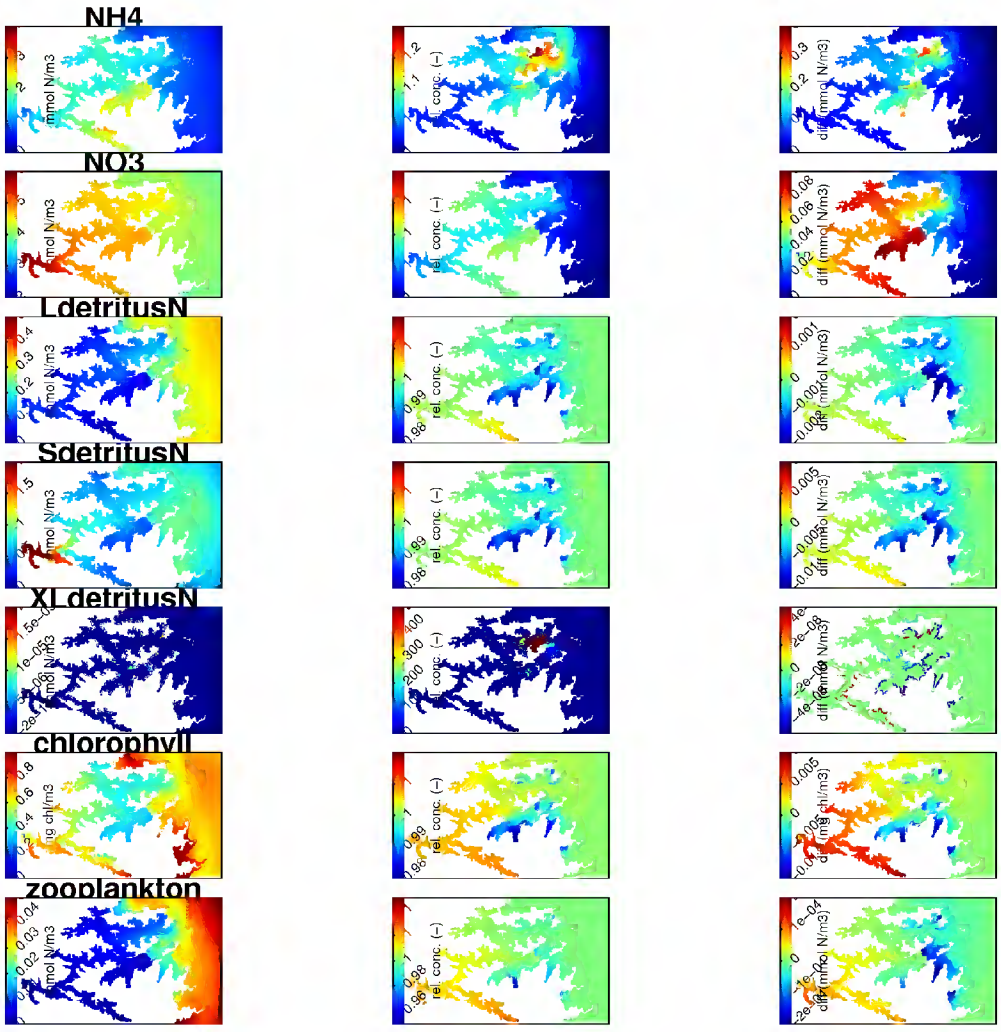

Figure 5-19: Comparison of winter time-averaged surface-layer concentrations in the EM-EF-WD and AM-AF-WD scenarios. Refer to the caption of Figure 5-13 for further explanation. These results are from simulations made with 200 m horizontal resolution.

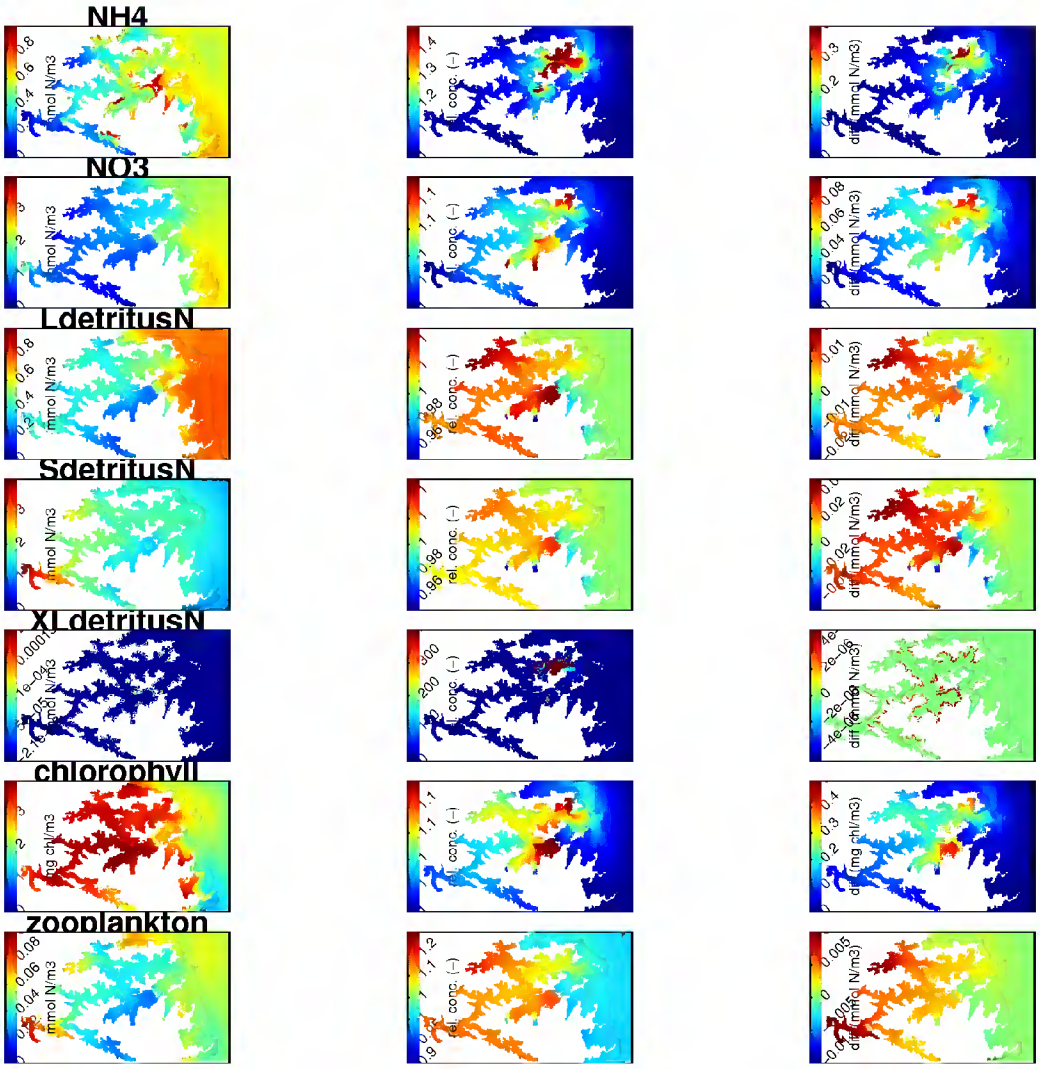

Figure 5-20: Comparison of summer time-averaged surface-layer concentrations in the EM-EF-WD and AM-AF-WD scenarios. Refer to the caption of Figure 5-13 for further explanation. These results are from simulations made with 200 m horizontal resolution.

5.4.5 "Existing mussel/no fish/with denitrification" versus "existing mussel/no fish/no denitrification"

Figure 5-21 (winter, surface layer) and Figure 5-22 (summer, surface layer) illustrate the differences between the EM-NF-WD[34] and EM-NF-ND results. As expected, when benthic denitrification is turned off, the system retains more nitrogen – and this effect is greatest in the shallower regions that are far from the Cook Strait mouth of Pelorus.

During winter, ammonium concentrations are predicted to rise by up to about 50% within Hikapu & Popoure reaches and Kenepuru. Nitrate is also predicted to rise by up to about 25% in inner Kenepuru (and 10–20% elsewhere). Phytoplankton concentrations increase very slightly (max

[34] Note, this reference scenario (EM-NF-WD) differs from the one (EM-EF-WD) that has been adopted previously.

increase circa 0.01 mg Chl m^{-3} within Kenepuru). Zooplankton concentrations are predicted to almost double in inner Kenepuru and to increase by 10–50% elsewhere in inner Pelorus.

During the summer, the changes are of similar nature, but larger magnitude. For example, chlorophyll concentrations are predicted to rise almost two-fold (an extra 3–4 mg Chl m^{-3}) in inner Kenepuru and zooplankton concentrations are predicted to rise more than 10-fold in that region.

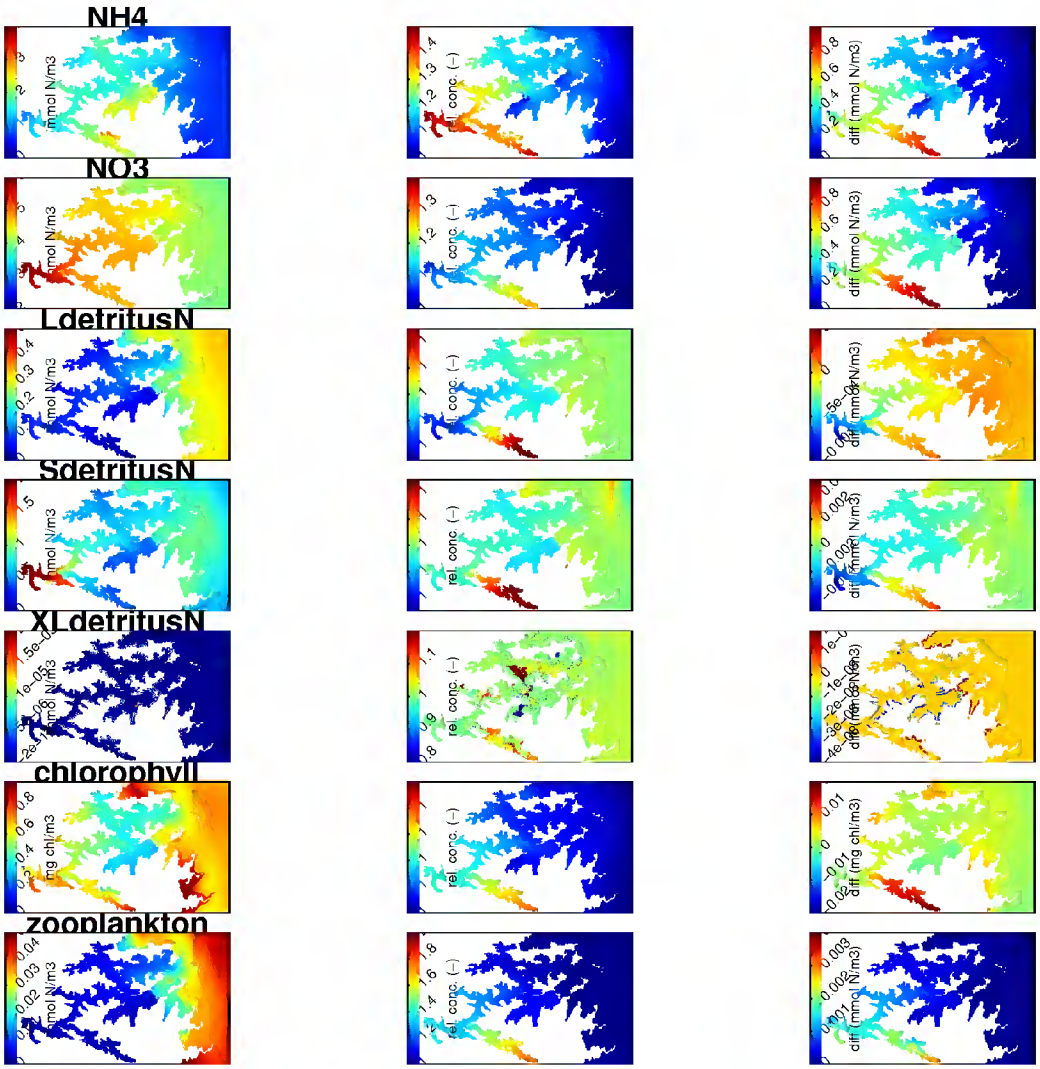

Figure 5-21: Comparison of winter time-averaged surface-layer concentrations in the EM-NF-WD and EM-NF-ND scenarios. Note that the reference simulation is EM-NF-WD rather than EM-EF-WD that was used for most other plots. Refer to the caption of Figure 5-13 for further explanation. These results are from simulations made with 200 m horizontal resolution.

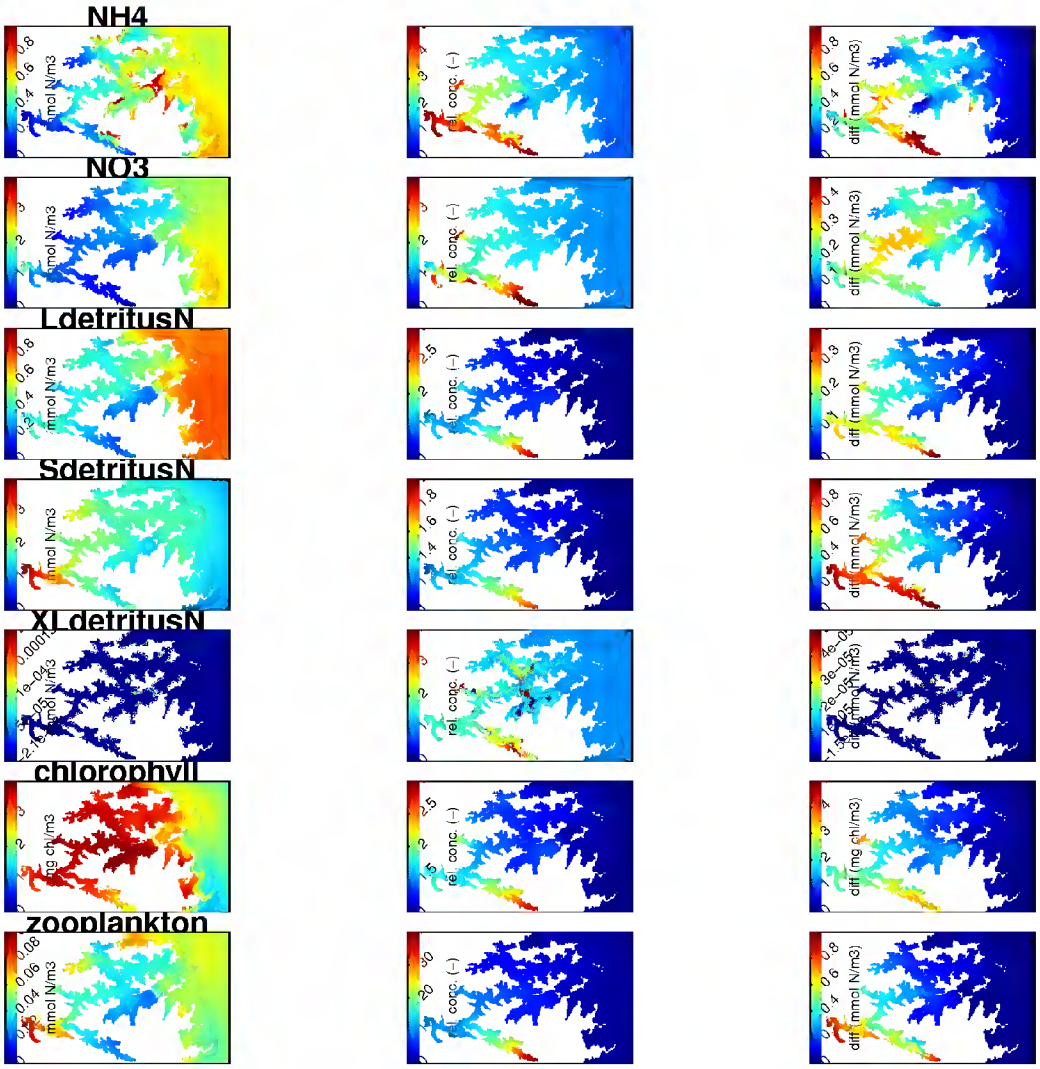

Figure 5-22: Comparison of summer time-averaged surface-layer concentrations in the EM-NF-WD and EM-NF-ND scenarios. Note that the reference simulation is EM-NF-WD rather than EM-EF-WD that was used for most other plots. Refer to the caption of Figure 5-13 for further explanation. These results are from simulations made with 200 m horizontal resolution.

5.4.6 "Existing mussel/existing fish/with denitrification" versus "approved mussel/approved fish/no denitrification"

Finally, in Figure 5-23 (winter, surface layer) and Figure 5-24 (summer, surface layer), results from the EM-EF-WD and AM-AF-ND simulation are compared. As expected, the combination of turning off nitrogen removal and adding more nitrogen into the system (from the additional fish farms) causes the concentrations of all state-variables to rise (the few additional mussel farms cannot induce sufficient depletion to offset this). Again, the changes tend to be much greater in summer than winter. Even in the summer, however, ammonium concentrations remain low relative to those that are toxic and time-averaged chlorophyll concentrations remain below 5 mg Chl m^{-3} throughout the Sounds[35].

[35] In the EPA Board of Inquiry decision into New Zealand King Salmon Ltd's application for additional farms, chlorophyll concentrations that are persistently (annual average) greater than 5 mg Chl a m^{-3} were deemed to be unacceptable Whiting, G., Beaumont, H., Ellison, E., Farnsworth, M., Briggs, M. (2012) Board of Inquiry New Zealand King Salmon requests for plan changes and applications for resource consents: 356.

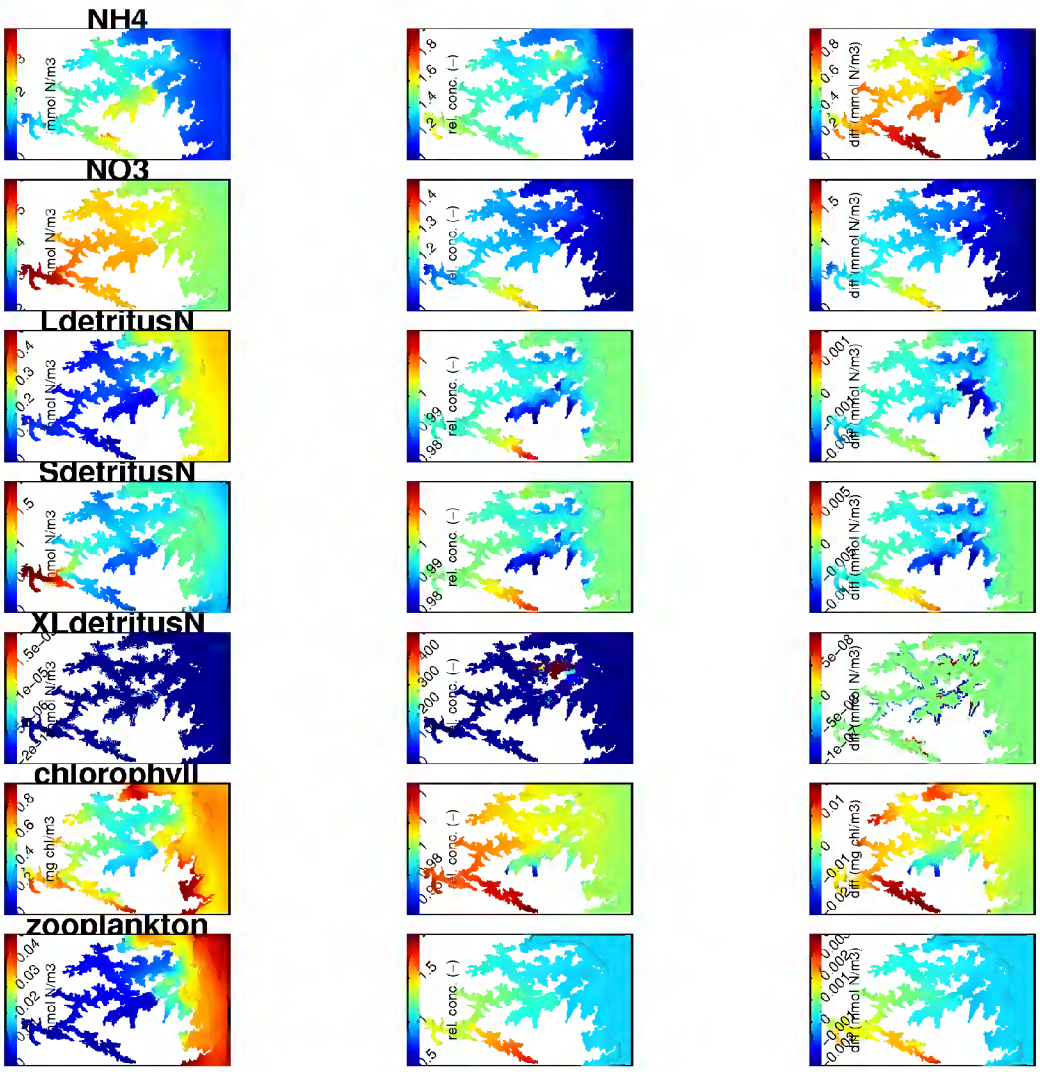

Figure 5-23: Comparison of winter time-averaged surface-layer concentrations in the EM-EF-WD and AM-AF-ND scenarios. Refer to the caption of Figure 5-13 for further explanation. These results are from simulations made with 200 m horizontal resolution.

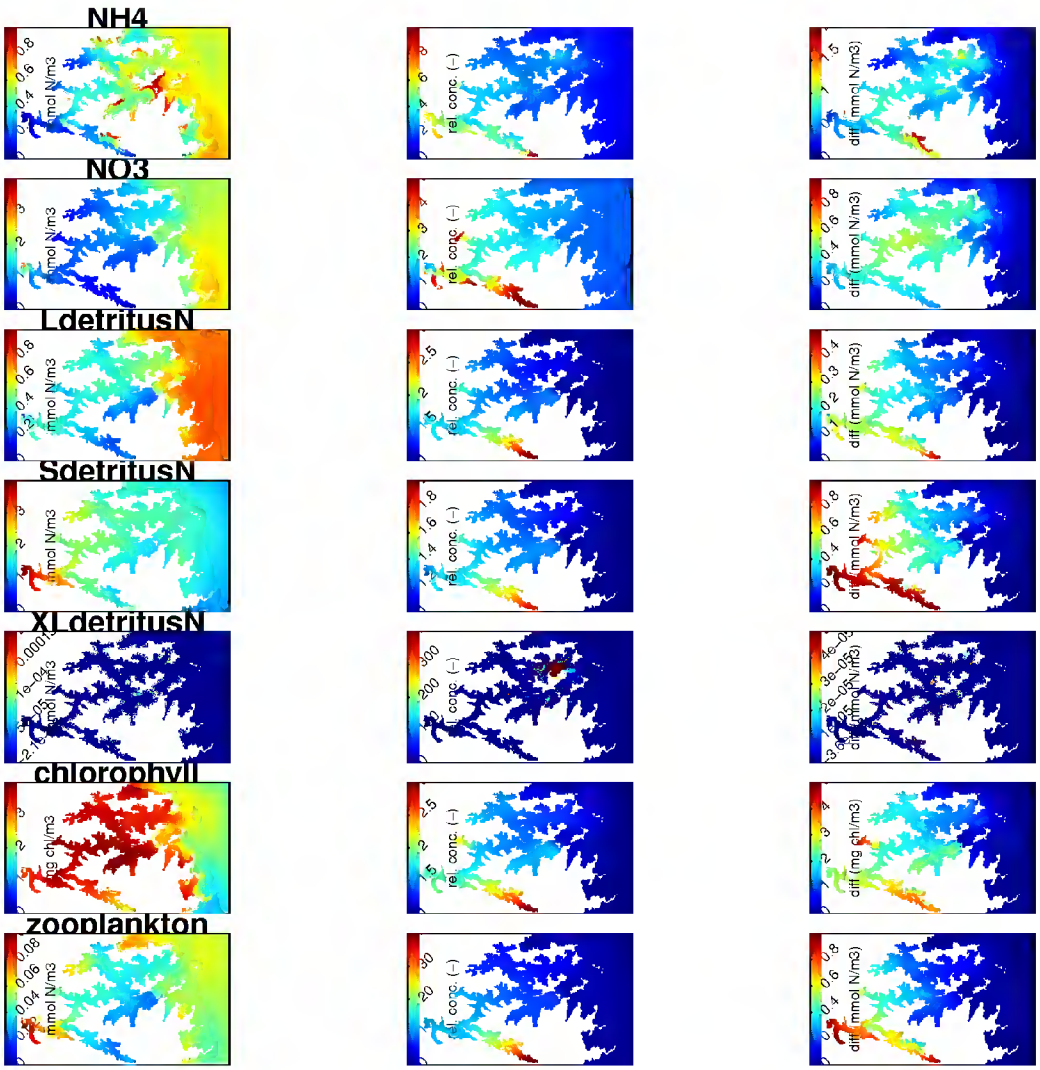

Figure 5-24: Comparison of summer time-averaged surface-layer concentrations in the EM-EF-WD and AM-AF-ND scenarios. Refer to the caption of Figure 5-13 for further explanation. These results are from simulations made with 200 m horizontal resolution.

5.5 Concentration changes in near-bed waters

The preceding sections have shown results from the surface-most layer of the model. We believe that the patterns will be similar throughout the vertical extent of the surface mixed layer that exists for much of the year within the Pelorus system. There are, however, reasons to believe that patterns may differ below the surface mixed layer. Firstly, there is less light at depth, so phytoplankton will be less able to respond to any fish-farm derived nutrient. Secondly, the mussel and fish-farms will not extend far (if at all) below the mixed layer, so seston will feel only weak (or indirect) effects of the farms. Finally, the main channel of Pelorus exhibits a strong estuarine flow. Water in the upper 20 m or so tends to flow out of the Sound into Cook Strait whilst deeper water flows into the Sound from Cook Strait.

Appendix E presents pictures (of the near-bed layer) that are conceptually equivalent to those presented for the surface layer within the preceding sub-sections. As one might expect:

- "Cook Strait-like" water-properties extend far further into Pelorus near-bed than near-surface. Furthermore, the change from Cook Strait-like to (inner) Pelorus-like is more gradual at depth (c.f. almost a sharp front at the Cook Strait mouth in the near-surface layer).
- Nutrient concentrations tend to be higher near-bed than near-surface (esp. in summer). Conversely, plankton concentrations tend to be lower.
- Effects of mussel farms and fish farms upon seston tend to be smaller near-bed than near-surface.
- In some instances, the effects of mussels and fish-farms upon nutrient may be greater near-bed (presumably, because XLdetritus from the farms quickly sinks to the bed and a fraction of that mineralizes into nutrient that returns the bottom-most layer).
- Turning off benthic denitrification has a larger impact upon near-bed nutrient concentrations than it has upon near-surface concentrations.

Despite these differences, the general inferences that can be drawn from the near-bed plots are similar to those that can be drawn from the near-surface ones:

- Mussel-farming (at today's extent) has greater influence upon water-quality than fish-farming (at today's extent).
- Increasing the scale of mussel and fish farming will induce further change (almost universally amounting to <10% percent of today's conditions (in a time-average), depending upon which property one chooses to examine and when/where one chooses to look).
- In the unlikely event that all benthic denitrification within the Pelorus system were to cease and mussel and fish-farming were to expand from today's operational farms to all consented farms, the time-averaged chlorophyll and detritus concentrations may double in the central and inner (especially Kenepuru) regions, but the seasonal average would remain below 5 mg Chl m^{-3}.
- The water-quality of Kenepuru and Beatrix/Crail/Clova (and, to a lesser extent, the landward reaches of Tawhitinui Reach) are more sensitive to changes in denitrification, mussel-farming and (even spatially distant) fish-farming than are the parts of the Sound that lie close to (or within) the main axis of estuarine flow.

5.5.1 Simulated changes of instantaneous water-quality at the seven MDC sampling stations

Figure 5-25 to Figure 5-31 illustrate the simulated dynamics of each state-variable in the near-surface layer at each MDC water-quality sampling station under five of the six different scenarios[36]. As noted earlier, the primary purpose of these plots is to demonstrate that the time-averaging process that was employed to generate the false colour plots (presented in the previous section) has not masked short-lived-but-much-larger differences between the dynamics stemming from differing scenarios. The plots certainly reveal that the time-averaging masks substantial high frequency (days to fortnight time scale) variations within any one scenario, but the patterns of fluctuations are similar across all scenarios. Thus, within any given season, the magnitudes of differences between scenarios remains similar day-to-day. The time-averaging is not masking short-lived-but-much-larger between scenario differences.

That is not to say that the between scenario differences are always small. Clearly:

- simulated 'present day' dynamics (EM-EF-WD) are markedly different from those of a notional, historical system in which catchment and oceanic inputs remain the same as they are now but neither mussel, nor fish-farms are present (NM-NF-WD),
- similarly, the model simulations indicate that, were benthic denitrification to cease *throughout* the domain (scenarios EM-EF-ND and AM-AF-ND), the system's dynamics would change markedly.

On the other hand, the model simulations indicate that the incremental changes (from the 'existing situation') associated with adding already-approved-but-not-operating marine farms will be small at the seven Marlborough District Council water quality sampling stations[37].

[36] To avoid generating even more cluttered/confusing plots, the sixth scenario was excluded from these plots. Results from that scenario are no more extreme.

[37] The MDC sampling stations are not close to any of the forthcoming new fish- or mussel farms. The incremental changes in the immediate vicinity of the new farms may be larger (see for example, Figure 5-19 & Figure 5-20).

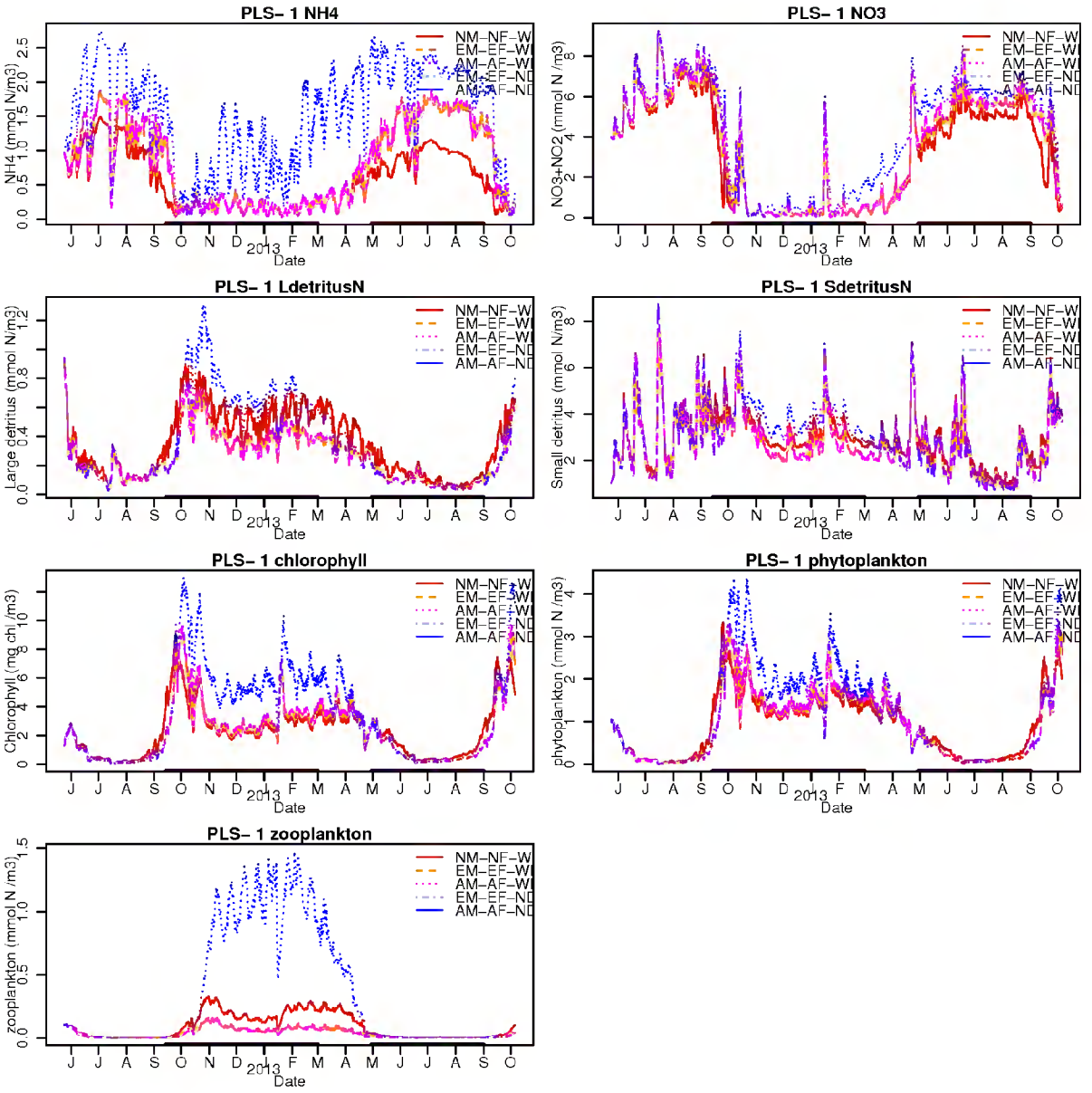

Figure 5-25: Simulated time-series of each state-variable in the surface-most layer at station 1 for five scenarios. The thick black lines running along the bottom of each plot indicate the periods used to produce the time-averaged plots. In this figure and the subsequent ones (for other MDC sites), the results for the EM-EF-ND and AM-AF-ND scenarios are almost coincident with one another (such that it is difficult to distinguish two separate lines). Similarly, the results from EM-EF-WD and AM-AF-WD are almost indistinguishable.

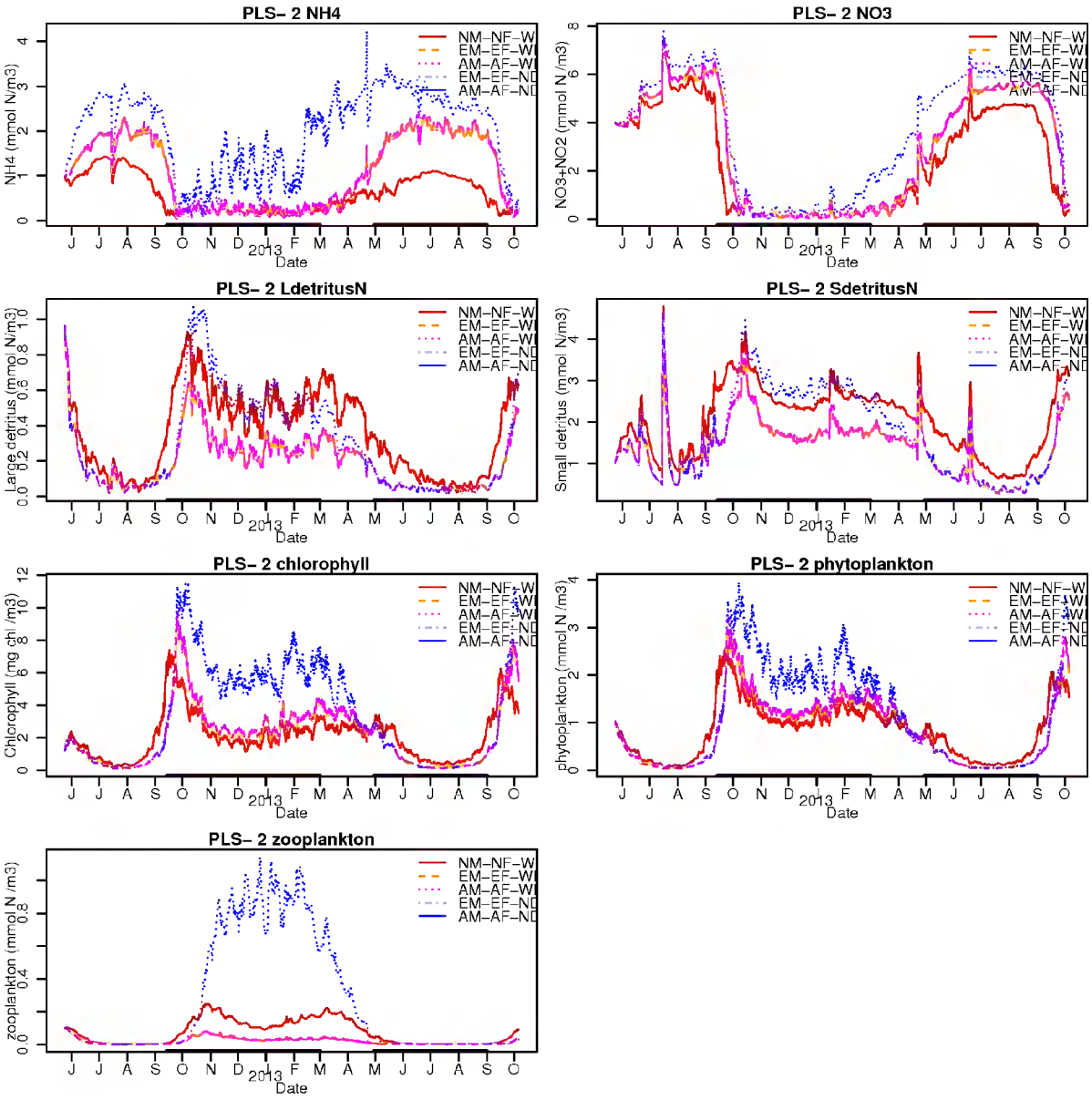

Figure 5-26: Simulated time-series of each state-variable in the surface-most layer at station 2 for five scenarios.

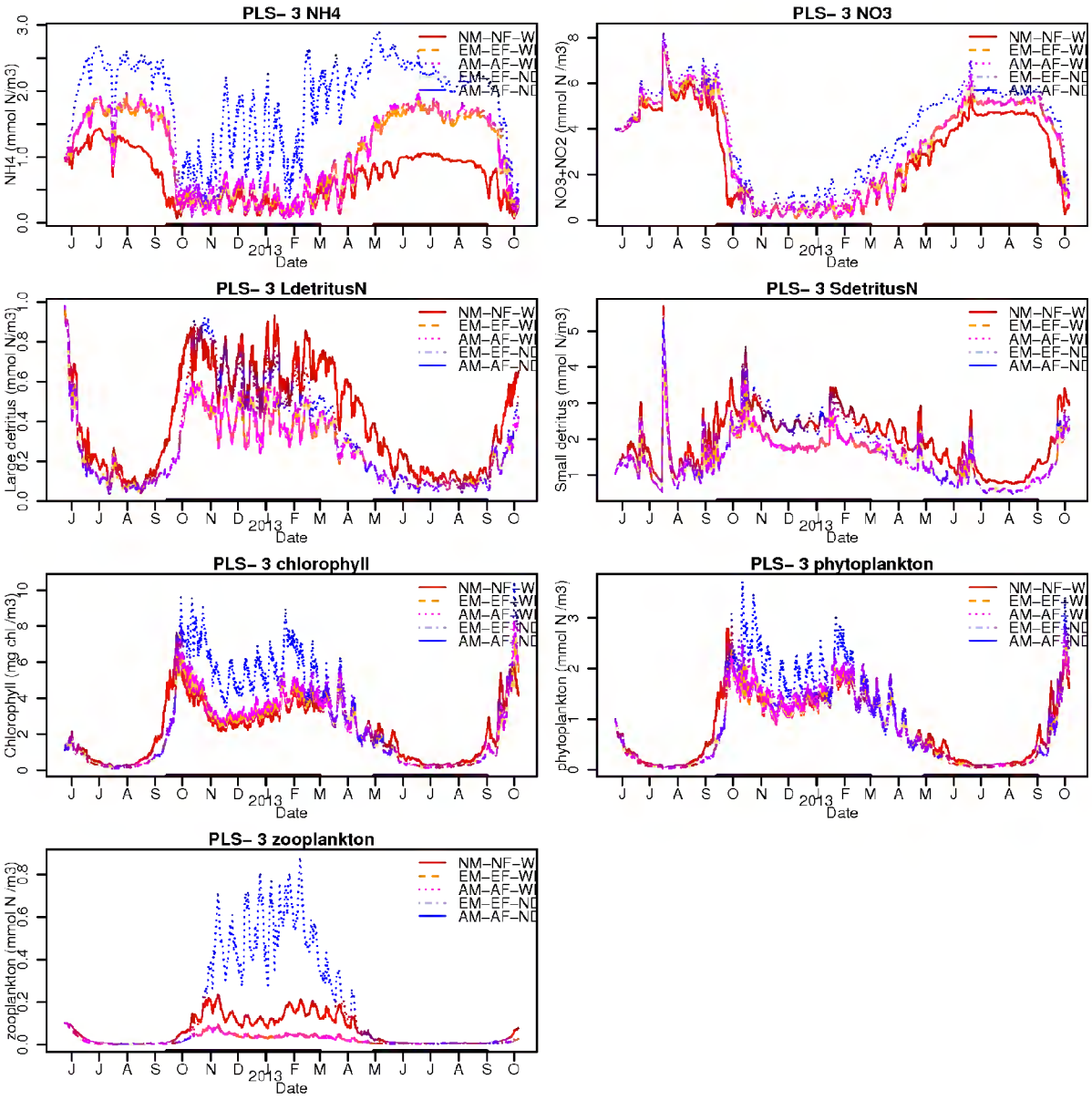

Figure 5-27: Simulated time-series of each state-variable in the surface-most layer at station 3 for five scenarios.

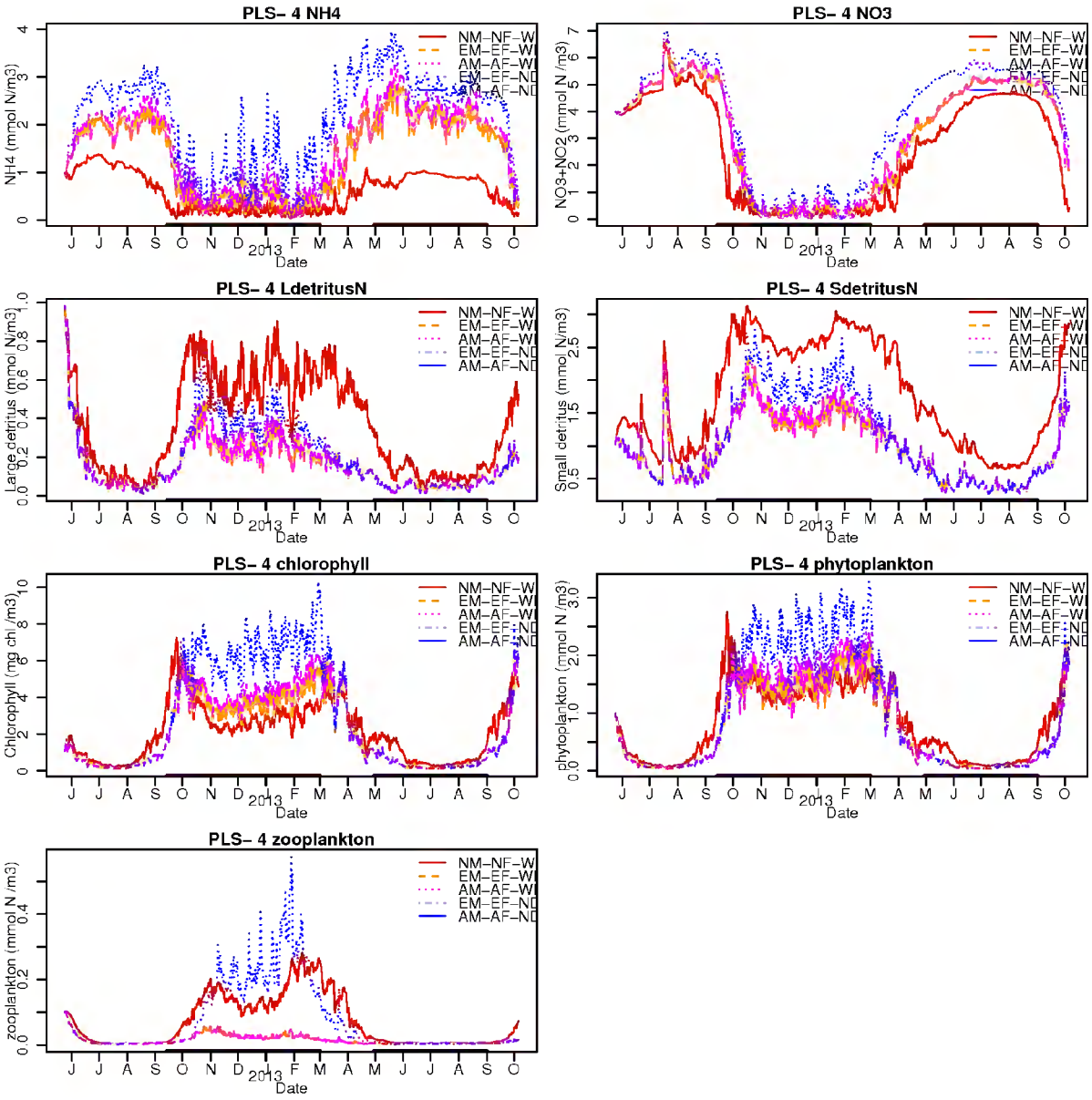

Figure 5-28: Simulated time-series of each state-variable in the surface-most layer at station 4 for five scenarios.

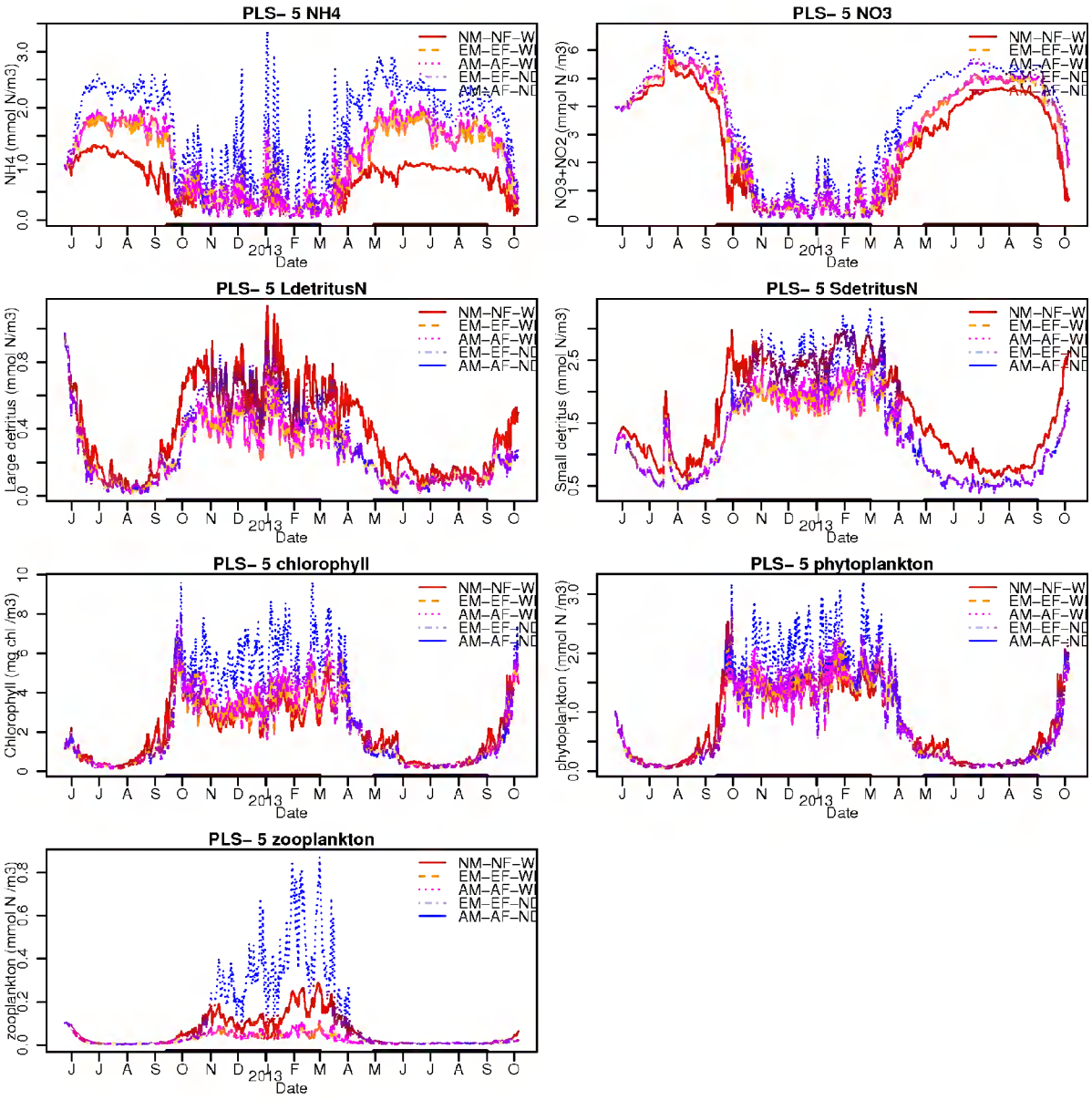

Figure 5-29: Simulated time-series of each state-variable in the surface-most layer at station 5 for five scenarios.

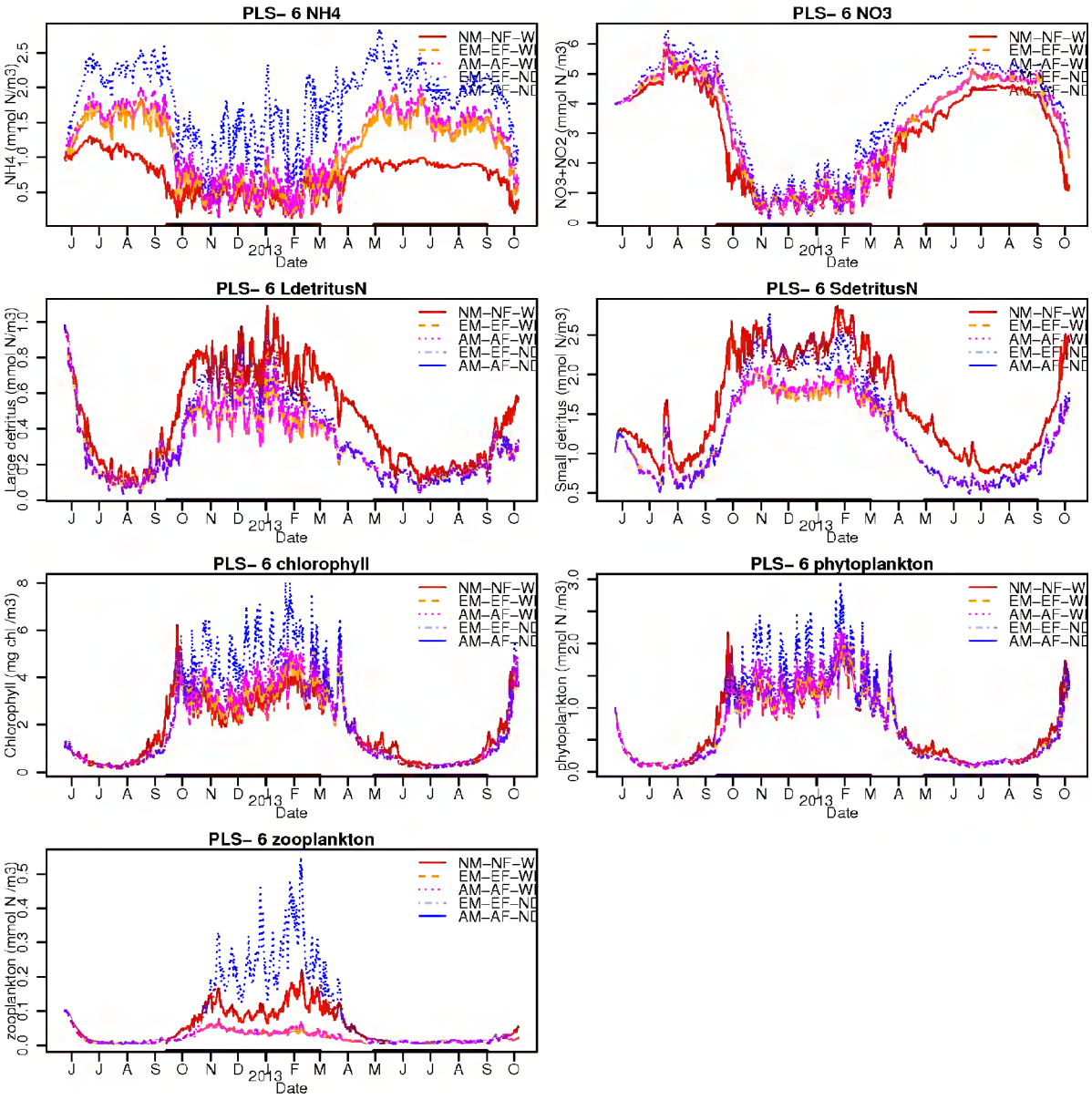

Figure 5-30: Simulated time-series of each state-variable in the surface-most layer at station 6 for five scenarios.

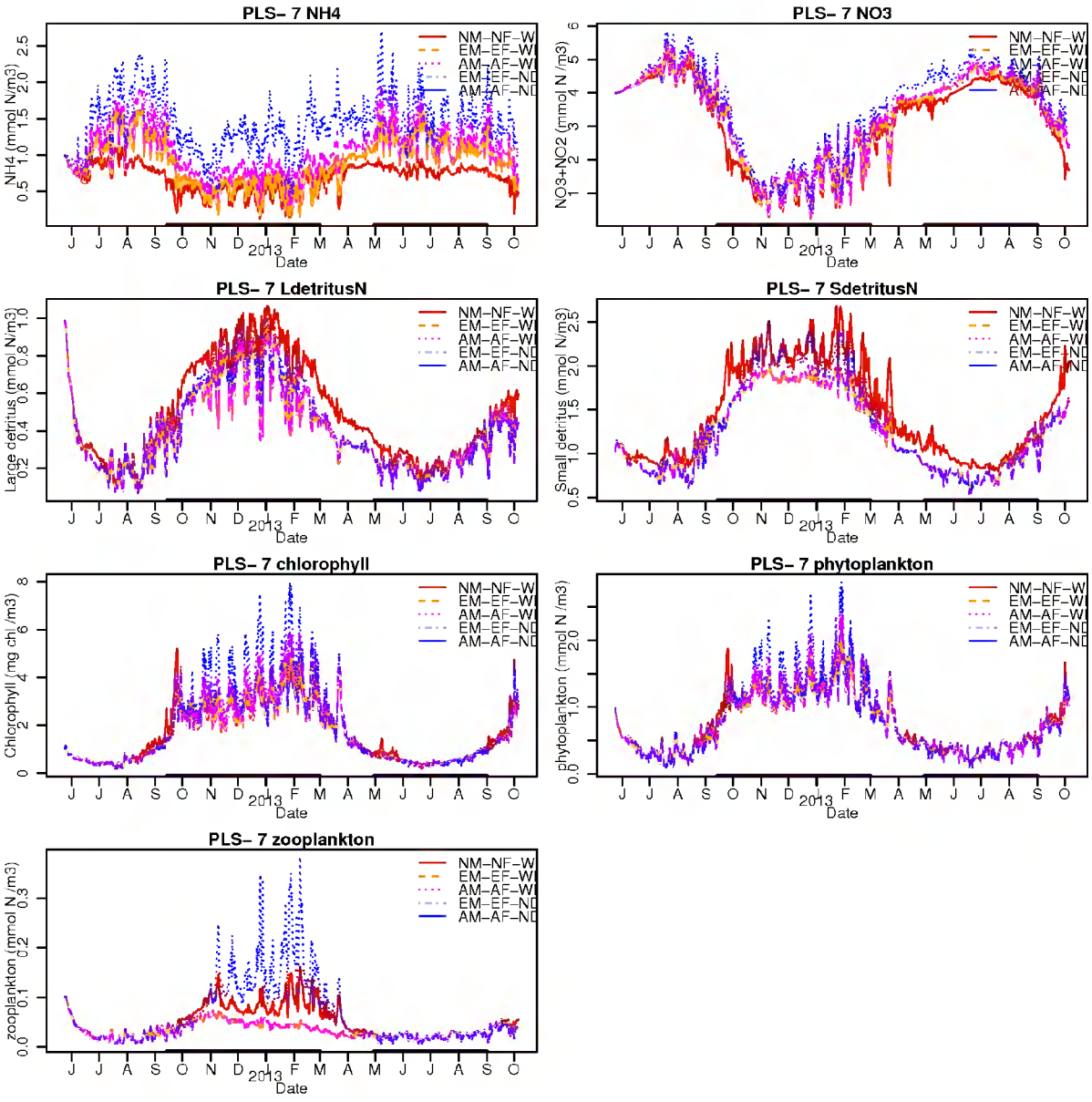

Figure 5-31: Simulated time-series of each state-variable in the surface-most layer at station 7 for five scenarios.

5.6 Comparison of the farming induced nitrogen fluxes

Figure 5-32 illustrates the magnitudes of the mussel farm nitrogen uptake and release fluxes at the whole-of-domain spatial-scale. In the graph, negative values imply that the material in question is suffering net removal from the water-column through the activity of the mussels. Conversely, positive values indicate net addition. The graph reveals that (in the model) the mussels gain the majority of their nutrition from small detrital material (grey) and from phytoplankton (red). This is a simple consequence of the greater abundance of these materials relative to zooplankton and large detritus (which the mussels also consume). The combination of higher summertime water temperatures (permitting greater specific filtration rates by the mussels) and higher summertime seston concentrations imply that the rates of ingestion and faeces/pseudofaeces production are

several times greater in summer than in winter. Ammonium release rates are also higher in summer, but the amplitude of the annual cycle of ammonium production is much smaller than that of (pseudo)faecal production. At the height of summer, the rate of nitrogen release as (pseudo)faeces slightly exceeds the rate of ammonium release, but for most of the year ammonium release rate is substantially greater than rate of release of nitrogenous detritus.

Figure 5-33 illustrates the temporal patterns of nitrogen release as (faeces, XLdetritusN) and as ammonium for the existing fish farms in Pelorus Sound. Ammonium excretion tends to be highest in summer reflecting the influence of water temperature upon basal respiration, and the fact that fish are growing most rapidly at that time of year. It also shows the feed input (as nitrogen). The feed input changes month-to-month in a stepwise manner – reflecting the fact that we made no attempt to smooth (interpolate) daily values from the monthly total feed input rates provided to us by NZKS Ltd. Rather, we calculated an average daily rate for each farm for each month and applied those rates throughout the month. Ammonium and detrital N production rates also change in stepwise manners, but the changes are less abrupt because there are various buffering/smoothing mechanisms within the model. For example, ammonium excretion arising from basal respiration is a significant part of the total ammonium flux. Its production rate is a function of fish size and water temperature but not of feed inputs. Total fish farm nitrogen input into the environment (sum of detritus and ammonium) is circa 1 tonne d^{-1}. During the summer months, this is considerably greater than the net nitrogen release rate from mussel crop (a negative value, indicating net nitrogen removal from the water-column into mussel flesh), but a bit less than the nitrogen loss from the mussel crop during winter (net export of flesh nitrogen into the water-column – indicative of condition loss).

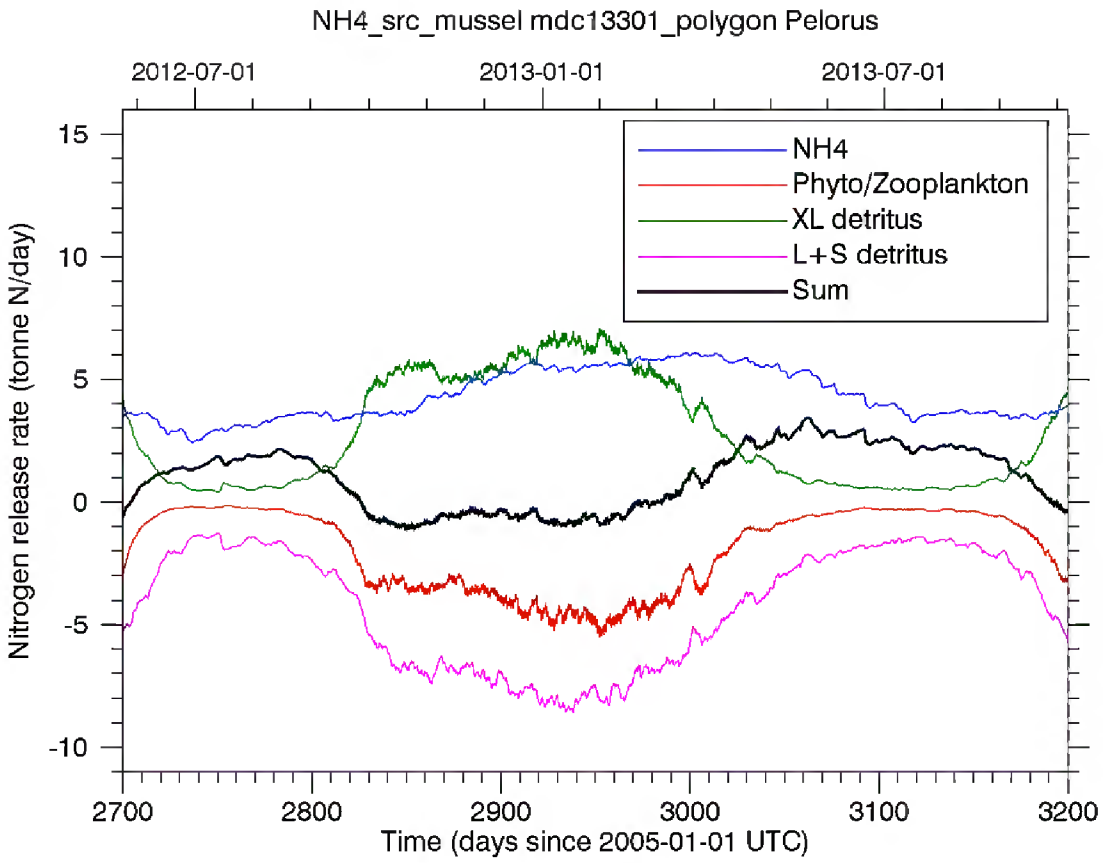

Figure 5-32: Nitrogen uptake (negative) and release (positive) release rates associated with mussel ingestion, respiration and excretion. blue - mussel excretion of ammonium; red – mussel ingestion of nitrogen within plankton; pink – mussel ingestion of small and large detrital nitrogen; green – mussel net egestion of extra large detrital nitrogen (faeces & pseudo-faeces); black – net sum (total egestion - ammonium excretion – total ingestion).

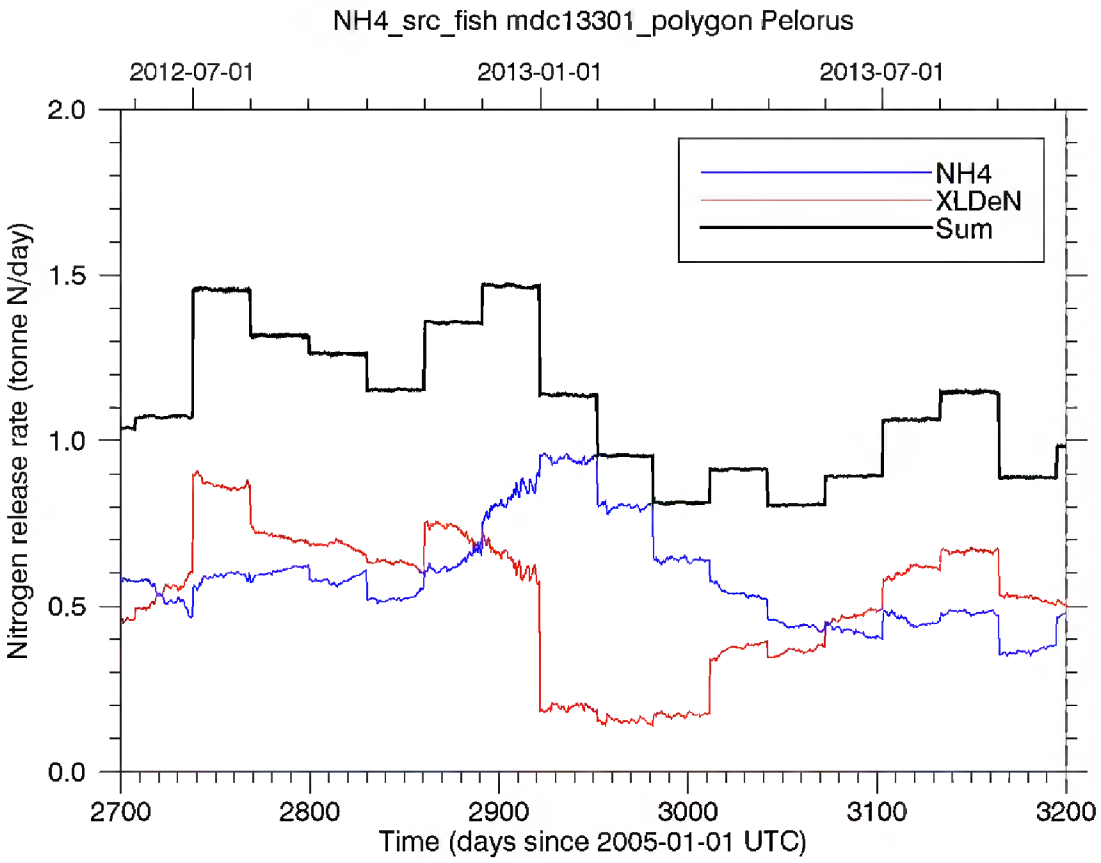

Figure 5-33: Nitrogen release to the water from fish farms. Red: sum of uneaten food and faeces; blue: ammonium excretion; black: sum of excretion and faeces/uneaten food.

6 Biophysical model: Discussion

6.1 Limitations of the biophysical model

Like all models, our biophysical model embodies many simplifications relative to reality. The foodweb is truncated. The highest explicit trophic group is zooplankton. The influence of predators of zooplankton is represented by imposing a specific mortality rate (d^{-1}) upon the zooplankton. In particular, the Fennel model assumes that the specific mortality rate increases linearly with rising zooplankton abundance. This assumption is not atypical of NPZD models, but Steele and Henderson (1992) and Edwards and Yool (2000) have shown that the dynamics of a nutrient-phytoplankton-zooplankton model can be very sensitive to the form (and parameterization) of this top-level predatory closure term. Under some situations, the system can be induced to exhibit high frequency oscillations (alternating booms and busts) even in an otherwise constant environment. The fact that the Fennel model assumes that the specific mortality rate increases linearly with rising zooplankton abundance reduces the likelihood of such oscillations. The implication is that it is possible that the Fennel model may under-estimate the frequency and/or extent of short-lived algal blooms. We have chosen to focus our attention upon time-averages. These are likely to be less sensitive to the form of the mortality closure term.

The model foodweb is deliberately simple. It does not include higher trophic levels. Perhaps more importantly, it does not include bacteria or macroalgae. Like the phytoplankton, bacteria and macro-algae will consume farm-derived nutrients. Since the model lacks these two groups, the phytoplankton have exclusive access to the farm derived nutrient. Since the model phytoplankton do not have to 'share' the fish-farm-derived nutrient with other taxa, it seems probable that the model over-estimates the extent to which the phytoplankton community may change (increase) in response to farm-derived nutrient. Another manifestation of the model's simple foodweb is that it contains only one phytoplankton group. In reality, the phytoplankton community of the Marlborough Sounds is composed of several tens of species. At any instant, phytoplankton biomass will be dominated by only a few species, but the dominant species change in a characteristic way through the year – primarily because differing species have differing nutrient and light requirements. As an emergent property, the apparent (emergent) kinetic 'coefficients' that govern nutrient-uptake and photosynthesis etc., of the real-world phytoplankton population change through the year. Since the model has only one phytoplankton group, it will not mimic these changes well and this may be one of the reasons that the model does not always adequately reproduce all aspects of the field data.

Some phytoplankton taxa are motile – notably dinoflagellates. Dinoflagellates comprise 10-50% of the Pelorus Sound phytoplankton community by biomass (in the >2 μm fraction). Motile algae have a competitive advantage in stratified waters that have a nutrient-depleted surface layer. This is because motile individuals are able to either: (a) actively hold position at a depth where photosynthetic- and nutrient-acquisition rates can be balanced, or (b) migrate between nutrient-rich deeper waters (where they can replenish their internal nutrient stores) and the light-rich surface layers (where they can replenish their carbon stores). The fact that the phytoplankton of the Fennel model are non-motile may help to explain why it fails to reproduce the deep chlorophyll maxima that are common in some parts of Pelorus Sound.

In the model, the instantaneous intensity of incoming photosynthetically active radiation (PAR) is derived from the user-specified incoming short-wave radiation. We used the short-wave radiation time-series stemming from the NCEP Reanalysis. This is a global product at 2 degree resolution. Real-world incident short-wave radiation in the Marlborough Sounds may differ from this synthetic time-

series (because of local, perhaps seasonally varying, effects such as cloud-cover, atmospheric dust and sub-2-degree scale latitudinal variations).

PAR is almost entirely restricted to the visible spectrum, but this is composed of light of many wave-lengths. Even pure water absorbs some wave-lengths of visible light (e.g., red) much more strongly than others (e.g., green). The PAR attenuation coefficient represents an empirical measure of PAR absorption. Because it is PAR-based (rather than wave-length specific), its value tends to decline with increasing depth (as the residual PAR becomes increasingly concentrated in the weakly absorbed wave-lengths). The Fennel model does not break PAR down into multiple wave-length bands. Thus, it cannot take account of this subtlety. Our estimate of the PAR attenuation coefficient is based upon PAR measurements made from more than 8 m below the sea-surface. By this depth, all the strongly absorbed PAR wavelengths (which make up about 50% of the visible spectrum at the sea surface) have disappeared. The implication is that we are probably over-estimating the quantity of PAR which penetrates to 8 m and deeper. To some extent, this can be (and has been) accommodated through calibration of the initial slope of the photosynthesis-irradiance curve (to data from Queen Charlotte Sound during an earlier modelling exercise), but it is possible that this weakness in the model is responsible for some of its deficiencies with respect to reproducing the field data.

Finally, we have chosen to make long-term simulations on a grid having 200 m horizontal resolution. Long term simulations would have been prohibitively expensive on a finer grid (Table 2-1). 200 m resolution is approximately the size of the collective pen structures that comprise a fish farm. The biophysical model does not have sufficient resolution to properly represent the steep concentration gradients (for example, of ammonium and very large detritus) that will exist in the immediate environs of a farm. Specifically, it will exhibit excessive numerical dispersion such that it will tend to under-estimate concentrations very close to the farm, and, perhaps, over-estimate them slightly further afield. At greater distances (perhaps, >1 km), natural dispersion will have eroded the steep gradients so the excessive numerical dispersion is of lesser import and the simulated concentrations will be more reliable. If near-field concentrations are to be examined using this model, we would need to adopt a finer grid (e.g., 50 m or finer resolution) and restrict ourselves to simulating shorter calendar periods.

6.2 Model skill

We noted that the model appears to have lower skill for phytoplankton (carbon biomass and chlorophyll) than for other state-variables. We believe that this is a misleading conclusion that stems from an inconsistency between the phytoplankton communities represented in the model and in the data. The model community is 'total phytoplankton' (all size-classes). In contrast, the phytoplankton community sampled in the field is phytoplankton larger than approximately 2 µm (being the nominal pore size used when filtering for chlorophyll and the approximate minimum dimension of cells that can be reliably seen and measured under the optical microscope). The size-structure of the phytoplankton community within Pelorus Sound is not well known, but Safi and Gibbs (2003) report that between May 1999 and September 1999 (incl.), an average of 29% (range 8–65%) of the total phytoplankton chlorophyll was composed of phytoplankton <2 µm. Thus, it should come as no surprise that the total phytoplankton (as simulated in the model) exceeds the phytoplankton (>2 µm) measured in the field. Indeed, it would be disturbing if the modelled phytoplankton did not exceed the field phytoplankton. Thus, whilst our naïve comparison between modelled phytoplankton and field phytoplankton appear to indicate that the model reproduces phytoplankton less well than it reproduces other state-variables, we are satisfied that that is not the case.

Nonetheless, we certainly cannot claim that the model is reproducing the dynamics of any of the state-variables very well.

There are several reasons why this should not be overly surprising:

- we have made no attempt to calibrate the model to the field-data
- the model has no ability to mimic seasonal changes in phytoplankton community structure
- our Cook Strait boundary conditions are based upon scarce field data (just one year's worth of monthly measurements at only two depths). Furthermore, the raw-data were smoothed before being applied as boundary conditions
- the insolation intensities that are applied are not corrected for possible seasonal-scale variations in cloud-cover or seasonal and hour-by-hour variations in topographic shade (though the latter will be significant only in narrow parts of the Pelorus system)
- the hydrodynamic model is yielding summertime water temperatures which are a bit too low. Since phytoplankton and zooplankton physiology is temperature dependent, this (or possibly incorrect parameterisation of the temperature dependence) could have subtle influences upon emergent population growth rates and standing stocks. We emphasize that the temperature effects that are mediated through physiological changes are likely to be small. As a rule of thumb, the rates at which physiological processes proceed approximately double for each 10 °C temperature increment[38]. Thus, the fact that simulated summertime water temperatures are approximately one °C too low implies that all temperature-dependent rates (primarily, ingestion (hence, egestion) and respiratory excretion) will be underestimated by about 5-10%
- the wind-fields that are applied derive from wind models that have low spatial resolution relative to widths of the Pelorus Channel. In combination with the steep topography, this implies that surface-flows and wind-driven mixing may not be well represented in the hydrodynamic model.

No specific numerical performance criteria have been set by which to assess the biophysical model's performance. In the context of this work, we are endeavouring to determine the relative changes induced by shellfish farming and fish-farming. With that in mind, it is appropriate to ask: 'does it matter that the model's performance is merely poor-moderate. For the reasons outlined in the following paragraph, we believe the answer is 'not greatly'.

Shellfish filter particulate matter out of the water column. The mussel model explicitly assumes that the quantity of water that each mussel pumps across its gills (the filtration apparatus) is independent of seston[39] concentration. Thus, the daily specific gross capture rate for seston is not influenced by the absolute quantity of seston in the water. On the other hand, the fraction of the captured seston that passes into the gut (rather than being rejected and converted to pseudo-faeces) is assumed to decline as the capture rate increases. That is, the relative quantity of captured seston that is rejected

[38] This is a rule-of-thumb that applies within an ectothermic organism's 'tolerable temperature range'. At more extreme (low or high) temperatures, the rates will drop rapidly toward zero due to temperature-induced damage to enzymes and cell structures. Differing functional forms (and/or coefficient values) have been adopted to describe the temperature dependencies of the various planktonic growth processes and mussel/fish ingestion, egestion and respiration processes (see appendices) but none imply a temperature-dependence that is markedly different from two-fold for ten degrees.

[39] Small, particulate organic matter in suspension within the water column (particulate organic detritus, phytoplankton and zooplankton)

as pseudofaeces (hence, returned to seston) increases with seston concentration. This means that even if the model over-predicts absolute seston concentration and, in consequence, initial capture of seston by mussels, much of 'excess' seston will be returned to the water-column (as pseudo-faeces-seston) rather than becoming incorporated into 'excess' mussel flesh (in effect, removed from the system).

Consequently, we infer that the model should be capable of adequately predicting near-field seston depletion levels if the near-field hydrodynamics are correct. Far-field change will be determined by a combination of many factors (hydrodynamics, plankton growth rates, detrital remineralization and settling rates etc.). The data do not allow us to determine whether the individual rates are close to being correct, but the fact that the far-field standing stocks are 'about right' on average offers some encouragement.

In the context of this model, fish farms are a source of nitrogen (as ammonium and particulate organic detritus). The rates of ammonium and detritus input are strongly correlated with the user-supplied fish-feed input rates, but also influenced by the parameterisation of the fish-physiology model. Those fish-feed input rates were based upon monthly rates provided to us by New Zealand King Salmon. We have recorded (but not reported) the derivative ammonium and detritus input rates calculated by our model and they are consistent with the prescribed inputs. It is worth emphasizing that the fish feed input rates reported by NZKS for the 2012/13 year were lower than they had been in earlier years – feed inputs had been reduced in order to reduce adverse impacts upon the seabed. Consequently, the nitrogen input rates for our *existing farms* scenario were lower than the maximum permitted by the consent conditions. By definition, that is appropriate for the *existing farms* simulation, but for the *approved farms* simulation it is less clear that this is appropriate. Nonetheless, for the most part, we chose to assume that the existing Pelorus fish farms would continue to operate in the same way as they did in 2012/13. The exceptions were Crail Li32 and Crail Li48. In reality, these were fallowed during 2012/13, but we assumed that they would be operating at their maximum permitted annual feed input rates in both the *existing* and *approved* farm scenarios.

The location (spatial and foodweb-level) and magnitudes of fish-farm induced change are dictated by myriad processes (currents, mixing, detrital sinking and mineralization rates, kinetics of plankton growth etc.). The hydrodynamic model has been shown to reproduce currents in the main stems of Pelorus moderately well (section 3.) The key biological processes governing how quickly (and how much) farm-derived nutrient is incorporated into the food chain are:

- Detrital denitrification rates.
- Detrital mineralization rates.
- Phytoplankton growth rates (particularly under nutrient-limiting conditions).

We have already established (section 5.2) that the denitrification rates are consistent with those measured in Pelorus Sound. Using the model output, it is possible to draw up nitrogen budgets. We do not present these in detail but the key conclusions are:

- At the whole of Pelorus scale, denitrification at the seabed (rather than export to Cook Strait) is the dominant means by which farm-derived nitrogen is removed from the system.

- Under the 'existing farms' scenarios, there is a net import of nitrogen from Cook Strait into Pelorus. Under the 'existing+approved farms' scenarios, there is a net export of nitrogen from Pelorus into Cook Strait.

We do not have data with which to validate any of the other biogeochemical rates predicted by our model but the coefficients that we have adopted to describe the various rate processes are typical of those seen in the water-column modelling literature. That said, though the specific detrital decay rates (0.01 d^{-1}) that we have adopted are typical of fresh plankton-derived material in the water-column (Enríquez, Duarte, Sand-Jensen 1993), they are high relative to those adopted when modelling the decay of fish-faeces in the seabed. For example, Brigolin, Pastres et al. (2009) adopted a value of 0.0027 d^{-1}. Since the bulk of farm-derived faeces will tend to arise in the summer, the implication is that too much of the farm-derived faecal nutrient will be mineralized during the summer (nutrient-limited months). Thus, the model may be over-estimating summertime fertilization potential. In reality, some of the faecal material which sinks to the seabed may not mineralize until autumn/winter. At that time of year, phytoplankton production will often be light-limited.

We have noted that, whilst the model appears to over-predict summertime, near-surface phytoplankton concentrations, there are reasons to believe that the over-prediction is not as bad as one might infer from a naïve comparison of simulation results (of total phytoplankton) and field-measurements (of phytoplankton > 2 µm). Caution must be applied whenever model results are compared with observations. It is not common practice to measure phytoplankton <2 µm in routine coastal plankton sampling (because the fine filters that are required to do so quickly become clogged with sediment and organic detritus).

6.3 Shifting baselines

In this work, we have regarded the 'existing conditions' simulation (i.e., EM-EF-WD) as our 'baseline'. Relative to that baseline, our modelling suggests that adding a (relatively) small number of additional mussel farms and three additional fish farms into the Pelorus system will induce water-quality changes that are small in comparison with present day seasonal variability. We have also shown that: (i) changes that might arise were benthic denitrification to be entirely lost[40] would be larger than those induced by the additional fish-farms and mussel farms that have been approved since 2010, (ii) that the changes arising from shifting from a notional 'no-farms' (i.e., pre-aquaculture development) stage to the present-day aquaculture stage ('existing farms') may have been several times greater than the changes that are predicted to be associated with the incremental addition of a relative small number of mussel farms [but a relatively large number of fish farms] between 2012 and a notional near-future state in which all of the approved mussel farms and forthcoming fish farms have been placed in the water.

In the model, all the simulated change that arises can legitimately be attributed to the aquaculture (we have changed nothing else in the model). In reality, however, the water-quality of the Sounds is likely to have been influenced by more than aquaculture expansion alone. Intensification of farming in some of the catchments may have caused nutrient inputs to climb. Probably more importantly, we believe that the nature of the seabed has changed dramatically over the past century. The evidence is laid out in detail within a recent report to Marlborough District Council (Handley 2015). In summary, there is substantial evidence that the surficial sediments of the seabed of Pelorus Sound

[40] An incomprehensibly unlikely event

used to be coarse grained sands, rock and biogenic reef (shellfish beds etc.). In contrast, the surficial seabed of Pelorus is now dominated by fine, soft, sediments. These are home to relatively few hard-bodied, long-lived organisms. We believe that the changes have been driven by a combination of increased sediment runoff from the catchment[41], over-fishing of historical shellfish beds, and destruction of biogenic structures on the seabed by shellfish dredges and other near-bed trawl devices. Collectively, the changes to the seabed may have changed its capacity to mineralize organic nitrogen and denitrify ammonium and nitrate.

We have no robust, quantitative measurements of the water-quality of the Sounds prior to the development of any aquaculture (or loss of seabed habitat and change in catchment inputs). We might be tempted to use the present model as a means of hind-casting the state of the system. Arguably, doing so is legitimate, but it is certainly fraught with difficulties. Our naïve 'no farms' simulation is unlikely to yield an accurate indication of the historical state of Pelorus water quality. We made no attempt to change the catchment inputs of nitrogen (or water volume, temperature etc.,) to reflect a reversion to a native forest catchment. We did not adjust the light attenuation coefficient to reflect a (presumed) lower concentration of suspended sediments (but, perhaps, higher dissolved colours) in the pristine waters of the historical Sounds. We did not make any attempt to modify the fraction of depositing particulate organic nitrogen which denitrifies to N_2 and nor did we make any attempt to introduce a population of benthic shellfish into the notional 'no farms' simulation. In short, our 'no farms' simulation is too simple/naïve for its results to be plausibly regarded as being representative of the past state of Pelorus water-quality.

By drawing upon data from analogous pristine catchments, it might prove relatively easy to develop plausible[42] (but always hypothetical) historical input loads for water and nutrient. We might also be able to develop plausible light attenuation coefficients and benthic grazing terms ,. Unfortunately, a fundamental scientific understanding of the manner in which seabed structure and faunal composition/activity etc., influence denitrification is poor. Developing plausible rules governing denitrification of sedimenting organic matter will certainly be much more difficult.

6.4 Implications of the biophysical modelling results: putting the changes in context

The MDC monitoring data indicate that near-surface nitrate concentrations vary more than ten-fold through the course of the seasons (Figure 5-1). Ammonium concentrations vary more than two-fold (Figure 5-2), phytoplankton and zooplankton concentrations vary five- to ten-fold (Figure 5-3 - Figure 5-10) and particulate detrital concentrations vary more than three-fold (Figure 5-4 - Figure 5-10). Even if one restricts attention to any one calendar month (taken from different years), the fluctuations can be substantial (compare pink and red circles and pink and blue triangles in Figure 5-4 - Figure 5-10). Unpublished historical data which NIWA gathered in Pelorus Sound indicates that a similar level of variability is also present there at a fortnightly time-scale.

Clearly, the predicted magnitudes of fish-farm-induced (or *denitrification associated*) change (relative to the *no farms* situation) are small relative to present-day natural variability. Furthermore, whilst we have chosen to focus upon seasonal-scale averages, inspection of time-series of instantaneous water-quality characteristics at a few specific locations have not revealed any relative changes which

[41] as a consequence of initial clearance of the native forests and subsequent intermittent logging operations
[42] In this context, not merely 'defensible/likely', but also 'sufficiently precise/tightly constrained to be useful'

are dramatically larger than are evident in the seasonal averages. That is, the time-averaging is not obviously masking any extreme, but short-lived events that are driven by the farms.

The additional fish farms are predicted to increase summertime near-surface total phytoplankton standing stocks by 5–10% relative to the existing conditions. Even so, the model suggests that they will only rarely (and locally) exceed 5 mg Chl m^{-3}. Concentrations of that magnitude would probably not be high enough to begin to change the perceived colour of the water. Nor are they sufficiently high (for long enough and over sufficiently large areas) for the system to be classified as eutrophic.

In comparison with the magnitudes of natural variability, it is tempting to argue that 5-10% changes in (for example) phytoplankton standing stock are negligibly small — even when they persist for an entire season and over a large fraction of the Sound. That may be slightly naïve. Given sufficient time, a 5% change in resource availability could, in theory, permit a disproportionate change in consumer abundance.

Hansen, Bjørnsen and Hansen (1997) made an extensive review of the literature concerning the feeding and growth of zooplankton in the 2- 2000 μm size range (protozoa to large copepods). They concluded that the half saturation food concentration (food concentration at which an organism's ingestion rate is one half of maximal) was about 240 mg C m^{-3} (though, there is substantial between taxon variability – the individual estimates in the source literature vary more than ten-fold). Ingestion (and, by implication, individual growth rate) will rise approximately linearly with food concentration up to food concentrations around the half-saturation concentration. At higher concentrations, the scaling will be sub-linear. Seston concentrations measured at the MDC sampling stations range between 39 and 335 mg C m^{-3} (median 215 mg C m^{-3}). Thus, they are usually below the 'typical' half saturation coefficient. This implies that changes in seston abundance (whatever the cause) will tend to induce zooplankton individual-level growth rate changes that are approximately proportionate to those in the seston. In our model, mussels consume zooplankton as well as detritus and phytoplankton. Thus, the zooplankton must contend with direct grazing pressure as well as wide-spread mussel-induced depletion of their phytoplankton prey during the winter. Together with their much lower maximum specific growth rates, this explains why the zooplankton tend to suffer greater depletion than phytoplankton or detritus.

Higher in the foodweb, a correlation between annual-scale average seston abundance and mussel yields has been found in Pelorus Sound (Zeldis, Howard-Williams et al. 2008; Zeldis, Hadfield, Booker 2013). If we make a leap of faith and assume that the correlation is indicative of causation, this opens the possibility that fish-farming could be beneficial to mussel farmers – however, the benefit will be small. In the analyses by Zeldis, there was a roughly two-fold difference between the maximum and minimum annual average particulate N abundances. That was associated with a yield difference of approximately 30% (of the long term average). Thus, the change at the upper end of the foodweb was certainly not super-proportionate. Our model predicts that seston concentrations will increase by only a few percent during the summer months in response to additional fish farming. Furthermore, they revert to (fish)farm-free levels during the winter months. This regular 'reset' may introduce a 'bottleneck' that would limit the extent to which populations of short-lived organisms can develop a multi-annual response to regular summer-time enhancement.

There are no definitive/universal standards which state what an acceptable quantum of change might be for any water-column property in the context of aquaculture. In the Firth of Thames, a negotiation process led to agreement that, averaged over a year, mussel farming in the Wilson Bay Aquaculture Management Area A (Zeldis, Felsing, Wilson 2005):

- should not induce phytoplankton depletion that exceeded 25% over an area twice that of the AMA (the AMA has an area of approx. 1200 ha)
- should not induce phytoplankton depletion that exceeds 20% over more than 10% of the Firth's surface area.

The AMA concept has no direct equivalent in the Marlborough Sounds but, relative to the simulated present-day conditions, none of the 'future farms' scenarios yield time-averaged phytoplankton depletion in excess of 25%.

The New Zealand King Salmon Board of Inquiry stipulated several water quality standards that must not be broken (Final report Appendices 4-7). For example Appendix 4 section 51 stipulates:

> *51 The farm shall be operated at all times in such a way as to achieve the following qualitative Water Quality Standards in the water column:*
> *a To not cause an increase in the frequency or duration of phytoplankton blooms (i.e., chlorophyll a concentrations ≥5 mg/m³)[43] [Note: water clarity as affected by chlorophyll a concentrations is addressed by this objective];*
> *b To not cause a change in the typical seasonal patterns of phytoplankton community structure (i.e., diatoms vs. dinoflagellates), and with no increased frequency of harmful algal blooms (HAB"s) (i.e., exceeding toxicity thresholds for HAB species);*
> *c To not cause reduction in dissolved oxygen concentrations to levels that are potentially harmful to marine biota [Note: Near bottom dissolved oxygen under the net pens is addressed separately through the EQS – Seabed Deposition];*
> *d To not cause elevation of nutrient concentrations outside the confines of established natural variation for the location and time of year, beyond 250m from the edge of the net pens;*
> *e To not cause a persistent shift from a mesotrophic to a eutrophic state;*
> *f To not cause an obvious or noxious build-up of macroalgal (eg sea lettuce) biomass [Note to be monitored in accordance with Condition 80h].*

Three of these (a, d, e) can be addressed with our present model. First, we note that the Board appears to have adopted a threshold of 5 mg chla m^{-3} as indicative of eutrophy. The Consent Conditions do not make it clear, but referring back to the underlying evidence[44], it is clear that this should be interpreted as an annual average. The mere fact that one (or even several) samples yield chlorophyll concentrations in excess of 5 mg chla m^{-3} need not indicate that the system is in a eutrophied state.

Whilst the biophysical modelling indicates that a time-averaged threshold of 5 mg chla m^{-3} may be approached (even exceeded) at some locations during the summer period, it certainly doesn't indicate that it will be exceeded over a large fraction of Pelorus during the summer period. Furthermore, it will not be exceeded on a year-round basis (the relevant time-scale for this threshold). Our modelling spans a period of 500 days. It suggests that, over that time-span, fish farming (including the new farms) in Pelorus will not cause the system to shift into a eutrophied state. We cannot entirely refute the possibility of a longer-term evolution towards eutrophy (whether exhibited as persistently and substantially increased phytoplankton or substantial change elsewhere in the foodweb). Nonetheless, it is our current opinion that the combination of winter-

[43] The conditions do not stipulate which phytoplankton size fractions were to be included when calculating chlorophyll concentration
[44] The figure of 5 mg Chl a m^{-3} appears to stem from evidence put forward by (Gillespie, P., Knight, B., MacKenzie, L. (2011) The New Zealand King Salmon Company Limited: assessment of environmental effects - water column: 79. citing Smith, V., Tilman, G., Nekola, J. (1999) Eutrophication: impacts of excess nutrient inputs on freshwater, marine, and terrestrial ecosystems. *Environmental Pollution*, 100(1-3): 179-196. and Wild-Allen, K., Herzfeld, M., Thomsen, P.A., Rosebrock, U., Parslow, J., Volkman, J.K. (2010) Applied coastal biogeochemical modelling to quantify the environmental impact of fish farm nutrients and inform managers. *Journal of Marine Systems*, 81: 134-147. 10.1016/j.marsys.2009.12.013).

time light limitation, relatively rapid flushing and benthic denitrification make it unlikely that the system will undergo extreme change in response to the levels of farming presently permitted in this system.

6.5 Biophysical modelling: summary of conclusions

- The model tends to predict overly high summertime surface-water phytoplankton concentrations in the baseline (existing conditions) scenario. Whilst we believe that the absolute concentrations increments that will arise when additional fish are added are small, the underlying 'baseline over-prediction' implies that : (a) the absolute summertime phytoplankton concentrations that may arise when more fish farms are added are probably also over-predicted by a similar increment, but (b) the relative concentration increments may be under-estimated.

- The 'no farms' simulation was run with the same (2012/2013-like) riverine, oceanic, climatic and seabed boundary conditions as the 'with farms' simulation. Thus, it may not be a good analogue for the true, historical no-farms situation. We know of no water-quality data stemming from prior to farm development. The earliest data that we know of stem from the mid/late 1990s (by which time there were already extensive mussel farms in Pelorus Sound). Analysis of those field data suggest that year-to-year variations in mussel yield were correlated with year-to-year variations in seston concentration and that those seston variations were best correlated with year-to-year climatic variations (El Nino/La Nina cycles). Whilst we have not made simulations for extreme El Nino or La Nina years, the discrepancy between model inferences and inferences drawn from the historical field data may indicate that the model is over-estimating the effects of mussels upon water-quality.

- Phytoplankton growth tends to be limited by low light intensities and short day-length during the winter months. During the summer months, it tends to be limited by a scarcity of nutrient (nitrogen). As a result of this difference, some of the effects of mussel and fish-farming differ between winter and summer months.

- Relative to the nominated baseline scenario (EM-EF-WD), a no mussel, existing fish with denitrification simulation (NM-EF-WD) yields:

  - Winter-time: lower concentrations of ammonium and nitrate but higher concentrations of particulate organic detritus (dead plankton etc.,) phytoplankton and zooplankton. The largest changes in relative concentration are seen in Kenepuru Sound and the largest relative concentration changes are within the zooplankton. There, time-averaged near-surface winter-time seston[45] concentrations in the NM-EF-WD simulation are more than double those of the EM-EF-WD scenario (for zooplankton in Kenepuru, substantially more than double). The Beatrix/Crail/Clova system also exhibits similar (but smaller) changes.

[45] Collectively, phytoplankton, zooplankton and other small particulate material are referred to as seston. The mussels feed upon phytoplankton, zooplankton and detritus. They release detritus (as faeces and pseudo-faeces). Fish also generate faeces. None of this faecal and pseudo-faecal material is part of the seston because they sink very rapidly whereas, by definition, seston is supposed to be approximately neutrally buoyant.

- Summertime: lower concentrations of ammonium, nitrate, higher concentrations of detritus and zooplankton, but phytoplankton concentrations which are similar to (or lower than) those of the EM-EF-WD scenario. During summer, mussels convert particulate organic nitrogen (not directly exploitable by phytoplankton) to ammonium (directly exploitable by phytoplankton). Phytoplankton growth is normally nutrient limited during this time, but in the immediate vicinity of the mussel farms, phytoplankton (which survive passage through the farms) find a plentiful ammonium supply. This enables them to grow quickly – more than offsetting the losses that the population suffered to mussel grazing (the 'excess accrued phytoplankton biomass being fuelled out of the detritus that was consumed). Once again, the largest changes are in Kenepuru Sound.

- Relative to the nominated baseline scenario (EM-EF-WD), a with mussel, no fish with denitrification simulation (EM-NF-WD) yields:

  - Winter-time: lower ammonium, nitrate and natural[46] detritus concentrations. With the exception of ammonium, the concentrations differ by less than approximately 1%. Phytoplankton and zooplankton concentrations that are almost identical to those of the EM-EF-WD scenario.

  - Summer-time: lower ammonium, nitrate, natural detritus, phytoplankton and zooplankton. The largest changes (declines in the absence of fish farms) are in Crail Bay (reflecting the presence of licensed farms in Crail Bay and Beatrix Bay and the slower flushing time of these bays in comparison with Waitata reach (which also harbours an existing fish farm at Waihinau Bay). Within Beatrix/Crail/Clova, time-averaged summertime phytoplankton concentration is predicted to be up to about 10% lower in the absence of fish farms. Zooplankton concentration is predicted to be up to about 15% lower.

- Turning to a comparison of the approved farms scenarios (AM-AF-WD) with the baseline (EM-EF-WD), the model predicts that the relatively few additional mussel farms present in the 'approved farms' scenarios (over and above those of the 'existing farms' scenario) induce water-quality changes that extend out to about bay-scale but amount to only a few percent of the simulated baseline (existing farms) concentrations. Changes are evident in nutrient (esp. ammonium) and seston concentrations. The changes include: increased ammonium concentrations in the vicinity of the farms and depressed concentrations of particulate organic detritus and zooplankton. During the winter, phytoplankton concentrations are slightly depressed by the additional mussel farms. During the summer, they are depressed in the immediate vicinity of the new mussel farms but can become slightly elevated further afield. The changes induced by these additional mussel and fish farms amount to a few percent of background concentrations. These are small relative to natural variability. For example, during winter, the incremental mussel grazing is predicted to induce local depletion of up to approximately 10% relative to the background/baseline (existing farms) simulation. In contrast, field data suggest that the extrema of phytoplankton population biomass can vary three or more fold over the course of a year. Indeed, it

[46] The small and large detritus classes of the model that receive dead plankton etc *cf* the XL-detritus class that receives faeces and pseudo-faeces from the mussels and fish.

can sometimes fluctuate by almost that much over time-scales of weeks and space scales of km or less.

- The model predicts that fish farming induces effects will extend through the entire Pelorus system. The effects upon nutrients are more localized (and, there, more intense) than the effects upon phytoplankton, zooplankton or natural detritus. Relative to the 'existing conditions' (EM-EF-WD), the modelling suggests that the approved additional fish- and mussel farms will induce winter-time changes of <5% and summer-time changes of <15% at most. In winter, phytoplankton biomass will increase slightly in the main channel of central and inner Pelorus but decline within Crail/Clova/Beatrix Bays. In summer, they will increase throughout Pelorus. The greatest (albeit, still relatively small) changes will be in the vicinities of the new fish farms (i.e., in Beatrix/Crail/Clova Bays, and around Richmond/Waitata/Port Ligar).
- Wintertime light limitation acts as a 'bottleneck' which limits the response of short-lived organisms to the increased nutrient concentrations.
- The additional fish-farms boost the predicted (overly high relative to field data) by a small quantum. Whilst the predicted summertime, near surface, phytoplankton concentrations would be higher than is the norm for New Zealand coastal waters, they would not be higher than values that are intermittently recorded in our coastal waters. They would probably not be high enough to begin to change the perceived colour of the water. Thus, we do not believe that the concentrations of nutrients and phytoplankton associated with the fish-farming scenarios are alarmingly high (particularly as we know the model is over-predicting the 'existing condition' summertime concentrations). We reiterate that the EM-EF_WD model over-predicts summertime phytoplankton concentrations relative to field data.
- At the whole of Pelorus scale, the majority of the farm derived nitrogen is predicted to be lost through denitrification at the seabed of the Pelorus system rather than by export to Cook Strait.
- Whilst we believe that the inferences that we draw from our modelling are robust, we caution that almost no sensitivity trials have been undertaken to justify that belief. We therefore recommend that further sensitivity trials be undertaken to determine the degree to which the model predictions are robust against assumptions regarding:
  - Denitrification potential. The largest changes (relative to the existing situation) arose when we turned off benthic denitrification throughout the domain. We consider domain-wide loss of denitrification to be vanishingly unlikely. Nonetheless, denitrification can become suppressed when organic loading rates are very high. Thus, one might legitimately ask what happens if denitrification is suppressed only in those parts of the domain where organic loading is exceptionally high (i.e., under the fish farms)?
  - Light attenuation (what happens if we take better account of the differential attenuation of different wavelengths?; what happens if seasonal variations in cloud cover etc., is introduced?).

- Sensitivity to the phytoplankton half-saturation coefficient for uptake of ammonium and nitrate.
- Formulation of the zooplankton mortality term.
- The role of dissolved organic nitrogen (by how much would the system's dynamics change if we assumed that catchment- and ocean-derived DON was biologically active rather than inert?).
- Sensitivity to Cook Strait boundary conditions (can phase errors be reduced by removing the three month smoothing that was applied to the Port Gore data? What are the consequences of inter-annual variability in the extent to which Cook Strait water intrudes into Pelorus and/or in the water-quality characteristics of the intruding Cook Strait water?).
- Sensitivity to assumptions concerning the efficiencies with which mussels capture detritus and zooplankton out of the water (relative to the efficiency with which they capture phytoplankton).

The coupled hydrodynamic and NPZD/aquaculture model is complex and represents a real-world system which is difficult to study in detail. It is impractical to try to undertake detailed validation of all components of the model using field data. Instead, one must rely upon comparing relatively few emergent properties from the model against corresponding field data. On the other hand, one might endeavour to study some components of the model in more detail by comparing against detailed laboratory-scale data. For example, one might excise the Fennel NPZD model from the remaining (3D hydrodynamics and aquaculture) components and apply the resultant NPZD model to data from laboratory-scale incubation data. In such incubations, the physical conditions can be more tightly regulated and some rate processes can be directly measured. Excising the NPZD code would not be too onerous, but gathering the requisite incubation data would be a substantial undertaking. Short-term incubations of this general type have been undertaken (e.g., Carter 2004) but a detailed comparison of the NPZD model against such data is outside the scope of this work. Furthermore, a quick examination of the material presented within Carter (2004) suggests that only chlorophyll and nitrate concentrations were recorded. Thus, the study provides no information concerning many of the state-variables of the Fennel NPZD model.

7 Deposition modelling

7.1 Methods

We simulated the first-time deposition foot-prints of farm waste (faeces + uneaten food) using a particle-tracking model. Each virtual particle represents a 'parcel' of waste material (measured as grams of carbon). Particles were released on a continuous basis from random horizontal locations within the perimeter of each farm. Where the information was available, the perimeter that was adopted was that of the fish pens[47]. In some cases (Port Ligar, Beatrix, Crail Li32 and Crail Li48) pen-perimeters were not available. For each of these farms, the perimeter was that of the licenced marine farm area. In these cases, the pens will occupy only a fraction of the area. At these farms, the model will: (a) underestimate maximal deposition under the pens and (b) over-estimate the area of the deposition footprint.

At release, each particle was also assigned a random initial depth between the sea-surface and 20 m below the surface. Subsequently, each particle moves under the influence of local-to-particle-currents, the intrinsic particle sinking velocity and turbulence.

The instantaneous local-to-particle currents were interpolated from an archive of 15 minute resolution hydrodynamic results generated by the 100 m resolution ROMS model. We adopted a sinking velocity of 5 cm s^{-1} (Brigolin, Pastres et al. 2009, and unpublished NIWA data). Turbulence was incorporated by adding a random velocity increment into each particle's equation of motion. The maximum absolute magnitude of this random term is proportional to the square-root of the estimated local dispersion coefficient. We assumed a horizontal dispersion coefficient of 1 $m^2 s^{-1}$. Vertical dispersion was derived from the shear, with a Richardson Number correction term. This yielded dispersion coefficients in the range $10^{-5} – 10^{-1}$ $m^2 s^{-1}$. We solved the resultant stochastic differential equation for particle motion by adopting Stratonovich Calculus and a second order Runge-Kutta method (Heun coefficients). For stochastic systems, this method is first-order strong convergent with respect to time-step. We adopted a time-step of 0.00025 d. This ensures that sinking (alone) cannot induce particles to pass through more than two layers within a single time-step. Thus, the particles will get to experience much (but not necessarily all) of any vertical variations in currents and mixing during their passage to the sea-bed.

At each farm, particles were released one at a time. The interval between particle releases was determined by the estimated daily rate of waste production (g C $farm^{-1}$ d^{-1}) and the nominal 'size' (g C) of each particle. The 'size' was chosen such that each farm generated 1000s of particles. The numbers of particles generated per farm ranged between approximately 15,000 (Waihinau) and 181,000 (Port Ligar). Each simulation spanned 30 simulated days. The farm-specific waste production rates were derived from monthly feed input rates (tonne feed $farm^{-1}$ $month^{-1}$), and an estimated carbon:feed weight fraction. This was derived from the C:dry weight ratios of protein, lipid and carbohydrate, and the typical proximate composition of salmon feed (Buschmann, Costa-Pierce et al. 2007). Refer to Table 7-1 for further details. For the Beatrix, Crail Li32, Crail Li48, Port Ligar, Richmond and Waitata farms, we applied monthly feed input rates that equated to 1/12 of the maximum permitted annual feed input rate. For Waihinau and Forsythe, we applied feed rates that were derived from projected feed schedules provided to us by NZKS. In both cases, the feed schedules included several months during which each farm would be empty. We derived an average

[47] Digitized from mooring plans provided to us by New Zealand King Salmon Ltd.

monthly input using only those months in which the farms would be occupied (ie, our deposition footprints for these farms are 'worst-case').

Table 7-1: Assumptions regarding composition of fish feed and assimilation of fish feed for deposition modelling.

Quantity	units	Value	Source
Fraction of ingested protein that is assimilated across gut wall	g assimilated g^{-1} ingested	0.90	(Buschmann, Costa-Pierce et al. 2007)
Fraction of ingested lipid that is assimilated across gut wall	g assimilated g^{-1} ingested	0.95	(Buschmann, Costa-Pierce et al. 2007)
Fraction of ingested carbohydrate that is assimilated across gut wall	g assimilated g^{-1} ingested	0.60	(Buschmann, Costa-Pierce et al. 2007)
Feed protein fraction	g protein g^{-1} feed	0.45	(Buschmann, Costa-Pierce et al. 2007)
Feed lipid fraction	g lipid g^{-1} feed	0.35	(Buschmann, Costa-Pierce et al. 2007)
Feed carbohydrate fraction	g carbohydrate g^{-1} feed	0.14	(Buschmann, Costa-Pierce et al. 2007)
Implied carbon content of feed	g C g^{-1} feed	0.47	
Implied assimilation efficiency for carbon	g assimilated g^{-1} ingested	0.82	
Assumed monthly feed input rate (Crail Bay Li48)	Tonne $month^{-1}$	125	(1/12) of maximum permitted annual feed input rate
Assumed monthly feed input rate (Crail Bay Li32)	Tonne $month^{-1}$	125	(1/12) of maximum permitted annual feed input rate
Assumed monthly feed input rate (Beatrix Bay)	Tonne $month^{-1}$	208	(1/12) of maximum permitted annual feed input rate
Assumed monthly feed input rate (Richmond)	Tonne $month^{-1}$	333	(1/12) of maximum permitted annual feed input rate
Assumed monthly feed input rate (Waitata)	Tonne $month^{-1}$	500	(1/12) of maximum permitted annual feed input rate
Assumed monthly feed input rate (Waihinau)	Tonne $month^{-1}$	172	Monthly average of projected input rates for period Dec '13 – Nov '14 [max permitted =333 $month^{-1}$]

Quantity	units	Value	Source
Assumed monthly feed input rate (Port Ligar)	Tonne month^{-1}	208	(1/12) of maximum permitted annual feed input rate
Assumed monthly feed input rate (Forsythe Bay)	Tonne month^{-1}	215	Monthly average of projected input rates for period Nov '14-Sep '15. [max permitted =250 month^{-1}]

7.2 Analysis and presentation of deposition model results

The location at which each particle first settled onto the seabed was recorded during the course of the simulation. Subsequently, all settlement locations were binned onto a 20 m resolution grid. This yields a bit-map of location-specific mass-accrual over the course of the 30-day simulation. Daily settlement rates are easily derived from that by dividing by the simulation length (30 d). We present the results as false-colour maps in which colour is indicative of the daily settlement rate (Figure 7-1).

Maximum deposition rates span the range 4.9 (Waitata) to 43.1 (Richmond) g C m^{-2} (3.8–33.55 kg dry weight m^{-2} year). The farm footprints range from 7.4 ha (Waihinau) to 32.5 ha (Port Ligar). Note, however that the latter is likely to be an over-estimate because particles were released from throughout the licenced area rather than from an (unknown) smaller pen-region within this area. The regions of maximum deposition are invariably within the farm perimeters and, in most cases, the deposition footprint is predicted to extend only approximately 100 m beyond the pen perimeter. Waitata and Richmond are exceptions. Their footprints are predicted to extend several hundred meters from the farm perimeters in the along-shore direction.

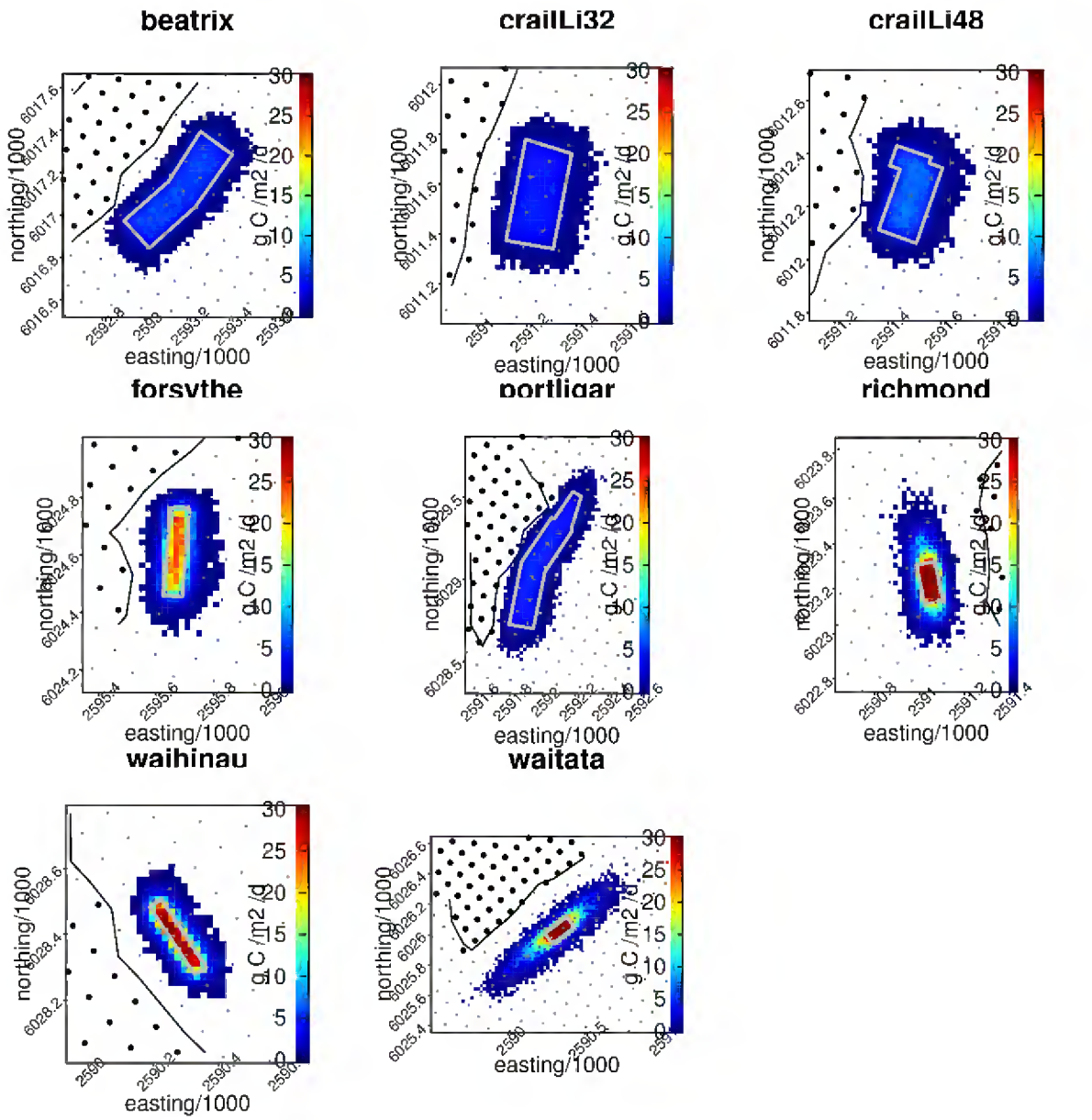

Figure 7-1: Maps of simulated daily deposition rates (g C /m2) for each farm. Simulations span the period 13 July – 12 August 2012. Pixel colour is indicative of the deposition rate. The grey line indicates the perimeter of the particle-release regions in the model. The black line is the model's zero-depth contour. The black circles are the mid-points of the water-columns of the hydrodynamic model. Large circles denote 'water-columns' that are prescribed as being unwettable (i.e., permanently dry land). Small dots denote water-columns that are wettable.

7.3 Discussion

Deposition rates of 5–45 g C m^{-2} d^{-1} have been measured at the edge of the pen at Waihinau in Pelorus Sound (D. Morrisey, NIWA, unpublished data). Keeley, Cromey et al. (2013) used the DEPOMOD particle-tracking tool to simulate deposition under Waihinau farms. At the pen edges, his modelled deposition rates were about 10 – 20 kg solids m^{-2} y^{-1} (13-26 g C m^{-2} d^{-1}). Our model yields deposition rates at the Waihinau pen edges which are within this range (Figure 7-1). Similarly, at Forsythe, DEPOMOD predicts deposition rates of about 26 g C m^{-2} d^{-1} – as do our simulations. Keeley

and Taylor (2011) present DEPOMOD simulation results for Richmond and Waitata farms. Under the maximum consented loading scenarios, DEPOMOD predicts peak deposition rates of 19-22 kg solids m^{-2} y^{-1} (24-28 g C m^{-2} d^{-1}) and a total footprint area of approximately 13 ha at Richmond. The corresponding figures from our simulations are 43 g C m^{-2} d^{-1} and 17 ha. At Waitata, the corresponding DEPOMOD figures are 10-13 kg m^{-2} y^{-1} (13-17 g C m^{-2} d^{-1}) and about 28 ha. Our model predicts 46 g C m^{-2} d^{-1} and 28 ha. Overall, it is encouraging that the two models yield similar near pen deposition rates and deposition footprint areas, despite using very different sources of hydrodynamic forcing[48] and having been parameterized independently of one another.

There is no single 'critical' deposition rate which can be used as an unequivocal threshold value to distinguish between rates of deposition which will not induce changes to the seabed fauna and biogeochemical structure and those that will. Observations elsewhere suggest that the structure of the benthic faunal community can be expected to change when deposition rates exceed about 1–5 g C m^{-2} d^{-1}. For the purposes of monitoring NZKS farms, a so-called benthic Enrichment Score[49] system has been adopted. The details are discussed in a recent 'benthic quality standards and monitoring' document (Keeley, Gillard et al. 2014) but, broadly, scores <= 5.0 are deemed acceptable. Historical data from existing NZKS farms indicate that this threshold is increasingly likely to be exceeded when deposition rates come to exceed 5-10 kg solids m^{-2} y^{-1} (6-12 g C m^{-2} d^{-1}) (Keeley, Cromey et al. 2013). On this basis, we suggest that few, if any of the farms will be able to operate at their maximum consented annual feed loads without breaching the agreed benthic standards. The aforementioned benthic quality standards document (Keeley, Gillard et al. 2014) provides an agreed framework by which stocking/feeding practices will be regulated in order to minimise the chances that farms will repeatedly violate the benthic standards.

8 Acknowledgements

We are grateful for the support that we have received from the staff of Marlborough District Council, notably Alan Johnson, Fleur Tiernan, Mike Ede and Steve Urlich. We are also grateful for the support that New Zealand King Salmon Ltd (notably Mark Gillard and Mark Preece) have provided. In particular, we thank them for providing detailed information about the historical feed input and stocking characteristics of each their existing farms.

[48] data from a single current meter resolved into three depth bins and having no horizontal resolution vs horizontally resolved hydrodynamic model output resolved into 20 layers

[49] A weighted measure of the state of the seabed as indicated by the benthic faunal composition and abundance, and a variety of biogeochemical and characteristics of the bed.

9 Glossary of abbreviations and terms

ADCP	An acoustic Doppler current profiler, an instrument for measuring velocity profiles.
bathymetry	The process of measuring and analysing seafloor depth. A bathymetric data set is often informally called a bathymetry.
CTD	A conductivity-temperature-depth instrument, typically lowered and raised in the water to measure vertical profiles of temperature and salinity.
denitrification	A bacterially mediated process through which nitrate (NO_3^+) is converted to nitrous oxide gas (N_2O) and, in some circumstances, free nitrogen gas (N_2). Denitrification occurs under anoxic conditions. It tends to occur most rapidly in zones where oxic and anoxic areas are in close proximity to one another.
light-limited	The realizeable phytoplankton growth rate is limited by low intensities of ambient photosynthetically available radiation (PAR). The term is usually applied when considering growth averaged over a 24 hour period. Since PAR intensity declines with increasing distance below the sea-surface, near-bed waters are more likely to be light-limited than near-surface waters. Similarly, light-limitation is more likely during the winter than summer.
nitrification	A bacterially mediated process by which ammonium is converted to nitrate via nitrite. Nitrification requires the presence of free oxygen and is suppressed by PAR.
nutrient-limited	The realizeable phytoplankton growth rate is limited by low concentrations of nutrient in the water-column. The term is usually applied when considering growth averaged over a 24 hour period.
PAR	Photosynthetically active radiation: that part of the solar spectrum that plants (including phytoplankton) can harvest and utilize to drive photosynthesis.
stratified	When the water column is stratified, a surface layer of lower density water floats above a sub-surface layer of higher density water. The surface layer can be less dense because it is cooler or more salty than the sub-surface water, or a combination of both.

10 References

Anon (2000) Anstralian and New Zealand Guidelines for Fresh and Marine Water Quality: Volume 2: Aquatic Ecosystems - rationale and background information. *New Zealand Guidelines for Fresh and Marine Water Quality*. http://www.environment.gov.au/water/publications/quality/index.html

Atlas, R., Hoffman, R.N., Ardizzone, J., Leidner, S.M., Jusem, J.C., Smith, D.K., Gombos, D. (2010) A Cross-calibrated, Multiplatform Ocean Surface Wind Velocity Product for Meteorological and Oceanographic Applications. *Bulletin of the American Meteorological Society*, 92(2): 157-174. 10.1175/2010BAMS2946.1

Attard, K.M. (2010) The degradation kinetics of organic materials in the marine environment - a case study using materials associated with sites of finfish aquaculture: 30.

Beers, J.R. (1966) Studies on the chemical composition of the major zooplankton groups in the Sargasso sea of Bermuda. *Limnology & Oceanography*, 11(4): 520-528.

Black, K.D. (2012) Benthic recovery project: 84.

Bowie, G.L., Mills, W.B., Porcella, D.B., Campbell, C.L., Pagenkopf, J.R., Rupp, G.L., Johnsom, K.M., Chan, P.W.H., Gherini, S.A., Chamberlin, C.E. (1985) *Rates, constants, and formulations in surface water quality modelling*. United States Environmental Protection Agency, Athens, Georgia: 455.

Bradford, J.M., Lapennas, P.P., Murtagh, R.A., Chang, F.H., Wilkinson, V. (1986) Factors controlling summer phytoplankton production in greater Cook Strait, New Zealand. *New Zealand Journal of Marine & Freshwater Research*, 20(2): 253-279.

Brigolin, D., Pastres, R., Nickell, T.D., Cromey, C.J., Aguilera, D.R., Regnier, P. (2009) Modelling the impact of aquaculture on early diagenetic processes in sea loch sediments. *Marine Ecology Progess Series*, 388: 63-80. 10.3354/meps08072

Broekhuizen, N., Hadfield, M.G. (2012) Review of evidence submitted by Mr Ben Knight on behalf of New Zealand King Salmon Co. Ltd. *NIWA Client Report*, HAM2012-110. http://www.epa.govt.nz/Publications/NIWA-Peer-rev-July-2012.pdf

Buschmann, A.H., Costa-Pierce, B.A., Cross, S., Iriarte, J.L., Olsen, Y., Reid, G. (2007) Nutrient impacts of farmed Atlantic Salmon (*Salmo salar*) on pelagic ecosystems and implications for carrying capacity. *World Wildlife Fund Salmon Aquaculture Dialogue by the Technical Working Group on nutrients and carrying capacity:* 68. http://www.worldwildlife.org/what/globalmarkets/aquaculture/WWFBinaryitem8844.pdf

Carter, C.M. (2004) Spatial and temporal dynamics of phytoplankton communities in a coastal ecosystem. University of Canterbury, Christchurch, New Zealand: 193.

Christensen, P.B., Glud, R.N., Dalsgaard, T., Gillespie, P.A. (2003) Impacts of longline mussel farming on oxygen and nitrogen dynamics and biological communities of coastal

sediments. *Aquaculture*, 218: 567-588. file://H:/was_p/pdf_reprints/christensen_et_al2003_aquaculture218_567.pdf

Cromey, C.J., Nickell, T.D., Treasurer, J., Black, K.D., Inall, M. (2009) Modelling the impact of cod (*Gadus morhua* L.) farming the in the marine environment CODMOD *Aquaculture*, 289: 42-53.

Edwards, A.M., Yool, A. (2000) The role of higher predation in plankton population models. *Journal of Plankton Research*, 22(6): 1085-1112.

Enders, E.C., Scruton, D.A. (2006) Potential application of bioenergetics models to habitat modeling and importance of appropriate metabolic rate estimates with special consideration for Atlantic Salmon. *Canadian Technical Report of Fisheries and Aquatic Sciences*, 2641: 40. http://www.dfo-mpo.gc.ca/Library/321568.pdf

Enríquez, S., Duarte, C.M., Sand-Jensen, K. (1993) Patterns in decomposition rates among photosynthetic organisms: the importance of detritus C:N:P content. *Oecologia*, 94: 457-471.

Fennel, K., Hetland, R., Feng, Y., Di Marco, S. (2011) A coupled physical-biological model of the Northern Gulf of Mexico shelf: model description, validation and analysis of phytoplankton variability. *Biogeosciences*, 8: 1881-1899. 10.5194/bg-8-1881-2011

Fennel, K., Wilkin, J., Levin, J., Moisan, J., O'Reilly, J., Haidvogel, D. (2006) Nitrogen cycling in the Middle Atlantic Bight: results from a three-dimensional model and implications for the North Atlantic nitrogen budget. *Global Biogeochemical Cycles*, 20: GB3007. 10.1029/2005GB002456

Fennel, K., Wilkin, J., Previdi, M., Najjar, R. (2008) Denitrification effects on air-sea CO_2 flux in the coastal ocean: simulations for the northwest North Atlantic. *Geophysical Research Letters*, 35: L24608. 10.1029/2008GL036147

Giles, H., Broekhuizen, N., Bryan, K., Pilditch, C.A. (2009) Modelling the dispersal of biodeposits from mussel farms: the importance of simulating biodeposit erosion. *Aquaculture*, 291: 168-178.

Giles, H., Pilditch, C.A. (2006) Effects of mussel (Perna canaliculus) biodeposit decomposition on benthic respiration and nutrient fluxes. *Marine Biology*, 150: 261-271.

Gillespie, P., Knight, B., MacKenzie, L. (2011) The New Zealand King Salmon Company Limited: assessment of environmental effects - water column: 79.

Hadfield, M., Broekhuizen, N., Plew, D. (2014a) A biophysical model for the Marlborough Sounds. *Part 1: Queen Charlotte Sound and Tory Channel,* CHC2014-116: 183.

Hadfield, M., Broekhuizen, N., Plew, D. (2014b) A biophysical model of the Marlborough Sounds: part 1: Queen Charlotte & Tory Channel. *NIWA Client Report (for Marlborough District Council)*: 183. http://www.marlborough.govt.nz/Environment/Coastal/Hydrodynamic-Models-of-the-Sounds.aspx

Hadfield, M.G. (2013) South Taranaki Bight Iron Sand Extraction Sediment Plume Modelling: Phase 3 studies. *NIWA Client Report* WLG2013-36: 86. http://www.epa.govt.nz/Publications/NIWA_sediment_plume_modelling_report.pdf

Hadfield, M.G., Zeldis, J.R. (2012) Freshwater dilution and transport in Canterbury Bight. *NIWA Client Report*, WLG2011-54: 39. http://ecan.govt.nz/publications/Pages/fresh-water-canterbury-bight.aspx

Haidvogel, D.B., Arango, H.G., Budgell, W.P., Cornuelle, B.D., Curchitser, E., Di Lorenzo, E., Fennel, K., Geyer, W.R., Hermann, A.J., Lanerolle, L., Levin, J., McWilliams, J.C., Miller, A.J., Moore, A.M., Powell, T.M., Shchepetkin, A.F., Sherwood, C.R., Signell, R.P., Warner, J.C., Wilkin, J. (2008) Ocean forecasting in terrain-following coordinates: Formulation and skill assessment of the Regional Ocean Modeling System. *Journal of Computational Physics*, 227(7): 3595-3624. doi: 10.1016/j.jcp.2007.06.016

Handley, S.J. (2015) The history of benthic change in Pelorus Sound (Te Hoiere), Marlborough, NEL2015-001 (project ELF15202): 47.

Hansen, P.J., Bjørnsen, P.K., Hansen, B.W. (1997) Zooplankton grazing and growth: scaling within the 2-2000 µm body size range. *Limnology and Oceanography*, 42(4): 687-704.

Heath, R.A. (1974) Physical oceanographic observations in Marlborough Sounds. *New Zealand Journal of Marine and Freshwater Research*, 8(4): 691-708. 10.1080/00288330.1974.9515538

Hickman, R.W. (1979) Allometry and growth of the Green-Lipped Mussel *Perna canaliculus* in New Zealand. *Marine Biology*, 51(4): 311-327.

Hickman, R.W., Illingworth, J. (1980) Condition cycle of the Green-Lipped Mussel *Perna canaliculus* in New Zealand. *Marine Biology*, 60(1): 27-38.

Jolliff, J.K., Kindle, J.C., Shulman, I., Penta, B., Friedrichs, M.A.M., Helber, R., Arnone, R.A. (2008) Summary diagrams for coupled hydrodynamic-ecosystem model skill assessment. *Journal of Marine Systems*, 76: 64-82. 10.1016/j.jmarsys.2008.05.014

Kalnay, E., Kanamitsu, M., Kistler, R., Collins, W., Deaven, D., Gandin, L., Iredell, M., Saha, S., White, G., Woollen, J., Zhu, Y., Chelliah, M., Ebisuzaki, W., Higgins, W., Janowiak, J., Mo, K.C., Ropelewski, C., Wang, J., Leetmaa, A., Reynolds, R., Jenne, R., Joseph, D. (1996) The NCEP/NCAR 40-year reanalysis project. *Bulletin of the American Meteorological Society*, 77(3): 437-471. 10.1175/1520-0477(1996)077<0437:tnyrp>2.0.co;2

Kaspar, H.F., Gillespie, P.A., Boyer, I.C., MacKenzie, A.L. (1985) Effects of mussel aquaculture on the nitrogen cycle and benthic communities in Kenepuru Sound, Marlborough Sounds, New Zealand. *Marine Biology*, 85(2): 127-136.

Keeley, N., Gillard, M., Broekhuizen, N., Ford, R., Schuckard, R., Urlich, S. (2014) Best Management Practice guidelines for salmon farms in the Marlborough Sounds: Part (II) benthic environmental quality standards and monitoring protocol. http://www.marlborough.govt.nz/Environment/Coastal/Best-Practice-Guidelines-for-Salmon-Farming.aspx

Keeley, N., Taylor, D. (2011) The New Zealand King Salmon Company Limited: Assessment of Environmental Effects - Benthic. *Cawthron Client Report*, 1983: 74 + appendices. http://www.epa.govt.nz/Publications/Appendix%204%20Seabed%20Report.pdf

Keeley, N.B., Cromey, C.J., Goodwin, E.O., Gibbs, M.T., Macleod, C.M. (2013) Predictive depositional modelling (DEPOMOD) of the interactive effect of current flow and resuspension on ecological impacts beneath salmon farms. *Aquaculture Environment Interactions*, 3: 275-291. 10.3354/aei00068

Knight, B.J. (2012a) Supplementary document of figures and tables - for evidence provided by Benjamin Robert Knight in relation to water column effects for the New Zealand King Salmon Co. Ltd. *Board of Inquiry appointed under section 149J of the Resource Management Act 1991 to consider The New Zealand King Salmon Co. Limited's private plan change requests to the Marlborough Sounds Resource Management Plan and resource consent applications for marine farming at nine sites located in the Marlborough Sounds*: 28.

Knight, B.R. (2012b) Statement of evidence of Benjamin Robert Knight in relation to water column effects for the New Zealand King Salmon Company Ltd. http://www.epa.govt.nz/Publications/13%20Benjamin%20Robert%20Knight%20-%20Water%20Column%20Effects%20-%20v1.pdf

Los, F.J., Blaas, M. (2010) Complexity, accuracy and practical applicability of different biogeochemical model versions. *Journal of Marine Systems*, 2010: 44-74. 10.1016/j.jmarsys.2009.12.011

Margolin, L.G., Smolarkiewicz, P.K. (1998) Antidiffusive Velocities for Multipass Donor Cell Advection. *SIAM Journal on Scientific Computing*, 20(3): 907-929. doi:10.1137/S106482759324700X

Monsen, N.E., Cloern, J.E., Lucas, L.V., Monismith, S.G. (2002) A comment on the use of flushing time, residence time, and age as transport time scales. *Limnology & Oceanography*, 47(5): 1545-1553.

Orban, E., Di Lena, G., Navigato, T., Cassini, I., Marzetti, A., Caproni, R. (2002) Seasonal changes in meat content, condition index and chemical composition of mussels (*Mytilus galloprovincialis*) cultured in two different Italian sites. *Food Chemistry*, 77(1): 57-65.

Petrell, R.J., Jones, R.E. (2000) Power requirement of swimming in chinook salmon and Atlantic salmon and implications for food conversion and growth performance. *Aquaculture Engineering*, 22: 225-239.

Reid, G.K., Liutkus, M., Robinson, S.M.C., Chopin, T.R., Blair, T., Lander, T., Mullen, J., Page, F., Moccia, R.D. (2009) A review of the biophysical properties of salmonid faeces: implications for aquaculture waste dispersal models and integrated multi-trophic aquaculture. *Aquaculture Research [AQUACULT. RES.]*, 40: 257-273. 10.1111/j.1365-2109.2008.02065.x

Ren, J.S., Ross, A.H. (2005) Environmental influence on mussel growth: a dynamic energy budget model and its application to the greenshell mussel *Perna canaliculus*. *Ecological Modelling*, 189: 347-362. file://H:/was_p/pdf_reprints/ren_and_ross2005_ecol_modelling189_p347_362.pdf

Ren, J.S., Ross, A.H., Hadfield, M.G., Hayden, B.J. (2010) An ecosystem model for estimating potential shellfish culture production in sheltered coastal waters. *Ecological Modelling*, 221: 527-539. 10.1016/j.ecolmodel.2009.11.003

Reynolds, R.W., Smith, T.M., Liu, C., Chelton, D.B., Casey, K.S., Schlax, M.G. (2007) Daily high-resolution-blended analyses for sea surface temperature. *Journal of Climate*, 20(22): 5473-5496. 10.1175/2007JCLI1824.1

Rickard, G.J., Hadfield, M.G., Roberts, M.J. (2005) Development of a regional ocean model for New Zealand. *New Zealand Journal of Marine and Freshwater Research*, 39(5): 1171–1191. 10.1080/00288330.2005.9517383

Ritter, J.J., Adams, N.K. (1976) Exponential dilution as a calibration technique. *Analytical Chemistry*, 48(3): 612-619. http://dx.doi.org/10.1021/ac60367a017

Safi, K., Gibbs, M.M. (2003) Importance of different size classes of phytoplankton in Beatrix Bay, Marlborough Sounds, New Zealand, and the potential implications for the aquaculture mussel *Perna canaliculus*. *New Zealand Journal of Marine and Freshwater Research*, 37(2): 267-272.

Schmidt-Nielsen, K. (1982) *Animal Physiology*. Cambridge University Press, Cambridge: 560.

Shchepetkin, A.F., McWilliams, J.C. (1998) Quasi-monotone advection schemes based on explicit locally adaptive diffusion. *Monthly Weather Review*, 126: 1541-1580. 10.1175/1520-0493(1998)126<1541:QMASBO>2.0.CO;2

Shearer, J.J. (1989) Pelorus Sound river water quality during low to medium flows: 43 + appendices.

Shearer, K.D., Åsgård, T., Andorsdöttir, G., Aas, G.H. (1994) Whole body elemental and proximate composition of Atlantic salmon (*Salmo salar*) during life cycle. *Journal of Fish Biology*, 44: 785-797.

Smith, S.D. (1988) Coefficients for sea surface wind stress, heat flux, and wind profiles as a function of wind speed and temperature. *Journal of Geophysical Research*, 93(C12): 15467-15472. doi: 10.1029/JC093iC12p15467

Smith, V., Tilman, G., Nekola, J. (1999) Eutrophication: impacts of excess nutrient inputs on freshwater, marine, and terrestrial ecosystems. *Environmental Pollution*, 100(1-3): 179-196.

Stanton, B.R., Goring, D.G., Bell, R.G. (2001) Observed and modelled tidal currents in the New Zealand region. *New Zealand Journal of Marine and Freshwater Research*, 35(2): 397–415. 10.1080/00288330.2001.9517010

Steele, J.H., Henderson, E.W. (1992) The role of predation in plankton models. *Journal of Plankton Research*, 14: 157-172.

Stigebrandt, A. (1999) Turnover of energy and matter by fish - a general model with application to salmon, 5: 28. http://www.biaoqiang.org/default.aspx?event=vd&docid=209

Sutton, P.J.H., Hadfield, M.G. (1997) Aspects of the hydrodynamics of Beatrix Bay. *New Zealand Journal of Marine and Freshwater Research*, 31(2): 271–279. 10.1080/00288330.1997.9516764

Thompson, R.O.R.Y. (1983) Low-Pass Filters to Suppress Inertial and Tidal Frequencies. *Journal of Physical Oceanography*, 13(6): 1077-1083. http://dx.doi.org/10.1175/1520-0485(1983)013<1077:LPFTSI>2.0.CO;2

Vincent, W.F., Howard-Williams, C., Downes, M., Dryden, S. (1989) Underwater light and photosynthesis at three sites in Pelorus Sound, New Zealand. *New Zealand Journal of Marine & Freshwater Research*, 23(1): 79-91. http://dx.doi.org/10.1080/00288330.1989.9516343

Walters, R.A., Goring, D.G., Bell, R.G. (2001) Ocean tides around New Zealand. *New Zealand Journal of Marine and Freshwater Research*, 35: 567-579.

Whiting, G., Beaumont, H., Ellison, E., Farnsworth, M., Briggs, M. (2012) *Board of Inquiry New Zealand King Salmon requests for plan changes and applications for resource consents*: 356.

Wild-Allen, K., Herzfeld, M., Thomsen, P.A., Rosebrock, U., Parslow, J., Volkman, J.K. (2010) Applied coastal biogeochemical modelling to quantify the environmental impact of fish farm nutrients and inform managers. *Journal of Marine Systems*, 81: 134-147. 10.1016/j.marsys.2009.12.013

Zeldis, J., Felsing, M., Wilson, J. (2005) Limits of acceptable change. *Coastal News*, 30: 1-3.

Zeldis, J.R., Hadfield, M.G., Booker, D.J. (2013) Influence of climate on Pelorus Sound mussel aquaculture yields: predictive models and underlying mechanisms. *Aquaculture Environment Interactions*, 4(1): 1-15. 10.3354/aei00066

Zeldis, J.R., Howard-Williams, C., Carter, C.M., Schiel, D.R. (2008) ENSO and riverine control of nutrient loading, phytoplankton biomass and mussel aquaculture yield in Pelorus Sound, New Zealand. *Marine Ecology Progress Series*, 371: 131-142.

Zeldis, J.R., Robinson, K., Ross, A.H., Hayden, B.J. (2004) First observations of predation by New Zealand Greenshell® mussels (*Perna canaliculus*) on zooplankton. *Journal of Experimental Marine Biology and Ecology*, 311: 287-299. file:///h:/was_p/pdf_reprints/zeldis/mussel_predation_final.pdf

Zimmerman, J.T.F. (1988) Estuarine residence times. In: B. Kjerfve (Ed). *Hydrodynamics of Estuaries*. CRC Press, Boca Raton, Florida: 75-84.

Appendix A Mathematical description of the Fennel NPZD model

$$\frac{\partial Phy}{\partial t} = \mu Phy - g_{Zoo}Zoo - m_{Phy}(Phy - PhyMIN)^{+} - \tau(SDet + Phy)Phy - w_{Phy}\frac{\partial Phy}{\partial z} - \sum_{i=1}^{N_{muss}} Mus_i\, V_i Phy \psi_{Phy}$$

The term $\sum_{i=1}^{N_{muss}} Mus_i\, V_i Phy \psi_{Phy}$ denotes the total local phytoplankton biomass loss rate (mmol N m^{-3} d^{-1}) due to the mussels of each size-class i. Mus_i denotes the local concentration of mussels (mussels of size i class m^{-3}). V_i (m^3 d^{-1} $mussel^{-1}$) denotes the volume of water filtered across the gills and ψ_{Phy} ($0<\psi_{Phy} \leq 1$) denotes the relative efficiency with which phytoplankton in the water passing over the gills is captured.

$$\mu = 0.59\mu_0 1.066^{T} \frac{\alpha I}{\sqrt{(0.59\mu_0 1.066^{T})^2 + (\alpha I)^2}} \left(\frac{NO3}{k_{NO3} + NO3}\right)\left(\frac{PhyIP}{k_{NH4} + NH4}\right)\left(\frac{NH4}{k_{NH4} + NH4}\right)$$

$$I = I_0\, par\, e^{-z\left(K_w + \frac{K_{Chl}\int_0^z Chl(\zeta)\, d\zeta}{z}\right)}$$

$$g_{Zoo} = g_{\max}\frac{Phy^2}{k_{Phy} + Phy^2}$$

$$\frac{\partial Chl}{\partial t} = \rho_{Chl}\mu Chl - g_{Zoo}Zoo\frac{Chl}{Phy} - m_p(Chl - ChlMIN) - \tau(SDet + Phy)Chl - w_{Phy}\frac{\partial Chl}{\partial z} - \sum_{i=1}^{N_{muss}} Mus_i\, V_i Chl \psi_{Phy}$$

$$\rho_{Chl} = \frac{\Theta_{\max}\mu Phy}{\alpha\, I\, Chl}$$

$$\frac{\partial Zoo}{\partial t} = g_{Zoo}\beta Zoo - l_{bm}(Zoo - ZooMin)^{+} - l_E\frac{Phy^2}{k_P + Phy^2}\beta Zoo - m_{Zoo}Zoo^2 - \sum_{i=1}^{N_{muss}} Mus_i\, V_i Zoo \psi_{Zoo}$$

$$\frac{\partial SDet}{\partial t} = g_{Zoo}(1-\beta)Zoo + m_{Zoo}Zoo^2 + m_{Phy}Phy - \tau(SDet + Phy)SDet - r_{SDet}SDet - w_{SDet}\frac{\partial SDet}{\partial z} - \sum_{i=1}^{N_{muss}} Mus_i\, V_i SDet \psi_{SDet}$$

$$\frac{\partial LDet}{\partial t} = \tau(SDet + Phy)^2 - r_{LDet}LDet - w_{LDet}\frac{\partial LDet}{\partial z} \sum_{i=1}^{N_{muss}} Mus_i\, V_i LDet \psi_{LDet}$$

$$\frac{\partial XLDet}{\partial t} = XLDet - w_{XLDet}\frac{\partial XLDet}{\partial z} - \sum_{i=1}^{N_{muss}} Mus_i\, V_i XLDet\psi X_{LDet} + \sum_{i=1}^{N_{fish}} faeces_i + uneatenfeed_i$$

$$\frac{\partial NO_3}{\partial t} = -\mu_{\max} f(I) L_{NO3} Phy + nNH_4$$

$$n = n_{\max}\left(1 - \frac{I - I_0}{k_I + I - I_0}\right)^+$$

$$\frac{\partial NH_4}{\partial t} = -\mu_{\max} f(I) L_{NH4} Phy - nNH_4 + l_{BM} Zoo + l_E \frac{Phy^2}{k_P + Phy^2}\beta Zoo + r_{SDet} SDet + r_{LDet} LDet + \sum_{i=1}^{N_{muss}} excretion_i + \sum_{i=1}^{N_{fish}} excretion_i$$

Table 10-1: Coefficients of the Fennel module. Unless otherwise noted, the values are those specified in the code that forms a part of the ROMS distribution. The coefficients are listed by both their Fennel-paper and ROMS-code names. A few coefficients are present only in the ROMS-code. A little additional explanation for those is presented in the Comment column.

Coefficient (Fennel 2006)	Coefficient (ROMS code)	Description	Units	Value	Comment
K_w	AttSW	Light attenuation coefficient due to seawater and components other than chlorophyll	m^{-1}	0.21	MDC data for Secchi disk depth in Queen Charlotte converted to a diffuse light attenuation coefficient using a correlation between attenuation and Secchi disk depth established with data from Pelorus Sound (Vincent, Howard-Williams et al. 1989) and applying discount of approx. 0.02 m^{-1} to avoid 'double counting' of attenuation due to chlorophyll
K_{chl}	AttChl	Light attenuation coefficient for chlorophyll	$m^2\ mg^{-1}$ chl	0.02486	
par	PARfrac	Fraction of incident shortwave radiation that is photosynthetically active	-	0.43	
μ_0	Vp0	Temperature limited phytoplankton growth parameter	-	1.0	
I_0	I_thNH4	Radiation threshold for nitrification inhibition	W m^{-2}	0.0095	
k_I	D_p5NH4	Half saturation radiation for nitrification inhibition	W m^{-2}	0.1	

Coefficient (Fennel 2006)	Coefficient (ROMS code)	Description	Units	Value	Comment
n_{max}	NitriR	Maximum rate of nitrification	d^{-1}	0.05	
$1/k_{NO3}$	K_NO3	Inverse half saturation for phytoplankton NO_3 uptake	m^3 $mmol^{-1}$ N	2	
$1/k_{NH4}$	K_NH4	Inverse half saturation for phytoplankton NH_4 uptake	m^3 $mmol^{-1}$ N	2	
k_{Phy}	K_Phy	Half saturation constant (squared) for zooplankton ingestion	(mmol N m^{-3})^2	2	
$\theta_{\max}$	Chl2C_m	Maximum Chl:phytoplankton carbon ratio	mg Chl mg^{-1} C	0.0535	
NA	ChlMin	Minimum Chl:phytoplankton carbon ratio	mg Chl mg^{-1} C	0.001	Additional coefficient present within ROMS. Chlorophyll background mortality falls to zero when the phytoplankton abundance falls below this value.
NA	PhyCN	Phytoplankton C:N ratio	mmol C $mmol^{-1}$ N	6.625	Additional coefficient present within ROMS. Required there for modelling of dissolved inorganic carbon and utilized in the mussel feeding model
$1/k_{NH4}$	PhyIP	Phytoplankton, coeff governing NH_4 dependent inhibition of NO_3 uptake	$mmol^{-1}$ N	1.5	Note that the ROMS implementation of the Fennel model distinguishes two coefficients (K_NH4, PhyIP) that correspond to two different usages of the original Fennel model's coefficient k_{NH4}
α	PhyIS	Initial slope of photosynthesis/irradiance curve	(W m^{-2} d)$^{-1}$	0.0125	In the code, PhyIS is defined in the manner of (Fennel, Hetland et al. 2011) rather than that of (Fennel, Wilkin et al. 2006). The numeric value that we have adopted was derived by calibration. It is half of the ROMS-default, but the ROMS default value is towards the upper end of the (large) range cited in the literature (Fennel, Wilkin et al. 2006)
NA	PhyMin	Phytoplankton mortality guard threshold	mmol N m^{-3}	0.001	Additional coefficient present within ROMS. Phytoplankton background mortality falls to zero when the phytoplankton abundance falls below this value.
m_{Phy}	PhyMR	Phytoplankton specific 'background' mortality rate	d^{-1}	0.15	
β	ZooAE_N	Zooplankton assimilation efficiency for ingested nitrogen	-	0.75	

Coefficient (Fennel 2006)	Coefficient (ROMS code)	Description	Units	Value	Comment
l_{bm}	ZooBM	Zooplankton specific basal metabolic rate	d^{-1}	0.1	
NA	ZooCN	Zooplankton C:N ratio	mmol C $mmol^{-1}$ N	6.625	Additional coefficient present within ROMS. Required there for modelling of dissolved inorganic carbon and utilized in the mussel feeding model
l_E	ZooER	Zooplankton specific excretion rate	d^{-1}	0.1	
$g_{\max}$	ZooGR	Zooplankton maximum specific ingestion rate	d^{-1}	0.6	
NA	ZooMin	Zooplankton guard threshold for basal metabolism	mmol N m^{-3}	0.001	Additional coefficient present within ROMS. Zooplankton respiratory losses when zooplankton concentration falls below this threshold.
m_{Zoo}	ZooMR	Zooplankton specific mortality rate	d^{-1}	0.025	
R_{LDet}	LDeRRN	Specific mineralization rate for N within large detritus	d^{-1}	0.01	Additional coefficient present within ROMS. Required there for modelling of dissolved inorganic carbon.
NA	LDeRRC	Specific mineralization rate for C within large detritus	d^{-1}	0.01	
τ	CoagR	Specific rate for coagulation of small detritus and phytoplankton to large detritus	d^{-1}	0.005	
R_{SDet}	SDeRRN	Specific mineralization rate for N within small detritus	d^{-1}	0.01	
NA	SDeRRC	Specific mineralization rate for C within small detritus	d^{-1}	0.01	Additional coefficient present within ROMS. Required there for modelling of dissolved inorganic carbon
	XLDeRRN	Specific mineralization rate for N within very fast sinking detritus	d^{-1}	0.01	Additional coefficient to accommodate degradation of the new state-variable. Black (2012) [citing Attard (2010)] suggests 0.005 – 0.06 d^{-1} for fish faeces and fish food. Giles and Pilditch (2006) estimated a rate of 0.16 d^{-1} for the degradation of mussel-derived organic matter.
	XLDeRRC	Specific mineralization rate for C within very fast sinking detritus	d^{-1}	0.01	Additional coefficient to accommodate degradation of the new state-variable
w_{phy}	wPhy	Sinking velocity for phytoplankton	m d^{-1}	0.1	
w_{LDet}	wLDet	Sinking velocity for large detritus	m d^{-1}	1.0	

Coefficient (Fennel 2006)	Coefficient (ROMS code)	Description	Units	Value	Comment
w_{SDet}	wSDet	Sinking velocity for small detritus	m d^{-1}	0.1	
	wXLDet	Sinking speed for very fast detritus (faeces & pseudo-faeces)	cm s^{-1} (m d^{-1})	5 (4320)	This coefficient applies to the additional state-variable (very fast sinking detritus) that is not found in the original Fennel model. The sinking speed is based upon unpublished measurements of faecal sinking speeds for material from Chinook salmon farmed in the Marl Sounds. It towards the upper range of published values for fish and mussel faecal sinking speeds (Cromey, Nickell et al. 2009; Giles, Broekhuizen et al. 2009; Reid, Liutkus et al. 2009)

Table 10-2: Coefficients required to link the Fennel NPZD model and the Ren mussel physiology model. The coefficients in this Table are not found in either of the original Fennel or Ren models but they are required in order to allow the models to be coupled. The coefficients used in our implementation of the mussel physiology are those specified within Ren & Ross (2005) or Ren et al. (2010).

Coefficient	Description	Units	Value	Comment
LDeCN	C:N ratio for large detritus	mmol C mmol^{-1} N	6.625	Assumed, but consistent with Fennel model C:N ratios of zooplankton and phytoplankton and the assumption that detrital C & N mineralize at the same rates
SDeCN	C:N ratio for small detritus	mmol C mmol^{-1} N	6.625	Assumed, but consistent with Fennel model C:N ratios of zooplankton and phytoplankton and the assumption that detrital C & N mineralize at the same rates
SIS	Concentration of suspended inorganic sediment	mg ash weight m^{-3}	2000	Marlborough District Council water quality samples from Queen Charlotte Sound
ψ_{Phy}	Relative search volume of mussels for phytoplankton	-	1.0	By definition
ψ_{Zoo}	Relative search volume of mussels for zooplankton	-	1.0	(Zeldis, Robinson et al. 2004)
ψ_{LDet}	Relative search volume of mussels for large detritus	-	1.0	Assumed, but consistent with (Zeldis, Robinson et al. 2004)
ψ_{SDet}	Relative search volume of mussels for small detritus	-	1.0	Assumed, but consistent with (Zeldis, Robinson et al. 2004)
ψ_{XLDet}	Relative search volume of mussels for small detritus	-	0.0	Assumed
PhyDWN	Dry weight to nitrogen ratio for phytoplankton	g DW mmol^{-1} N	1.02	(Bowie, Mills et al. 1985)
ZooDWN	Dry weight to nitrogen ratio for phytoplankton	g DW mmol^{-1} N	0.89	(Beers 1966)
LDeDWN	Dry weight to nitrogen ratio for large detritus	g DW mmol^{-1} N	1.0	Assumed, chosen to lie between the corresponding ratios for phytoplankton and zooplankton (closer to the former)
SDeDWN	Dry weight to nitrogen ratio for small detritus	g DW mmol^{-1} N	1.0	Assumed, chosen to lie between the corresponding ratios for phytoplankton and zooplankton (closer to the former)

Appendix B Mathematical description of the mussel farm model

The full Ren et al. (2010) mussel growth model includes explicit dynamic descriptions of the rates of change of mussel energy reserves and structural volume. In his model, the reserve:structure ratio can vary through time (it provides an index of mussel condition or level of starvation). Some of the physiological rates are influenced by the ratio. We do not go to these lengths. The mussels of our population are described only in terms of numbers per length class. Length and structural volume are closely related, but instantaneous length provides no information about mussel condition. For the purposes of calculating all physiological rates, we assume that our mussels have replete reserves.

An individual mussel is defined by its shell length (M_L, mm). In turn, this defines various body-weight characteristics. The whole animal wet-weight (inclusive of shell, gram) is denoted M_{WW+S}:

$$M_{WW+Shell} = 0.00025\ M_L^{2.726}$$

The wet-weight exclusive of shell (gram) is:

$$M_{WW} = 0.32 M_{WW+Shell}$$

The dry weight (exclusive of shell, gram) is:

$$M_{DW} = 0.2 M_{WW}$$

We assume that our mussels have replete reserves, and that reserves amount to 40% of the dry body mass (exclusive of the shell). Thus, the dry weight mass (gram) of structural tissue (ie proteins, carbohydrates etc., which once laid down, cannot be remobilized to meet energetic demands etc.,) is:

$$M_S = 0.6 M_{DW}$$

and, the dry weight mass (gram) of mussel reserve materials is:

$$M_R = M_{DW} - M_S = 0.4 M_{DW}$$

The energy content (J) of these reserves is

$$E = \frac{1000 M_R}{\mu_E}$$

The biovolume (M_V) of the structural material is

$$M_V = \frac{M_S}{\rho}$$

In the original Ren model, the maximum energy reserves (J cm^{-3}) are denoted $[E_m]$. In our derivation of this model, we assume $E = [E_m] M_V$.

$$M_V = \frac{M_{DW}}{0.2} = M_{WW}$$

The energy content of the mussel (Joules, exclusive of shell) is

$$M_J = 1000(M_S \mu_S + M_R \mu_R)$$

As noted previously, we assume the mussels have replete reserves, so

$$M_R\mu_R = \frac{M_J - 1000 M_S \mu_S}{1000} = 2600\, M_V$$

Mussels are assumed to consume seston. We measure its abundance (as perceived by the mussels) as: carbon (S_C, mg C m^{-3}), nitrogen (S_N, mg N m^{-3}) and dry weight (S_{DW}, mg dry weight m^{-3}). Seston is assumed to comprise of small and large detritus, phytoplankton and zooplankton and suspended inorganic matter. The carbon (S_C, mmol C m^{-3}), nitrogen (S_N, mmol N m^{-3}), dry-weight (S_{DW}, mg m^{-3}) and energy concentrations (S_J, J m^{-3}) of perceived seston are given by:

$$S_C = Phy.\varphi_{C:N}^{Phy}\psi_{Phy} + Zoo.\varphi_{C:N}^{Zoo}\psi_{Zoo} + LDet.\varphi_{C:N}^{LDet}\psi_{LDet} + SDet.\varphi_{C:N}^{SDet}\psi_{SDet}$$

$$S_N = Phy\psi_{Phy} + Zoo\psi_{Zoo} + LDet\psi_{LDet} + SDet\psi_{SDet}$$

$$S_{DW} = Phy.\varphi_{DW:N}^{Phy}\psi_{Phy} + Zoo.\varphi_{DW:N}^{Zoo}\psi_{Zoo} + LDet.\varphi_{DW:N}^{LDet}\psi_{Zoo} + SDet.\varphi_{DW:N}^{SDet}\psi_{Zoo} + SIS$$

$$S_J = Phy.\varphi_{C:N}^{Phy}.\varphi_{J:C}^{Phy}\psi_{Phy} + Zoo.\varphi_{C:N}^{Zoo}.\varphi_{J:C}^{Zoo}\psi_{Zoo} + LDet.\varphi_{C:N}^{LDet}.\varphi_{J:C}^{LDet}\psi_{LDet} + SDet.\varphi_{C:N}^{SDet}.\varphi_{J:C}^{SDet}\psi_{SDet}$$

The volume of water pumped across the mussel gill surface is:

$$V = U_{mm}{M_V}^{2/3} f(K)$$

Where $f(K)$ denotes the temperature dependence function (temperature in Kelvin)

$$f(K) = k_{T0} e^{\left(\frac{T_A}{T_0} - \frac{T_A}{K}\right)} \left[1 + e^{\left(\frac{T_{AL}}{K} - \frac{T_{AL}}{T_L}\right)} + e^{\left(\frac{T_{AH}}{T_H} - \frac{T_{AH}}{K}\right)}\right]^{-1}$$

The quantities of phytoplankton, zooplankton, large detritus, small detritus and energy captured on the gills are:

$$C_{Phy} = VPhy\psi_{Phy}$$

$$C_{Zoo} = VZoo\psi_{Zoo}$$

$$C_{LDet} = VLDet\psi_{LDet}$$

$$C_{SDet} = VSDet\psi_{SDet}$$

$$C_J = V\left(Phy\psi_{Phy}\varphi_{C:N}^{Phy}\varphi_{J:C}^{Phy} + Zoo\psi_{Zoo}\varphi_{C:N}^{Zoo}\varphi_{J:C}^{Zoo} + LDet\psi_{LDet}\varphi_{C:N}^{LDet}\varphi_{J:C}^{LDet} + SDet\psi_{SDet}\varphi_{C:N}^{SDet}\varphi_{J:C}^{SDet}\right)$$

Of this material, a fraction is lost as pseudo-faeces. The remainder passes into the gut. The fraction passing into the gut is given by:

The rate at which energy is assimilated across the gut wall is

$$A_J = V\frac{S_C}{S_C + H_{pm}} p_{A\max}$$

The rates of carbon and nitrogen assimilation are:

$$A_C = \frac{V\left(Phy\psi_{Phy}\varphi_{C:N}^{Phy} + Zoo\psi_{Zoo}\varphi_{C:N}^{Zoo} + LDet\psi_{LDet}\varphi_{C:N}^{LDet} + SDet\psi_{SDet}\varphi_{C:N}^{SDet}\right)}{C_J} I_J$$

$$A_N = \frac{V\left(Phy\psi_{Phy} + Zoo\psi_{Zoo} + LDet\psi_{LDet} + SDet\psi_{SDet}\right)}{C_J} I_J$$

Material which is not assimilated across the gut wall is lost as faeces and pseudo-faeces and passes into the large-detrital pool.

The mussel energy expenditure rate (J mussel^{-1} d^{-1}) is made up of a basal term (p_M) and a growth-and-filtration-related term (p_g).

$$p_M = \left(\frac{[E]}{[E_G] + \kappa[E]}\right) f(K)[p_m] M_V$$

$$p_g = \left(\frac{[E]}{[E_G] + \kappa[E]}\right) [E_G] p_{A_{\max}} {M_V}^{2/3}$$

The mussel carbon respiration rate (E_C, mmol CO_2-C mussel^{-1} d^{-1}) is:

$$E_C = max\left[A_C - \frac{p_M + p_g}{\mu_R}, A_C - A_N \varphi_{C:N}^{Mus}\right]$$

The mussel nitrogen excretion rate (E_N, mmol NH_4-N mussel^{-1} d^{-1}) rate is:

$$E_N = A_N - \frac{1}{\varphi_{C:N}^{Mus}}\left[A_C - \frac{p_M + p_g}{\mu_R}\right]$$

Symbol	Description	Units	Value	Comment
	Scaling coefficient relating whole animal wet weight (incl. of shell) to shell length	g mm$^{-2.726}$	0.00025	(Hickman 1979)
	Exponent in wet-weight:length relationship	-	2.76	(Hickman 1979)
	Fraction of whole animal wet weight that is not shell	-	0.32	
	dry weight: wet weight ratio of mussel soft tissue	-	0.2	
	Structural tissue dry weight mass/soft tissue dry weight mass for a well fed mussel	-	0.6	
μ_S	Energy density of mussel structural tissue	J mg^{-1} structural dry weight		
μ_R	Energy density of mussel reserve tissue	J mg^{-1} reserve dry weight		

Symbol	Description	Units	Value	Comment
$\varphi_{C:N}^{Phy}$	C:N ratio of phytoplankton	mol C / mol N		
$\varphi_{C:N}^{Zoo}$	C:N ratio of zooplankton	mol C / mol N		
$\varphi_{C:N}^{LDet}$	C:N ratio of large detritus	mol C / mol N		
$\varphi_{C:N}^{SDet}$	C:N ratio of small detritus	mol C / mol N		
$\varphi_{DW:N}^{Phy}$	C:N ratio of phytoplankton	g dry weight / mol N		
$\varphi_{DW:N}^{Zoo}$	C:N ratio of zooplankton	g dry weight / mol N		
$\varphi_{DW:N}^{LDet}$	C:N ratio of large detritus	g dry weight / mol N		
$\varphi_{DW:N}^{SDet}$	C:N ratio of small detritus	g dry weight / mol N		
$\varphi_{J:C}^{Phy}$	Energy density of phytoplankton	J / mmol C		
$\varphi_{J:C}^{Zoo}$	Energy density of zooplankton	J / mmol C		
$\varphi_{J:C}^{LDet}$	Energy density of large detritus	J / mmol C		
$\varphi_{J:C}^{SDet}$	Energy density of small detritus	J / mmol C		
ψ^{Phy}	Mussel filtration efficiency for phytoplankton	$m^3 m^{-3}$		
ψ^{Zoo}	Mussel filtration efficiency for zooplankton	$m^3 m^{-3}$		
ψ^{LDet}	Mussel filtration efficiency for large detritus	$m^3 m^{-3}$		
ψ^{SDet}	Mussel filtration efficiency for small detritus	$m^3 m^{-3}$		
H_{pm}	Half saturation seston concentration	mmol C m^{-3}	295/12	
$p_{A_{\max}}$	Maximum surface area specific assimilation rate	J cm^{-2} d^{-1}		
ρ	Biovolume-specific concentration of structural materials	g structural cm^{-3} biovolume	0.2	

Appendix C Mathematical description of the fish farm model

Stigebrandt derived a model for salmon growth that is based upon energy conservation. Fish size is expressed as live weight (W, gram), and energy content (Q, Joules). The energy density of fish flesh (C_{fi},J g^{-1} live weight) is assumed to be constant.

$$Q = WC_{fi}$$

The maximal fish growth rate ($G_{\max}$, g live weight fish^{-1} d^{-1}) is assumed to scale allometrically with fish weight and exponentially with temperature (T, Celsius).

$$G_{\max} = aW^b e^{\tau T}$$

The realized ingestion rate (Q_r, J fish^{-1} d^{-1}) is the lesser of the per-capita feed provision rate (Q_{feed}, J fish^{-1} d^{-1}) or the maximal ingestion rate ($Q_{r_{\max}}$, J fish^{-1} d^{-1}, to be defined in greater detail later)

$$Q_r = \min\left(Q_{feed}, Q_{r_{\max}}\right) \alpha W^{\gamma} e^{\tau T}$$

The feed is deemed to consist of a water fraction (F_w, g water g^{-1} feed), a protein fraction (F_p, g protein g^{-1} feed), a lipid fraction (F_l, g lipid g^{-1} feed) and a carbohydrate fraction (F_c, g carbohydrate g^{-1} feed). The energy densities (J g^{-1} substrate) for lipid and carbohydrate are denoted C_l and C_c respectively. For protein, we define two energy densities. $C_p^{NO_3}$ denotes the energy density if the protein is fully catabolised to yield NO_3 as the nitrogenous end-product. $C_p^{NH_4}$ denotes the (smaller) energy density that arises when protein is catabolised to yield ammonium as an end-product. The energy density of food is defined to be:

$$\delta = F_p C_p^{NO_3} + F_l C_l + F_c C_c$$

The fractional contributions of protein, lipid and carbohydrate to the total ingested energy are:

$$E_p^{NO_3} = \frac{F_p C_p^{NO_3}}{\delta}, E_p^{NH_4} = \frac{F_p C_p^{NH_4}}{\delta} \; E_l = \frac{F_l C_l}{\delta} \text{ and } E_c \frac{F_c C_c}{\delta}$$

A fraction of the ingested energy is lost in faeces. The loss rate (Q_f, J fish^{-1} d^{-1}) is determined by the assimilation efficiencies for protein (A_p, dimensionless), carbohydrate (A_c) and lipid (A_l) and by the fractional contributions which each makes to total energy ingestion.

$$Q_f = Q_r \left((1 - A_p) E_p^{NO_3} + (1 - A_l) E_l + (1 - A_c) E_c \right)$$

The process of breaking proteins, lipids and carbohydrates into simpler molecules and assimilating those across the gut wall incurs an energy expenditure (so-called specific dynamic action, (Q_{SDA}, J fish^{-1} d^{-1}). The SDA for protein amounts to 30% of the assimilated protein energy whilst the SDAs for lipid and carbohydrate amount to 5% of their respective energy assimilation rates:

$$Q_{SDA} = Q_r \left(0.3 A_p E_p^{NO_3} + 0.05 (A_c E_c + A_l E_l) \right)$$

A fish is assumed to use dietary lipid and carbohydrate preferentially to fuel its energy demands (thereby conserving as much nitrogen as possible to synthesize new proteins). Nonetheless, when a fish assimilates more nitrogen than it requires to meet the nitrogen demands associated with building new flesh, it uses the excess protein to meet energetic expenditure. Similarly, when the total energy assimilation rate is insufficient to meet the basal energy demand, the fish is assumed to

meet the deficit by catabolising lipid, carbohydrate and protein at rates which maintain a fixed proximate body composition. $E_p^{NO_3}$ is based upon full oxidation to NO_3, but fish catabolise proteins only to NH_4^+. Thus, account must be taken of the energy that is lost as NH_4^+ when protein is catabolised. The result is an additional growth-related energy loss (Q_N, J fish^{-1} d^{-1})

$$Q_N = \frac{E_p^{NO_3} - E_p^{NH_4}}{E_p^{NO_3}} C_p \left(F_p A_p \frac{Q_r}{\delta} - P_p \frac{dW}{dt} \right)$$

The energetic cost of growth (net accrual of new fish flesh; Q_g, J fish^{-1} d^{-1}) is assumed to be proportional to the rate of growth.

$$Q_g = C_{fi} \left[\frac{dW}{dt} \right]^+$$

Basal energetic costs (Q_s, J fish^{-1} d^{-1}) are assumed to scale allometrically with fish weight and exponentially with temperature.

$$Q_s = \alpha W^\gamma e^{\tau T}$$

In the original Stigebrandt model, locomotory costs (Q_l, J fish^{-1} d^{-1}) were set to zero because basal metabolism was explicitly assumed to include a locomotory component. In our implementation, we have retained an explicit locomotory term (set proportional to the basal respiration – which explicitly excludes locomotion)

$$Q_l = \vartheta Q_s$$

Since farmed salmon are usually harvested before reaching sexual maturity, we assume that the energetic costs of gamete synthesis (Q_p, J fish^{-1} d^{-1}) are zero.

Collectively, the expressions for basal metabolism, maximal growth rate, maximal ingestion rate, digestive efficiencies, specific dynamic action, and protein catabolism efficiency imply an expression for the maximum ingestion rate (J fish^{-1} d^{-1})

$$Q_{r_{\max}} = \frac{\left[\alpha W^\gamma + a W^b \left(C_{fi} - \frac{E_p^{NO_3} - E_p^{NH_4}}{E_p^{NO_3}} C_p P_p \right) \right] e^{\tau T}}{1 - \left((1 - A_p) E_p + (1 - A_l) E_l + (1 - A_c) E_c \right) - \left(0.3 A_p E_p^{NO_3} + 0.05 (A_c E_c + A_l E_l) \right) - \frac{E_p^{NO_3} - E_p^{NH_4}}{E_p^{NO_3}} A_p E_p}$$

The rate of change of energy content $\frac{dQ}{dt}$ (J fish^{-1} d^{-1}) is given by the difference between the rates of energy ingestion (Q_r) and energy loss though: faeces Q_f, catabolism of protein ingested in excess of growth requirements (Q_N), basal metabolism (Q_s), locomotory metabolism (Q_l), specific dynamic action, energy expended in synthesis of new flesh (Q_g) and energy expended in synthesis of gametes (Q_p).

$$\frac{dQ}{dt} = Q_r - Q_f - Q_N - Q_s - Q_l - Q_{SDA} - Q_g - Q_p = C_{fi} \frac{dW}{dt}$$

Since Q_N and Q_g are dependent upon $\frac{dW}{dt}$, the equation does not have an analytic solution. We use the bisection method to calculate a realized instantaneous value for $\frac{dQ}{dt}$ that satisfies this equation. Conceptually similar equations can be set up for carbon. Again, we use the bisection method to solve that equation. The final realized growth rate (which may be negative) is the lesser of the two growth rates (expressed in energy units). Realized carbon, nitrogen etc., uptake and release fluxes are then calculated on the basis of that growth rate. Oxygen demand can be derived from the calculated assimilation rates of protein, carbohydrate and lipid, the realized fish growth rate and the respiratory quotient of each substrate. (Buschmann, Costa-Pierce et al. 2007)

Table 10-3: Coefficients for the fish physiology module. WW: wet weight. The majority of coefficients are derived from data concerning Atlantic salmon. Chinook salmon is the species that farmed in the Marlborough Sounds).

Coefficient (Stigebrandt 1999)	Coefficient (ROMS code)	Description	Units (Stigebrandt) [ROMS]	Value	Comment
$C_p^{NO_3}$		Energy protein when fully oxidized to nitrate	J g^{-1}	23.0x10^3	http://www.fao.org/docrep/003/aa040e/aa040e08.htm
$C_p^{NH_4}$		Energy density of protein when catabolized to ammonium	J g^{-1}	19.0x10^3	(Schmidt-Nielsen 1982)
C_l		Energy density of lipid	J g^{-1}	39.33x10^3	(Schmidt-Nielsen 1982)
C_c		Energy density of carbohydrate	J g^{-1}	17.57x10^3	(Schmidt-Nielsen 1982)
	FeedWaterFrac	Energy density of ingested carbohydrate	g water g^{-1} feed	0.085	(Buschmann, Costa-Pierce et al. 2007)
F_p	FeedProteinFrac	Protein content of the fish feed	g protein g^{-1} feed	0.45	(Buschmann, Costa-Pierce et al. 2007); http://en.wikipedia.org/wiki/Chinook_salmon
F_l	FeedLipidFrac	Lipid content of the fish feed	g lipid g^{-1} feed	0.22	http://en.wikipedia.org/wiki/Chinook_salmon; but see (Buschmann, Costa-Pierce et al. 2007) – which suggests 0.35
F_c	FeedCarbFrac	Carbohydrate content of fish feed	g carbohydrate g^{-1} feed	0.14	http://en.wikipedia.org/wiki/Chinook_salmon; but see (Buschmann, Costa-Pierce et al. 2007) – which suggests 0.10
	FishWaterFrac	Water content of the fish feed	g water g^{-1} fish	0.75	(Shearer, Åsgård et al. 1994)
P_p	FishProteinFrac	Protein content of the fish	g protein g^{-1} fish	0.14	(Shearer, Åsgård et al. 1994)
P_l	FishLipidFrac	Lipid content of the fish	g lipid g^{-1} fish	0.10	(Shearer, Åsgård et al. 1994)
P_c	FishCarbFrac	Carbohydrate content of fish	g carbohydrate g^{-1} fish	0.015	(Shearer, Åsgård et al. 1994)

Coefficient (Stigebrandt 1999)	Coefficient (ROMS code)	Description	Units (Stigebrandt) [ROMS]	Value	Comment
δ	Derived property (see right)	Energy density of fish feed	J g^{-1}	$\delta = F_p C_p^{NO_3} + F_l C_l + F_c C_c$	$1 \leq F_p + F_l + F_c$, allowing that fish feed may have a small water content
C_{fi}	Derived property (see right)	Energy density of live fish	J g^{-1}	$C_{fi} = P_p C_p^{NO_3} + P_l C_l + P_c C_c$	
A_p	FishAssimEfficProt	Assimilation efficiency for protein content of fish feed	-	0.9	(Buschmann, Costa-Pierce et al. 2007)
A_l	FishAssimEfficLipid	Assimilation efficiency for lipid content of fish feed	-	0.95	(Buschmann, Costa-Pierce et al. 2007)
A_c	FishAssimEfficCarbo	Assimilation efficiency for carbohydrate content of fish feed	-	0.6	(Buschmann, Costa-Pierce et al. 2007)
	SDAProt	Specific dynamic action for digestion of protein	J expended J^{-1} protein assimilated across gut wall	0.3	(Stigebrandt 1999)
	SDALipid	Specific dynamic action for digestion of lipid	J expended J^{-1} lipid assimilated across gut wall	0.05	(Stigebrandt 1999)
	SDACarbo	Specific dynamic action for digestion of carbohydrate	J expended J^{-1} carbohydrate assimilated across gut wall	0.05	(Stigebrandt 1999)
NA	WLs	Scale coefficient in fish weight:length allometry	kg WW $mm^{-1/WLe}$ fork length	2.84627×10^{-9}	(Petrell and Jones 2000)
NA	WLe	Exponent in fish weight:length allometry	-	3.27	(Petrell and Jones 2000)
a	GWs	Exponent in fish allometric relation between maximal growth rate and live weight	$(g\ WW)^{1-GWe}\ d^{-1}$	0.038	(Petrell and Jones 2000)

Coefficient (Stigebrandt 1999)	Coefficient (ROMS code)	Description	Units (Stigebrandt) [ROMS]	Value	Comment
b	GWe	Exponent in fish allometric relation between maximal growth rate and live weight	-	0.667	(Petrell and Jones 2000)
α	resps	Exponent in fish allometric relation between basal respiration rate and live weight	J (g WW)$^{-\gamma}$ d^{-1}	46.024	(Stigebrandt 1999)
γ	respe	Exponent in fish allometric relation between basal respiration rate and live weight	-	0.74	(Enders and Scruton 2006) but see (Stigebrandt 1999) who suggests 0.8
	Tmptrs	Scale coefficient in exponential relationship governing fish maximal growth and basal respiration	-	1.0	(Stigebrandt 1999). The reference temperature is 0 °C
τ	Tmptre	Exponent coefficient in exponential relationship governing fish maximal growth and basal respiration	°C^{-1}	0.08	(Stigebrandt 1999)
	SwimCostFrac	Energy expended in swimming relative to basal energy expenditure	J J^{-1}	1.1	(Petrell and Jones 2000)
	Nresid	Fraction of the protein energy assimilated across the gut wall which is lost as ammonium during protein catabolism	J J^{-1}	$\frac{E_p^{NO_3} - E_p^{NH_4}}{E_p^{NO_3}}$	(Stigebrandt 1999). Careful reading of (Stigebrandt 1999) reveals that his value for the energy content of protein is based upon complete oxidation. He introduces Nresid=0.15 to account for the energy that is lost because fish oxidize protein only to a NH_4^+ endpoint. That is a little smaller than the value derived from our chosen values for $E_p^{NO_3}$ and $E_p^{NH_4}$

Appendix D Hydrodynamic model vs observations: additional graphs and tables

Tidal height tabulated parameters

Table D-1: Comparison of N2 tidal height parameters for Pelorus 1994–1995 and 1997–1998 tide gauges. N2 tidal sea level parameters from measurements and model. Here "ratio" means model value divided by observed value and "diffce" means model value minus observed value.

Tide gauge site and deployment	Record length (days)	Amplitude (m)			Phase (°)		
		Obs.	Model	Ratio	Obs.	Model	Diffce
Beatrix East 1994-1995 Deployment 1	54	0.158	0.167	**1.06**	258.7	264.7	**6.0**
Pelorus Entrance 1997-1998 Deployment 1	46	0.083	0.077	**0.92**	201.4	200.8	**-0.7**
Pelorus Entrance 1997-1998 Deployment 2	69	0.230	0.239	**1.04**	239.3	242.7	**3.4**
Pelorus Entrance 1997-1998 Deployment 3	78	0.136	0.147	**1.08**	276.7	278.7	**2.1**
Beatrix North 1997-1998 Deployment 1	46	0.089	0.082	**0.92**	202.0	201.3	**-0.7**

Table D-2: Comparison of O1 tidal height parameters for Pelorus 1994–1995 and 1997–1998 tide gauges. As Table D-1 but for the O1 constituent.

Tide gauge site and deployment	Record length (days)	Amplitude (m)			Phase (°)		
		Obs.	Model	Ratio	Obs.	Model	Diffce
Beatrix East 1994-1995 Deployment 1	54	0.019	0.021	**1.13**	257.1	264.3	**7.2**
Pelorus Entrance 1997-1998 Deployment 1	46	0.014	0.018	**1.35**	263.2	236.9	**-26.3**
Pelorus Entrance 1997-1998 Deployment 2	69	0.020	0.022	**1.07**	259.0	253.1	**-5.9**
Pelorus Entrance 1997-1998 Deployment 3	78	0.017	0.016	**0.92**	236.7	244.3	**7.5**
Beatrix North 1997-1998 Deployment 1	46	0.013	0.019	**1.46**	264.1	237.1	**-27.0**

Tidal velocity graphs

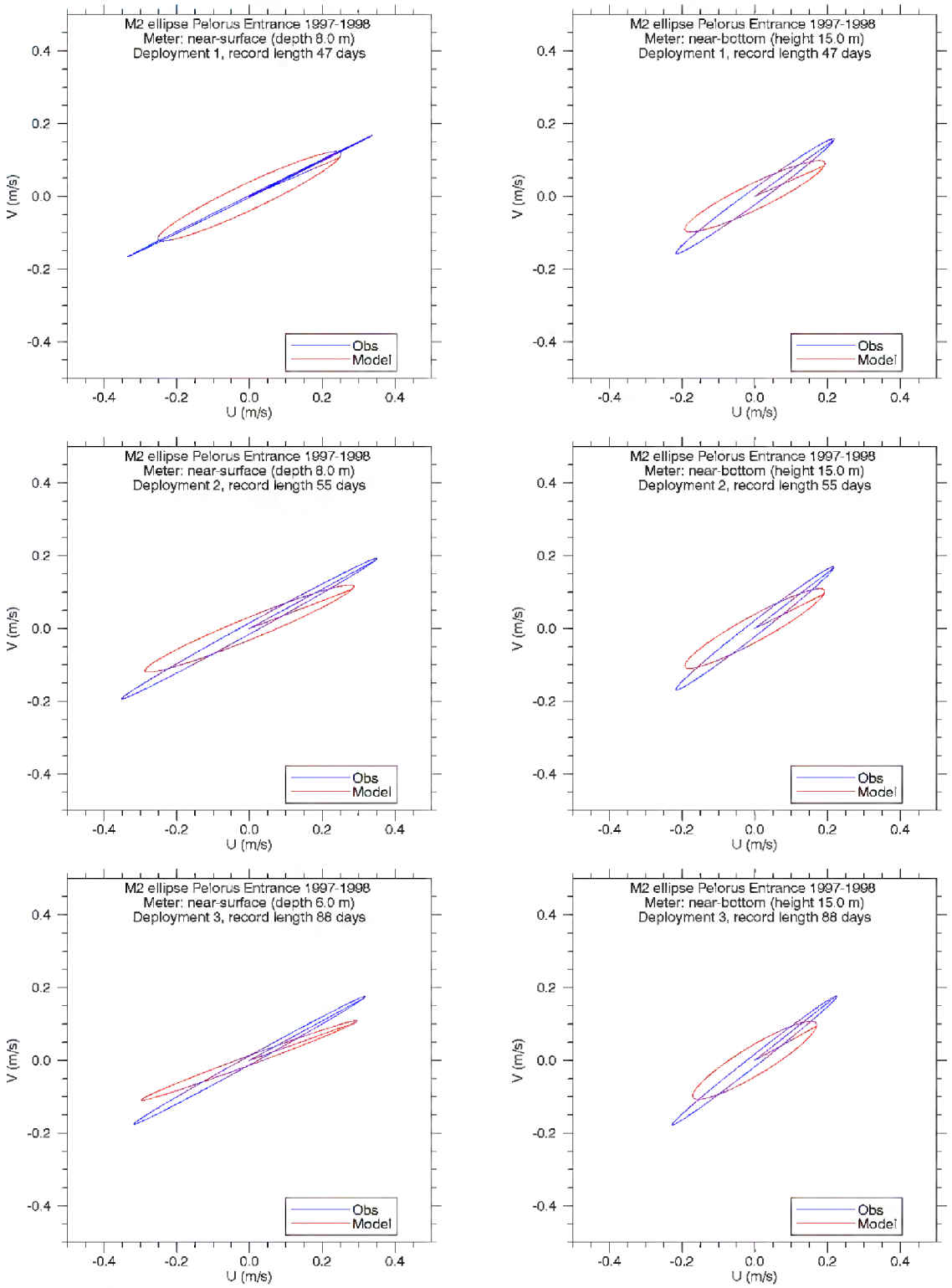

Figure D-1: M2 tidal velocity comparison for Pelorus Entrance 1997–1998. M2 tidal ellipses from current meter (blue) and model (red) at the Pelorus Entrance site, deployments 1 (upper), 2 (middle) and 3 (lower), for near-surface (left) and near-bottom (right) meters. The format of the graphs follows Figure 3-5.

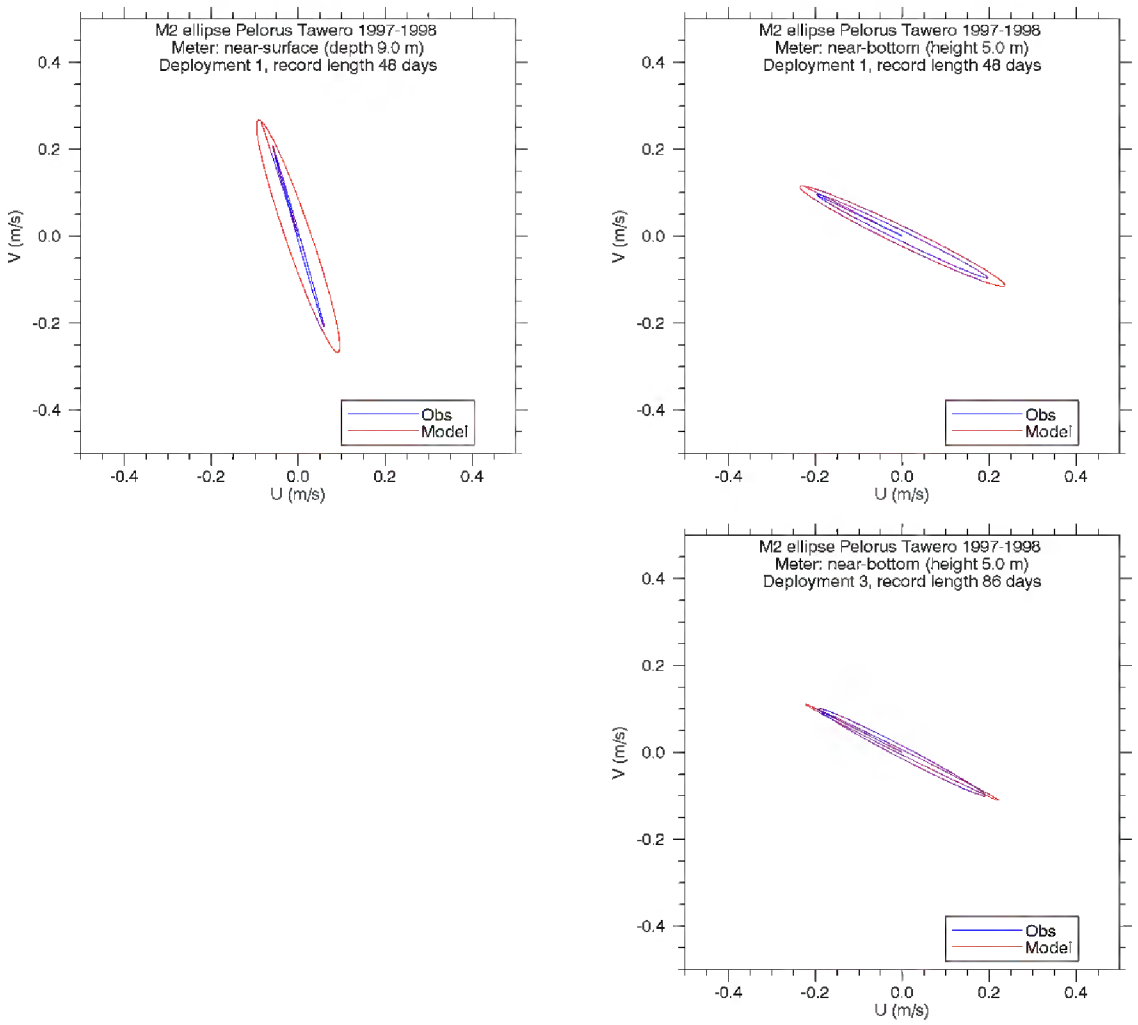

Figure D-2: M2 tidal velocity comparison for Pelorus Tawero 1997–1998. M2 tidal ellipses from current meter (blue) and model (red) at the Pelorus Entrance site, deployments 1 (upper) and 3 (lower), for near-surface (left) and near-bottom (right) meters. The format of the graphs follows Figure 3-5.

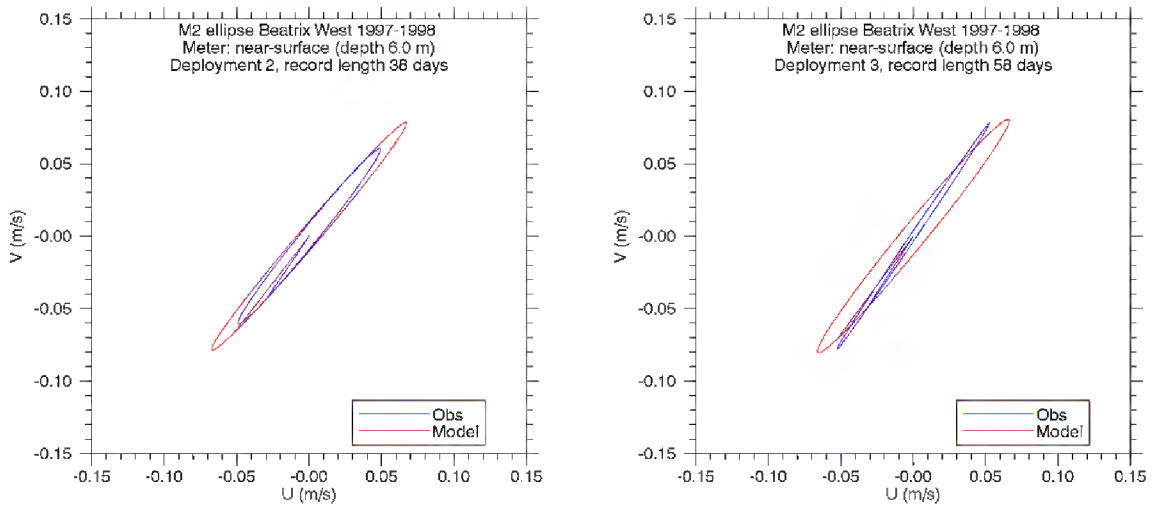

Figure D-3: M2 tidal velocity comparison for Beatrix West 1997–1998. M2 tidal ellipses from current meter (blue) and model (red) at the Beatrix West site, near-surface meters, for deployments 2 (left) and 3 (right). The format of the graphs follows Figure 3-5.

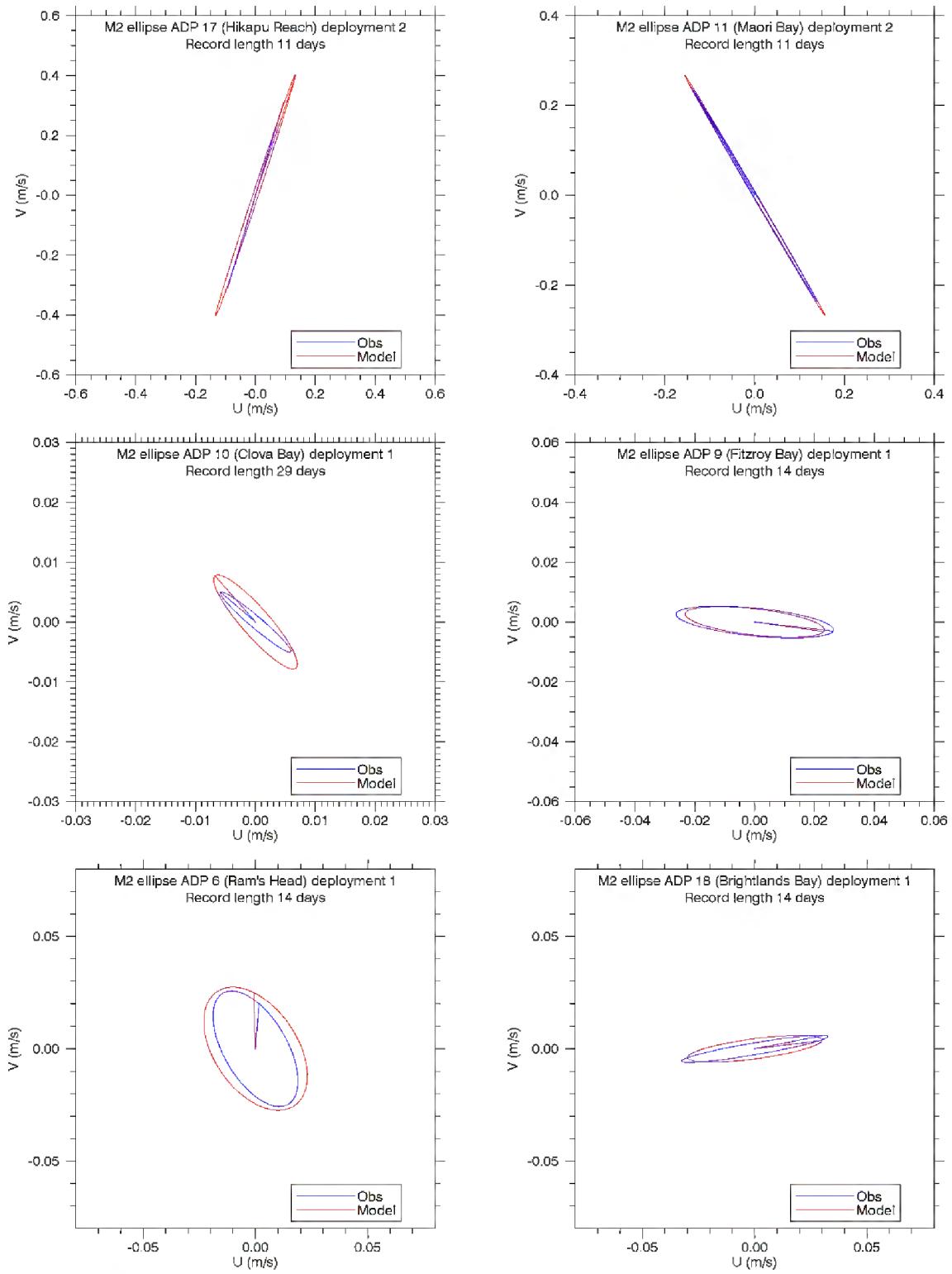

Figure D-4: M2 tidal velocity comparison for 6 FRIA 2005 ADCPs. M2 tidal ellipses of depth-averaged current from ADCP (blue) and model (red). Sites and deployments as indicated. The remaining 3 sites are shown in Figure D-5.

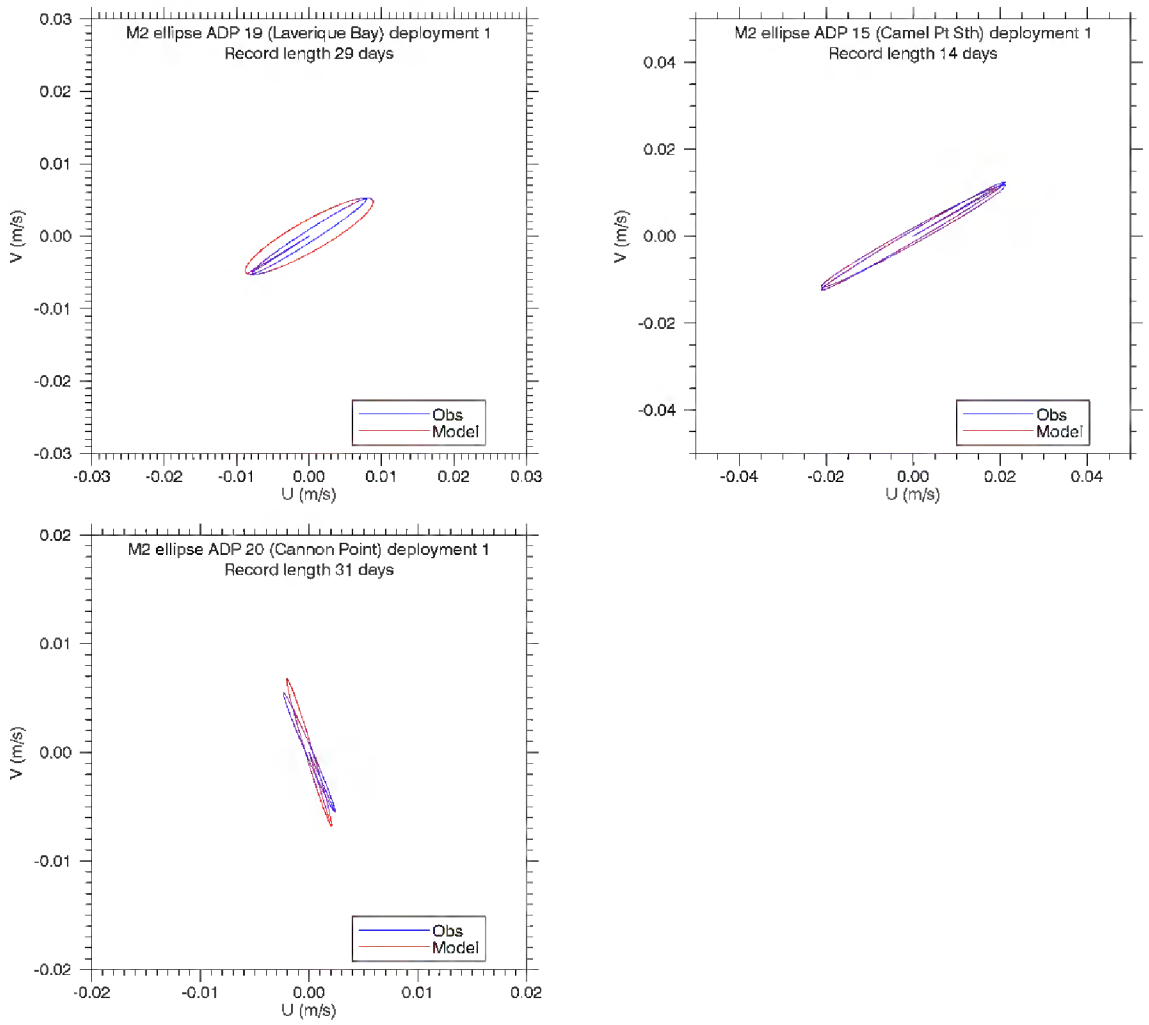

Figure D-5: M2 tidal velocity comparison for 3 FRIA 2005 ADCPs. M2 tidal ellipses of depth-averaged current from ADCP (blue) and model (red). Sites and deployments as indicated. The previous 6 sites are shown in Figure D-4.

Subtidal velocity scatter plots

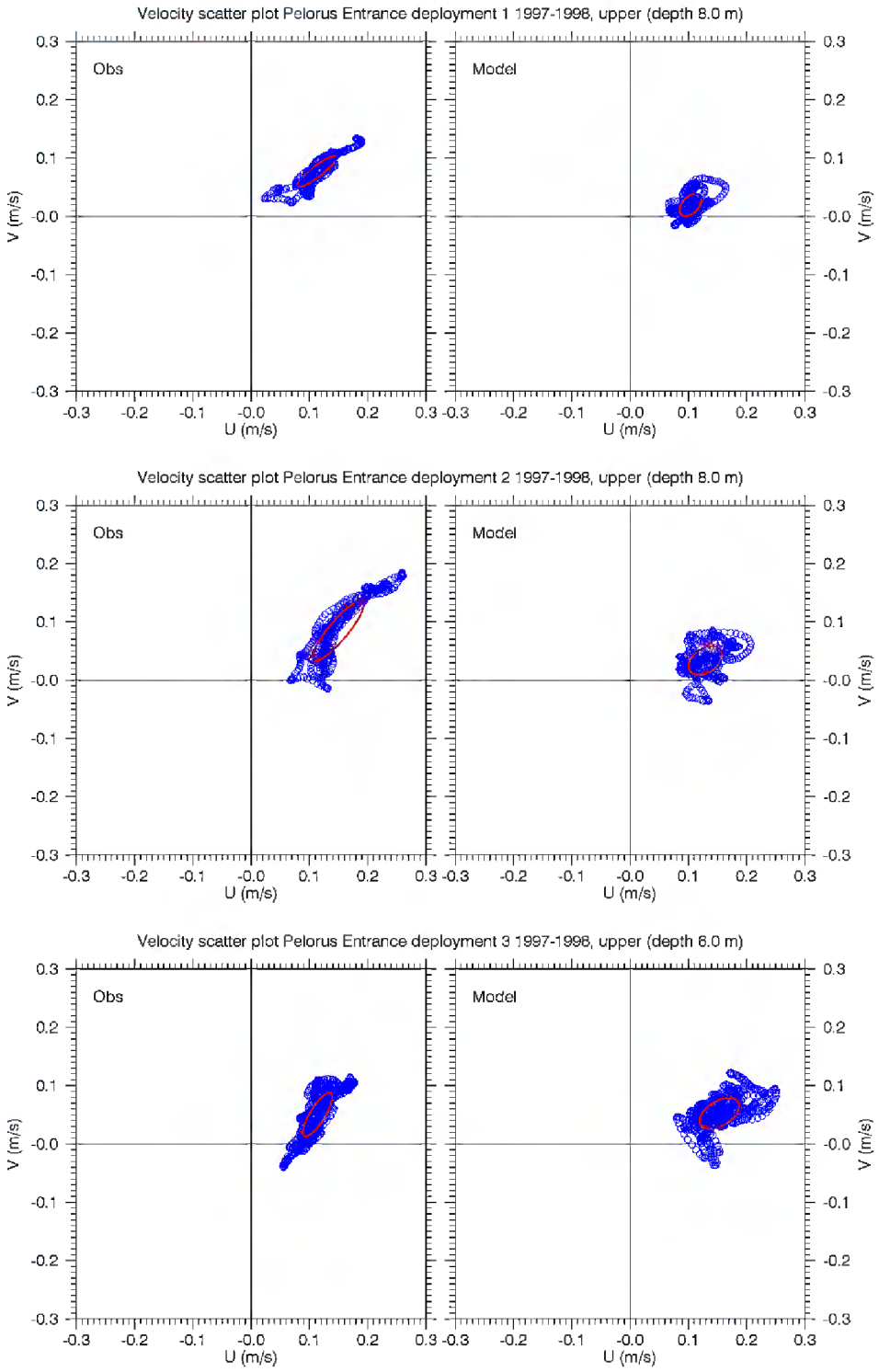

Figure D-6: Subtidal velocity comparison for Pelorus Entrance upper current meter. Subtidal velocity scatter plots from current meter (left) and model (right) at the Pelorus Entrance upper site, deployments 1 (upper), 2 (middle) and 3 (lower). The format of the graphs follows Figure 3-6.

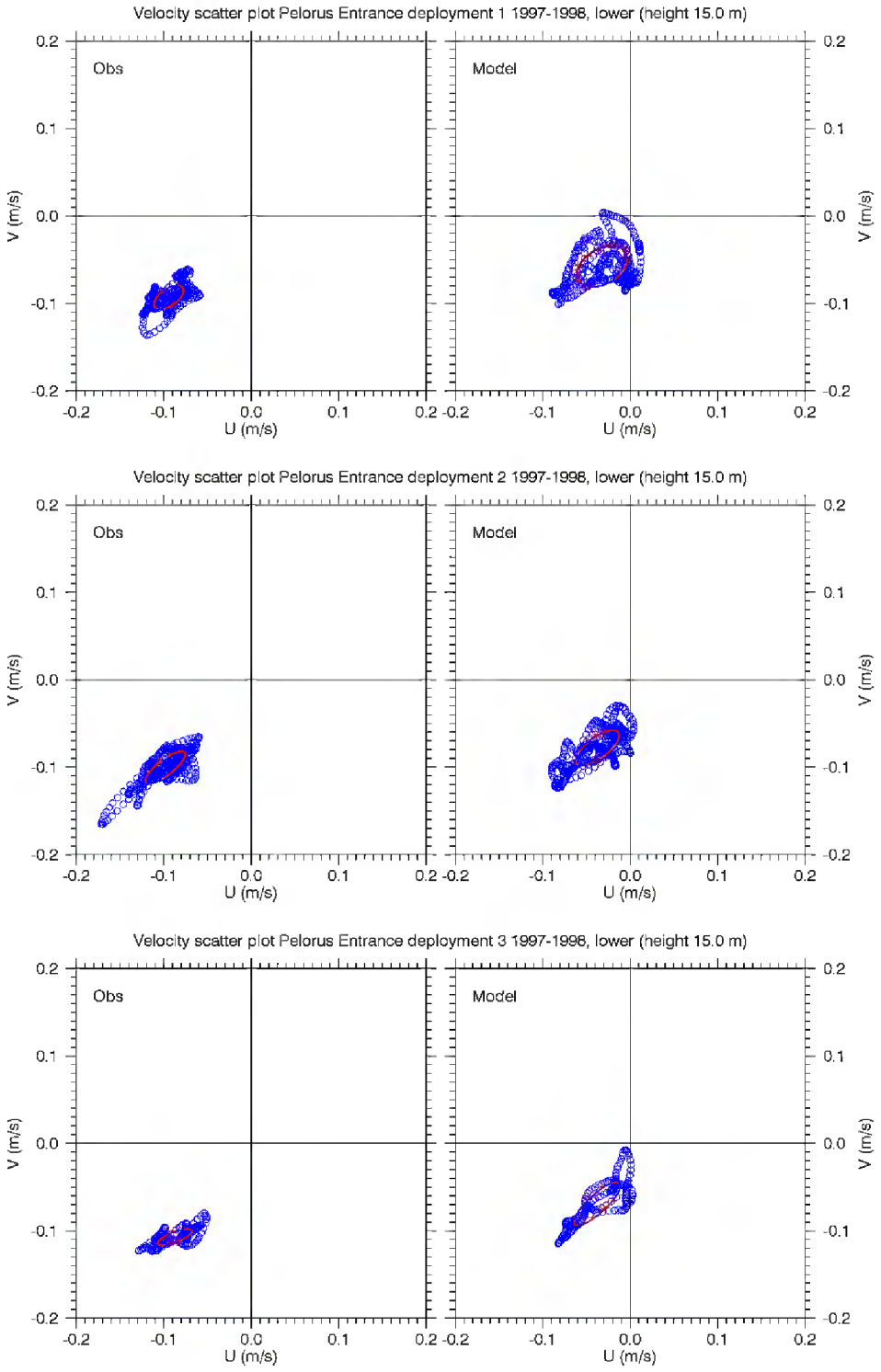

Figure D-7: Subtidal velocity comparison for Pelorus Entrance lower current meter. As Figure D-6 but for the lower current meter.

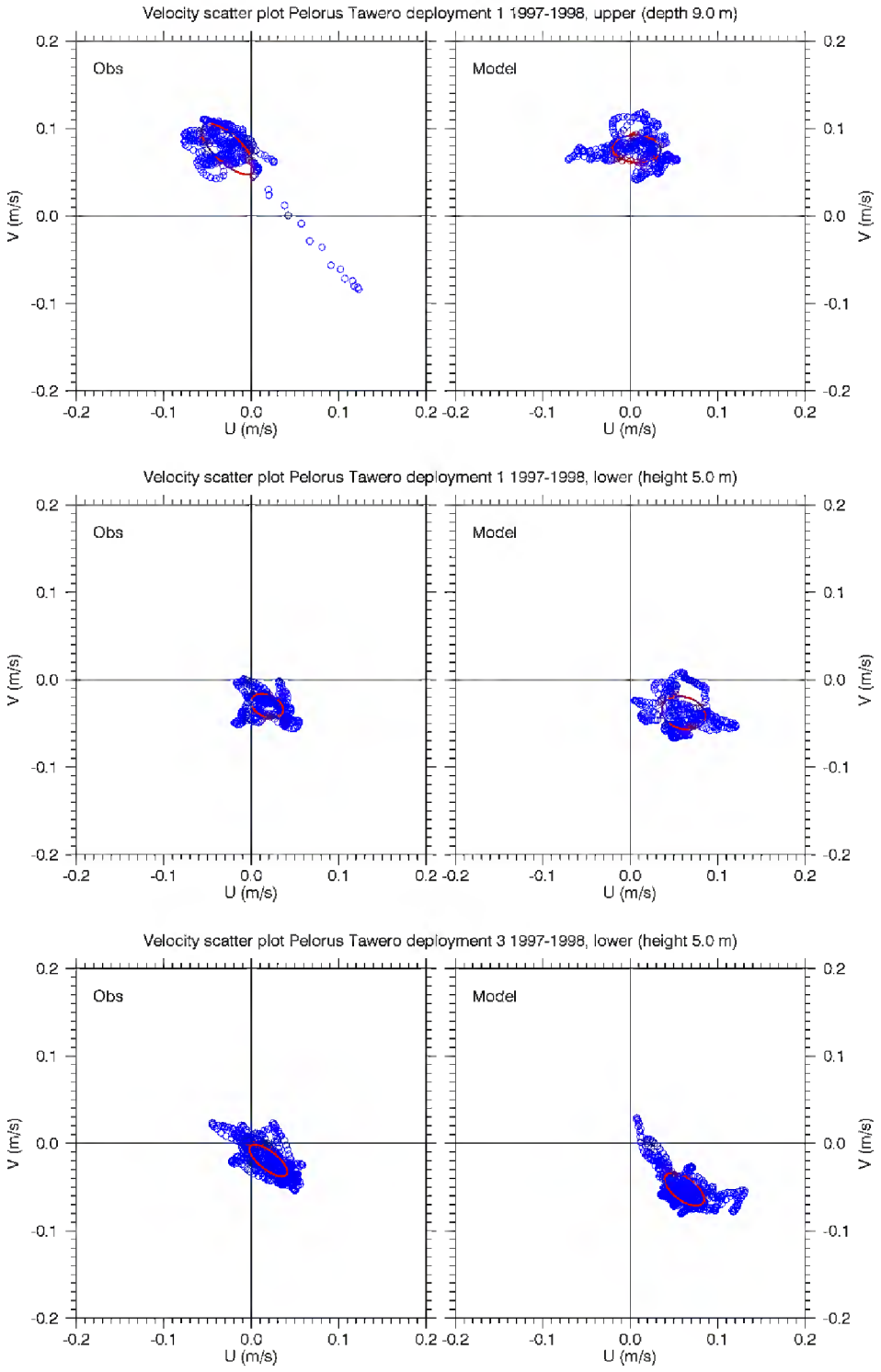

Figure D-8: Subtidal velocity comparison for Pelorus Tawero current meters. Subtidal velocity scatter plots from current meter (left) and model (right) at the Pelorus Tawero site, from top: deployment 1 upper; deployment 1 lower; deployment 3 lower.. The format of the graphs follows Figure 3-6.

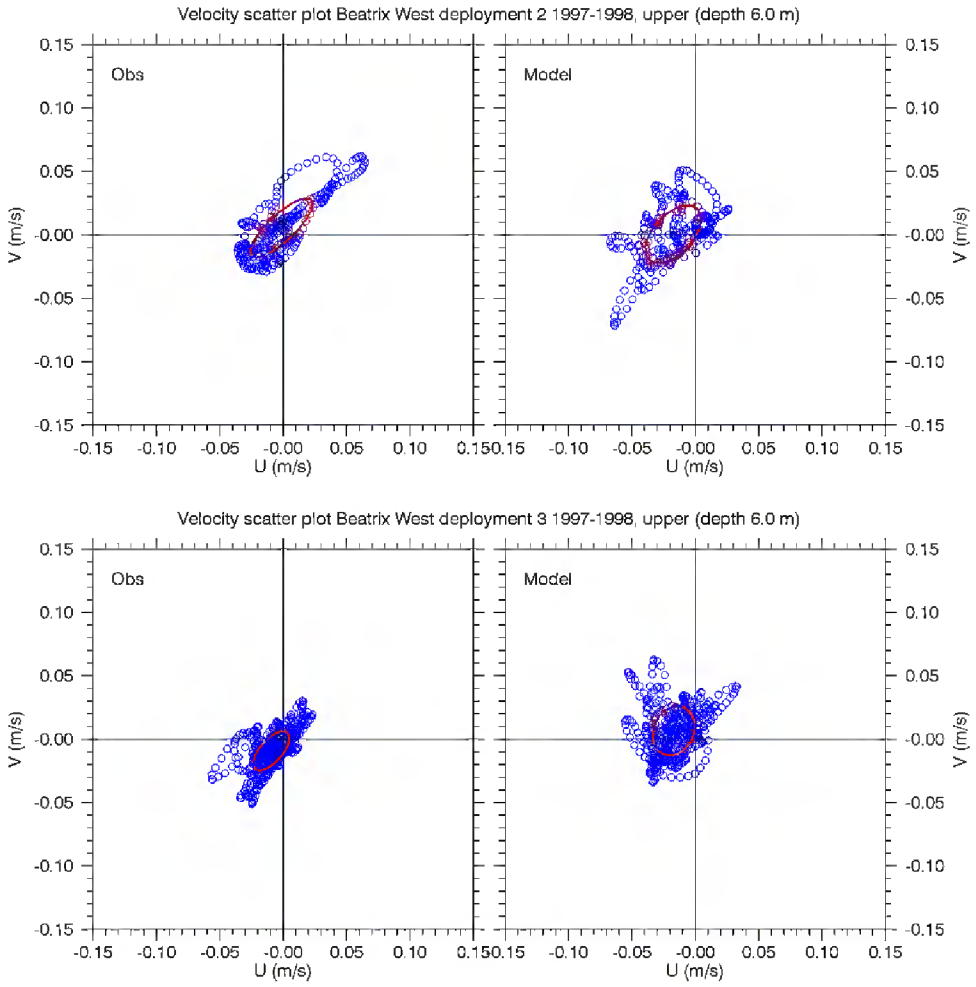

Figure D-9: Subtidal velocity comparison for Beatrix West current meters. Subtidal velocity scatter plots from current meter (left) and model (right) at the Beatrix West site, from top: deployment 2 upper; deployment 3 upper. The format of the graphs follows Figure 3-6.

Tidal velocity tabulated parameters

Table D-3: Comparison of M2tidal ellipse parameters for Pelorus 1994–1995 and 1997–1998 current meters. M2 tidal ellipse parameters from current meter measurements and model. Here "ratio" means model value divided by measured value and "diffce" means model value minus measured value.

Current meter Site/Level/Deployment	Record length (days)	Semi-major axis (m/s)			Eccentricity			Inclination (°T)			Phase (°)		
		Meas.	Model	Ratio	Meas.	Model	Diffce	Meas.	Model	Diffce	Meas.	Model	Diffce
Pelorus Entrance near-surface (depth 8.0 m) deployment 1	47	0.376	0.278	**0.74**	0.01	0.13	**0.12**	63.6	64.8	**1.2**	9.2	14.6	**5.4**
Pelorus Entrance near-surface (depth 8.0 m) deployment 2	55	0.401	0.310	**0.77**	0.03	0.09	**0.06**	61.2	67.8	**6.6**	11.6	13.6	**2.0**
Pelorus Entrance near-surface (depth 6.0 m) deployment 3	88	0.364	0.317	**0.87**	0.03	0.04	**0.01**	61.1	69.9	**8.7**	11.4	12.2	**0.8**
Pelorus Entrance near-bottom (height 15.0 m) deployment 1	47	0.268	0.214	**0.80**	-0.07	0.16	**0.23**	54.1	64.2	**10.1**	352.1	12.2	**20.2**
Pelorus Entrance near-bottom (height 15.0 m) deployment 2	55	0.275	0.219	**0.80**	-0.06	0.16	**0.22**	52.1	61.3	**9.1**	354.0	14.2	**20.2**
Pelorus Entrance near-bottom (height 15.0 m) deployment 3	88	0.288	0.198	**0.69**	-0.05	0.20	**0.24**	52.0	58.9	**6.9**	5.2	10.8	**5.6**
Pelorus Tawero near-surface (depth 9.0 m) deployment 1	48	0.217	0.283	**1.30**	-0.01	0.10	**0.12**	164.2	161.1	**-3.1**	359.3	9.3	**10.0**
Pelorus Tawero near-bottom (height 5.0 m) deployment 1	48	0.219	0.262	**1.20**	-0.05	0.08	**0.13**	116.0	115.8	**-0.2**	3.3	13.8	**10.5**
Pelorus Tawero near-bottom (height 5.0 m) deployment 3	86	0.216	0.248	**1.15**	-0.06	0.02	**0.08**	117.5	116.4	**-1.1**	10.7	15.2	**4.5**
Beatrix West near-surface (depth 6.0 m) deployment 2	38	0.078	0.103	**1.33**	0.07	0.06	**-0.01**	39.0	40.5	**1.5**	132.0	144.7	**12.7**
Beatrix West near-surface (depth 6.0 m) deployment 3	58	0.094	0.104	**1.10**	0.02	0.08	**0.06**	34.0	39.3	**5.3**	134.7	147.3	**12.6**

Table D-4: Comparison of S2tidal ellipse parameters for Pelorus 1994–1995 and 1997–1998 current meters. As Table D-3 but for the S2 constituent.

Current meter Site/Level/Deployment	Record length (days)	Semi-major axis (m/s)			Eccentricity			Inclination (°T)			Phase (°)		
		Meas.	Model	Ratio	Meas.	Model	Diffce	Meas.	Model	Diffce	Meas.	Model	Diffce
Pelorus Entrance near-surface (depth 8.0 m) deployment 1	47	0.126	0.106	**0.85**	0.05	0.16	**0.12**	63.2	59.6	**-3.6**	92.2	84.7	**-7.6**
Pelorus Entrance near-surface (depth 8.0 m) deployment 2	55	0.161	0.136	**0.84**	0.06	0.10	**0.04**	56.5	58.3	**1.8**	60.7	51.7	**-8.9**
Pelorus Entrance near-surface (depth 6.0 m) deployment 3	88	0.110	0.093	**0.85**	0.07	0.23	**0.16**	55.8	59.7	**3.9**	82.3	67.8	**-14.5**
Pelorus Entrance near-bottom (height 15.0 m) deployment 1	47	0.136	0.114	**0.84**	-0.09	0.00	**0.09**	54.3	55.3	**1.0**	67.1	95.8	**28.6**
Pelorus Entrance near-bottom (height 15.0 m) deployment 2	55	0.165	0.133	**0.81**	-0.09	0.04	**0.13**	53.4	53.1	**-0.3**	44.6	61.7	**17.1**
Pelorus Entrance near-bottom (height 15.0 m) deployment 3	88	0.132	0.095	**0.72**	-0.11	0.02	**0.12**	54.9	50.1	**-4.8**	49.9	75.2	**25.3**
Pelorus Tawero near-surface (depth 9.0 m) deployment 1	48	0.092	0.120	**1.30**	-0.21	-0.23	**-0.02**	1.6	175.1	**-6.5**	86.9	85.4	**-1.6**
Pelorus Tawero near-bottom (height 5.0 m) deployment 1	48	0.109	0.147	**1.35**	-0.03	0.15	**0.18**	108.0	101.2	**-6.8**	85.6	92.6	**7.0**
Pelorus Tawero near-bottom (height 5.0 m) deployment 3	86	0.089	0.112	**1.27**	0.02	0.16	**0.14**	113.2	110.1	**-3.0**	79.5	73.6	**-5.9**
Beatrix West near-surface (depth 6.0 m) deployment 2	38	0.028	0.050	**1.74**	0.04	0.10	**0.06**	37.2	41.0	**3.8**	186.8	193.6	**6.7**
Beatrix West near-surface (depth 6.0 m) deployment 3	58	0.031	0.032	**1.06**	0.14	0.19	**0.06**	29.0	24.3	**-4.8**	202.9	217.3	**14.4**

Table D-5: Comparison of M2tidal ellipse parameters for FRIA 2005 ADCPs. M2 tidal ellipse parameters from ADCP measurements and model. Here "ratio" means model value divided by measured value and "diffce" means model value minus measured value.

ADCP Site/Deployment	Record length (days)	Semi-major axis (m/s)			Eccentricity			Inclination (°T)			Phase (°)		
		Meas.	Model	Ratio	Meas.	Model	Diffce	Meas.	Model	Diffce	Meas.	Model	Diffce
Site 17 deployment 2	11	0.326	0.424	**1.30**	0.00	0.02	**0.02**	16.8	18.3	**1.5**	11.7	11.8	**0.2**
Site 11 deployment 2	11	0.274	0.309	**1.13**	0.01	-0.01	**-0.03**	149.5	149.7	**0.2**	19.9	16.1	**-3.8**
Site 10 deployment 1	29	0.008	0.010	**1.33**	0.13	-0.23	**-0.36**	130.3	138.7	**8.4**	0.1	359.7	**-0.4**
Site 9 deployment 1	14	0.026	0.023	**0.89**	-0.18	-0.19	**-0.01**	95.7	96.7	**1.0**	174.8	173.6	**-1.3**
Site 6 deployment 1	14	0.029	0.031	**1.07**	-0.49	-0.60	**-0.11**	149.5	145.7	**-3.8**	305.0	313.7	**8.7**
Site 18 deployment 1	14	0.033	0.030	**0.91**	0.08	0.15	**0.07**	80.4	82.4	**2.0**	344.7	3.7	**19.1**
Site 19 deployment 1	29	0.009	0.010	**1.07**	-0.08	0.21	**0.29**	57.1	60.5	**3.4**	173.6	171.9	**-1.7**
Site 15 deployment 1	14	0.025	0.024	**0.98**	0.05	0.07	**0.02**	59.6	61.1	**1.5**	359.8	350.8	**-9.0**
Site 20 deployment 1	31	0.006	0.007	**1.19**	-0.05	0.05	**0.1**	156.6	163.2	**6.6**	180	185.9	**5.9**

Subtidal velocity tabulated parameters

Table D-6: Sub-tidal velocity comparison. Sub-tidal mean and variance ellipse parameters from ADCP measurements and model, and temporal correlations between measured and modelled time series. Here "ratio" means model value divided by measured value and "diffce" means model value minus measured value.

ADCP Site & Deployment	Mean magnitude (m/s)			Mean direction (°T)			Semi-major axis (m/s)			Eccentricity			Inclination (°T)			Correlation	
	Meas.	Model	Diffce	Meas.	Model	Diffce	Meas.	Model	Ratio	Meas.	Model	Diffce	Meas.	Model	Diffce	Along-chann.	Across-chann.
Pelorus Entrance 1997-1998 upper deployment 1	0.136	0.105	**-0.031**	55.7	79.5	**23.8**	0.043	0.023	**0.54**	0.22	0.61	**0.39**	52.60	43.50	**-9.00**	0.60	0.38
Pelorus Entrance 1997-1998 upper deployment 2	0.172	0.133	**-0.038**	60.4	75.5	**15.0**	0.067	0.032	**0.48**	0.25	0.65	**0.40**	40.00	55.00	**15.10**	0.53	0.64
Pelorus Entrance 1997-1998 upper deployment 3	0.124	0.162	**0.038**	66.3	71.2	**4.9**	0.044	0.038	**0.86**	0.30	0.56	**0.27**	31.60	58.90	**27.40**	0.50	0.33
Pelorus Entrance 1997-1998 lower deployment 1	0.133	0.066	**-0.066**	225.3	208.9	**-16.4**	0.020	0.031	**1.59**	0.50	0.65	**0.15**	55.20	60.20	**5.10**	0.39	0.51
Pelorus Entrance 1997-1998 lower deployment 2	0.140	0.087	**-0.054**	224.3	205.6	**-18.7**	0.028	0.030	**1.07**	0.32	0.40	**0.08**	52.10	53.30	**1.20**	0.71	0.39
Pelorus Entrance 1997-1998 lower deployment 3	0.138	0.079	**-0.060**	219.1	208.5	**-10.6**	0.021	0.035	**1.68**	0.29	0.30	**0.01**	68.70	47.20	**-21.40**	0.80	-0.04
Pelorus Tawero 1997-1998 upper deployment 1	0.081	0.077	**-0.004**	340.9	5.7	**24.8**	0.039	0.028	**0.71**	0.40	0.57	**0.17**	133.10	93.20	**-39.90**	0.40	0.40
Pelorus Tawero 1997-1998 lower deployment 1	0.035	0.072	**0.037**	148.8	121.9	**-26.9**	0.019	0.026	**1.32**	0.65	0.71	**0.07**	114.20	106.80	**-7.50**	0.44	-0.41
Pelorus Tawero 1997-1998 lower deployment 3	0.028	0.081	**0.053**	135.0	130.3	**-4.7**	0.026	0.027	**1.01**	0.40	0.49	**0.09**	128.10	126.90	**-1.20**	0.08	-0.24
Beatrix West 1997-1998 upper deployment 2	0.006	0.017	**0.012**	345.8	271.1	**-74.7**	0.032	0.028	**0.86**	0.32	0.56	**0.24**	46.70	43.00	**-3.80**	0.45	0.30
Beatrix West 1997-1998 upper deployment 3	0.013	0.018	**0.005**	225.2	291.0	**65.8**	0.019	0.020	**1.05**	0.46	0.79	**0.33**	41.70	24.50	**-17.20**	0.29	0.21

Appendix E Time-averaged water-quality properties in the bottom-most layer of the water-column

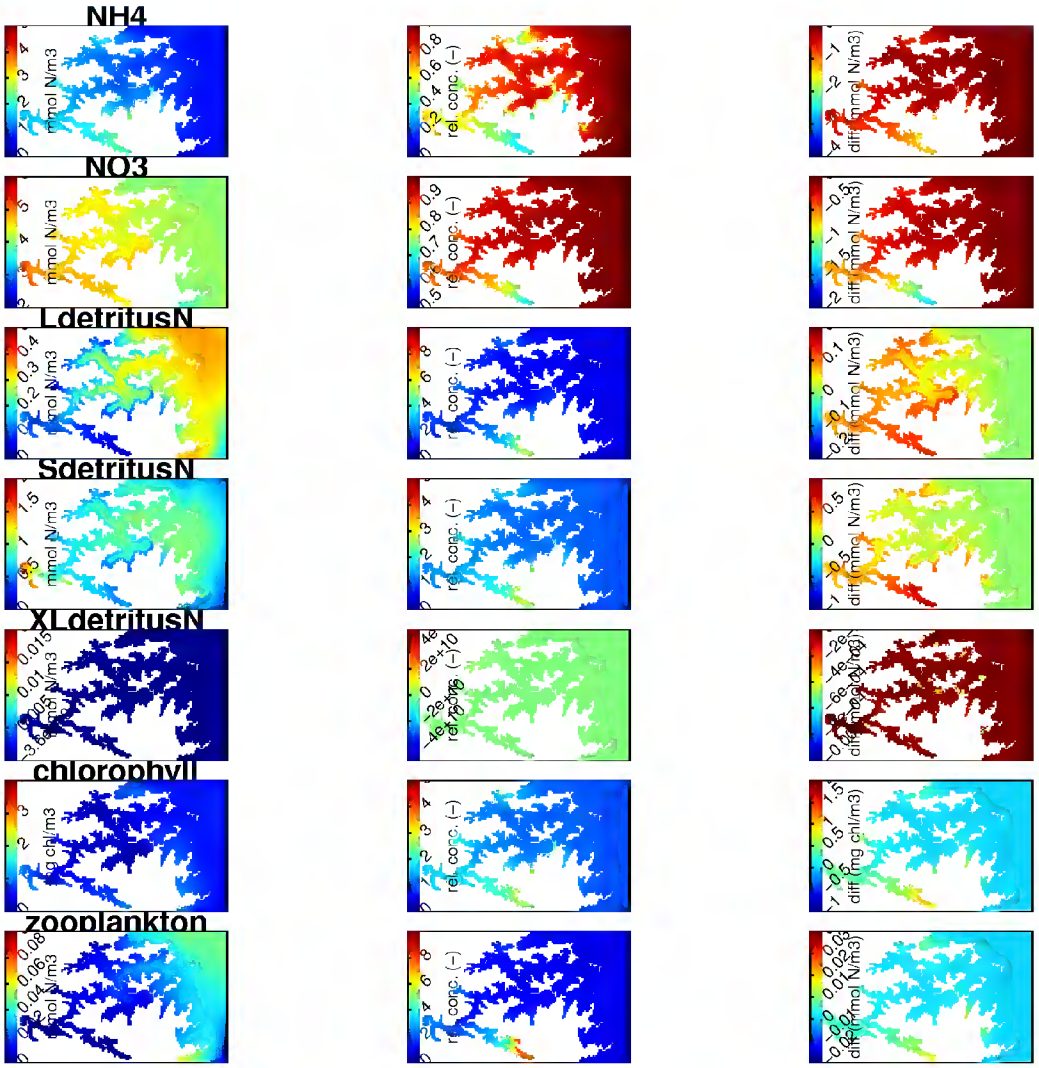

Figure E-1: Comparison of winter time-averaged concentrations in the EM-EF-WD and NM-EF-WD scenarios in the bottom-most layer of the water-column. The left-hand panel illustrates the time-average in the surface-most layer for the reference scenario (EM-EF-WD). The central panel illustrates the time-averaged relative concentration (alternative scenario relative to reference). The right hand column illustrates the time-averaged concentration difference (alternative scenario - reference scenario). These simulations were made on a 400 m horizontal resolution grid.

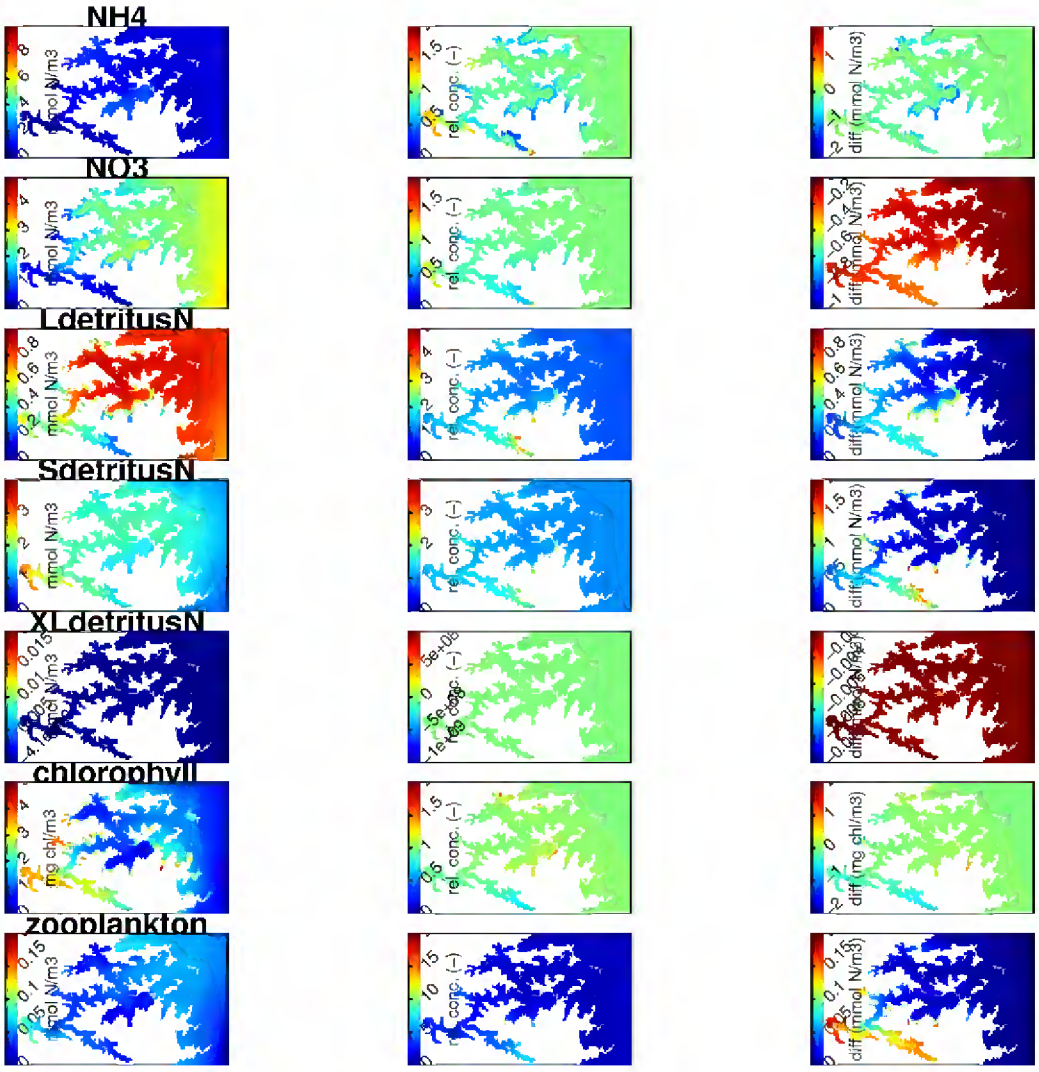

Figure E-2: Comparison of summer time-averaged concentrations in the EM-EF-WD and NM-EF-WD scenarios in the bottom-most layer of the water-column. Refer to the caption of Figure E-1 for further details. These simulations were made on a 400 m horizontal resolution grid.

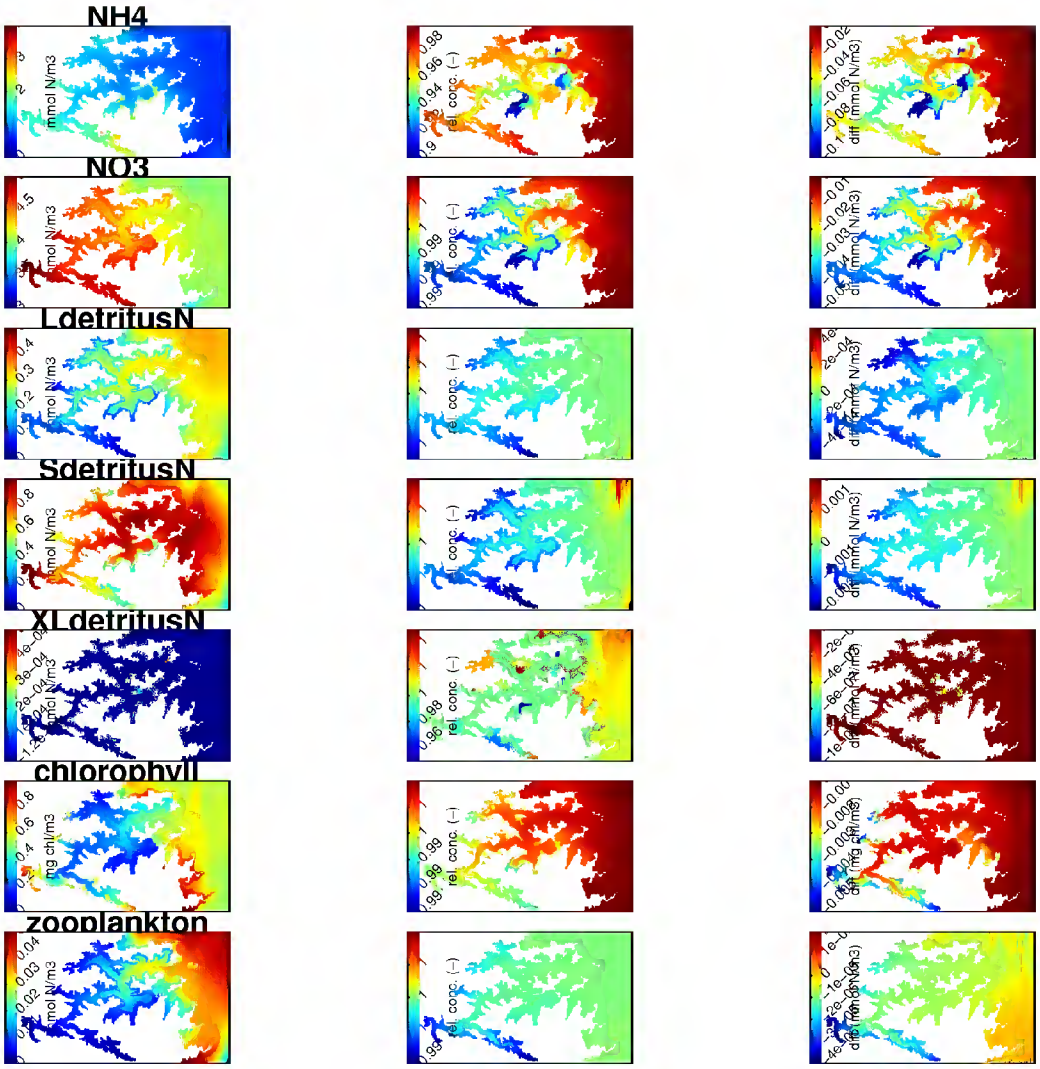

Figure E-3: Comparison of winter time-averaged concentrations in the EM-EF-WD and EM-NF-WD scenarios in the bottom-most layer of the water-column. Refer to the caption of Figure E-1 for further details.

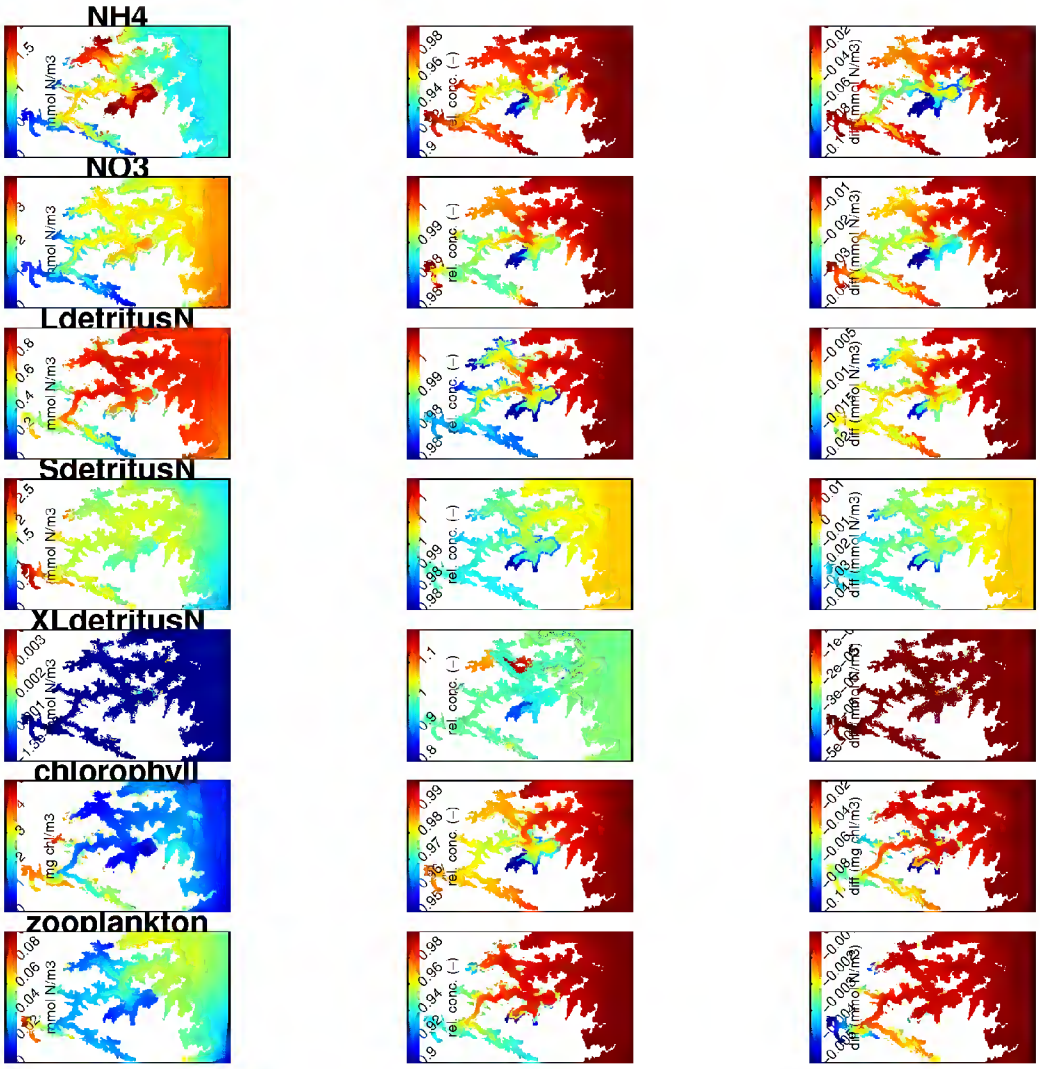

Figure E-4: Comparison of summer time-averaged concentrations in the EM-EF-WD and EM-NF-WD scenarios in the bottom-most layer of the water-column. Refer to the caption of Figure E-1 for further details.

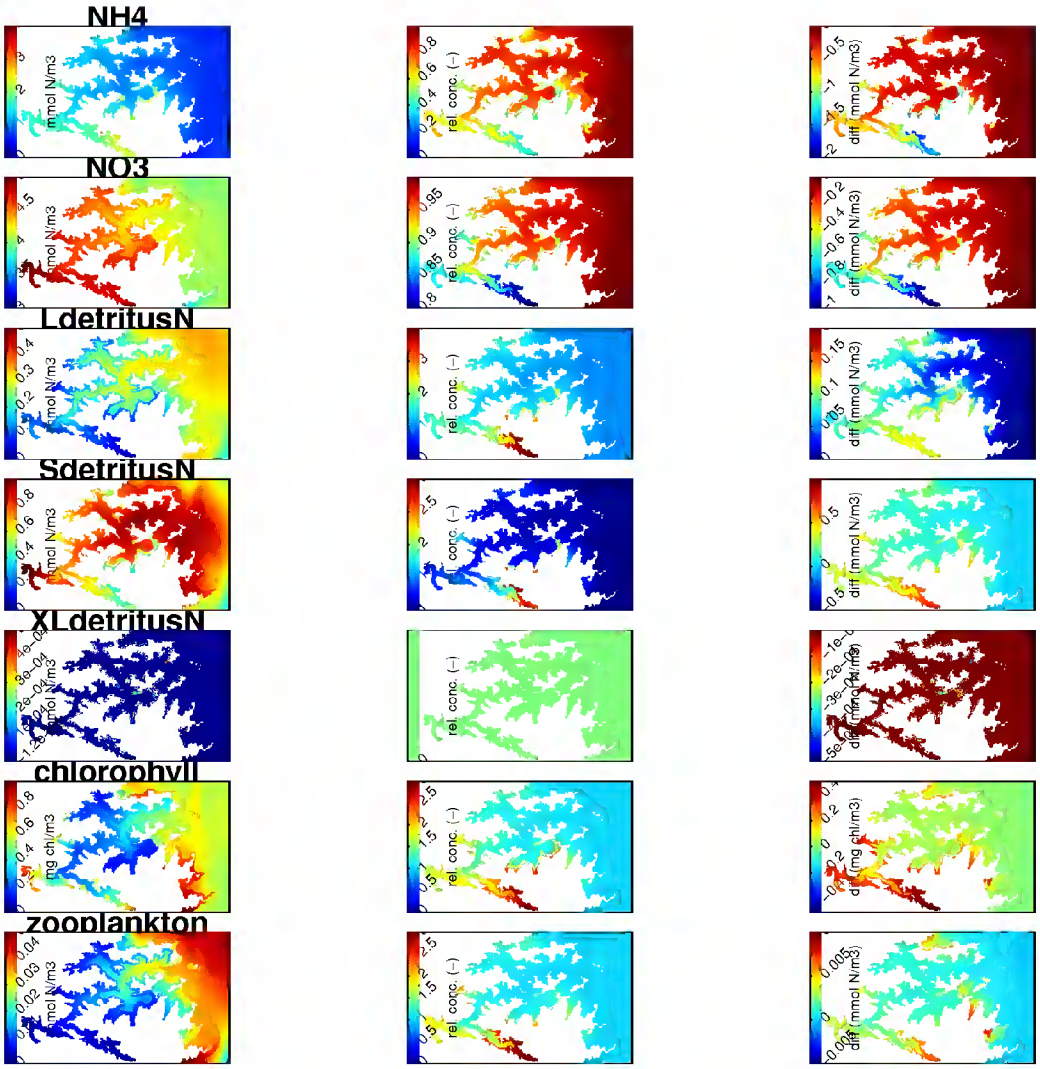

Figure E-5: Comparison of winter time-averaged concentrations in the EM-EF-WD and NM-NF-WD scenarios in the bottom-most layer of the water-column. Refer to the caption of Figure E-1 for further details.

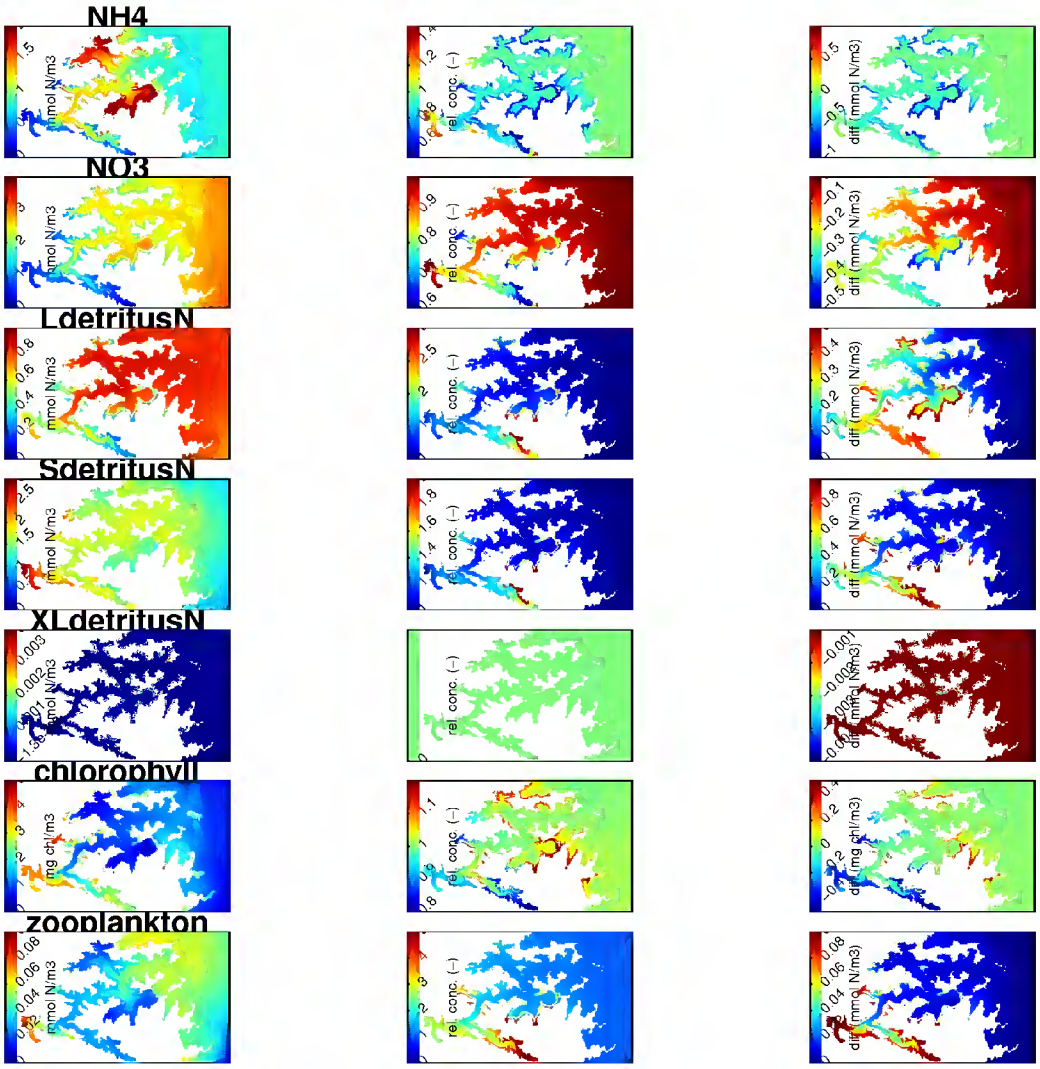

Figure E-6: Comparison of summer time-averaged concentrations in the EM-EF-WD and NM-NF-WD scenarios in the bottom-most layer of the water-column. Refer to the caption of Figure E-1 for further details.

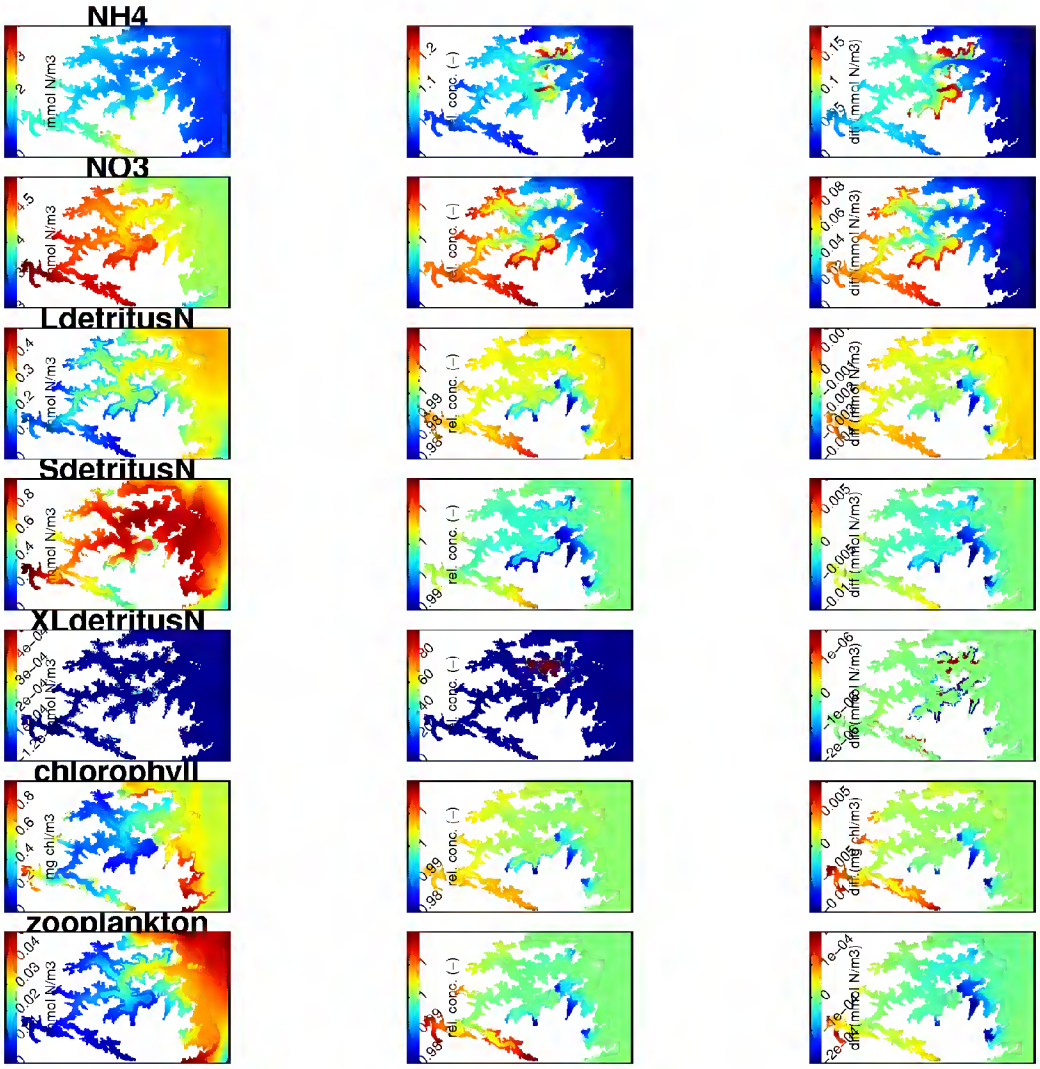

Figure E-7: Comparison of winter time-averaged concentrations in the EM-EF-WD and AM-AF-WD scenarios in the bottom-most layer of the water-column. Refer to the caption of Figure E-1 for further details.

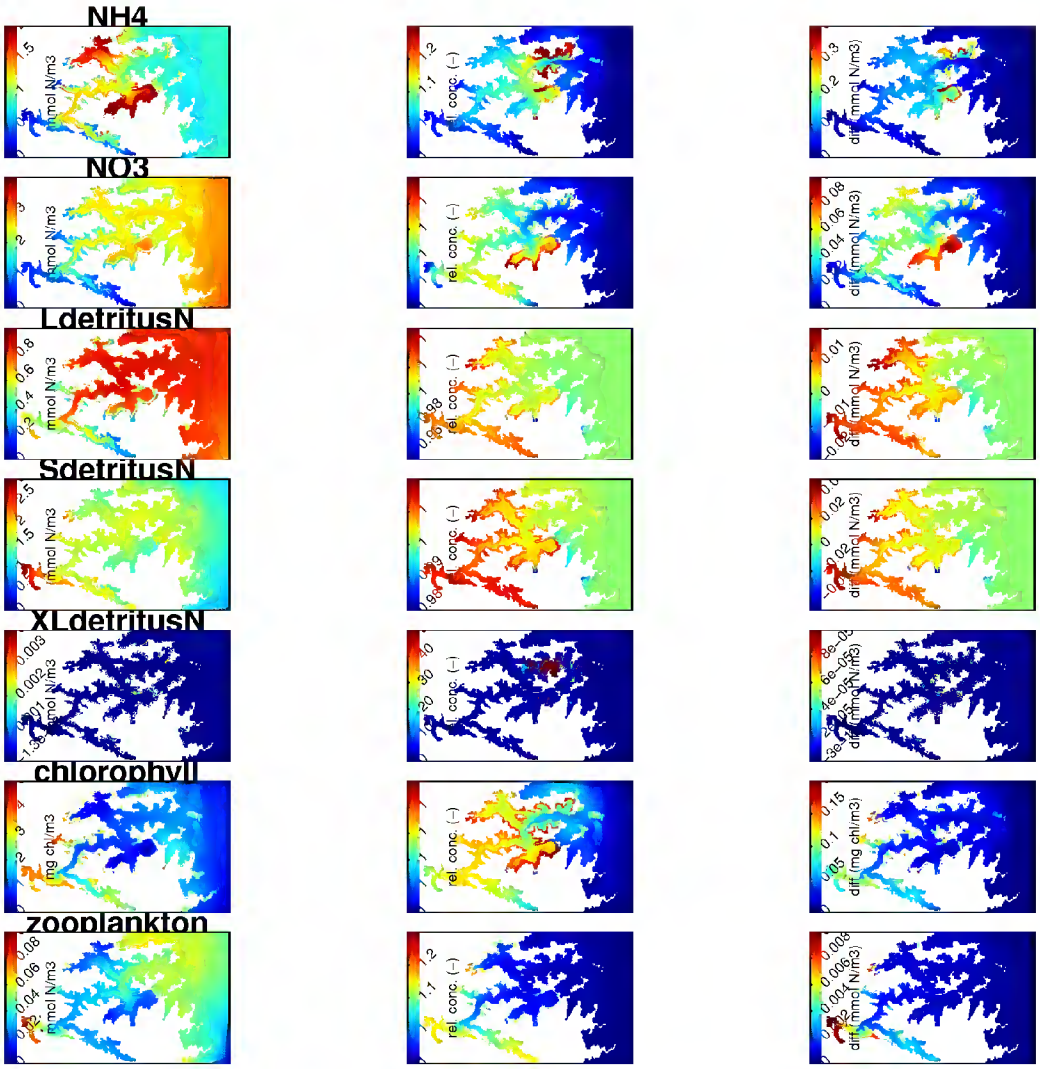

Figure E-8: Comparison of summer time-averaged concentrations in the EM-EF-WD and AM-AF-WD scenarios in the bottom-most layer of the water-column. Refer to the caption of Figure E-1 for further details.

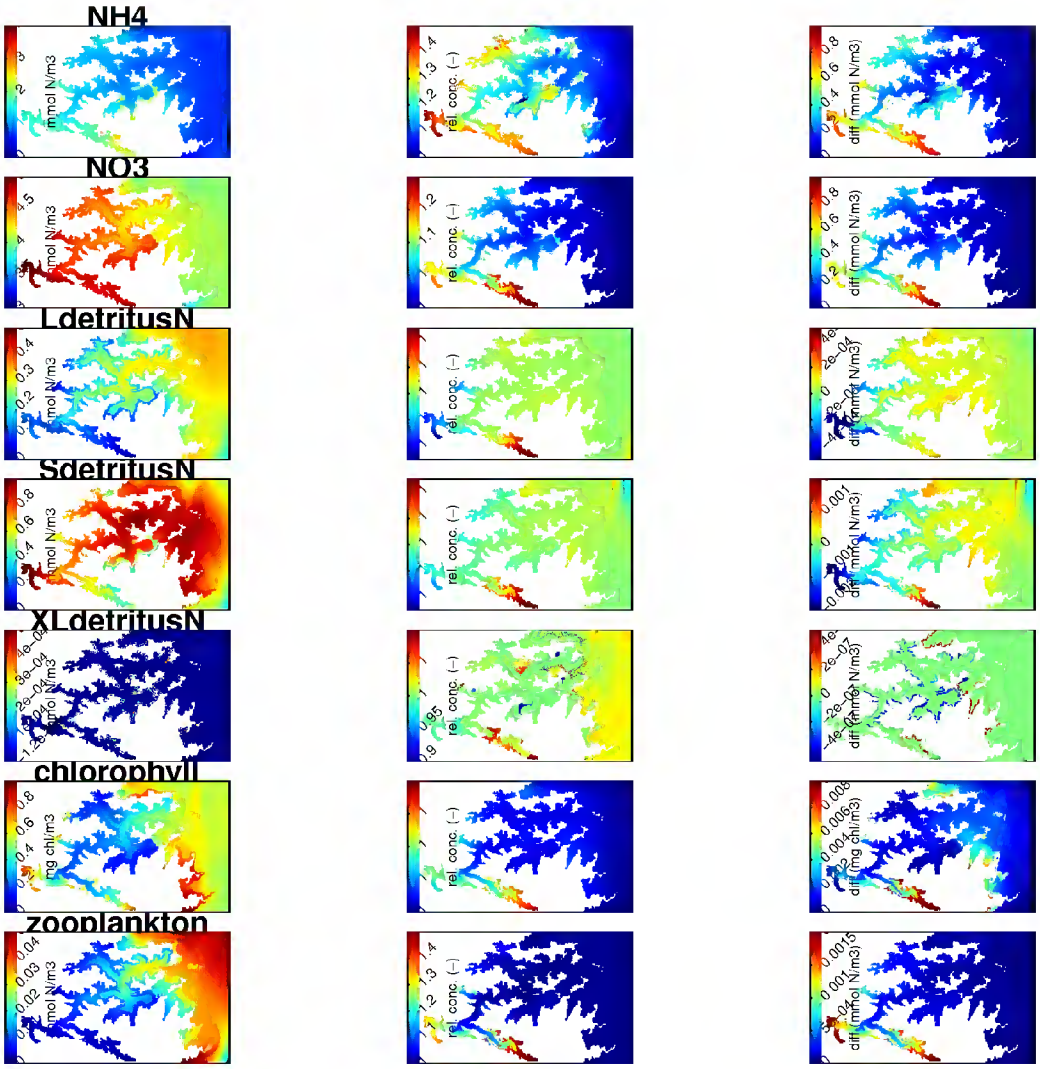

Figure E-9: Comparison of winter time-averaged concentrations in the EM-NF-WD and EM-NF-ND scenarios in the bottom-most layer of the water-column. Note that the reference scenario (EM-NF-WD) differs from that used in most comparisons. Refer to the caption of Figure E-1 for further details

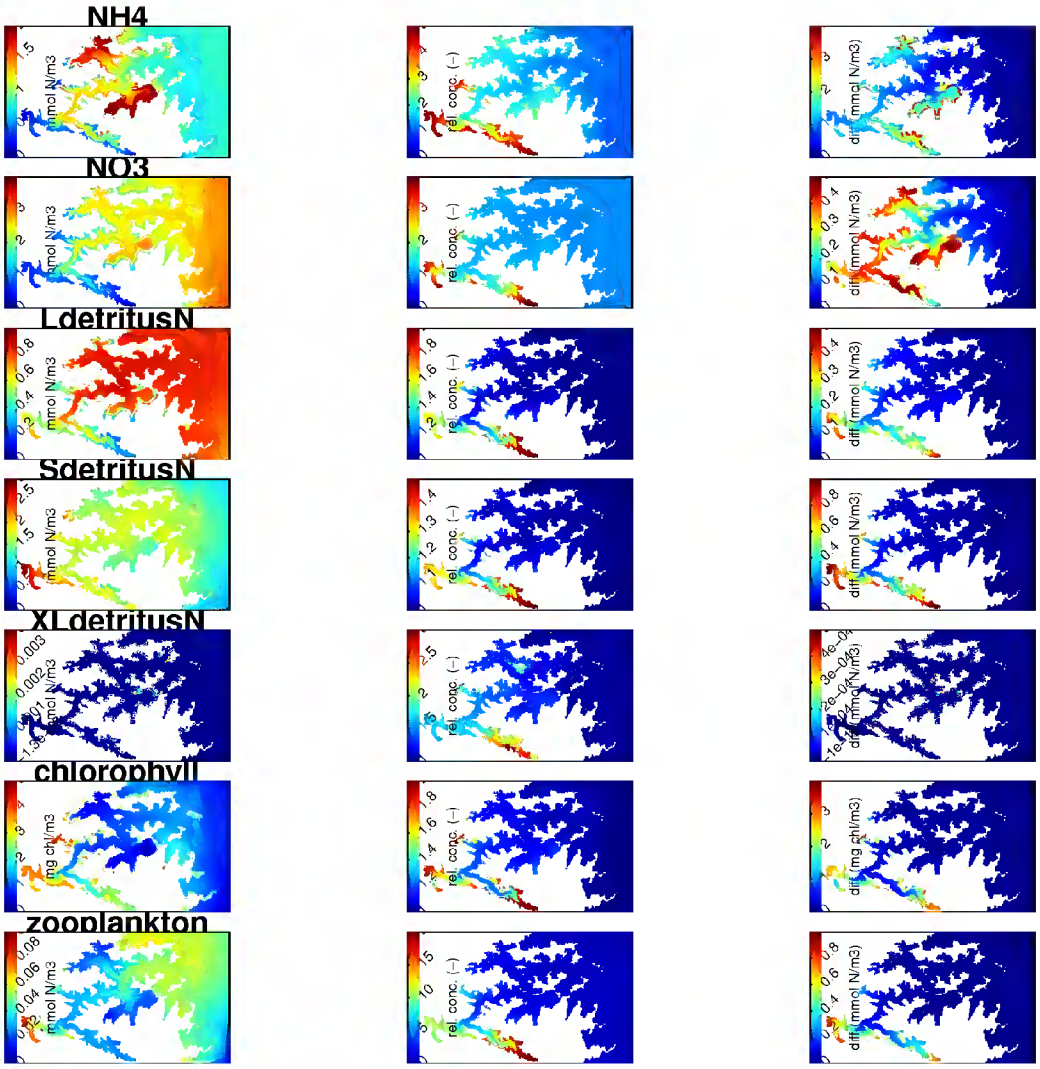

Figure E-10: Comparison of summer time-averaged concentrations in the EM-NF-WD and EM-NF-ND scenarios in the bottom-most layer of the water-column. Note that the reference scenario (EM-NF-WD) differs from that used in most comparisons. Refer to the caption of Figure E-1 for further details

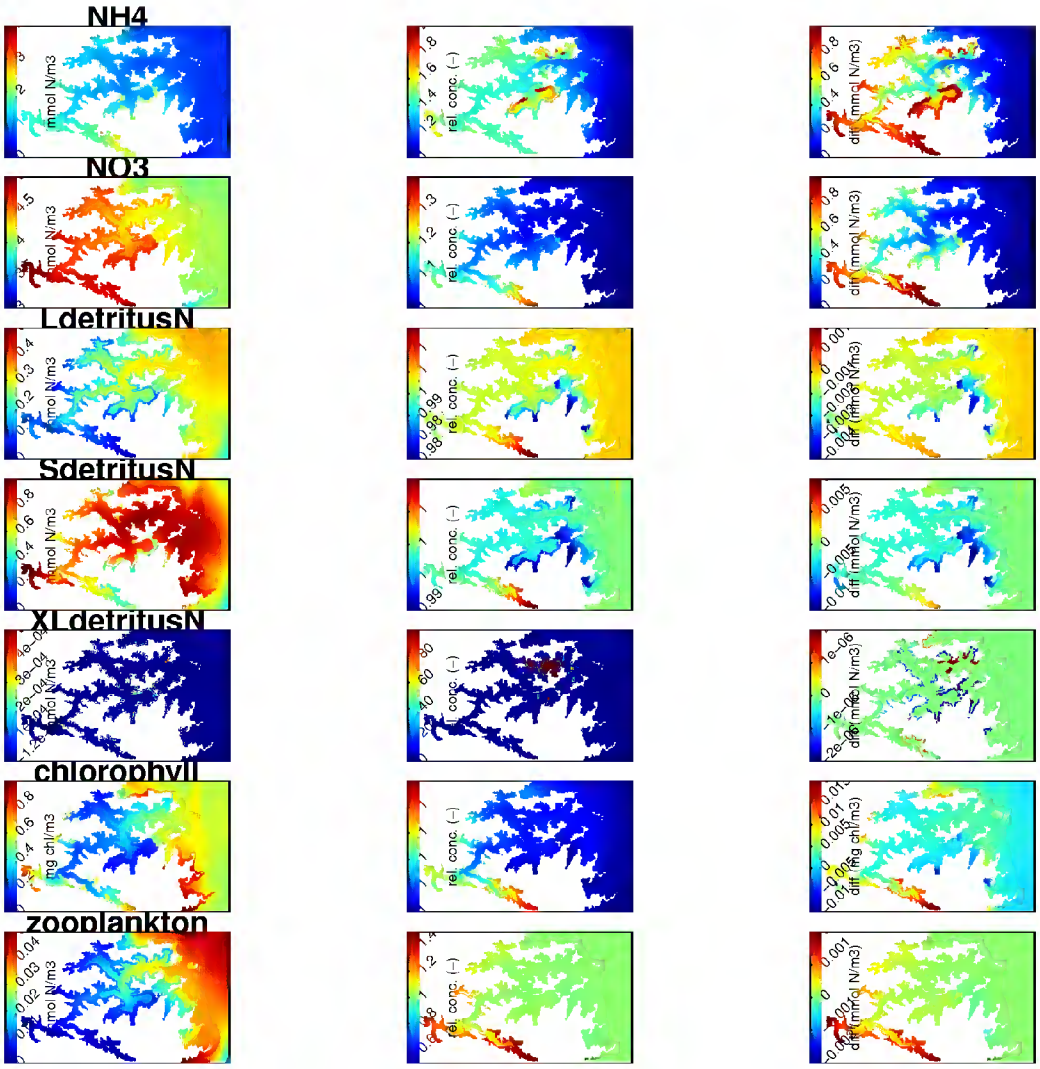

Figure E-11: Comparison of winter time-averaged concentrations in the EM-EF-WD and AM-AF-ND scenarios in the bottom-most layer of the water-column. Refer to the caption of Figure E-1 for further details.

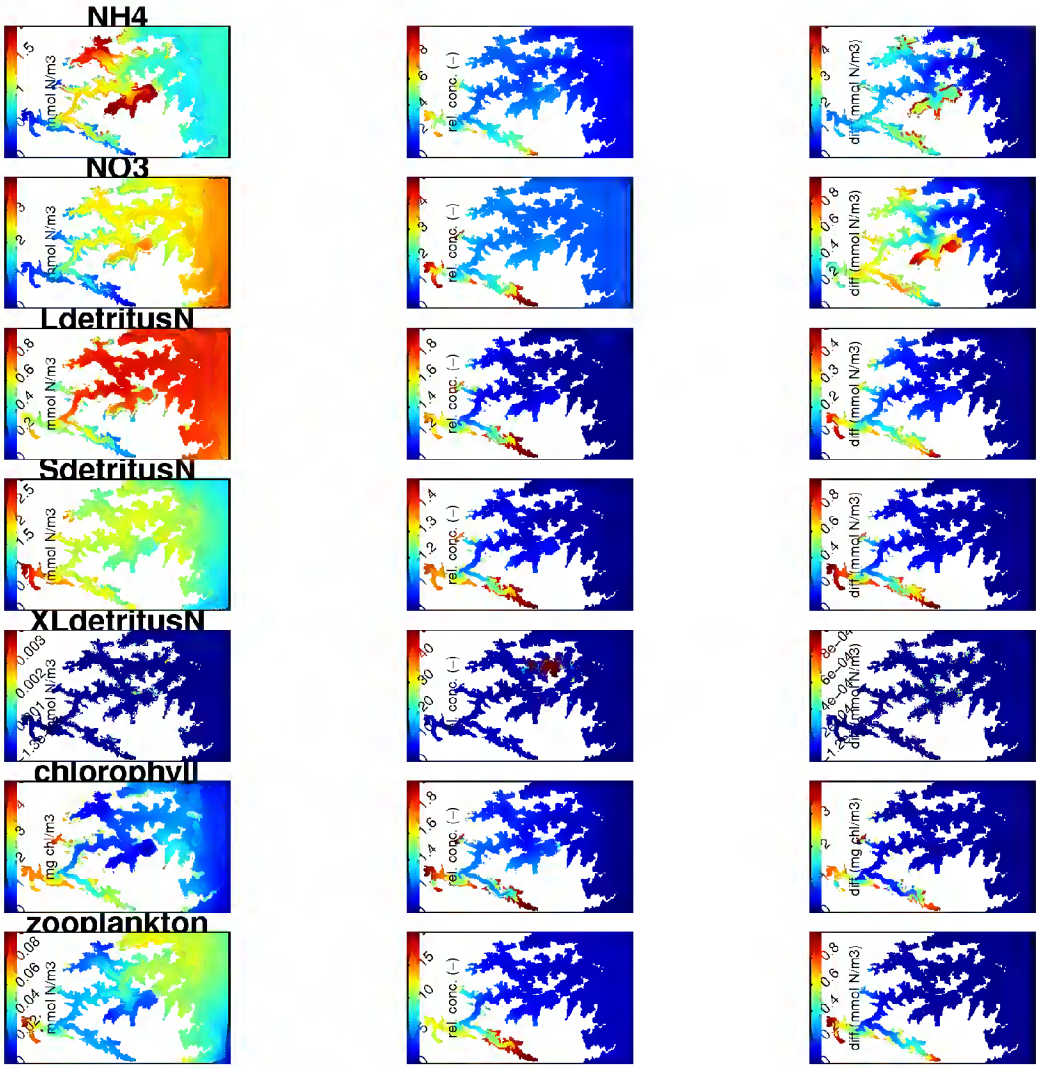

Figure E-12: Comparison of winter time-averaged concentrations in the EM-EF-WD and AM-AF-ND scenarios in the bottom-most layer of the water-column. Refer to the caption of Figure E-1 for further details.